Department of Civil and Environmental Engineering
The University of South Florida

Strength of Repaired Piles

Jeffrey Fischer, Gray Mullins and Rajan Sen
Department of Civil and Environmental Engineering

March 2000

A Report on a Research Project Sponsored by the
Florida Department of Transportation
Contract BB-036
Tampa, Florida

DISCLAIMER

The opinions, findings and conclusions expressed in this publication are those of the authors and not necessarily those of the State of Florida Department of Transportation.

CONVERSION FACTORS, US CUSTOMARY TO METRIC UNITS

Multiply	*by*	*to obtain*
inch	25.4	mm
foot	0.3048	meter
square inches	645	square mm
cubic yard	0.765	cubic meter
pound (lb)	4.448	newtons
kip (1000 lb)	4.448	kilo newton (kN)
newton	0.2248	pound
kip/ft	14.59	kN/meter
pound/in^2	0.0069	MPa
kip/in^2	6.895	MPa
MPa	0.145	ksi
ft-kip	1.356	kN-m
in-kip	0.113	kN-m
kN-m	0.7375	ft-kip

PREFACE

The investigation reported was funded by a contract awarded to the University of South Florida, Tampa by the Florida Department of Transportation. Dr. Moussa Issa was the Project Manager. It is a pleasure to acknowledge his contribution to this study.

This project could not have been successfully completed without the enormous support and help from FDOT's District Maintenance Offices. We especially acknowledge the contribution of Mr. Pepe Garcia, Mr. Hamid Kashani, (Districts One & Seven), Mr. Jorge Martos, Mr. Ralph Leever (District Four) and Mr. Alan Hyman (District Five).

We wish to thank Mr. Sam Lande, Florida Wire & Cable Company, Jacksonville for donating the prestressing strands needed for the test specimens. The specimens were cast at Henderson Prestress, Tarpon Springs. We are very grateful to Mr. Henderson for accommodating us and for facilitating fabrication of the specimens. We thank Mr. Jay Gregg of Applied Concrete Technologies for his assistance.

This study could not have been completed without the support and invaluable assistance of the College of Engineering's Machine Shop staff of Mr. Bob Smith, Mr. Jerry Miller and Mr. Bryan O'Steen. We thank Mr. Mike Konrad in our department for his assistance. The contribution of graduate students (not in any order) Mr. Chris Lewis, Mr. George Atluri, Mr. Reuben Sosa, Mr. Ed Garbin, Mr. Rob Donaldson and Mr. Syed Jani is gratefully acknowledged. We are especially grateful to Mr. David Folk, Mr. Chris Bailey and Dr. Andres Torres-Acosta, for their help in testing and to numerous volunteers from the undergraduate concepts class who helped with the repairs in Phase I. The expert assistance of Mr. Niranjan Pai, a graduate student in Mechanical Engineering, who carried out the finite element analysis for the study and completed all the plots included in this report is gratefully acknowledged.

EXECUTIVE SUMMARY

This report presents results from a two-year laboratory study to assess the strength of repaired piles and to identify measures that would lead to improved efficiency. One third scale model pile specimens fabricated at a commercial prestressing facility were repaired and tested to failure.

Two types of repair were investigated : non-structural repairs using concrete as a filler (Type II) and structural repairs (Type V). In the latter case, severe corrosion was simulated by cutting all the strands and installing a reinforcing cage. A total of 42 specimens were tested under axial and eccentric loading in two phases. In Phase I, only methods and materials used by FDOT were investigated. In Phase II, modifications that potentially enhanced the interface bond between the pile core and repair material were tested.

The results of Phase I indicated that existing repairs led to significant improvement in structural capacity. Under axial loads, non-structural repairs regained about 60% of the capacity of the undamaged pile; structural repairs regained about 75%. Under eccentric loading, the corresponding percentages increased to 70% and 86% respectively. In absolute terms, these percentages represent very significant capacities. Failure in the repaired pile generally occurred due to debonding. This was particularly noticeable in case of non-structural repairs.

The focus on Phase II was on improving the pile core-repair material bond. Two basic schemes were tested. The first used shear connectors and the second tested a new additive material. Two different types of shear connectors were tested - powder activated nails and epoxied doweled bars - in two different schemes. In one, based on specifications used by District IV, the nails were driven in the top region of the pile above the high water level. In the second, they also extended below the water line. In that results were poorer under axial loads, all Phase II tests focused on this loading. As in Phase I, all repair methods increased the capacity of the damaged piles. Additional increases were realized in Phase II in all but one repair scheme. The results showed the doweled epoxy bars provided the greatest additional benefit (12%), followed by the additive material (7.7%). The powder activated nails damaged the core and led to smaller increases (3.3%) or even reduced capacities (-6.3%) when nails extended below the water line.

The results of the study show that current practice yields satisfactory results though simple measures that improve interface bond can further enhance capacity. It should be noted however that these findings are based on short term testing where effects of differential shrinkage between the pile core and the repair material did not play a significant role. Moreover, the long-term integrity of the jacket was not addressed. This may have far reaching effects on the structural performance of any such repair.

TABLE OF CONTENTS

LIST OF TABLES

LIST OF TABLES (Contd.)

LIST OF FIGURES

LIST OF FIGURES (Contd.)

LIST OF FIGURES (Contd.)

LIST OF FIGURES (Contd.)

1. INTRODUCTION

1.1 Introduction

Corrosion damaged piles are commonly repaired by jacketing the pile. These jackets consist of removable or stay-in-place forms installed around the pile that are subsequently filled with concrete, mortar or epoxy. Jackets can be flexible (*constructed of industrial strength fabric*) or rigid though semi-rigid fiberglass jackets have become popular because of their light weight.

Pile jackets are widely used in Florida: a survey completed in 1996 showed that the state had 279 bridges with jacketed piles with a cumulative jacket length of 83,068 ft [1.1]. Depending on the extent and position of damage, Florida uses six different fiberglass jackets designated as Type I to Type VI. Types I-IV are *non-structural* and are used to repair minor damage. Types V and VI are *structural* and are used in cases of severe damage where there is a need to provide reinforcing steel to replace prestressing strands that have corroded away. The vast majority of the repairs carried out, however, are minor repairs with structural repairs constituting a tiny fraction of the total number [1.1].

Although much information is available on the manner in which repairs are to be carried out and on the performance of repair materials [1.2-1.3], relatively little information is available on the structural efficiency of the repaired piles. Without information on the strength of repaired piles, rational decisions that could potentially lead to savings are more difficult to justify. The majority of the studies reported in the literature relate to structural elements or connections used in a non-marine environment. Earlier studies focused on the use of conventional repair materials like concrete or steel, e.g. Refs. 1.4-1.5. More recently, there has been considerable interest in the application of fiber reinforced polymer materials, e.g. Ref. 1.6.

Studies have shown that *full composite action* can be achieved across a repaired section using concrete, though this requires exacting conditions. For example, in a recent study completed in UK in which both beams and columns in a H frame were repaired and tested, full composite action was achieved by the selection of proper materials and in their correct application [1.7]. Material parameters that were deemed critical were modulus of elasticity, tensile strength, coefficient of thermal expansion, shrinkage, creep and tensile adhesion to the concrete substrate. As conditions during pile repair are less than ideal, such complete composite action is unlikely to be realized. In this situation, the extent to which loads are transferred to the repair material is unknown and needs to be established.

1.2 Objectives

The study attempted to answer the following questions through experimentation:

What is the capacity increase due to repair of corroded piles?
When a pile corrodes, the load it supports is re-directed through the reduced corroded cross-section thereby increasing its stress. Because the load path is already set, there is uncertainty as to the extent of increase in capacity arising out of a repair.

Can this repair efficiency be improved?
The critical parameter for efficient load transfer to the repair material is the interface bond between the pile core and the repair material. Efficiency would improve if the bond could be improved. Some FDOT districts have already instituted measures to enhance bond. For example, District IV have a repair option that utilizes powder activated nails as shear connectors. Confinement provided by steel ties is known to improve the material properties of concrete. Advances in concrete technology can also lead to enhanced bond. However, the extent of improvement achieved by such measures in piling applications is not known.

As the name implies, non-structural jackets are intended simply to restore appearance and protect reinforcement against subsequent chloride attack. Structural repairs on the other hand, are intended to restore the ultimate capacity of the cross-section. In the original scope of this project, the goal was to examine only structural (Type V) repairs. However, as there are far greater non-structural repairs than structural ones, the experimental investigation was expanded to include non-structural (Type II) repairs as well.

To meet the above objectives, the study was divided into two distinct phases. In Phase I, simulated repairs were carried out on model piles and their ultimate capacity assessed under concentric and eccentric loads. The results of Phase I, were used to establish a test program for Phase II. In this phase, the effect of shear connectors and a new material were evaluated.

Repairs were carried out largely using materials and procedures stipulated by FDOT. Non-linear finite element analyses were carried out using ANSYS. These compared predictions from the analyses with experimental results. The analysis allows results from the study to be extrapolated to model different conditions.

1.4 Organization of Report

This report is organized into twelve chapters and four appendices that describe various aspects of the study. For convenience, all references cited are listed at the end of the chapter.

An overview of the experimental program for Phase I is provided in Chapter 2. Information on materials used for piles and on repairs is contained in Chapter 3. Chapter 4 describes the fabrication of the pile specimens used in the study while Chapter 5 provides information on how the various repairs were carried out. The results of the concentric and

eccentric tests on the repaired specimens are covered in Chapters 6 and 7 respectively. An assessment of these results is given in Chapter 8.

Phase II experimentation is covered in Chapters 9 and 10. Chapter 9 presents an overview of the experimental program while Chapter 10 contains all the results and a discussion of its findings. Finite element modeling of testing in Phase I and II is covered in Chapter 11. The principal conclusions and recommendations from the study are summarized in Chapter 12.

The appendices contain supplementary results and information relating to results contained in the text of the report. Experimental results from Phase I are contained in Appendices A and B. Results from Phase II are in Appendix C. Finite element comparisons are contained in Appendix D.

References

1.1 Amrhein, W.J. (1996). Letter Report Dated Dec. 11, Florida Department of Transportation, Tallahassee, FL.

1.2 Standard Specifications for Road and Bridge Construction (1994). Florida Department of Transportation, Tallahassee, Revision, September 12.

1.3 Emmons, P. H. (1993). *Concrete Repair and Maintenance Illustrated*, R.S. Means & Company, Kingston, MA.

1.4 Trikha, D.N., Jain, S.C. and Hali, S.K. (1991). "Repair and Strengthening of Damaged Concrete Beams,". Concrete International, Vol 13, No 6, June, pp. 53-59.

1.5 Frangou, M, Pilakoutas, K. and Dritsos, S. (1995). "Structural repair/Strengthening of RC Columns,". Construction and Building Materials, Vol 9, No 5, Oct., pp. 259-266.

1.6 Saadatmanesh, H. and Ehsani, M. (Eds). (1998). Fiber Composites in Infrastructure, Proceedings of the Second International Conference on Composites in Infrastructure, Tucson, AZ, Vol. I pp. 113-328.

1.7 Mays, G.C. and Barnes, R.A. (1995). "The Structural Effectiveness of Large Volume Patch Repairs to Concrete Structures,". Proceedings Institute of Civil Engineers Structures and Buildings, Vol 110, Nov., pp. 351-360.

2. EXPERIMENTAL PROGRAM

2.1 Introduction

The experimental program consisted of two inter-dependent phases. In the first phase, the ultimate capacity of repaired piles was assessed. The results obtained from this phase were used to develop Phase II. This chapter provides an overview of the experimental program for Phase I. Phase II testing was more limited and is presented in Chapter 9.

The basis for the selection of the scale size, dimensions and materials used for the repair specimen is discussed in Section 2.2. Damage simulation is described in Section 2.3. Comments concerning the repair interface are presented in Section 2.4. The device utilized to simulate a load on the damaged piles is described in Section 2.5. The test matrix for this study is presented in Section 2.6. This chapter also introduces the nomenclature used in identifying the test specimens that are referenced in subsequent chapters.

2.2 Specimen Size

Detailed investigation in an earlier study [2.1] had established the key geometric parameters defining typical damage in prototype piles. This had shown that damage was typically most severe in prestressed piles 18 in. x 18 in. or 20 in. x 20 in. with pile slenderness ratios in the 50-60 range. The extent of the damage varied but typically it was assumed to be around 4 ft 6 in.

Based on available testing facilities and fabrication considerations, a one-third scale model for 18 in. piles was deemed the most appropriate as used in the previous study. This gave a 6 in. x 6 in. model section with a clear cover of one inch. Four 5/16 in. Grade 250 strands, each jacked to 11.6 kips, provided a jacking stress of 1300 psi that is consistent with values of 1.2-1.38 ksi in prototype piles.

The same No 5 gage spirals used in prototype piles was also used for the model but with the pitch modified in the middle region to be in the same ratio as 12 in. x 12 in. piles. Calculations had shown that the spirals did not provide any significant confinement.

The pile length was selected to be 8 ft pile to provide a slenderness ratio of 53. Fig. 2.1 provides details of the test specimens.

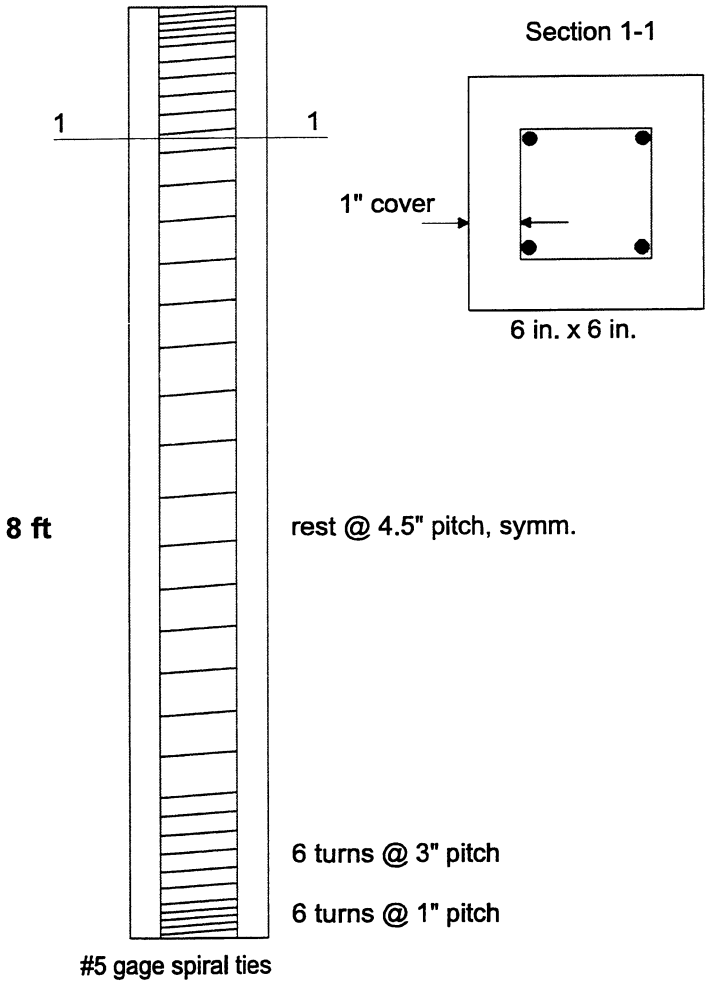

Figure 2.1 Details of Model Piles.

2.3 Damage Simulation

The goal of this study was to determine the effectiveness of two distinct types of repair - structural and non-structural. The most commonly reported repair type is the nonstructural or patch repair. This repair type is prescribed on piles that have not suffered significant section losses in the pre-stressing strands. A structural repair includes mild steel reinforcing and is used in the most extreme cases. In some cases it is the remedy for piles that have fully compromised strands.

Damage was formed in the specimen during fabrication with the use of plywood cutouts. This formed damage was centered about the midpoint of the pile. As in the

previous study, the typical uniform damage was taken as 4 feet 6 inches in the prototype, i.e., 18 inches in the model. A 3:1 transition slope was provided at each end of the uniformly damaged surfaces to the 6 in. by 6 in. section. As 3/4 in. plywood was used, this meant the damage length was an additional 4.5 in. as shown in Fig. 2.2. The resulting *formed* surface provided the texture that was used in half of the repairs. The remaining repairs were carried out on a chipped surface described in Section 2.4.

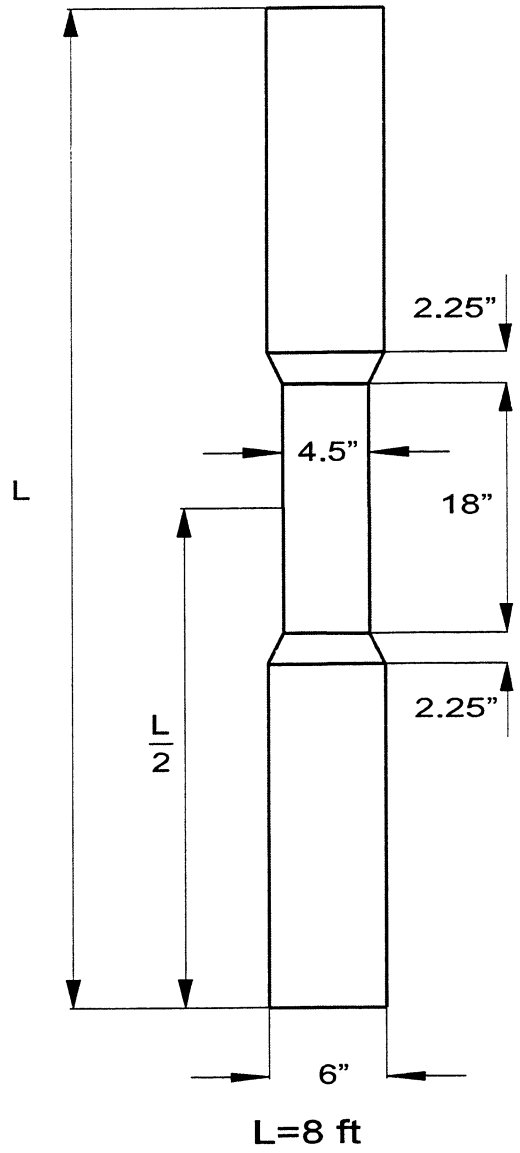

Figure 2.2 Simulated Damage.

The specimens that were patch repaired are designated in this report by a three alphanumeric identifier that begins with the letter N (*to signify non-structural repairs*). The second alphanumeric relates to the surface of the pile core. Repairs on formed surfaces use the letter F. Chipped surfaces are identified by the letter C. The third identifier defines the specimen number.

The same type of identifier is used for the structural repairs excepting that the letter N is replaced by the letter S (*to signify structural repairs*). To model the complete loss of prestressing steel, the strands were all cut at two locations approximately three inches from the center of the 18 in. damaged zone. These cuts were made while the specimen was under simulated dead load.

The cementitious material specified for the pile jacket filler material was of course different for the structural and nonstructural repairs

2.4 Repair Interface

A repair system may be idealized as three distinct zones. The substrate zone or core pile is connected to the repair zone at a common surface often called a bond interface. A chain analogy is helpful in the understanding that a repair system is only as strong as its weakest link. Therefore, a failure in any single zone often spells failure in the entire system. The bond interface is critical in transferring shear. This bond is dependent upon a number of factors including the roughness of the interface. Although the formed surface is unlikely to be encountered in the field it was used on the model as it provided a uniformly consistent surface that was easier to measure and model numerically. As indicated, the second letter identifying this formed surface on a repair is the letter F.

Prior to any repair procedure it is necessary to prepare the surface. The objective is to remove unsound concrete, latency and anything that could have an adverse effect on bonding strength. Frequently this is accomplished with light pneumatic hammers. Consequently, the second surface type examined in this study is a chipped surface that is identified by the letter C. As one can imagine, this surface is highly irregular and more challenging to measure.

2.5 Preload Simulator

Damaged piles in service support both dead and live loads. The removal of such loads are impractical if not impossible. As a consequence most repair systems can do little in redistributing these loads. To simulate these loads a device was designed that would enable a compressive load to be maintained prior to the repair and remain through testing.

This device was required to fit inside the testing frame and not interfere with the ends of the pile necessary for testing.

Service loads from a number of bridges using 18 in. piles were obtained from design information. The reported service stress in the prototype pile ranged from 300 - 550 psi. Using the upper bound of expected service stress a device capable of maintaining a 20 kip load was designed.

This device was constructed from a pair of steel angle sections secured in place at each end by friction. Four high strength bolts were connected to opposing angles and tightened to a specified torque. The angle pairs at each end were connected by two threaded rods which were similarly torqued to the specified setting which produced a tensile force in the rods resulting in a compressive force on the concrete pile in the region of the repair. Fig. 2.3 is a schematic of the initial rendering of the preload simulator. In the final design two sets of bolts were used to connect the clamping brackets that were stiffened (see Chapter 6 for details).

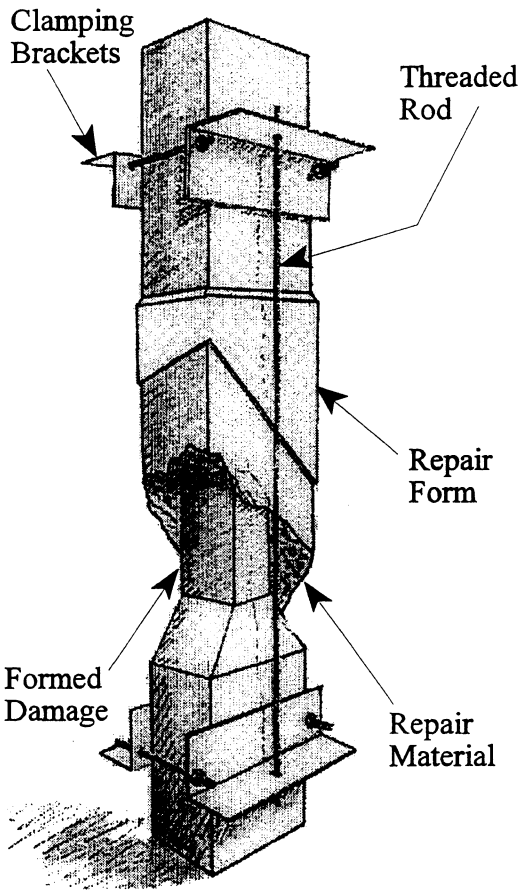

Fig. 2.3 Preload Simulator.

2.6 Test Matrix

In order to assess efficacy of the repairs, both damaged and undamaged specimens needed to be tested as controls. The undamaged controls are identified by the letter C followed by their line number (1 or 2) and the position number in the prestressing bed. The numbering format is identical for damaged controls excepting that C is replaced by D.

Two series of tests were carried out on the formed damaged sections that had been repaired. One series pertained to structural repairs (S) in which the strands were all cut (cs). The other series pertained to the nonstructural repairs (N).

Two types of loads were considered - axial and eccentric loads. The eccentricity ratio, e/h, was taken as 0.2, based on typical design loads for piles. The eccentric loading tests will be referred to frequently in the report as "bending tests".

The test matrix is summarized in Table 2.1. In all, 30 tests were proposed with an identical number of axial and eccentric tests. In general, two specimens were tested in each test set. Additional information on the breakdown of the specimens for the different tests may be found in Chapters 6 and 7.

Table 2.1 Phase I Test Matrix.

Type of Test Specimen	Test ID	Axial	Bending
Undamaged Controls	Cx-x	3	2
Damaged Controls	Dx-x	2	3
Damaged Controls Strands Cut	D-cs	2	2
Structural Repair Formed Surface	SF-x	2	2
Structural Repair Chipped Surface	SC-x	2	2
Non-Structural Repair Formed Surface	NF-x	2	2
Non-Structural Repair Chipped Surface	NC-x	2	2
Totals		15	15

References

2.1 Sen, R., Mullins, G. and Snyder, D. (1999). Ultimate Capacity of Corrosion Damaged Piles. Final Report for Florida Department of Transportation, March.

3. MATERIAL PROPERTIES

3.1 Introduction

This chapter provides information on material properties of the concrete, reinforcing steel and prestressing steel used in the fabrication and repair of the test specimens. Information on the concrete mix design used in fabrication is summarized in Section 3.2. Corresponding properties of the steel used as spiral ties and for prestressing steel are contained in Sections 3.3 and 3.4 respectively. Section 3.5 provides details on the mild steel reinforcement used on the structural repairs in Phase I. Details of the mix designs used in the structural and non-structural repairs in Phase I are presented in Sections 3.6 and 3.7 respectively. Section 3.8 provides details of the mix design used in Phase II.

3.2 Class V Concrete

The test specimens were fabricated at Henderson Prestress, Tarpon Springs using FDOT's Class V Special mix, typically used for piles. The approved mix design was supplied by Florida Rock Industries (Mix No 07-0002). The design strength is 6000 psi. This mix uses Type II cement and Fly Ash with a water to cementitious ratio of 0.30. Details of the mix are summarized in Table 3.1.

Table 3.1 Concrete Mix Design for Class V Special.

Item	**Quantity** per yd^3
Cement (Type II)	702 lbs
Coarse Aggregate (#57 Crushed Limestone)	1730 lbs
Fine Aggregate (Silica Sand)	1027 lbs
Water	258 lbs
Fly Ash Class F	150 lbs
Air Entrainment Admixture (Darex AEA)	10 oz
Water Reducing Agent (WRDA 19)	85 oz
Water/Cementitious Ratio	0.3
Slump Range (in.)	3.50 to 7.50

The piles were fabricated on March 9, 1998. Thirty cylinders were cast at the time of the pour. Two cylinders were tested prior to release. Their 24 hour strength was 4,100 psi. Other cylinders were tested relative to the testing schedule to reflect the strength of the test specimens. Generally six cylinders were tested at a time. The compressive strength averaged 8,620 psi.

3.3 Spiral Ties

Spiral ties using #5 gage wire were used. The spirals were fabricated by Wire Products Inc. The material properties of the certified domestic steel as provided by their manufacturer [3.1] are summarized in Table 3.2.

Table 3.2 Material Properties of Spiral Ties.

Property	Standard
Diameter	0.208 in.
Area	0.034 in^2
Tensile Strength	110 ksi
Yield Strength	97 ksi

3.4 Prestressing Steel

All specimens were prestressed using 5/16 inch diameter, seven wire, Grade 250, low relaxation steel strands. The strands were donated by Florida Wire and Cable Company, Jacksonville, Florida. The properties of the strands as provided by their manufacturer [3.2] are presented in Table 3.3.

Table 3.3 Prestressing Steel Properties.

Property	Standard
Ultimate Breaking Strength	15,959 lb.
Load at 1% Extension	14,740 lb.
Ultimate Elongation in 24 in., in/in.	5.5%
Modulus of Elasticity	29.3 x 10^6 psi

3.5 Reinforcing Bars

Structural pile jackets specify a reinforced steel cage. CTL of Chicago supplied the deformed bar size #2 which was also used to fabricate the stirrups. In Phase II, these reinforcing bars were also used as shear connectors that were epoxied in pre-drilled holes in the repair zone. Material properties for the model reinforcing steel as provided by their supplier [3.3] are summarized in Table 3.4.

Table 3.4 Properties of Reinforcing Steel [3.3]

Item	Standard
Diameter	0.25 in.
Area	0.05 in^2
Yield Strength	60 ksi

3.6 Class III Concrete

The structural repairs in Phase I were carried out adjacent to the University of South Florida's engineering research building using a Class III mix design typically used for pile repair. The approved mix design was supplied by Ewell Industries (Mix ID 63018). The design strength is 3000 psi. This mix uses Type I/II cement and Fly Ash with a water to cementitious ratio of 0.51. Details of the mix are summarized in Table 3.5.

Table 3.5 Class III Concrete Mix Design.

Item	Quantity /cy
Cement (TypeI/II)	560 lbs
Coarse Aggregate (Crushed Limestone)	1450 lbs
Fine Aggregate (Silica Sand)	1054 lbs
Water	367 lbs
Fly Ash Class F	155 lbs
Air Entrainment Admixture (MBAE - 90)	7 oz
Water Reducing Agent (MBL - 80)	64.4 oz
Water/Cementitious Ratio	0.51
Slump Range	7 to 9 in.

The repairs were carried out on November 19, 1998. Several cylinders were cast at the time of the repair. Tests conducted on January 14, 1999 indicated that the strength of this mix was 5,670 psi.

3.7 Portland Grout Filler

The nonstructural repairs were carried out using a grout filler at the same location as the structural repairs adjacent to the University of South Florida's engineering research building. The mix design was supplied by Ewell Industries (Mix ID 60010). The expected 28 day strength of this mix is 4000 psi. This mix uses Type I/II cement and Fly Ash with a water to cementitious ratio of 0.5. There are no coarse aggregates in this grout. Details of the mix are summarized in Table 3.6.

Table 3.6 Portland Grout Mix Design.

Item	**Quantity** (per $yd^{3)}$
Cement (Type I/II)	658 lbs
Fine Aggregate (Silica Sand)	2169 lbs
Water	471 lbs
Fly Ash Class F	282 lbs
Water Reducing Agent (MBL-80)	84.6 oz
Water/Cementitious Ratio	0.5
Slump Range	8 to11 in.

Several cylinders were cast and tested at intervals corresponding to the test schedule. The compressive strength averaged 3,920 psi.

3.8 Class IV Concrete

Repairs carried out in Phase II used Class IV concrete. The approved mix design using 3/8 in. aggregate was supplied by RMC Ewell (Mix No 99778). The design strength is 5500 psi. This mix uses Type I/II cement and Fly Ash with a water to cementitious ratio of 0.30. Details of the mix are summarized in Table 3.7.

The nine specimens repaired on June 4 1999 used Class IV concrete supplied by Ewell Industries. The average compressive strength at the time of testing was 7,880 psi.

Table 3.7 Concrete Mix Design for Class IV Special.

Item	Quantity per yd^3
Cement (Type II)	630 lbs
Coarse Aggregate (Crushed Limestone)	1215 lbs
Fine Aggregate (Silica Sand)	1478 lbs
Water	292 lbs
Fly Ash Class F	150 lbs
Air Entrainment Admixture (MBAE-90)	5 oz
Water Reducing Agent (MBL - 80)	90 oz
Water/Cementitious Ratio	0.37
Slump Range	4.0 to 6.0 in.
Unit Weight	139.3 lbs/ft^3

The two PROTECRETE specimens repaired two weeks later also used Class IV concrete but with the following changes (1) Type I cement (2) no admixtures (3) additional PROTECRETE's mix water conditioner. These were individually batched at USF (see Chapter 10 for mix details). Average concrete strength for the first batch was 4,980 psi and that of the second batch was 4,530 psi.

References

3.1 Wire Products Inc. (1997). Properties of 4 x 4 Spirals. Fax dated Dec 1.

3.2 Florida Wire and Cable Inc. (1997). Fax dated November 19.

3.3 Construction Technology Laboratories, Inc. (1998). Properties of Model Reinforcement, Skokie, IL. Fax from Adrian Ciolko dated October 9.

4. FABRICATION OF SPECIMENS

4.1 Introduction

The pile specimens used for repair were fabricated at a commercial prestressing facility, Henderson Prestress, in Tarpon Springs about 30 miles from the USF campus. This chapter provides an outline of some of the considerations that went into the fabrication of the specimens. Details relating to the facilities utilized in casting the specimens are contained in Section 4.2. The forming operations are described in Section 4.3. The placement of the concrete is presented in Section 4.4. An assessment of the initial prestressing force is included in Section 4.5.

4.2 Prestressing Facilities

Although the original intent was to test about thirty specimens, extra specimens were cast to allow additional testing. As the prestressing bed was approximately 240 ft long, it was possible to cast twenty five, eight ft long specimens in one line. An additional line was created so that fifty specimens could be cast simultaneously. They were batched from a single truck and therefore the concrete used and curing conditions were identical for all the specimens. Thirty-six of the specimens had stimulated damage by using plywood inserts (see Fig. 3.2). The remaining 14 specimens were cast with nominally constant cross section each side measuring six inches (see Fig. 3.1).

Dirk Henderson, president of Henderson Prestress, permitted us to cast the piles on an existing bed used for double-T sections. These steel forms provided an excellent base for welding six inch angle irons which were used as forms. Reinforced abutments located at each end of the bed were well suited for our stressing operations. In addition this bed offered a safe work platform to facilitate the fabrication of our specimens.

At the Henderson Prestress yard only a couple problems cropped up. The 3/4 in. aggregate in the mix (see Table 4.1) was at times difficult to consolidate near the ends of pile where the spiral pitch was the narrowest. This difficulty was compensated for by running the vibrator inside the spirals toward the ends. An unexpected cold snap plummeted temperatures which retarded the strength gain required for release. It also hindered mounting the strain gages which were intended to estimate the initial prestress. Fortunately, this site is near the Gulf which protected the specimens from the frost that was experienced further inland.

4.3 Details of Fabrication

Two factors were crucial for success in the laboratory testing. These were the condition of the ends of the column and the uniformity of the simulated damage. The ends of the columns needed to be absolutely square to prevent failing prematurely especially under axial loading. Uniformity of the simulated damage was essential for obtaining a consistent bonding surface for the repairs.

Plywood boxes were used to form the ends of the specimens and allow access to facilitate cutting the strands. These boxes were constructed from three 6 inch square pieces and two 5in. by 6 in. rectangles to form an open cube. Two of the square parts cut for each assembly had four holes drilled utilizing a jig assuring the final assembly would accommodate the prestressing strands and provide the specified cover for the spirals. These parts were assembled with glue in a clamping device that assured squareness of each box form.

Box form assembly

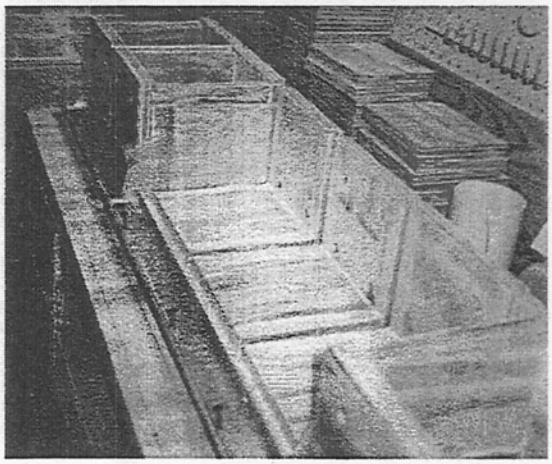

Form clamping device.

Figure 4.1. Fabrication of Plywood Boxes.

Three sides of the plywood inserts used to form the simulated damage were also glued in a clamping device. Waxed paper was used to prevent the formed boxes from sticking to the clamping jig. Finishing nails were driven to improve the durability of these three-sided forms during handling. The fourth side of the plywood insert could only be placed after the concrete was consolidated and finished in the simulated damage region. A few small holes drilled in this top form would have minimized the surface blemishes created by entrapped air.

The fabrication of the specimens was carried out in accordance with standard prestressing practice. The double-T bed was wire brushed to remove any scale and rust

deposits. A string line was set to insure that the form, six by six by 5/8 inch angle was aligned. This angle was tack welded to the double-T bed at appropriate intervals. Form oil was placed on this angle and the other metal pieces used as forms. The plywood boxes were not oiled to prevent contamination of the strands.

Each of the wooden forms was positioned in pairs along the length of the bed. Similarly, the spirals were located along the bed with a precaution not to contaminate them with the form oil. The four prestressing strands were individually threaded through each of the end forms and through each spiral along the bed. The strands were stressed slightly to remove the slack. A flat plate measuring six inches by one quarter inch was stood on edge forming the third side of the pile providing a common form for the adjacent prestressing lines. The next four strands were threaded like the previous four strands. Finally, a second line of angles was secured with welds completing the form work.

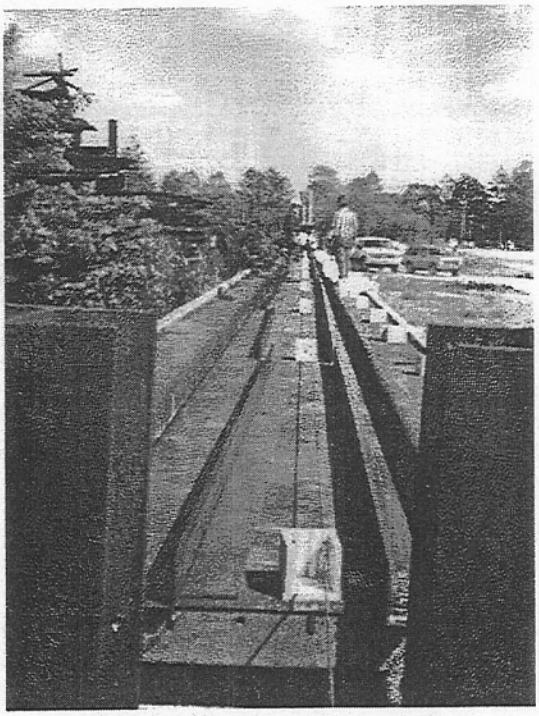

Setting the First Steel Angle

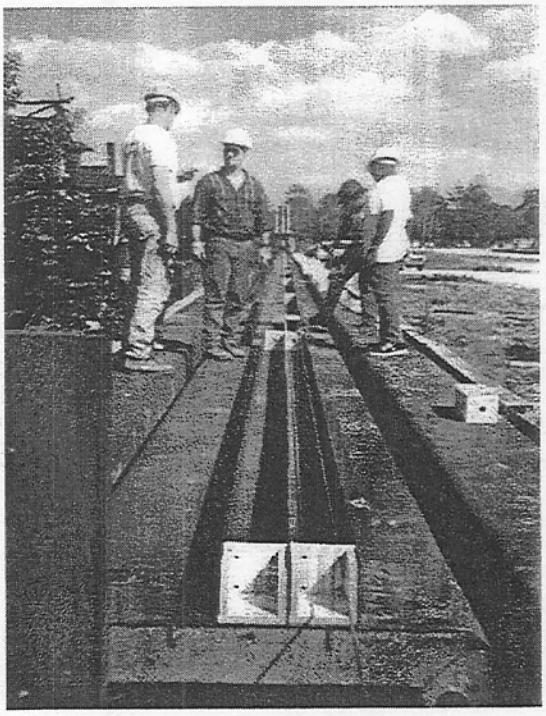

Aligning the Third Form

Figure 4.2. Forming the Specimens.

Care was taken in the layout of the controls and the damage sections. Since the test matrix required pairs of specimens to form each set of tests, a specimen from each line was desired. Specimens from the same bed position made up the test pair whenever practical. The numerical sequence began at the live end. The position of the controls was dictated by a practical forming concern. The flat plate, used as a common form between the two lines, relied on the support of a wooden form to align two plate ends. Therefore, the controls were situated along the bed where the flat plate was continuous.

Welding the Steel Forms

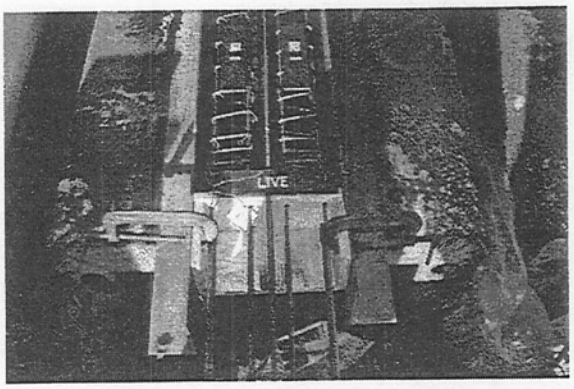

View at Live Stressing End

Figure 4.3. Securing the Specimen Forms

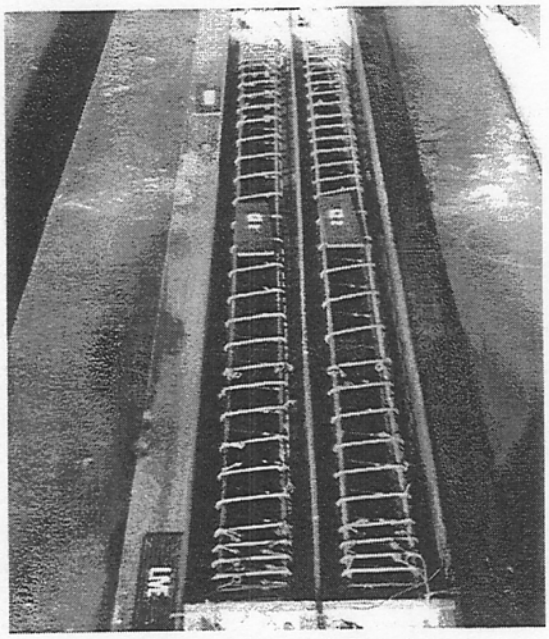

Undamaged Control Specimens

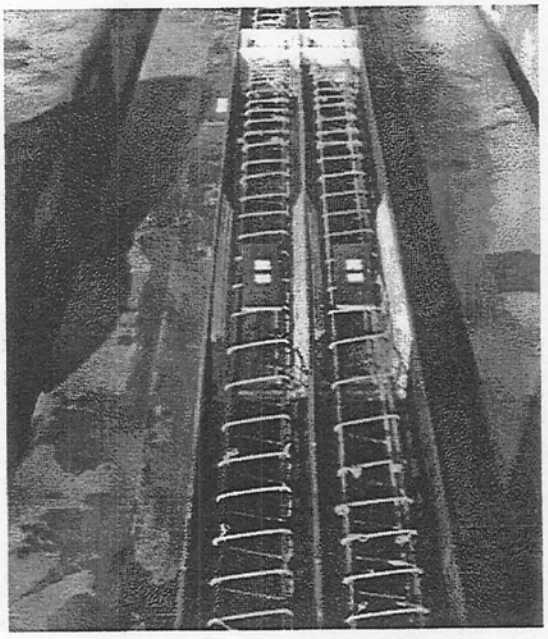

Formed Damaged Specimens

Figures 4.4. View of the Two Specimen Types.

The strands were stressed to the target level of 11.5 kips and were monitored with load cells located at both ends of the prestressing bed. After the stressing operation, the forms were repositioned to the proper location. Clamps were installed to hold the plywood box spacers in place. The spirals were then stretched and tied to the stressed prestressing strands with tie wire.

4.4 Concrete Placement

Each specimen required approximately two cubic feet of Class V concrete. The volume of concrete required to cast all the fifty specimen piles was approximately four cubic yards. An approved mix designed was used. The concrete was batched at Florida Rock's ready mix plant located only a mile from the prestressing yard. The truck was dispatched at 10:30 am. The concrete pour began at 11:15 and lasted one hour and 15 minutes. Throughout the pour cylinders were being prepared following ASTM guidelines. A total of thirty 6 in. concrete cylinders was cast.

The concrete was placed into the forms directly from the ready mix truck and by using hand shovels. Immediately following placement, the fresh concrete was consolidated with a vibrator. The forms were again filled to the appropriate level and the top surface was struck off. Where there were formed damaged inserts along the bed approximately 3/4" of material was removed and the form lid was tamped into place and secured with nails. After some time had elapsed, the top surface was finished with hand floats. A curing compound was applied to the exposed surface.

4.4 Initial Prestress

Two different kinds of measurements were made to estimate the initial prestress in the test specimens. These were (1) load cells (2) strain measurements in concrete using both strain gages and vibrating wire gages. However, because of the inclement weather, the strain gages did not fully bond to the concrete and results were inconclusive.

Load cells were used to monitor the force in each prestressing strand. A total of sixteen loads cells - eight each at the live (pulling) and dead ends - were used. The load cells were hooked to a computerized data acquisition system that allowed both the jacking force, P_j and the initial prestress, P_i to be obtained directly. The results from the load cell readings are summarized in Table 4.1. The initial prestress values are higher than the jacking force because of a drop in temperature at the time of release.

Table 4.1 Average Initial Prestress in Each Strand in Test Specimens.

Bed	f'c (psi)	Load Cell (lb)	
		P_j	P_i
#1	4,100	10,092	11,146
#2		9,873	10,704

Concrete Placement

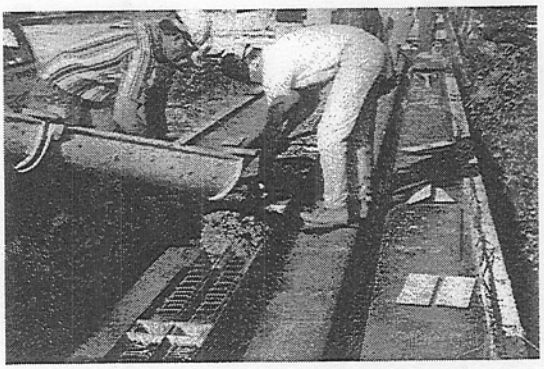

Consolidation of Concrete

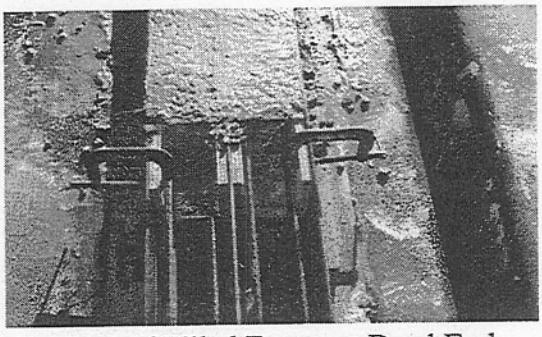

View of Filled Forms at Dead End

Floating the Specimens Surface

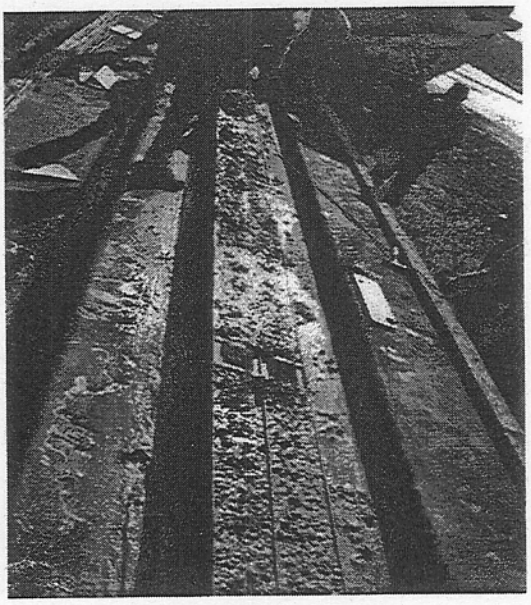

View of Filled Forms

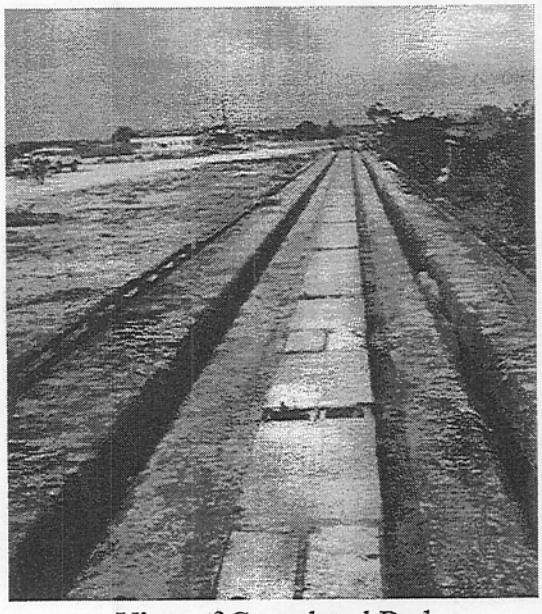

View of Completed Bed

Figure 4.4. Placement of Concrete.

5. STRUCTURAL/NON STRUCTURAL PILE REPAIRS

5.1 Introduction

Two types of repairs - structural (Type V) and non-structural (Type II) were carried out in Phase I. This chapter provides an overview of the repair procedures used. Background information on the FDOT specifications for these repairs and variations used in modeling are summarized in Section 5.2. As the piles are repaired under sustained superstructure dead load stresses, it was necessary to model this condition. Technical details relating to the dead load simulator (Section 2.5) appear in Section 5.3. Surface preparation for the repairs is presented in Section 5.4 and general procedures followed for conducting the repairs are discussed in Section 5.5. In addition, procedures unique to structural jacket repairs are covered in Section 5.6; those for non-structural jacket repairs are described in Section 5.7.

5.2 Modeling FDOT Repairs

The repair most commonly used by FDOT is the non-structural patch repair using either epoxy (Type I) or grout (Type II). In this study, only Type II repair using grout was tested. Section 457 of the FDOT Standard Specifications for Road and Bridge Construction Special Provisions covers requirements [5.1] for the repair materials. Details of the mix design complying with these specifications may be found in Section 3.7 of this report.

The less common structural repairs require reinforcing steel to be additionally provided. The specifications [5.1] stipulate that these are to be epoxy coated and used in conjunction with Class III concrete. Because of the short interval between repair and testing, epoxy coated bars were not used.

Fig. 5.1 shows standard FDOT repair details for prototype piles. It may be seen that 12 # 3 bars ($A_s = 1.32$ in^2) provide longitudinal reinforcement; #3 bars are also used as ties. The ties are spaced at 12 in. regardless of the pile dimensions. In the model, the area of steel should be 1/9th that of the prototype, i.e. 0.147 in^2. If four bars are used, this translates to bars having a diameter of 0.21 in.

Deformed wires could be used to provide this area. However, they were not recommended because of inherent difficulties in annealing them to reproduce the properties of mild steel. Construction Technologies Laboratories, IL previously annealed deformed

wires but stopped doing so because it did not duplicate elongation. Consequently, larger diameter #2 bars (dia. 0.25 in.) were used. Their properties matched those of the #3 bars.

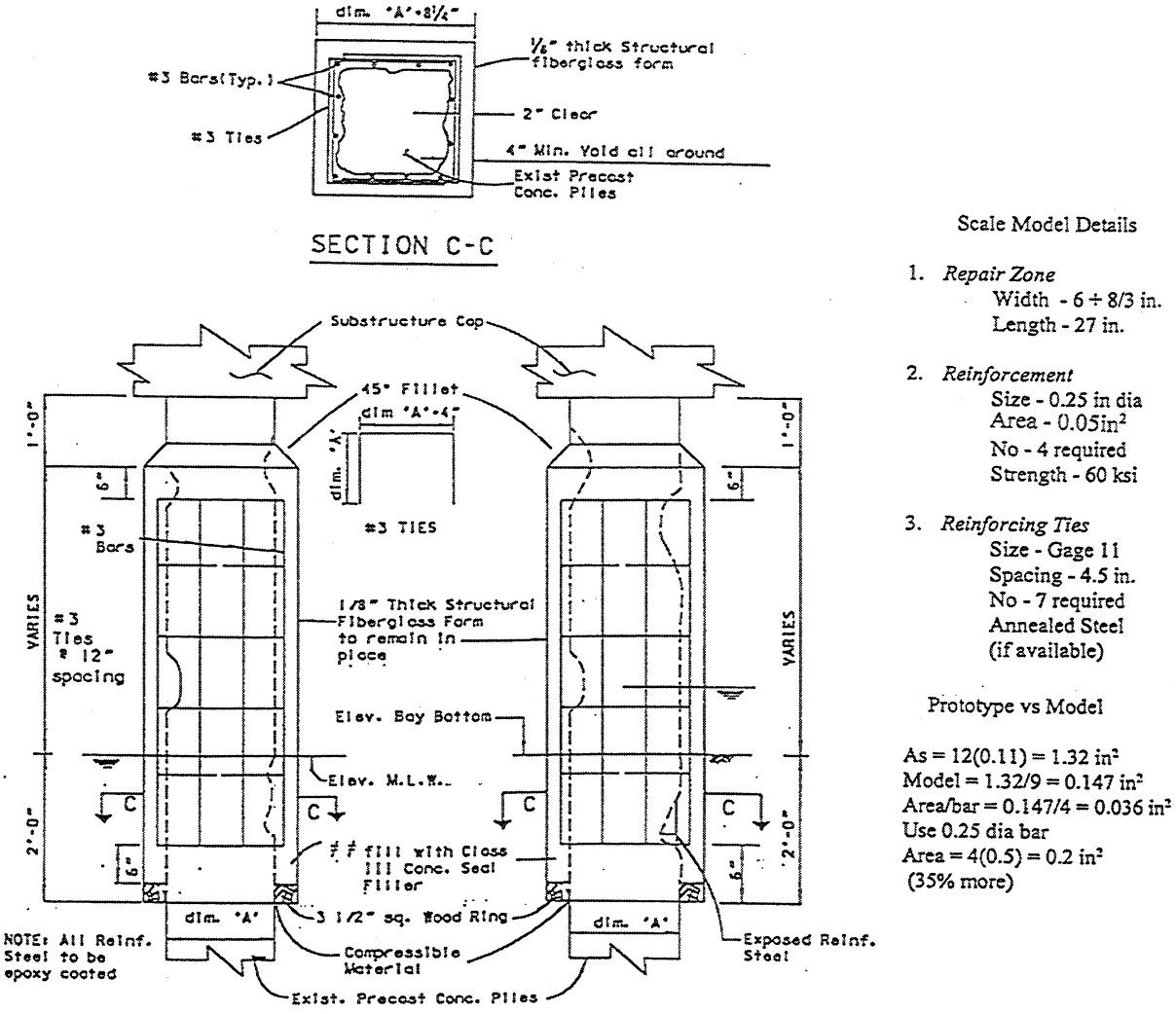

Figure 5.1 FDOT Type V Repair and Model Details.

The use of larger diameter deformed bars leads to a 36% greater steel area than dictated by modeling principles. However, as the object of the study is to determine whether repairs result in strength gain, this is not a critical consideration. Details of the reinforcement and ties used for repairing the model are shown in Fig. 5.2. It may be seen that #2 bars are also used as ties and are spaced at 4.5 in. - the same spacing as in the model piles. The overall repair length is 30 in. to accommodate the seven ties.

The stay-in-place fiberglass jacket used by FDOT was also not used in the models. These jackets are constructed with at least one seam which runs the entire length of the repair. Furthermore, it was found [5.2] that square sections are not as effective as circular sections in confining concrete core. Thus, its omission is not expected to be critical.

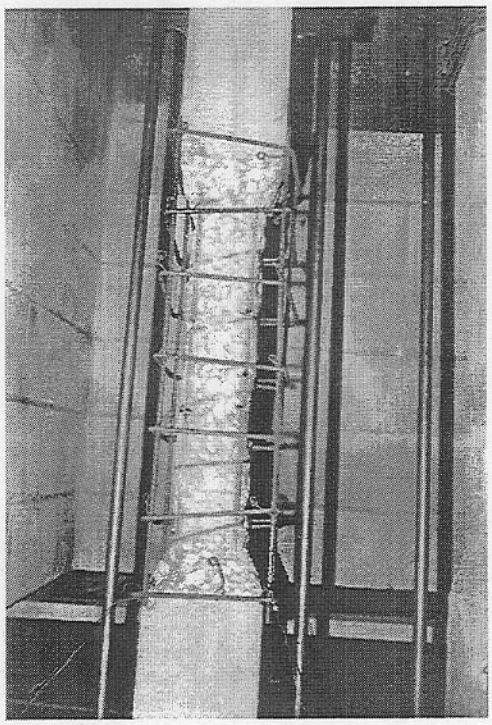

Figure 5.2 Type V Repair in Model.

5.3 Load Simulator

Field repairs are carried out on loaded bridges where the piles support both service dead loads and vehicular loads. Consequently, test specimens need to be subjected to similar sustained stress levels prior to repair. Moreover, this load cannot be released after the repair has been completed and ultimate load tests are to be carried out, i.e. the assembly used to apply the sustained load should fit inside the reaction frame.

Design calculations [5.3-5.4] indicated that the sustained stress levels in 18 in prototype piles range between 300-600 psi. As higher levels are likely to be more detrimental, stress levels in the 500-550 psi range were used in the testing. This translates to a load of 20 kips in the model.

As discussed earlier (see Section 2.5), a simple assembly comprising two high strength threaded rods connected to four angle iron brackets was used to maintain the required compressive load. Prior to the mass production of the sixteen sets needed for the

study, the assembly was tested to verify its performance. A single assembly was secured on a test pile. Two load cells were installed to measure the reaction of the rod in response to various levels of applied torque. The nut on the rod was tightened using a standard mechanical torque wrench. The load simulator test met the performance criteria of maintaining the required load for several days (see Fig. 5.3).

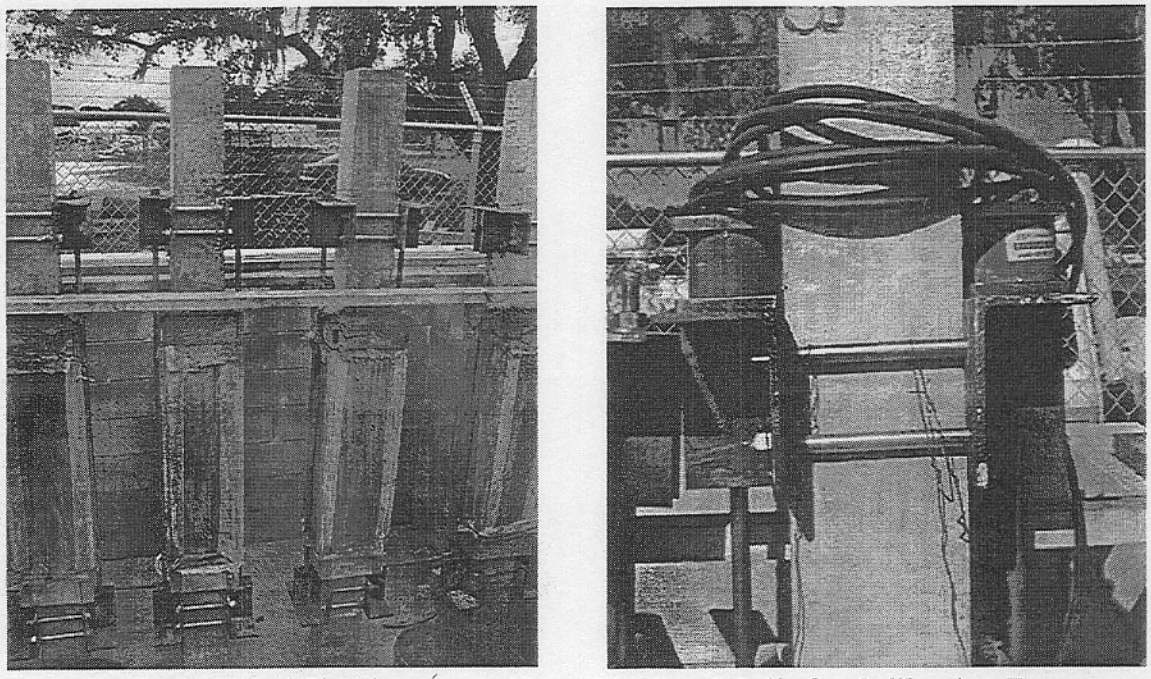

Installed Load Simulator Load Cells for Calibrating Torque

Figure 5.3 View of Load Simulator.

This test proved invaluable. It became apparent that the costlier 5/8 in. high strength threaded rod in the original design could be replaced by regular 3/4 in. rods whose ends could be threaded in the machine shop. This single change, significantly lowered costs. More importantly, the test provided assurance that a given torque would produce a given load under similar conditions. This eliminated the need to instrument and monitor each of these rods.

Following fabrication of sixteen sets of the pre-load simulator, the load in the tension rods was calibrated against load cell readings. A pair of angles forming a clamp was attached to a pile end with four 5/8 inch grade eight bolts. A torque of 220 foot-pounds prevented slippage of these clamps. Both of the 3/4 in. rods with threads on each end were dressed with an anti seizing compound and fitted with washers and nuts. A pair of load cells indicated that target level of 20 kips (10 kips in each rod) required 98 ft-lbs applied to each nut. The same torque was used in all the piles repaired.

This torque was set at installation of the load simulator. It was re-checked immediately proceeding the installation of the pile jacket repair. Furthermore, it was checked prior to testing of each of the sixteen repaired piles. With minor exceptions, the nuts remained stationary during both re-checks. The removal of this device was accomplished in the testing frame under a load and is detailed in subsequent chapters.

5.4 Surface Preparation

Two distinct bonding surfaces were investigated in Phase I (see Fig. 5.4). Although all sixteen repaired specimens had formed damage at the time of casting, a rough interface was provided on half (eight) of the repairs. This surface was created using an electric chipping hammer to remove a layer of concrete. The target depth of this chipped surface was to the level of the confining spirals. Each of the four pile faces was prepared in this manner.

Approximately ½ inch of the concrete cover was removed to reveal the confining spirals. The hammer chisel was directed along the spiral removing the concrete cover and exposing the spiral. After exposing all of the spirals in a repair zone the chipping hammer was used to remove the concrete to this level. Also, on each end of the repair zone approximately ½ inch of cover was removed in the transition zone. Following this procedure the piles were water blasted to remove fine dust particles.

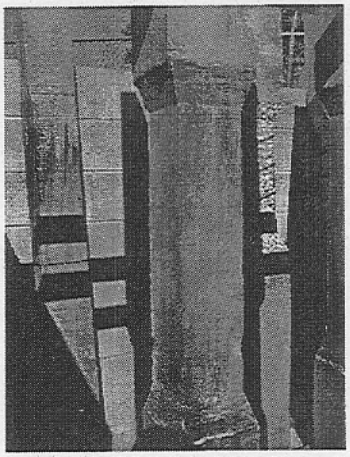

Specimen with Formed Damage

Specimen with Chipped Damage

Figure 5.4 Surface Types Investigated in Phase I.

The remaining eight specimens were cleaned with water blasting to remove any surface latency and dust. Three of these formed surfaces were quite uniform in appearance. There were, however, irregularities caused by air pockets trapped beneath the top form at the time of casting. This surface usually faced the "back" during testing for aesthetic reasons. A number of measurements were recorded on each of the damaged specimens.

5.5 Repair Procedures

The form work used for the repairs was filled with water prior to concreting to saturate the repaired surface. The forms were fabricated from 3/4 inch plywood. Each plywood piece was lined with a six-mil plastic covering. A router was used to provide a groove on the opposite faces of four part form to house the rods from the pre-load simulator. This groove centered the jacket form and also maintained its position. Each of the form parts were sealed with caulking before assembly. The bottom of the form was sealed with an expandable foam strip. A small piece copper tubing was inserted through a hole in the foam strip to accommodate filling and draining of the forms.

Each repair area was saturated for at least two days prior to the installation of the repair system to prevent localized dehydration at the interface. A toilet float valve located in a bucket provided constant head pressure through tubing connected at the base of each pile jacket forms (see Fig. 5.5). These forms were drained just prior to placement of the pile jacket filler material. The repaired piles were cured at least 28 days with the plastic lined plywood forms in place.

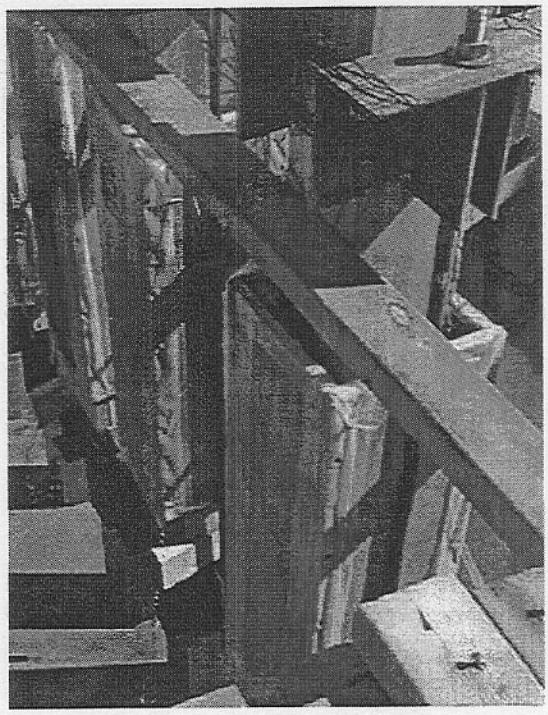

Pile Jacket Formwork

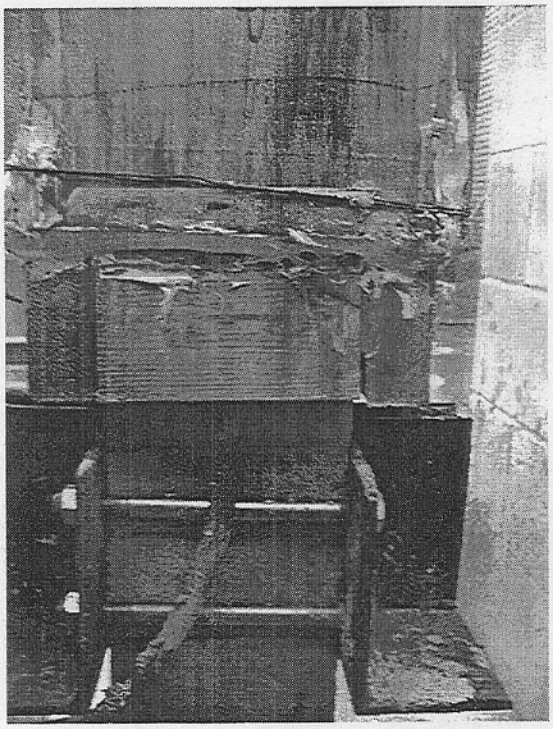

Water Tube for Filling and Draining

Figure 5.5 Details of Repair Formwork

The two different types of repairs - Type V and Type II - were carried out in this phase. Items unique to each of these types are covered in the next two sections. The following is the procedure common to both types of repairs:

1. Surfaces prepared as outlined in a preceding section.

2. Application of appropriate load using the pre-load simulators fitted for each repaired pile.

3. Maintenance of full water level inside the forms for a minimum of two days.

4. The orientation of the piles during repair was nearly vertical.

5. Curing occurred with the forms intact for a minimum of 28 days.

6. The repaired specimens with load simulators were instrumented and loaded.

7. Load simulator removal followed an equivalent load impressed at testing.

5.6 Structural Repair

FDOT's Type V or structural repairs are used when severe damage to the strands is apparent. To model this type of repair, the strands in the pile specimens were cut. This operation occurred after the damaged piles' surfaces were prepared and each was fitted and loaded with the load simulation device. Each of the four strands were cut in two places approximately three inches offset from the center of the repair area (see Fig. 5.6). The surface was then cleaned to remove fine dust particles.

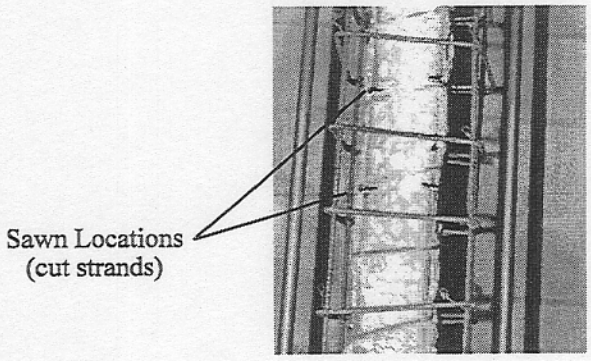

Figure 5.6 Slits in Concrete Show Strand Cut Locations.

The reinforcing steel cage was then installed around the damaged area (see Fig. 5.6). The form was fitted around the pile and sealed. The forms were filled with water and the water levels were maintained for three days. Prior to the placement of the Class III concrete filler the forms were drained. Space limitations prevented utilizing the vibrator, however, consolidation was accomplished by tapping the exterior of the form with hammers. Eighteen 6 inch cylinders were prepared following ASTM standards.

Ewell Ready Mix provided an approved mix design for this application. The concrete was placed utilizing a concrete pump truck. Immediately preceding any concrete placement, it was determined that the mix had become stiff therefore required additional water. Water was added to the drum which was then rotated 75 additional turns. With a consistency that could be pumped, the pump lines were cleared and the concrete was placed. There was moderate difficulty in placing the concrete as the top of the form was somewhat congested with the reinforcing steel. Detailed material information is presented in Chapter 3.

5.7 Non-Structural Repair

Type II or nonstructural repairs specify Portland grout filler. These repairs are specified when a distressed pile has retained a significant amount of its original prestressing strand. This repair primarily provides cover to the existing, often exposed strands. There is no reinforcing steel used in conjunction with this type of repair (see Fig. 5.7)

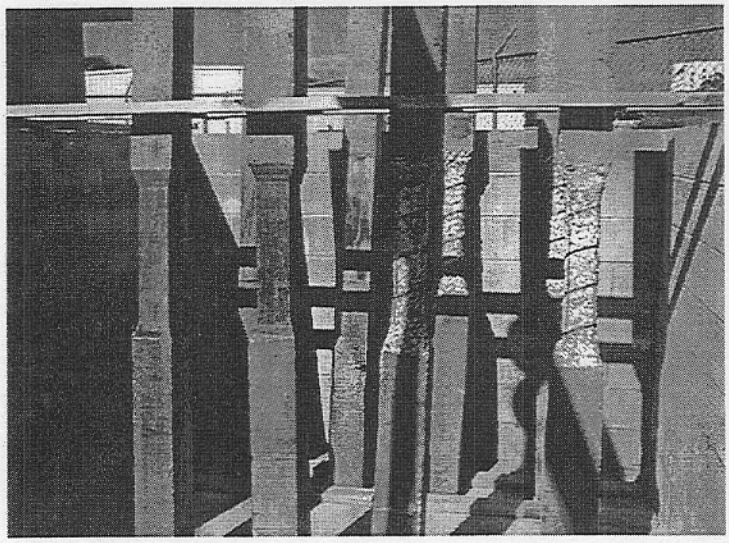

Figure 5.7 Non Structural Repair.

As in the preceding section the surfaces were prepared and the forms were installed. These forms were filled with water and maintained for seven days. Ewell Ready Mix

provided a mix design approved for this application. The nonstructural repairs were conducted on December 7, 1998 on eight specimens. A number of cylinders were prepared following ASTM specifications. Also three sets of molds to measure shrinkage were prepared.

The mix arrived in a high slump condition. The material was nearly self leveling. The driver was instructed two turn the mix 50 additional turns to assure homogeneous mix. Despite these efforts the mix was quite fluid. Nevertheless, it was placed using wheelbarrows and buckets. The placement and consolidation of this mix were performed without difficulty.

References

5.1 Florida Department of Transportation (1996). Standard Specifications for Road and Bridge Construction, Tallahassee, FL

5.2 Mirmiran, A. (1997). FRP-Concrete Composite Column and Pile Jacket Splicing. Final Report submitted to Florida Department of Transportation, August.

5.3 Compton, D. (1998). Service Pile Design Loads for SR 207 over Branch Creek, HDR, Tampa, FL, Sept. 21, 3 pp.

5.4 Menke, T. (1998). Service Pile Design Loads for Western Beltway Ramp F over SR 50, URS Greiner, Sept. 9, 5 pp.

6. AXIAL TEST RESULTS

6.1 Introduction

This chapter presents the results from the concentric load tests. Eight of the specimens tested were repaired piles. The remainder were controls. Results from corresponding eccentric load tests are contained in Chapter 7. Two types of repairs were investigated. Structural (Type V) and nonstructural (Type II) repairs were carried out on two different surface types. The ultimate capacities of these jacketed piles are compared with identically tested control specimens.

A description of the test set-up is presented in Section 6.2. Details of specimens tested and instrumentation appears in Section 6.3 while the results from the seven series of tests are described in Section 6.4 and constitutes the largest section of the chapter. The principal conclusions are summarized in Section 6.5.

6.2 Test Set-Up

The experimentation called for the columns to be pinned at the supports. This meant that the column had to be free to rotate in *any* direction at its ends. Although roller supports are sometimes used, they only permit rotation in one direction. Consequently, they were not used in the axial tests.

Pinned support was provided by a two-part 8 in. diameter hemispherical steel member that was attached to the load cell at the bottom and to the piston ram of a 300-ton hydraulic cylinder at the top. The outer surfaces of this member were flat but the curved interface permitted rotation in all directions. Grease was generously applied to the interface to reduce friction and to promote relative rotation. Two 18 in. x 18 in. square steel plates were bolted to the exposed flat surfaces and served as supports for the column ends. This arrangement allowed the ends of the column to rotate freely without permitting any translation (Fig. 6.1).

To prevent premature end failure, the column ends were placed on lead plates to facilitate uniform distribution of the applied loads. Additionally, the ends were confined over a 6 in. length by ½ in. thick steel plates. Bolts were used to secure the plates to the columns. The entire confinement assembly was adjusted on the basis of strain readings with the column under nominal loads to position it exactly in the center of the reaction frame.

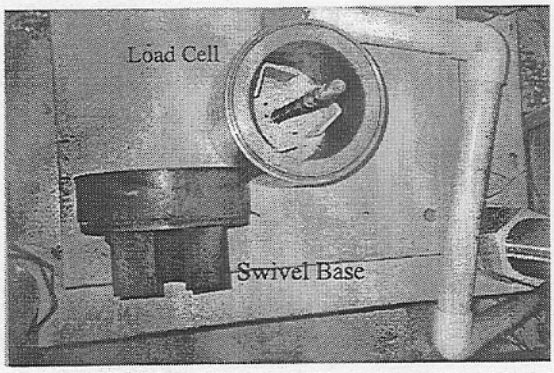

Swivel/Load Cell Assembly

Applying Grease to Swivel Base

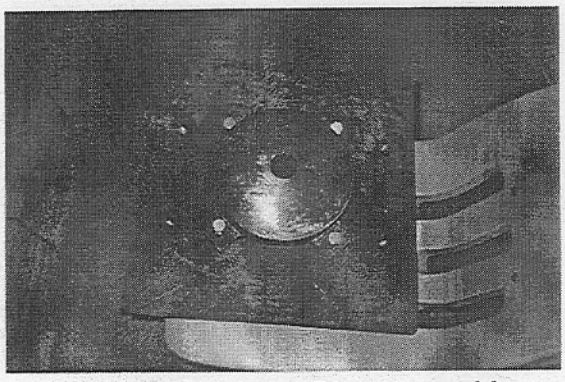

Swivel Top/Plate Assembly

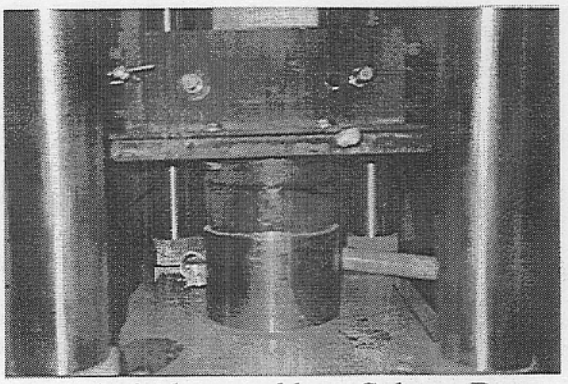

Swivel Assembly at Column Base

Greased Swivel Top

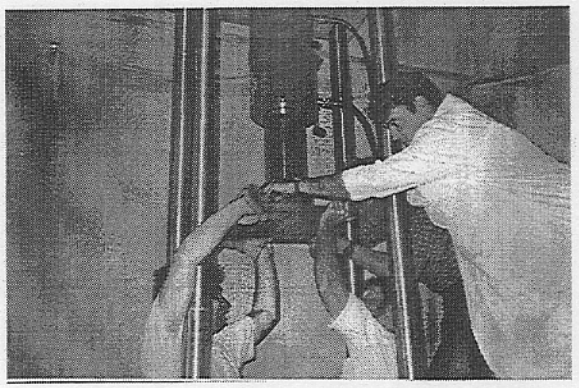

Attaching Swivel Assembly at Top

Fig. 6.1 End Conditions in Axial Testing.

6.3. Test Program

Although only eight repaired specimens were tested under concentric loads, the need to assess comparative strength gains necessitated additional tests on controls. Three types of controls - undamaged, formed damage and formed damage with strands cut - were tested. The original intent was to test three undamaged specimens (because of the importance as a baseline measurement) and two controls each for the other two types. However, as one of the undamaged controls failed at the ends an additional specimen had to be tested.

Details of the sixteen specimens tested in seven series are summarized in Table 6.1. The specimen designation is as explained previously in Section 2.6 with 'C' identifying controls, 'SF and SC' identifying Type V repairs on formed/chipped surfaces, 'NF and NC' identifying Type II repairs on the same surfaces and 'D' designating formed damage.

Table 6.1 Specimen Details.

Type of Test Specimen	Number	Specimen ID
Undamaged Controls	4	C1-5,6,7 C2-6
Structural Repair Formed Surface	2	SF-1 SF-2
Structural Repair Chipped Surface	2	SC-1 SC-2
Non-Structural Repair Formed Surface	2	NF-1 NF-2
Non-Structural Repair Chipped Surface	2	NC-1 NC-2
Damaged Controls	2	D1-10 D2-10
Damaged Controls with Strands Cut	2	D2-9 D2-4
Totals	16	

6.3.1 Instrumentation

In order to center the specimens accurately in the reaction frame, a total of twelve strain gages - one each on the four surfaces of the pile at three different locations - were bonded to the concrete surface. As the pre-load simulator (see Fig. 2.3) extended beyond the quarter point in the repaired specimens, this location could not be used. Instead, gages were affixed one foot from each end and at mid-span in all the specimens.

In addition to strain gages, LVDTS were also used to monitor axial shortening and any movement in the horizontal direction. A total of eight LVDTs was used - two for

measuring axial shortening and six others to monitor lateral movement in two directions. These were positioned at the same three locations as the strain gages.

6.3.2 Specimen Preparation

Before specimens were tested, the cross-sectional dimensions were carefully measured at the strain gage locations. For damaged specimens additional measurements were made at the ends and at the midpoint of the damaged zone. Where strands were cut, the section became irregular and additional measurements were made to allow its section properties to be determined.

The calculated cross-sectional areas correspond to measurements taken at the mid-point are summarized in Table 6.2. Inspection of Table 6.2 shows that the core cross-section is the largest for the undamaged section. Of the specimens that were repaired, the chipped surfaces have considerably smaller cores compared to the formed surfaces. The area of repair shown in the table was calculated by subtracting out the core area from the gross area.

Table 6.2. Cross-Sectional Area of Concentrically Loaded Specimens.

Item #	Test Type	Specimen	Gross Area in^2	Core in^2	Area of Repair in^2
1	Undamaged Control	C2-5	35.2	Same	
2	Undamaged Control	C1-6	38.7		
3	Undamaged Control	C1-7	37.9		
4	Undamaged Control	C2-6	36.8		
5	SF-1	D1-11	75.5	21.4	54.1
6	SF-2	D2-11	75.7	21.7	54.1
7	SC-1	D1-16	75.2	13.1	62.1
8	SC-2	D2-16	74.8	13.4	61.4
9	NF-1	D1-12	75.5	20.7	54.8
10	NF-2	D2-12	75.5	21.7	53.8
11	NC-1	D1-14	74.9	12.3	62.6
12	NC-2	D2-14	74.4	13.0	61.4
13	Damaged Control	D2-10	20.1	Same	
14	Damaged Control	D1-10	21.4		
15	D. Control Cut Strands	D2-9	21.1	15.3	
16	D. Control Cut Strands	D2-4	20.4	14.7	

The operation of cutting the strands was carried out while the specimen was in the reaction frame under a nominal load of 10 kips. The applied compressive load helped balance tensile stresses introduced in the cross-section as a result of release of the prestressing force. An electrical hand saw with an abrasive masonry blade was used to cut through each of the strands at two locations three inch above and below the center. The observation of the sparks indicated when the strands had been completely severed.

On the repaired specimens, the pre-load simulator was removed under a load of about 20 kips. This was done only after the specimen was centered as verified by strain measurements recorded from the eight gages located 1 foot from the ends and not affected by the load simulator. Each of the two rods was removed carefully followed by the removal of the four brackets. The data acquisition was then balanced with the applied load in place. Finally, the specimens were loaded until they failed.

6.3.3 Test Procedure

All strain gage, LVDT channels and the 500 kip load cell from GEOKON were hooked up to a MEGADAC 3100 data acquisition system. The load was applied using a 300 ton, 13 in stroke hydraulic jack from Force Resources, Inc. that was connected to an electrically operated hydraulic pump.

The procedure was different for the repaired specimens than for the controls in that the eight repaired piles were fitted with a pre-load simulator. Where the simulators were used, a twenty-kip load was applied prior to the removal of the device. Otherwise, a ten-kip load was used to ensure concentric loading. The strain readings at each end were compared and if they varied by more than 10%, the position of the column inside the frame was adjusted through tightening and loosening of the bolts used to confine the column ends (see Fig. 6.1). When the column was accurately centered, loads were incremented and readings recorded continuously by the data acquisition system.

Because compression failures are explosive with debris ejected a considerable distance away, a protective plywood sheet was used to protect all personnel involved with the testing. Plexiglass glass windows allowed the testing to be monitored from a safe distance.

6.4 Results

This section presents results from the seven series of tests conducted. The load cell readings were found to have a sensitivity constant error that led to an over estimation of the loads. The correct loads were obtained by reducing all the test values by a constant of 0.8524 as in the earlier study [6.1]. These corrected values are reported throughout this text.

A summary of the ultimate load values from all the axial tests appears in Table 6.3. For convenience, the results in this table are also re-plotted in bar form in Fig. 6.2.

Table 6.3 provides information on the individual failure load, the average failure load and the *average* failure load from each of the seven series as a percentage of the *average* of the three undamaged controls that failed in compression.

Table 6.3. Summary of Results of Axially Loaded Specimens.

Test#	Type	Specimen	Failure Load kips	Average kips	% U. Control
1	U. Control	C2-5	246.3		
2	U. Control	C1-6	222.6	239.0	100.0
4	U. Control	C2-6	248.0		
3	U. Control	C1-7	226.0	End Failure	
8	Type V	SF-1	179.9		
5	Type V	SF-2	205.9	192.9	80.7
7	Type V	SC-1	174.4		
6	Type V	SC-2	176.4	175.4	73.4
25	Type II	NF-1	134.3		
30	Type II	NF-2	163.1	148.7	62.2
24	Type II	NC-1	128.5		
31	Type II	NC-2	141.7	135.1	56.5
27	F. Control	D1-10	145.5		
26	F. Control	D2-10	150.0	147.8	61.8
29	Control- SC	D2-4	87.3		
28	Control-SC	D2-9	112.8	100.0	41.8

Inspection of Table 6.3 shows that Type V structural repairs are quite effective regaining over 70% of the original capacity. In contrast, the Type II non-structural repairs were far less effective. In particular, Type II repairs for formed surfaces showed practically no gain in capacity (148.7 vs 147.8 kips). As a result of this, the axial response of non-structural repairs was the focus of the Phase II investigation (see Chapter 9).

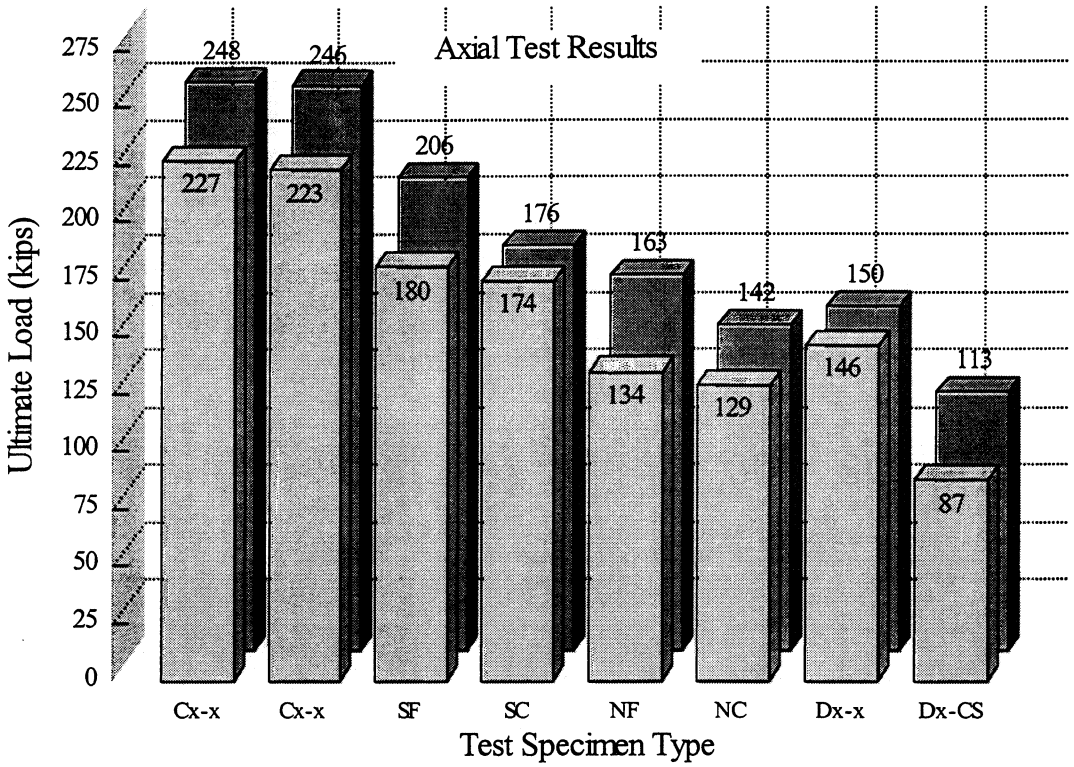

Figure 6.2 Summary of All Phase I Axial Test Capacities.

With the exception of one control C1-7 that failed prematurely at the end, all specimens failed in compression in the middle. As such they were explosive accompanied by a very loud noise. Failure of the structural repairs was, however, not as violent. The added steel helped to confine the core and limited the amount of material that spewed out.

Failure modes from all the tests are shown in Figs. 6.3-6.9. Figs. 6.3-6.5 show the failure modes of the three types of controls that were tested - undamaged controls, damaged controls and damaged controls with the strands cut. All failures occurred in the middle and were accompanied by buckling of the prestressing strands.

Figs. 6.6-6.7 show the failure modes that were observed in case of repairs on formed specimens. In case of non-structural repairs, the segments of the concrete jacket separated from the core (Fig. 6.6). In contrast, in the structural repairs, there was no such separation though there was cracking at the edges of the jacket. The ties holding the structural steel that was added appeared to be intact (see Fig. 6.7).

Figs. 6.8-6.9 show the failure modes for repairs where the interface was chipped (Fig. 5.4). The bond between the repair material and the core was far superior and the jacket did

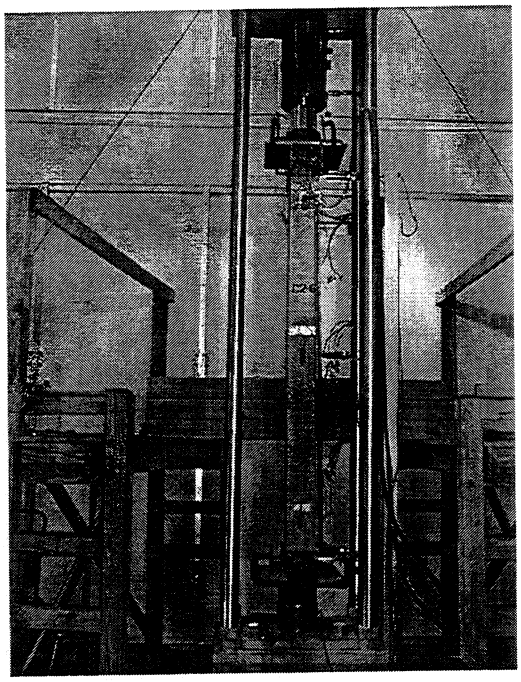

Test Set-Up

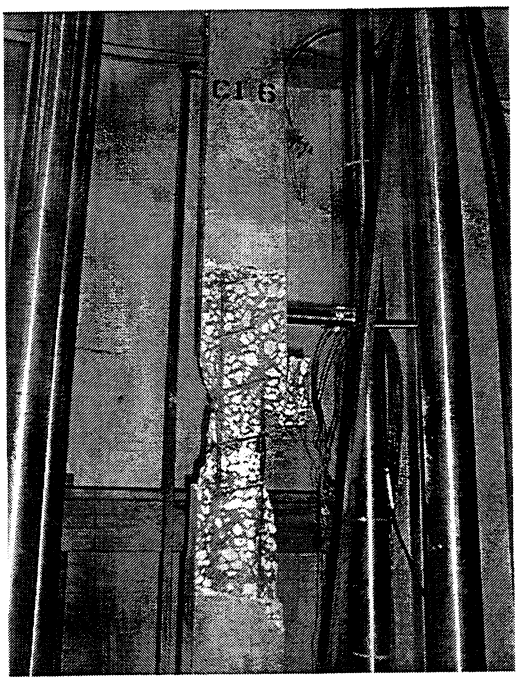

Compression Failure in Middle

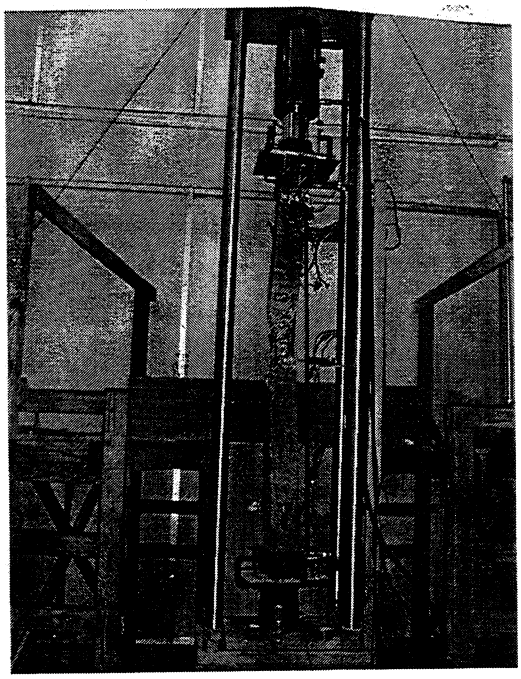

View of Failed Column

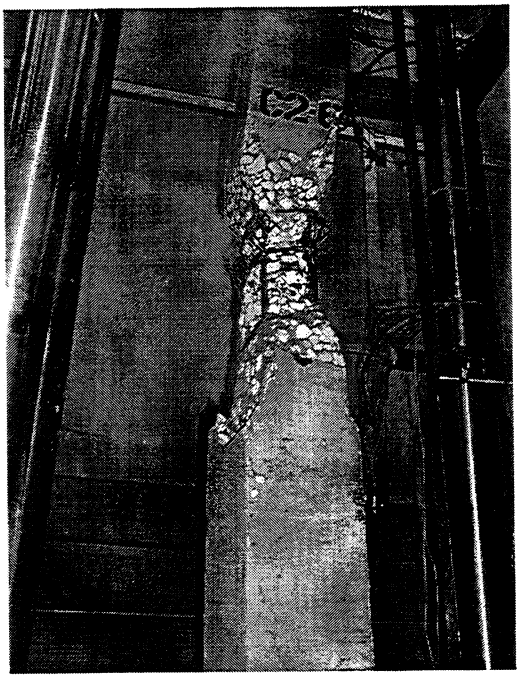

Note Buckling of Failed Strand

Figure 6.3 Undamaged Controls Under Concentric Loads.

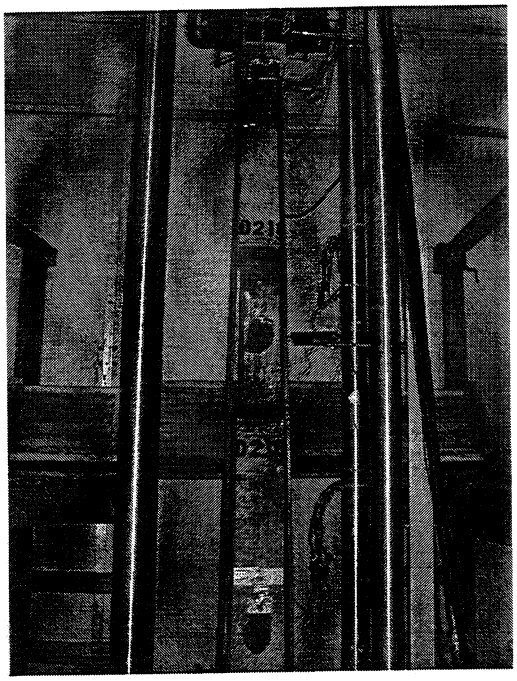

Test Set-Up

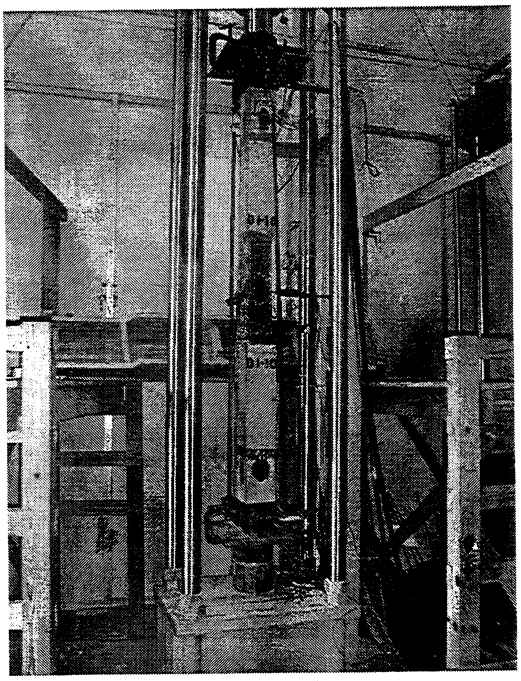

Compression Failure in Middle

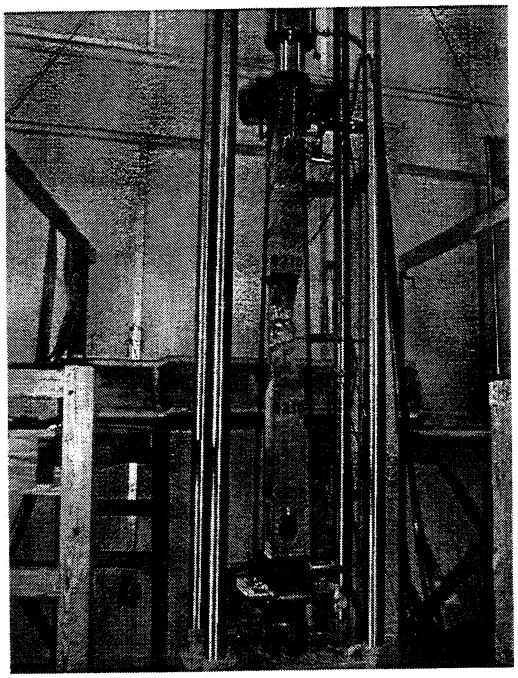

View of Failed Column

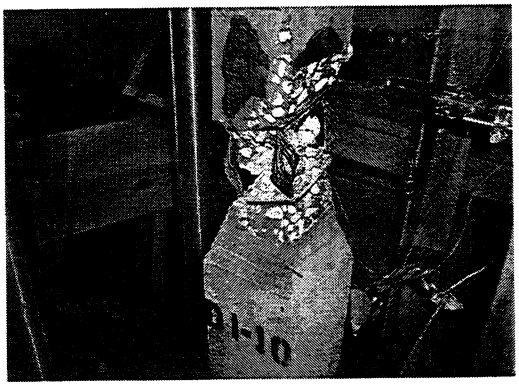

Note Buckling of Failed Strand

Figure 6.4 Damaged Controls Under Concentric Loads.

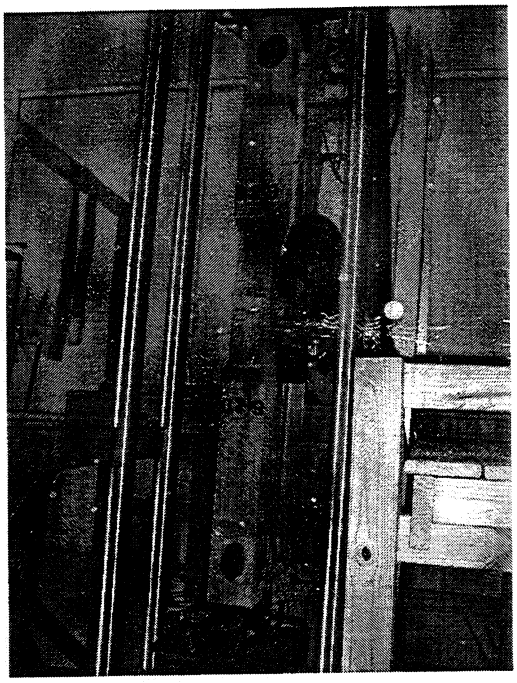

Cutting Strands with a Grinder

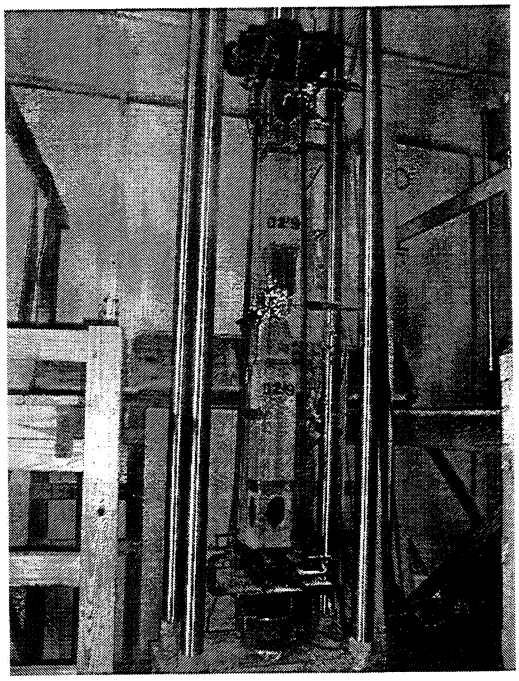

Compression Failure in Middle

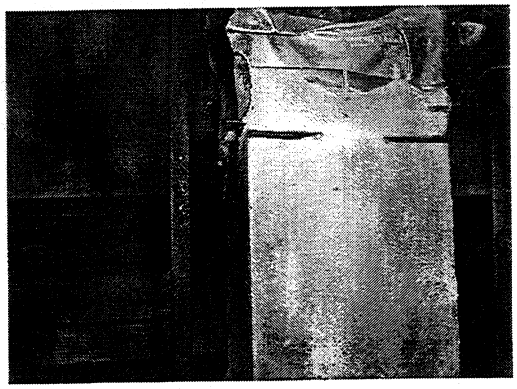

Cut in Pile Core

Note Cut Strands

Figure 6.5 Damaged Controls With Strands Cut Under Concentric Loads.

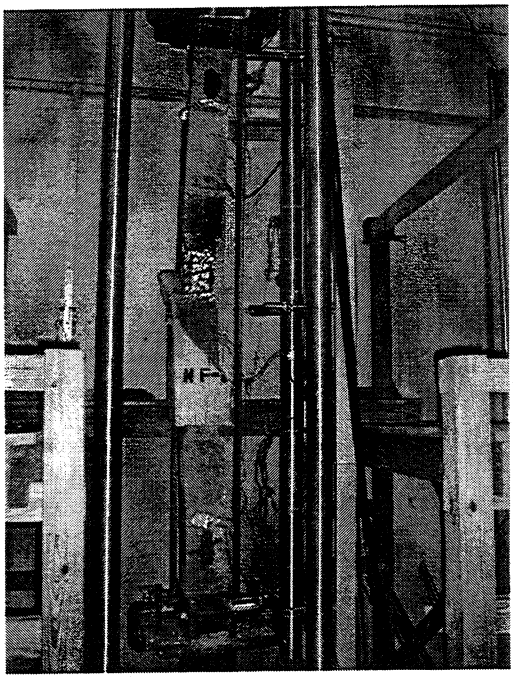

Failed Specimen

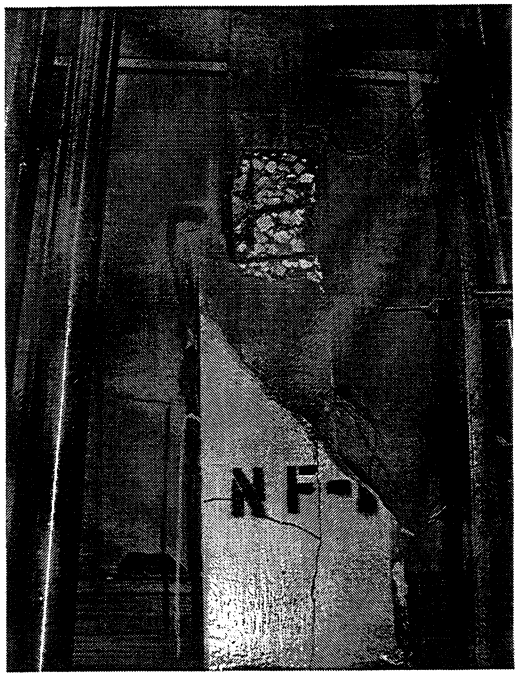

Separation of Jacket

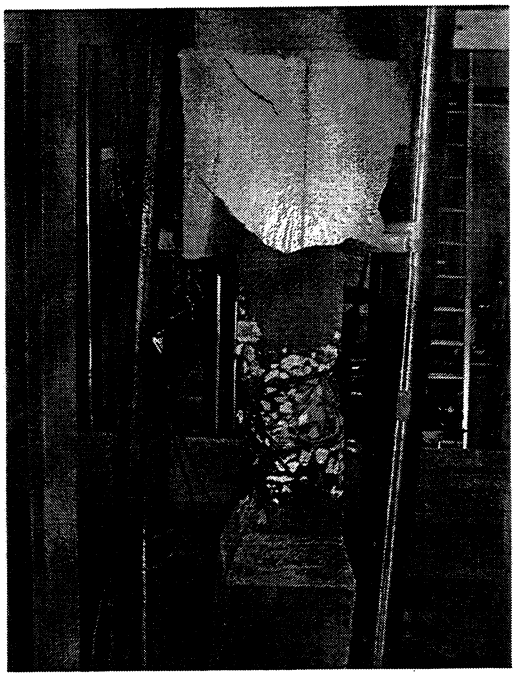

Core Buckled After Debonding

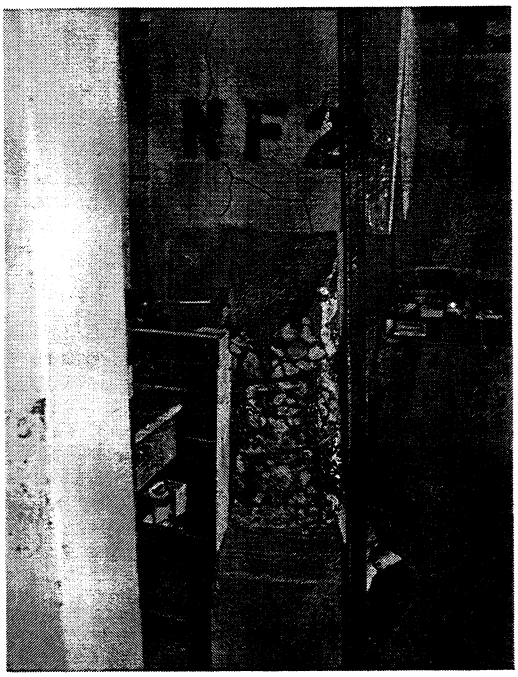

Note Buckling of Failed Strand

Figure 6.6 Failure of Non-Structural Formed Repairs Under Concentric Loads.

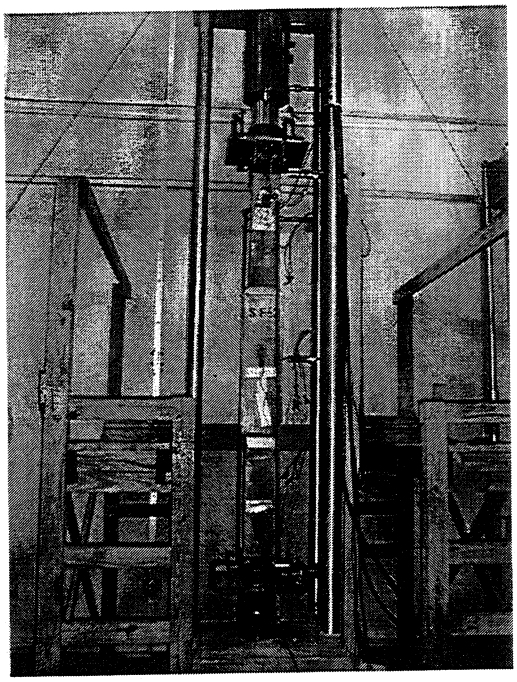

Set Up

Separation of Jacket

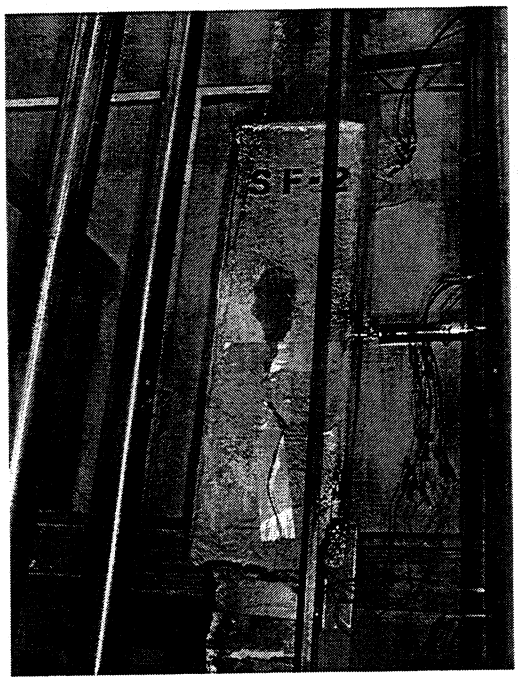

View of Failed Specimen

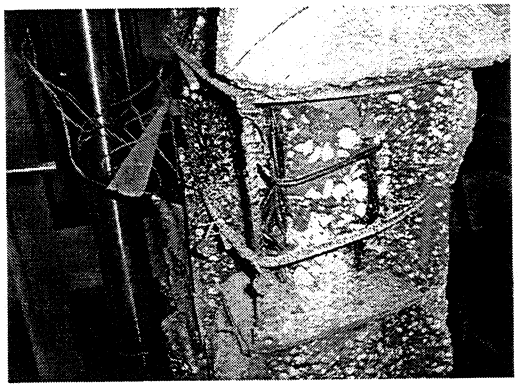

View of Failed Core and Rebar Cage

Figure 6.7 Failure of Structural Formed Repairs Under Concentric Loads.

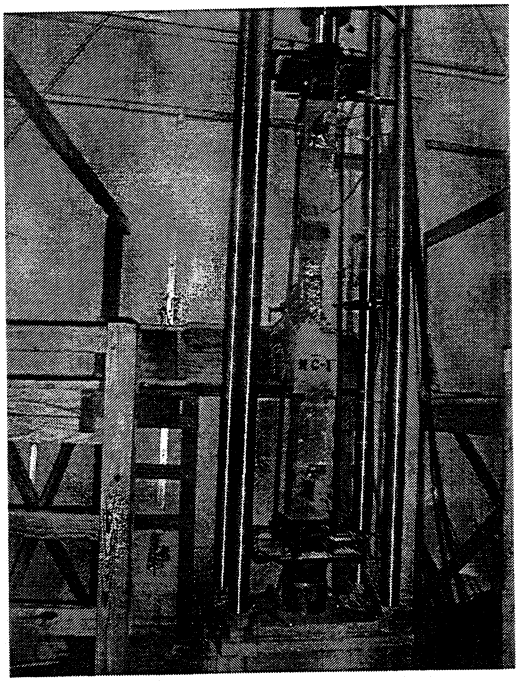

View of Failed Specimen

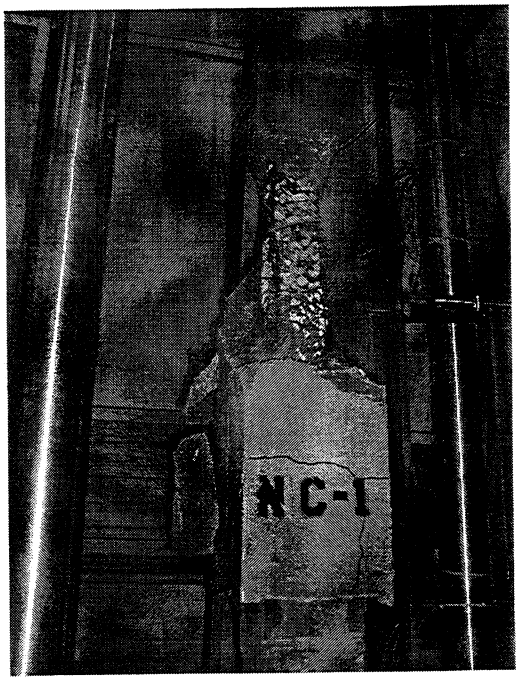

Separation of Jacket

View of Chipped Core

Effect of Explosive Failure

Figure 6.8 Failure of Non-Structural Chipped Repair Under Concentric Loads.

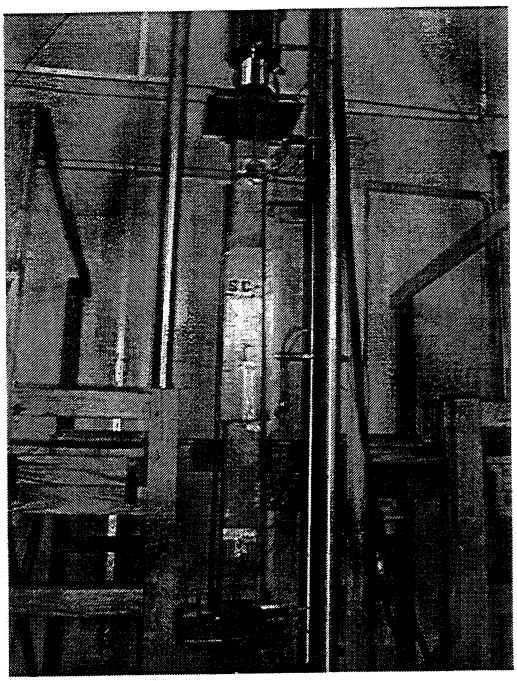

View of Failed Specimen SC-1

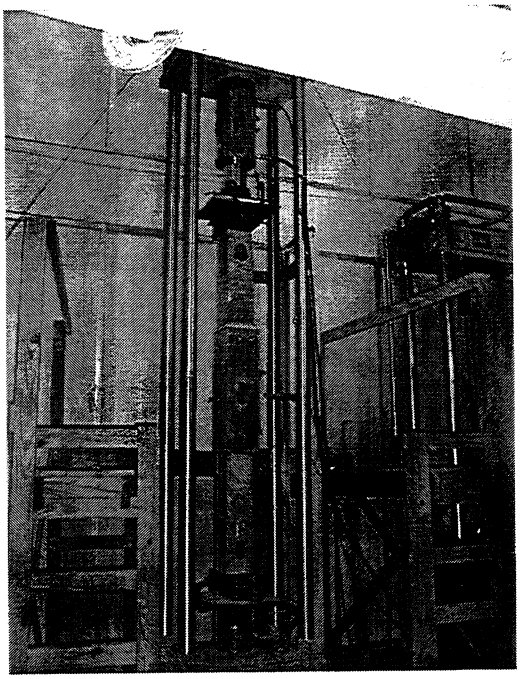

View of Failed Specimen SC-2

Close Up of Jacket

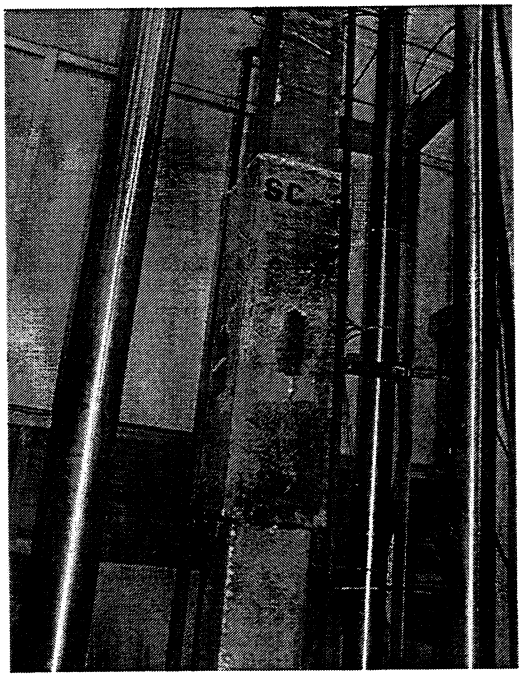

Note Limited External Damage

Figure 6.9 Failure of Structural Chipped Repair Under Concentric Loads.

not simply separate as in the cases of formed surfaces (Fig. 6.8). In the structural repair, there was less damage than its formed counterpart (Fig. 6.9).

In order to gain an increased understanding, further detailed analyses are presented. The results are presented for groups of similar tests. In general, two tests are considered in each group. The results are presented for the three sets of controls followed by the remaining results. Thus, they begin with the three series of controls - undamaged controls, formed damage controls and the controls where the strands were cut. This is followed by results for the four series of nonstructural (Type II) and structural (Type V) repairs for the two different surface preparations - formed and chipped. All plots showing strain variation with load are included in Appendix A to prevent clutter.

6.4.1 Undamaged Controls

Four undamaged controls were tested to failure. The ultimate loads at failure were 248.0, 246.3, 226.8, and 222.6 kips. Discarding the faulty test, the average failure load is 239 kips. The maximum compressive strain in these plots is somewhat lower than the true value since it does not incorporate strain due to the prestress.

Table 6.4 provides a summary of the three undamaged piles tested as controls. Plots showing the strain variation with load for all the controls are shown in Fig. A.1-A.3 in Appendix A.

Inspection of Figs. A.1-A.3 shows that the response of the pile is linear until about 85% of the ultimate load. Variation in the average strain at the three locations along the pile overlapped (not shown here) indicating that the load on the column was largely concentric.

Table 6.4. Test Results for Undamaged Controls.

Specimen	Test #	Ultimate Load kips
C2-5	1	246.3
C1-6	2	222.6
C2-6	4	248.0
	Averages	239.0

6.4.2 Control with Formed Damage

Two controls with formed damage were tested to failure. The results are summarized in Table 6.5. Inspection of this table shows that the average failure load was 147.8 kips or 61.8% of the average capacity of the undamaged controls though its available cross-section is about 56% (see Table 6.2).

Typical plots to show the variation of the load vs strain are shown in Figs.A.4-A.5 in Appendix A. Inspection of these plots show that the response is largely linear. These controls are appropriate to compare the nonstructural formed damage quite directly.

Table 6.5 Axial Test Results for Damaged Controls.

Specimen	Test #	Ultimate Load kips	Percentage of Undamaged Control
D1-10	27	145.5	60.9
D2-10	26	150.0	62.8
	Averages	147.8	61.8

6.4.3 Control with Formed Damage and Strands Cut

Two controls with formed damage were tested to failure. The average load at failure was 100.1 kips (see Table 6.6) that is 41.9% of the undamaged controls. The variation in load is large compared to the formed damage (Table 6.5) because of the difficulty in ensuring identical damage while cutting the strands. Plots showing the variation of the load vs strain are shown in Figs. A.6-A.7. The plot of average strain for each of these tests is linear throughout the range of loading up to 90% of the failure load.

Table 6.6. Axial Test Results for Damaged Controls with Cut Strands.

Specimen	Test #	Ultimate Load kips	Percentage of Undamaged Control
D2-4	29	87.3	36.5
D2-9	28	112.8	47.2
	Averages	100.1	41.9

6.4.4 Nonstructural Repair with Formed Surface

The average failure load for the Type II repairs was over 100% of the formed control (Table 6.5) but about 62% of the undamaged control. Failure was initiated by debonding. The average debonding load was nearly 85% of the ultimate capacity. Evidence of debonding may be clearly seen from the strain vs load plot in Figs. A.8-A.9.

Table 6.7. Axial Results for Nonstructural Repairs (Type II) on Formed Surface.

Specimen	Test #	Debond Load	Ultimate Load	Debond % Ultimate	% Formed Control	%Undamaged Control
NF-1	25	118	134.3	87.9	90.9	56.2
NF-2	30	133	163.1	81.5	110.4	68.2
	Average	126	148.7	84.7	100.6	62.2

6.4.5 Structural Repair with Formed Surface

In contrast to the non-structural repairs, the structural repairs show significant capacity beyond the debonding load. This averages 64.3% of the ultimate compared to 84.7% for the non-structural case. The overall strength gains are also impressive and are nearly 80% of the undamaged section (see Table 6.8).

Typical plots to show the variation of the load, strain and deflection are shown in Figs. A.10-A.11. Data from Test #08 (SF-1) was reconstructed from the hard copy printed at the time of the test, therefore, it has much fewer data points.

Table 6.8. Axial Test Results for Structural Repairs on Formed Surface.

Specimen	Test #	Debond Load	Ultimate Load	Debond % Ultimate	% Formed Control SC	%Undamaged Control
SF-1	8	128	179.9	71.2	179.7	75.2
SF-2	5	119	205.9	57.8	205.7	86.2
	Average	124	192.9	64.3	192.7	80.7

6.4.6 Nonstructural Repair with Chipped Surface

The average failure load for the Type II repairs was over 90% of the formed control (Table 6.5) but about 56% of the undamaged control (see Table 6.9). There was no debonding and failure occurred due to crushing of the core. Ultimate capacities were lower because of the smaller core area (see Table 6.2). Strain plots are shown in Fig. A.12-A.13.

Table 6.9. Axial Results for Nonstructural Repairs (Type II) on Chipped Surface.

Specimen	Test #	Debond Load	Ultimate Load	Debond % Ultimate	% Formed Control	%Undamaged Control
NC-1	24	129	128.5	100.0	86.9	53.8
NC-2	31	142	141.7	100.0	95.9	59.4
	Average	135	135.1	100.0	91.4	56.6

6.4.7 Structural Repair with Chipped Surface

Structural repairs have significantly greater capacity because of the contribution of the re-bar. In the tests, one specimen debonded at 85% of ultimate load while the other did not debond. The average capacity was 73.4% of the undamaged control compared to 56.6% for the corresponding non-structural repair.

Plots showing the variation of the load vs strain are shown in Figs. A.14-A.15.

Table 6.10. Axial Test Results for Structural Repairs on Chipped Surface.

Specimen	Test #	Debond Load	Ultimate Load	Debond % Ultimate	% Formed Control SC	%Undamaged Control
SC-1	7	174	174.4	100.0	174.2	73.0
SC-2	6	150	176.4	85.0	176.2	73.8
	Average	162	175.4	92.5	175.2	73.4

6.5 Conclusions

The following conclusions may be drawn from the test results:

1. Structural repairs provide higher increase in axial capacity. Non-structural repairs on *formed* surfaces led to practically zero increase in capacity (see Table 6.11).

2. The roughness of the interface contributes significantly to composite action. Chipped surfaces resulted in composite action practically to failure. The repair material debonded more readily in case of formed specimens and was the same for structural and non-structural repairs.

3. None of the repairs led to piles regaining their original strength. The highest increase was 80.7% (Type V - formed); the lowest was 56.6% (Type II - chipped).

Table 6.11. Axial Test Results Summary.

Test Series	Debond Load	Ultimate Load	Debond Percent of Ultimate	Percent of Undamaged Control
	kips	kips	%	%
Undamaged Controls		239.0		100.0
Damaged Controls		147.8		61.8
Damaged Controls with Cut Strands		100.1		41.9
Nonstructural Formed	126	148.7	84.7	62.2
Structural Formed	124	192.9	64.3	80.7
Nonstructural Chipped	135	135.1	100.0	56.6
Structural Chipped	162	175.4	92.5	73.4

References

2.1 Sen, R., Mullins, G. and Snyder, D. (1999). Ultimate Capacity of Corrosion Damaged Piles. Final Report for Florida Department of Transportation, March.

7. ECCENTRIC LOAD RESULTS

7.1 Introduction

This chapter presents the results from the eccentric load tests. Eight of the specimens tested were repaired specimens. The remainder were controls. Results from the corresponding concentric load tests are contained in Chapter 6.

Two types of repairs were investigated. Structural (Type V) and non-structural (Type II) repairs were carried out on two different surface types. The ultimate capacities of these jacketed piles were compared with identically tested control specimens.

A description of the test set-up is presented in Section 7.2. Details of specimens tested and instrumentation appears in Section 7.3 while the results from the seven series of tests are described in Section 7.4 and constitutes the largest section of the chapter. The principal conclusions are summarized in Section 7.5.

7.2 Test Set-Up

The swivel head assembly used in the axial load testing permitted rotation about any axis. In the bending tests, however, only uniaxial bending was being considered. Consequently, the end conditions used in the axial load testing had to be appropriately modified for these tests.

Rollers permit rotation in one direction and were therefore used in the bending tests. In the testing, a steel roller was positioned between two steel plates and offset exactly 1.2 in. from the center line of the column to meet the target eccentricity ratio, e/h of 0.2 (e is the eccentricity, h is the depth). Guides were welded to the two plates sandwiching the roller to prevent any translation. One of these plates was bolted to the swivel head assembly. Details are shown in Fig. 7.1.

No changes were made to the assembly used to confine the column ends in the axial testing. As before, confinement was provided by using four 6 in. high steel plates that were secured to the column by adjustable bolts. The confinement was restricted to a depth equal to that of the member (also 6 in.) where stresses were non-uniform. Additionally, the ends of the column were supported on lead plates to ensure uniform distribution and prevent premature

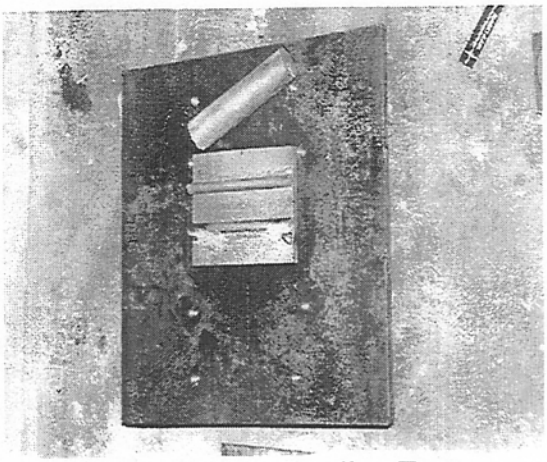

Roller Used in Bending Tests

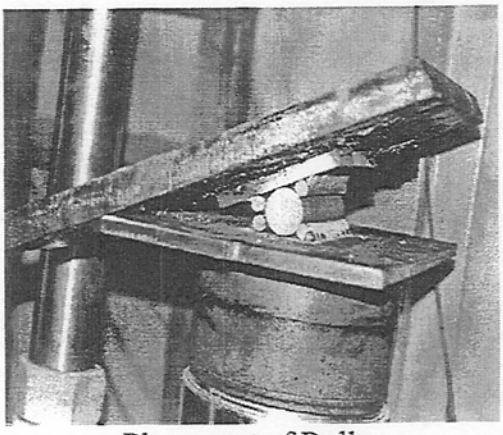

Placement of Roller

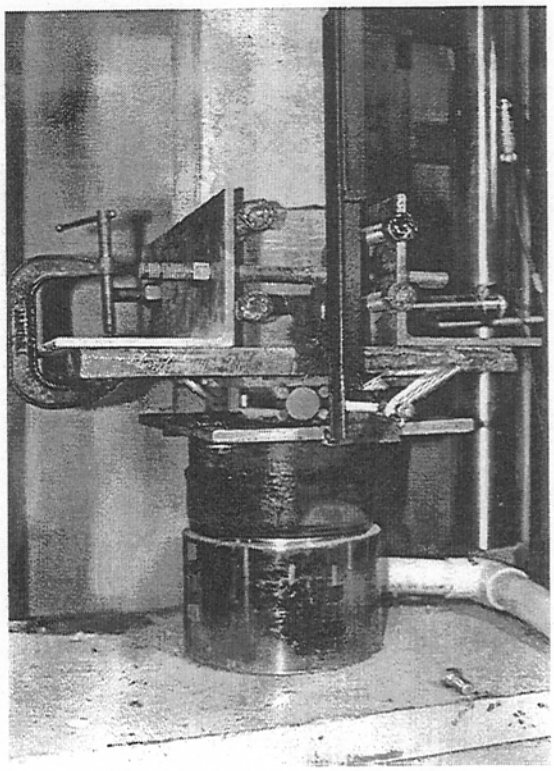

Bottom Support Assembly

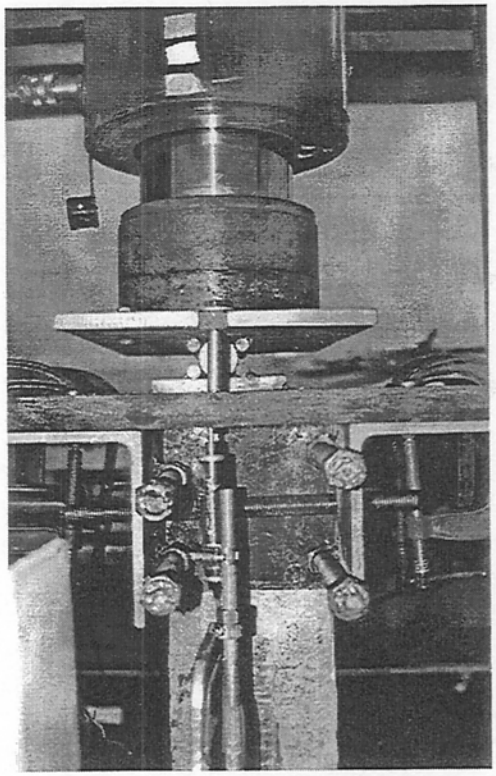

Eccentric Load at Top Support

Fig. 7.1 End Conditions in Bending Test.

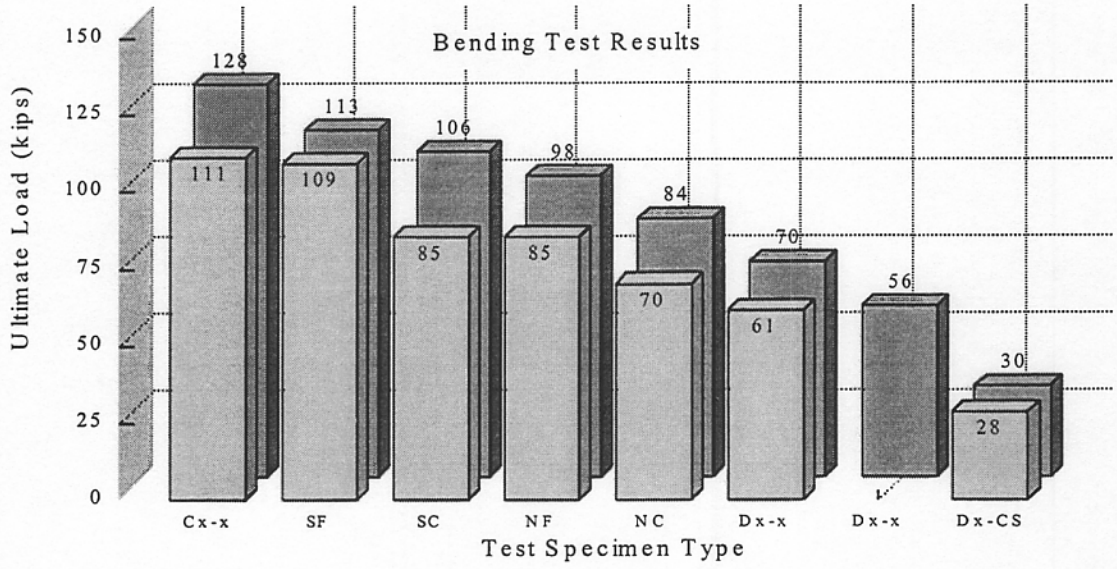

Figure 7.2. Summary of Phase I Capacities Under Eccentric Loading.

Typical failure modes from the repaired specimens are shown in Figs. 7.3-7.9. Failure was initiated by compression with cracks forming on the tension side. In cases of non-structural repair with the strands cut, the specimen broke in two pieces.

Figs. 7.3-7.5 show the failure mode for the controls. All failures occurred in the mid-region. In cases of the formed surface repair, separation occurred but not to the same extent as under axial loading (Fig. 6.6). The structural repairs developed additional capacity after cracking (Fig. 7.7). In cases of the chipped surface repair, debonding occurred more readily in non-structural jackets (Fig. 7.8). The structural repair deflected very little and exhibited moderate cracking (Fig. 7.9).

In order to gain an increased understanding, further detailed analyses are presented in the same format as that for concentric loading. For each pile, two sets of plots are shown in a single page. The first provides information on the load vs lateral deflection; the second shows the variation of mid-strain compressive and tensile strains with load. Because the gages were affixed to the exterior surface of the repair, the loads applied to the member did not necessarily give rise to tensile and compressive stresses on the opposite faces.

end failure. The final position of the column in the test frame was determined by tightening or loosening the bolts as needed while the column was under nominal loading.

7.3 Test Program

The testing program for eccentric loading was conducted much like the concentric axial test. As before, seven controls were tested along with eight repaired specimens. Two surface types - formed and chipped were investigated and two repair types (Types II and V) were tested in pairs. The controls tested were similar to the ones tested axially excepting that they were tested under eccentric loading. Aside from the differences identified the test setup and the following sections, the procedure was quite analogous.

Details of the specimens tested in the four series of repairs and the three series of controls are summarized in Table 7.1.

Table 7.1 Specimen Details.

Type of Test Specimen	Number	Specimen ID
Undamaged Controls	2	C2-5 C2-7
Structural Repair Formed Surface	2	SF-3 SF-4
Structural Repair Chipped Surface	2	SC-3 SC-4
Non-Structural Repair Formed Surface	2	NF-3 NF-4
Non-Structural Repair Chipped Surface	2	NC-3 NC-4
Damaged Controls	3	D1-7 D2-7,8
Damaged Controls with Strands Cut	2	D1-8 D1-9
Totals	15	

7.3.1 Instrumentation

Twelve strain gages were mounted to the surfaces at one foot from each end and in the middle as for the axial tests. Eight of these gages were located outside of the region of the pile compressed by the pre-load simulator. These were useful in centering the pile with precision. Also, these gages provided useful measurements for analyzing the preload strain.

Both axial and lateral deflections were measured by seven LVDT's. The plots included in this chapter are the average of the two gages measuring axial deflection. The plots also indicate the lateral deflection at the mid point. Additional lateral measurements were taken at the ends and at quarter points of the pile which provided a independent reference from the testing frame.

7.3.2 Specimen Preparation

Specimens were prepared identically to those tested under concentric loading. In essence, dimensions were measured and gages attached. Where strands had to be cut, the operation was carried out exactly as before. A nominal load was applied to the specimen and the strands cut under this load. The compression load served to counter tensile forces released as the strand was cut.

The calculated cross-sectional areas of the specimens tested under eccentric loading are summarized in Table 7.2. Inspection of Table 7.2 shows that the column cross-section was somewhat larger than the 36 in^2 obtained on the basis of the nominal column dimension. The section reduces by more than 64% in cases where strands were cut.

Table 7.2. Cross-Sectional Area of Specimens Tested under Eccentric Loads.

Item #	Test Type	Specimen	Gross Area in^2	Core in^2	Area of Repair in^2
1	Undamaged Control	C2-7	37.3		
2	Undamaged Control	C1-5	40.0	Same	
3	SF-3	D1-17	75.7	21.1	54.6
4	SF-4	D2-17	78.2	21.6	56.6
5	SC-3	D1-18	76.0	12.9	63.1
6	SC-4	D2-18	77.1	12.8	64.3
7	NF-3	D1-13	74.9	20.7	54.2
8	NF-4	D2-13	75.5	21.5	54.0
9	NC-3	D1-15	73.6	12.3	61.3
10	NC-4	D2-15	74.1	12.5	61.6
11	Damaged Control	D1-7	20.0		
12	Damaged Control	D2-8	20.3	Same	
13	Damaged Control	D2-7	20.5		
14	D. Control Cut Strands	D1-8	20.4	14.2	
15	D. Control Cut Strands	D1-9	20.4	14.3	

As for the concentric tests, the calculated cross-sectional areas correspond to measurements taken at the mid-point. Of the specimens that were repaired, the chipped surfaces have considerably smaller cores (about 60%) compared to the formed surfaces. The area of repair shown in the table was calculated by subtracting out the core area from the gross area.

7.3.3 Test Procedure

All strain gages, LVDTs and the 500 kip load cell from GEOKON were hooked up to a MEGADAC 3100 data acquisition system. The load was applied using a 300 ton, 13 in stroke hydraulic jack from Force Resources, Inc. that was connected to an electrically operated pump.

The data acquisition system was zeroed and a small initial load applied. The calculated strains under nominal load were compared against test results and the position of the specimen in the frame was adjusted by tightening and loosening of the bolts used to confine the column ends (see Fig. 7.1) until strains readings were in good agreement with the expected values.

With the column accurately centered, a 20 kip load was applied to relieve the tension in the long-slender threaded rods. Care had to be taken to place the pre-load simulator at right angles to the eccentricity to ensure that the two rods would be subjected to the same loads; otherwise, the rods would be subjected to unequal loads. The hardware used to load the piles prior to the repair procedure were then removed. The columns were then loaded and readings were taken continuously by the data acquisition system.

7.4 Results

This section presents results from the seven series of tests conducted. As for the concentric load results, load cell readings were found to have a sensitivity constant error that led to an over estimation of the loads.

A summary of the ultimate load values from all the axial tests appears in Table 7.3. For convenience, the results in this table are also re-plotted in bar form in Fig. 7.2.

Table 7.3 provides information on the individual failure load, the average failure load and the *average* failure load from each of the seven series as a percentage of the *average* of the undamaged controls that failed in compression.

Table 7.3. Summary of Results for Eccentrically Loaded Specimens.

Test#	Type	Specimen	Failure Load kips	Average kips	% U. Control
9	U. Control	C2-7	127.9	119.5	100.0
10	U. Control	C1-5	111.2		
12	Type V	SF-3	112.8	110.9	92.8
14	Type V	SF-4	109.1		
11	Type V	SC-3	105.8	95.5	79.9
13	Type V	SC-4	85.2		
16	Type II	NF-3	85.2	91.8	76.8
15	Type II	NF-4	98.4		
18	Type II	NC-3	84.2	76.7	64.2
17	Type II	NC-4	69.2		
19	F. Control	D1-7	55.5	62.3	52.1
21	F. Control	D2-8	61.4		
20	F. Control	D2-7	70.1		
22	Control- SC	D1-8	28.2	28.9	24.1
23	Control-SC	D1-9	29.6		

Inspection of Table 7.3 shows that strength gains under eccentric loading are more substantial than those for concentric loading (Table 7.3). Increase in capacity of structural repairs (Type V) was as much as nearly 93% of the original undamaged capacity compared to 81% under concentric loading. Non-structural repairs (Type II) showed increases of over 76% of the original undamaged capacity compared to 62% under concentric loading.

As for the concentric loading, increases were greater for formed interface rather than for the chipped one. This is because the area of the core for the chipped case was only 60% of that for the formed case (see Table 7.2).

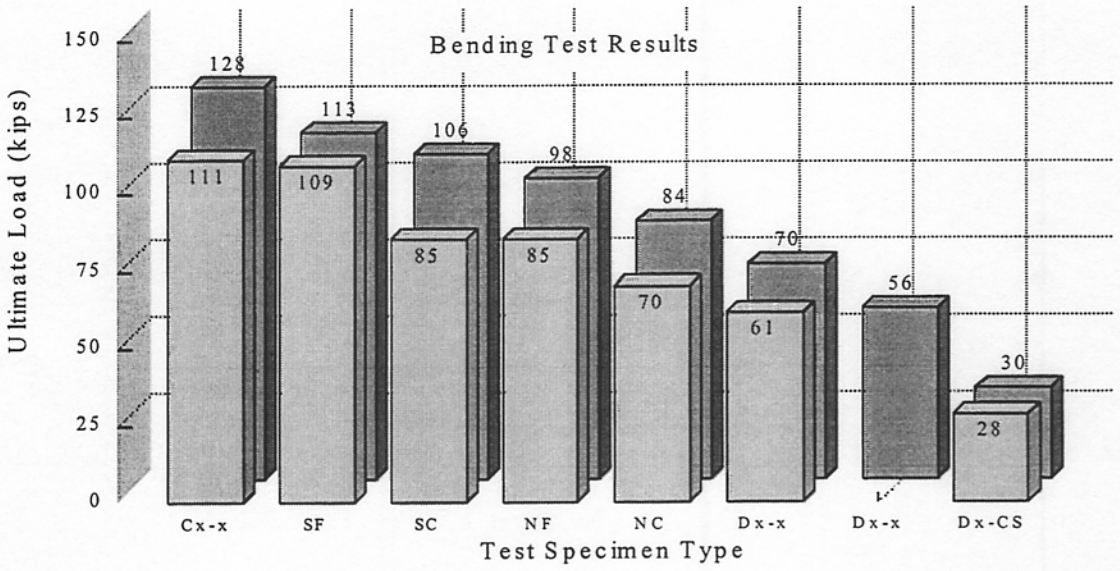

Figure 7.2. Summary of Phase I Capacities Under Eccentric Loading.

Typical failure modes from the repaired specimens are shown in Figs. 7.3-7.9. Failure was initiated by compression with cracks forming on the tension side. In cases of non-structural repair with the strands cut, the specimen broke in two pieces.

Figs. 7.3-7.5 show the failure mode for the controls. All failures occurred in the mid-region. In cases of the formed surface repair, separation occurred but not to the same extent as under axial loading (Fig. 6.6). The structural repairs developed additional capacity after cracking (Fig. 7.7). In cases of the chipped surface repair, debonding occurred more readily in non-structural jackets (Fig. 7.8). The structural repair deflected very little and exhibited moderate cracking (Fig. 7.9).

In order to gain an increased understanding, further detailed analyses are presented in the same format as that for concentric loading. For each pile, two sets of plots are shown in a single page. The first provides information on the load vs lateral deflection; the second shows the variation of mid-strain compressive and tensile strains with load. Because the gages were affixed to the exterior surface of the repair, the loads applied to the member did not necessarily give rise to tensile and compressive stresses on the opposite faces.

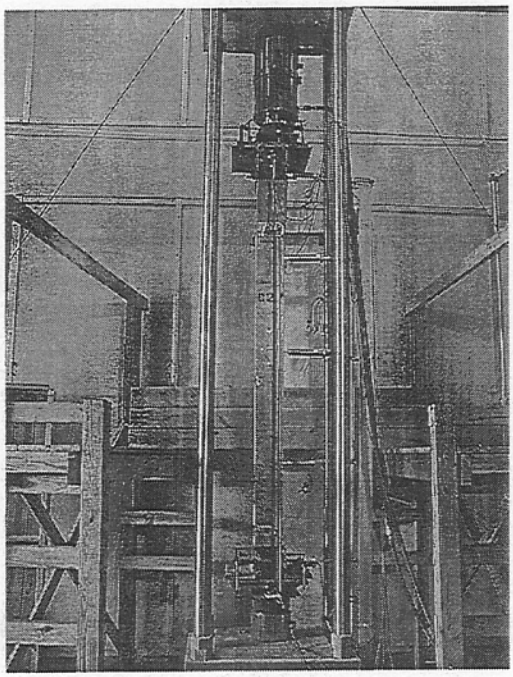

Test Set-Up

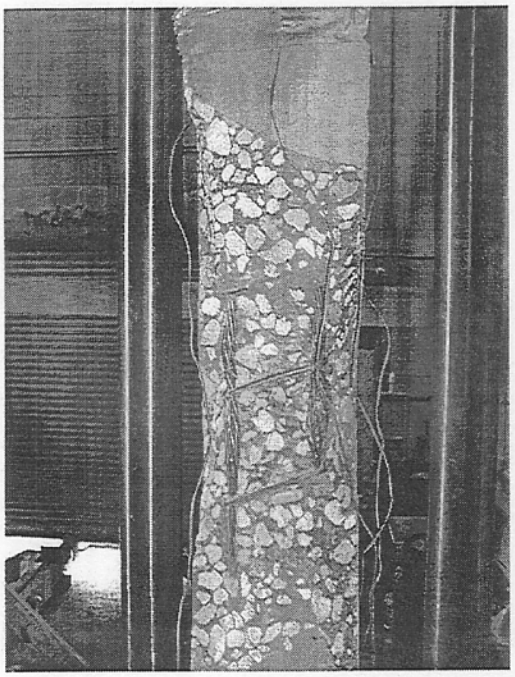

Close-Up of Damage

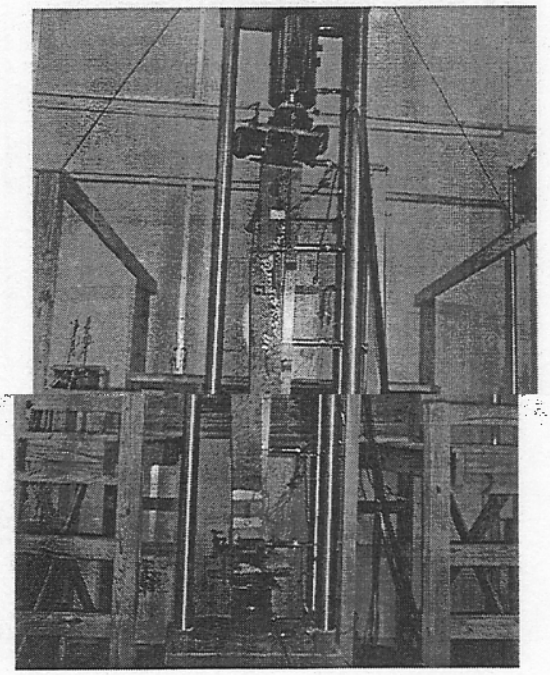

View of Failed Control

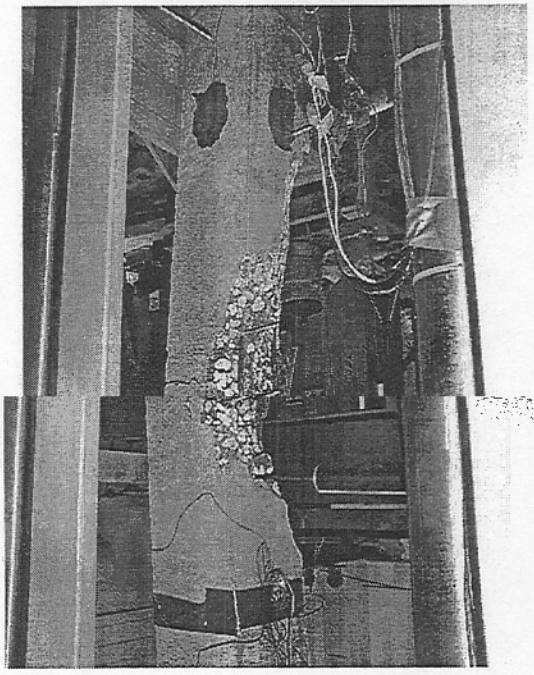

Close-Up of Failed Zone

Figure 7.3 Undamaged Control in Bending.

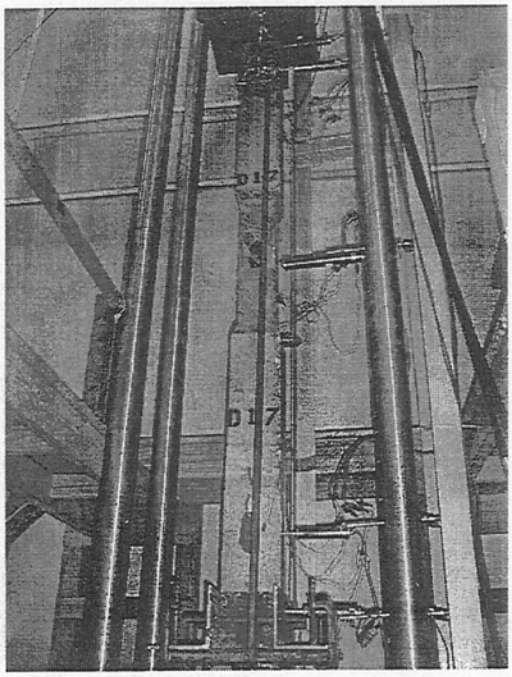

Test Set-Up

View of Failed Damaged Control

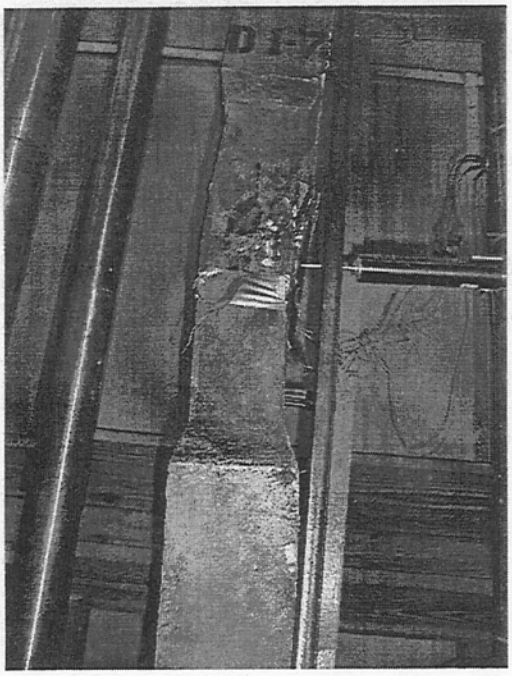

Close-Up of Failed Control

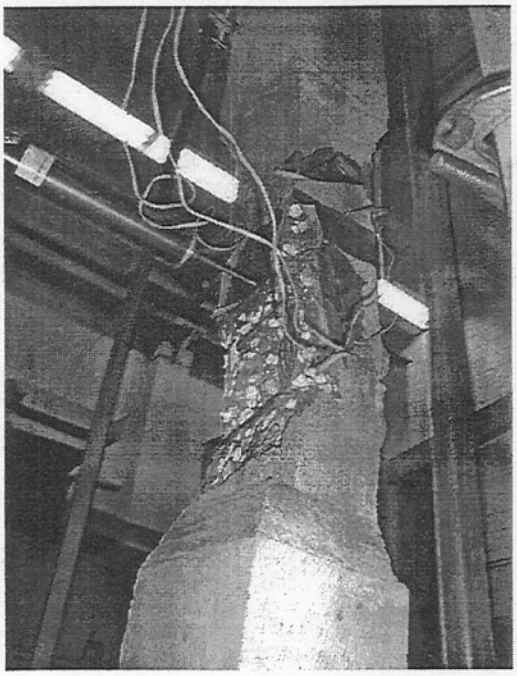

Close-Up of Failed Zone

Figure 7.4 Damaged Control in Bending.

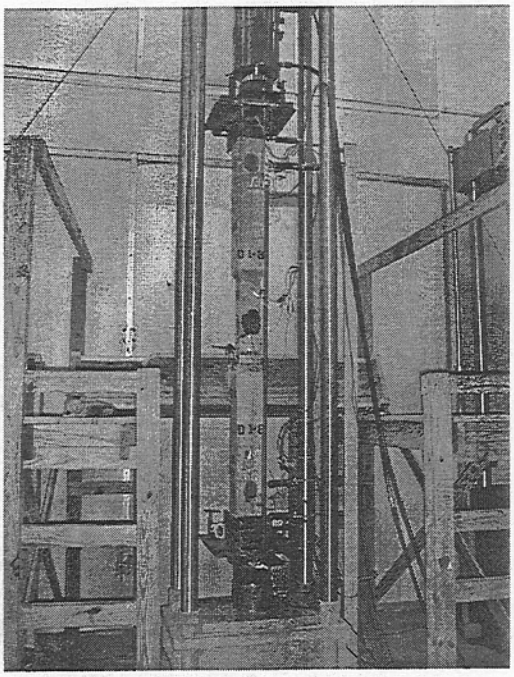

Test Set-Up

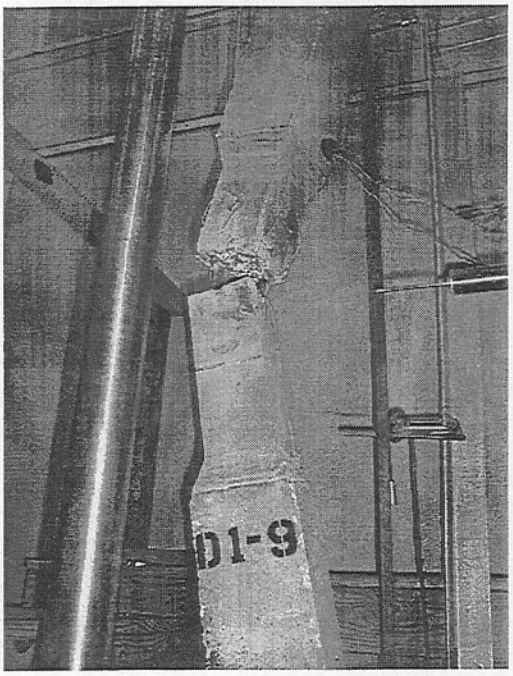

View of Failure

Control Fails in Two Pieces

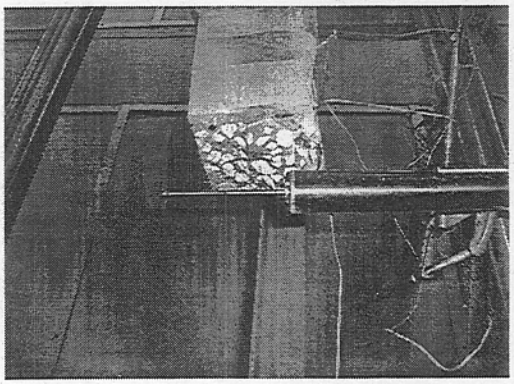

View of Top Part

Figure 7.5 Damaged Control with Strands Cut in Bending.

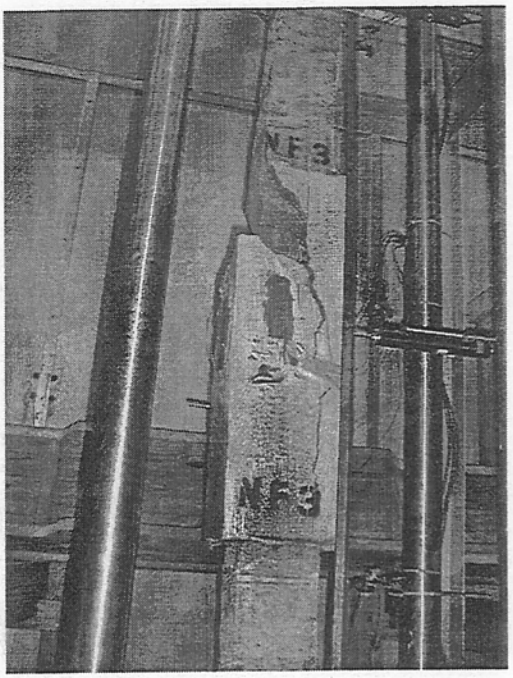

View of Failed Member

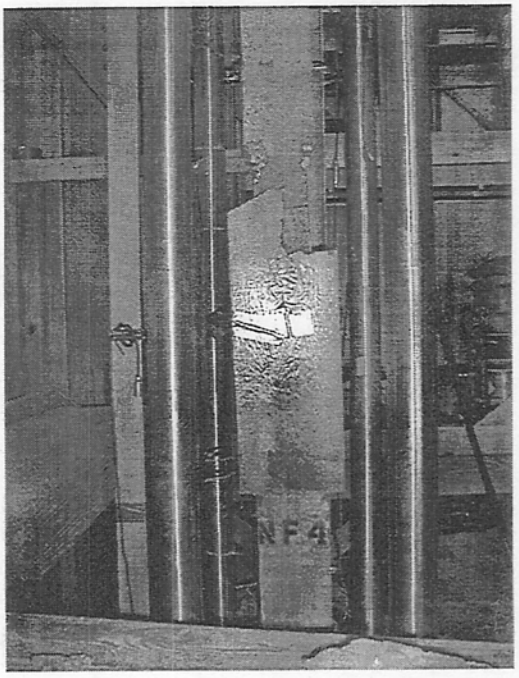

View of Second Failure

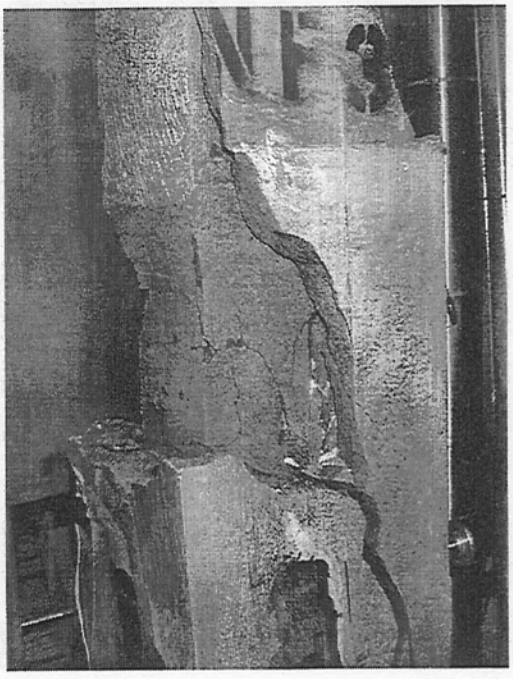

Debonding on Tension Face

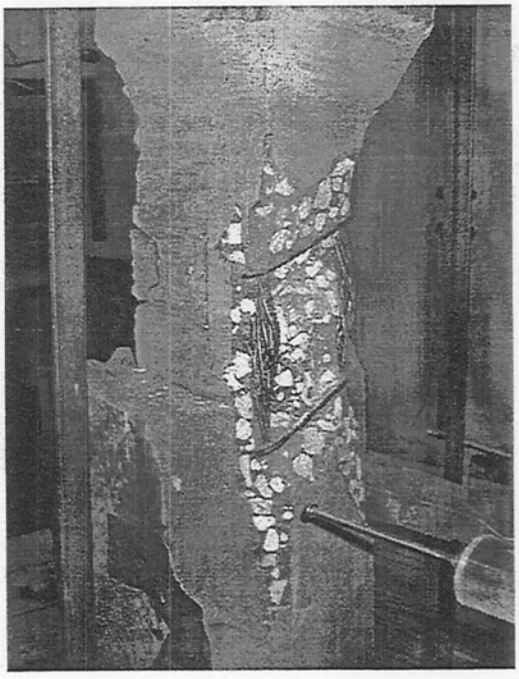

Close-Up of Core

Figure 7.6 Non-Structural Repair With Formed Surface in Bending.

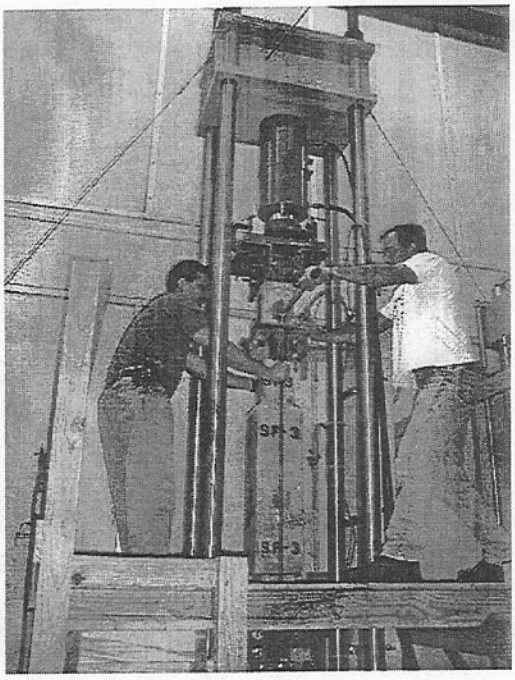

Preload Removal

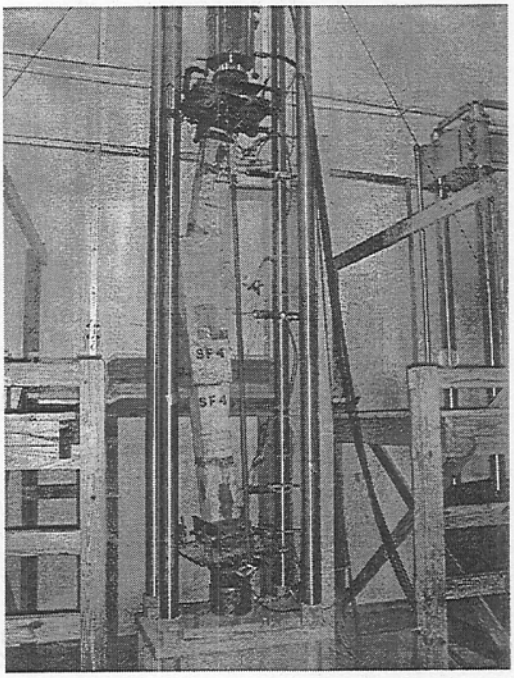

View of Failure

Debonding on Jacket

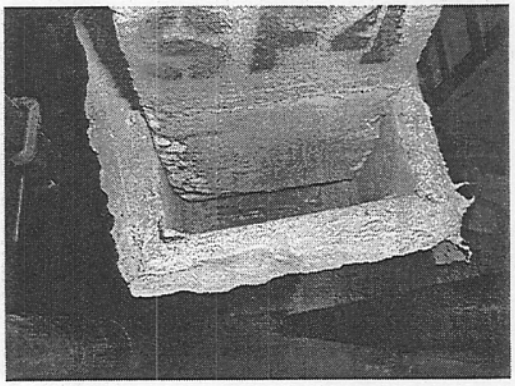

Separation of Jacket

Figure 7.7 Structural Repair With Formed Surface in Bending.

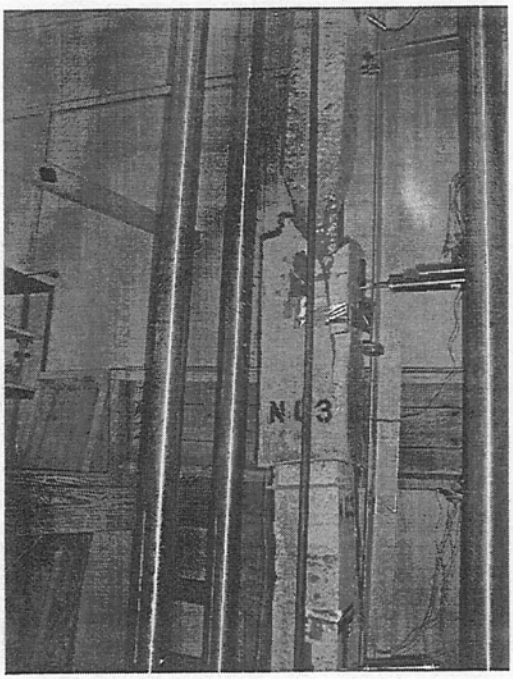

View of Failed Specimen

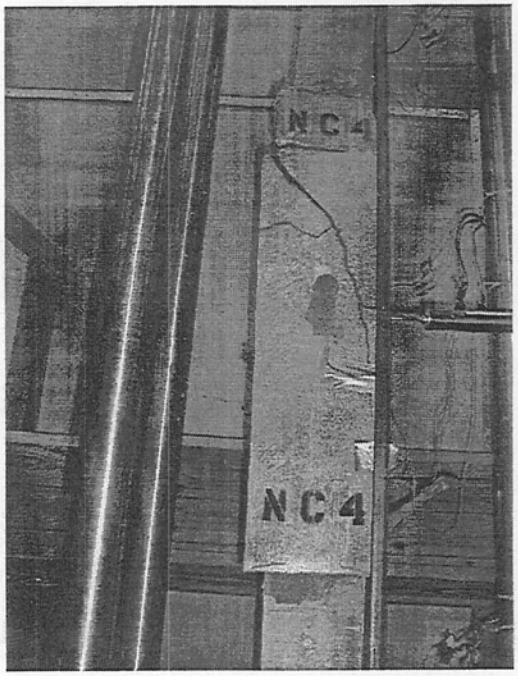

View of Failure

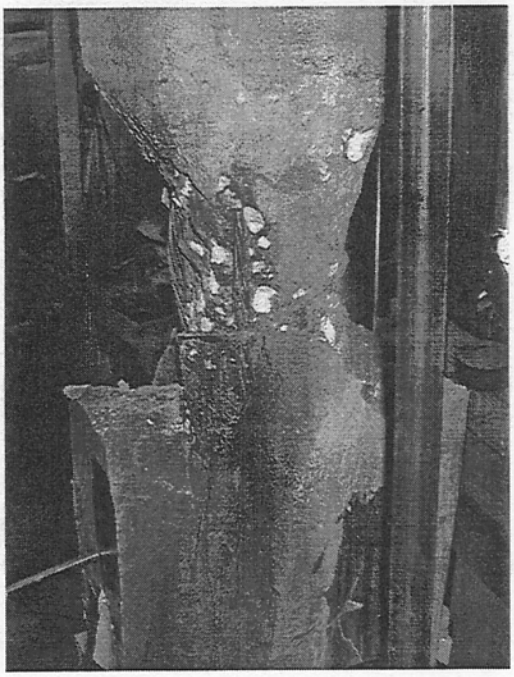

Debonding on Jacket

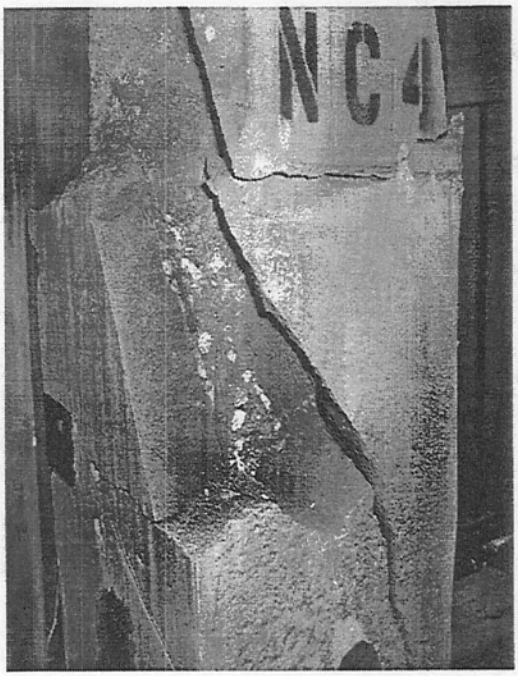

Separation of Jacket

Figure 7.8 Non-Structural Repair With Chipped Surface in Bending.

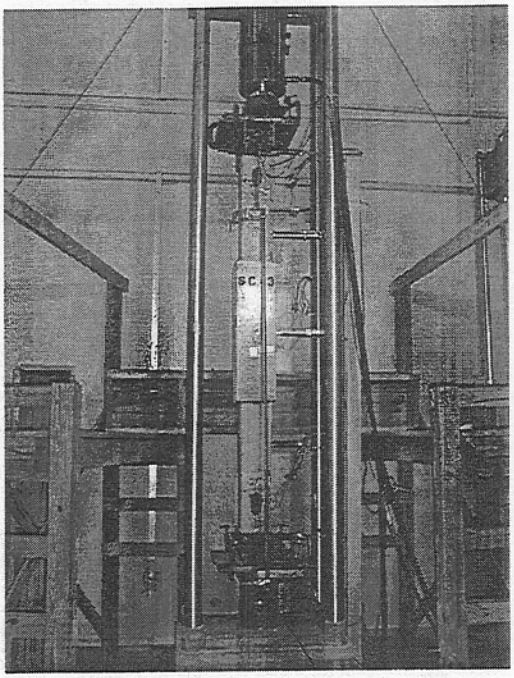

Test Set-Up

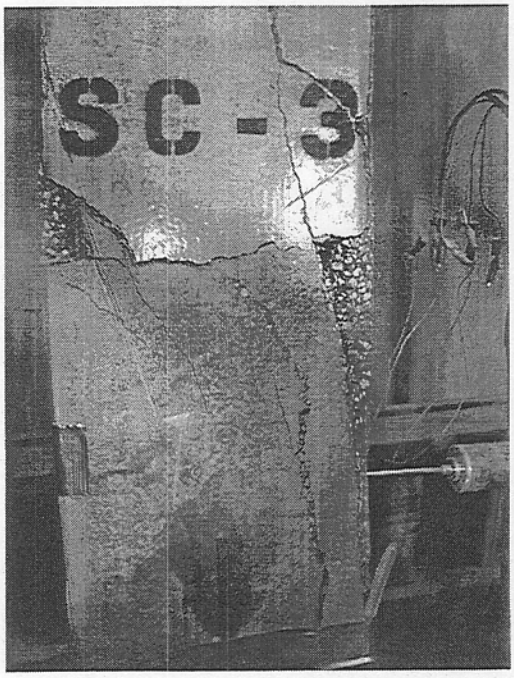

View of Failure

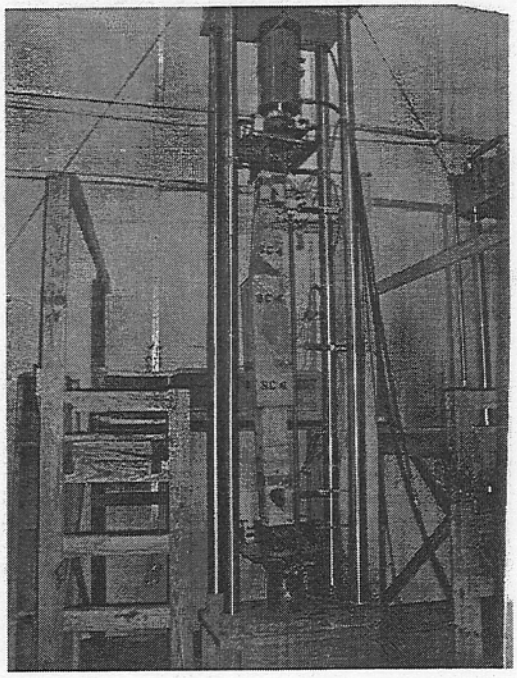

View of Failure

Separation of Jacket

Figure 7.9 Structural Repair With Chipped Surface in Bending.

The results are presented for groups of similar tests. In general, two tests are considered in each group. First, the results from the three sets of controls - undamaged controls, formed damage controls and the cut strand - are discussed. This is followed by results for the four series of repairs. These consist of nonstructural (Type II) and structural (Type V) repairs for the two different surface preparations - formed and chipped. All plots referred may be found in Appendix B.

7.4.1 Undamaged Controls

Two undamaged controls were tested to failure. Table 7.4 provides a summary of the results. The average ultimate load at failure was 119.5 kips. This value is used in the sections that follow to assess the strength gain in repaired piles.

Plots showing the mid-span lateral deflection and strain variation with load for a typical control are shown in Figs B.1-B.4 in Appendix B. Compressive and tensile strains that developed may be clearly seen.

The eccentric load was applied to cause E-W bending about the N-S axes as oriented in the test frame. The results showed that there was no bending about the E-W axes. As the results do not incorporate the effect of prestress they do not represent the absolute magnitude of the strains that developed. Had these been included, the compressive strains would be higher and the tensile strains lower.

Table 7.4. Eccentric Test Results for Undamaged Controls.

Specimen	Test #	Ultimate Load kips
C1-5	10	111.4
C2-7	9	127.9
	Averages	119.5

7.4.2 Control with Formed Damage

Two controls, D1-7 and D2-8 with formed damage were initially tested to failure. As there was significant disparity in the ultimate loads, an additional control D2-7 was also tested. Unfortunately, part of the data for D2-7 was lost. The results are summarized in Table 7.5. Inspection of this table shows that the average failure load was 62.3 kips or 52.1% of the average capacity of the undamaged controls, lower than that from axial tests (see Table 7.5). Typical plots to show the variation of the load vs mid-span lateral deflection and strain are shown in Figs. B.5-B.10 in Appendix B.

Table 7.5 Eccentric Test Results for Damaged Controls.

Specimen	Test #	Ultimate Load kips	Percentage of Undamaged Control
D1-7	19	55.5	46.4
D2-7	21	61.4	51.4
D2-8	20	70.1	58.7
	Averages	62.3	52.1

7.4.3 Control with Formed Damage and Strands Cut

Two controls with all four strands cut were tested to failure. The average load at failure was 28.9 kips (see Table 7.6) that is 24.1% of the undamaged controls. Plots showing the variation of the load, strain and deflection for all the specimens are shown in Figs. B.11-B.14 in Appendix B.

Table 7.6. Eccentric Test Results for Damaged Controls with Cut Strands.

Specimen	Test #	Ultimate Load kips	Percentage of Undamaged Control
D1-9	23	29.6	24.8
D1-8	22	28.2	23.6
	Averages	28.9	24.2

7.4.4 Nonstructural Repair with Formed Surface

The average failure load for the Type II repairs were nearly 150% of the formed control (Table 7.5) and about 77% of the undamaged control. Failure was initiated by debonding. The average debonding load was 65% of the ultimate capacity, much lower than that for axial loading.

Plots of the average mid-span deflection and strain variation with load are shown in Figs. B.15-B.18 in Appendix B.

Table 7.7. Eccentric Results for Nonstructural Repairs (Type II) on Formed Surface.

Specimen	Test #	Debond Load	Ultimate Load	Debond % Ultimate	% Formed Control	%Undamaged Control
NF-3	16	60	85.1	70.5	136.6	71.2
NF-4	15	60	98.4	61.0	157.9	82.3
	Average	60	91.8	65.4	147.4	76.8

7.4.5 Structural Repair with Formed Surface

The structural repairs debonded at lower loads under eccentric rather than under axial loading presumably because of the tensile strains that were introduced by the eccentricity. Strength gains were impressive with the average capacity being over 93% of the undamaged control (see Table 7.8).

Typical plots showing the variation of the load, strain and deflection are shown in Figs. B.19-B.22. The debonding load is not obvious looking at the strain variation. Non-linear strain variation may be seen at higher loads.

Table 7.8. Eccentric Test Results for Structural Repairs on Formed Surface.

Specimen	Test #	Debond Load	Ultimate Load	Debond % Ultimate	% Formed Control SC	%Undamaged Control
SF-3	12	93	113.4	82.0	182.0	94.9
SF-4	14	79	109.1	72.4	175.1	91.3
	Average	86	111.3	77.2	178.6	93.1

7.4.6 Nonstructural Repair with Chipped Surface

The average failure load for the Type II repairs was over 120% of the formed control (Table 7.5) but about 64% of the undamaged control (see Table 7.9). Unlike axial tests where there was no debonding until failure, there was some debonding under eccentric loading. As before, ultimate capacities were lower because of the smaller core area (see Table 7.2). Deflection and strain plots are shown in Figs. B.23-26. Because of the relatively large dimension of the repair, the application of loading led to compressive strains on both surfaces.

Table 7.9. Eccentric Results for Nonstructural Repairs (Type II) on Chipped Surface.

Specimen	Test #	Debond Load	Ultimate Load	Debond % Ultimate	% Formed Control	%Undamaged Control
NC-3	18	73	84.3	86.6	135.3	70.5
NC-4	17	55	69.3	79.4	111.2	58.0
	Average	64	76.8	83.3	123.3	64.3

7.4.7 Structural Repair with Chipped Surface

Structural repairs led to greater strength gain than the non-structural repairs. Average capacity was 79.9% of the undamaged control (Table 7.10) compared to 64.3% for non-structural repairs (Table 7.9). Debonding loads were greater. In contrast to axial tests, debonding load as a percentage of the ultimate load were lower.

Typical plots to show the variation of the load, strain and deflection are shown in Figs. B.27-30.

Table 7.10. Eccentric Test Results for Structural Repairs on Chipped Surface.

Specimen	Test #	Debond Load	Ultimate Load	Debond % Ultimate	% Formed Control SC	%Undamaged Control
SC-3	11	70	105.8	66.2	169.8	88.5
SC-4	5	67	85.1	78.7	136.6	71.2
	Average	69	95.5	72.3	138.4	79.9

7.5 Conclusions

The following conclusions may be drawn from the test results:

1. Structural repairs are very efficient and lead to significant increases in ultimate capacity. Non-structural repairs on *formed* surfaces are much more efficient under eccentric loading rather axial loading where there was practically no increase in capacity (see Table 7.11).

2. The bond between the old concrete and the repair material is less important under eccentric load than with concentric loading.

3. None of the repairs led to piles regaining their original strength. The highest increase was 93.1% (Type V - formed); the lowest was 64.3% (Type II - chipped). These are however, higher than those for concentric loads.

Table 7.11. Eccentric Test Results Summary.

Test Series	Debond Load	Ultimate Load	Debond Percent of Ultimate	Percent of Undamaged Control
	kips	kips	%	%
Undamaged Controls		119.5		100.0
Damaged Controls		62.3		52.1
Damaged Controls with Cut Strands		28.9		24.2
Nonstructural Formed	60	91.8	65.4	76.8
Structural Formed	86	111.3	77.2	93.1
Nonstructural Chipped	64	76.8	83.3	64.3
Structural Chipped	69	95.5	72.3	79.9

8. ASSESSMENT OF PHASE I RESULTS

8.1 Introduction

The goal of Phase I was twofold: first, to determine if repairs led to increased capacity under concentric and eccentric loads and second, to identify measures, if any, could be taken to improve efficiency. This chapter critically evaluates the test results presented in the two preceding chapters with emphasis on identifying measures to increase capacity.

Aspects of the results from the axial and eccentric tests are examined in Sections 8.2 and 8.3 respectively. A comparative analysis of the strength gains from the four series of repairs is presented in Section 8.4. A discussion of these findings and their implications for prototype piles is presented in Section 8.5. The principal conclusions are summarized in Section 8.6. These form the basis of the test program for the second phase that is described in the next chapter.

8.2 Capacity of Controls for Axial Tests

In order to assess strength gain, comparisons need to be made with appropriate controls. Although four types of repairs were carried out (Type II, Type V with formed and chipped surfaces), only three types of controls were tested (undamaged control, formed damage control, formed damage with strands cut - note that this is not an exact control since the gaps left by the removal of the strand are filled by the repair material). Thus, there is a need to first of all estimate the capacity of a chipped control.

Finite element analysis could, of course, be used to estimate the capacity of a chipped control. However, as the capacity was found to be related to the reduction in cross-section in an earlier study [8.1], a reasonable estimate can also be made by interpolation. This simpler approach is used here.

Table 8.1 examines the relationship between axial capacity and cross-sectional area reduction. For formed damage, an average reduction in area of 43.7% results in a somewhat smaller load loss of 38.2%. For cut strands, the corresponding loss is 58.1% for a 59.4% reduction. The latter value is used to estimate the loss for the chipped section as the cross-section loss is similar. In this case the average reduction in area is 64.9%. This is estimated to produce a reduction of 63.5% (64.9 x 58.1/59.4) giving an estimated magnitude of 87.3 kips.

Table 8.1 Axial Capacity vs Cross-Section Reduction

Test #	Control Type	Area in^2	Failure Load kips	Reduction of Area (%)	Reduction of Load (%)
1	Undamaged	35.24	246.3		
2	Undamaged	38.66	222.6		
4	Undamaged	36.75	248.0		
	Average	36.88	239.0		
26	Formed Damage	20.11	150.0	45.5	37.2
27	Formed Damage	21.39	145.5	42.0	39.1
	Average	20.75	147.8	43.7	38.2
28	Cut Strands	15.25	112.8	58.6	52.8
29	Cut Strands	14.68	87.3	60.2	63.5
	Average	14.97	100.1	59.4	58.1
	Chipped Damage				
6	Structural Chipped	13.37	*Estimate*	63.7	*Estimate*
7	Structural Chipped	13.08		64.5	
24	Nonstructural Chip	12.32		66.6	
31	Nonstructural Chip	12.99		64.8	
	Average	12.94	87.3	64.9	63.5

8.3 Capacity of Controls for Eccentric Tests

Because the type of damage induced in the sections was symmetric, the reduction in bending capacity under eccentric loading is also related to the reduction in cross-section as pointed out in the previous study [8.1]. Therefore, the same procedure used to assess the capacity of a chipped control under axial load may also be used to establish capacity under eccentric loads.

Table 8.2 provides the relationship between load reduction and loss of cross-section. For formed damage, the average reduction is 47.9% for an average cross-sectional loss of 47.6%. For cut strands, reduction in load capacity is greater - a 75.8% load reduction for a 61.3% reduction in cross-section.

As the chipped sections have cross-sections comparable to the cut-strand case, these values are used to estimate the capacity. The 66.7% reduction in area is estimated to lead to a 82.5% capacity loss.

Table 8.2 Bending Capacity vs Cross-Section Reduction

Bending Test #	Control Type	Area in^2	Failure Load kips	Reduction of Area (%)	Reduction of Load
9	Undamaged	37.32	127.9		
10	Undamaged	40.02	111.2		
	Average	38.67	119.6		
19	Formed Damage	19.97	55.5	48.4	53.6
20	Formed Damage	20.25	70.1	47.6	41.4
21	Formed Damage	20.53	61.4	46.9	48.6
	Average	20.25	62.3	47.6	47.9
22	Cut Strands	15.25	28.2	60.6	76.4
23	Cut Strands	14.68	29.6	62.0	75.2
	Average	14.97	28.9	61.3	75.8
	Chipped Damage				
11	Structural	12.89		66.7	
13	Structural	12.84	*Estimate*	66.8	*Estimate*
17	Nonstructural	12.54		66.2	
18	Nonstructural	12.25		67.0	
		12.63	21.0	66.7	82.5

8.4 Strength Gain

Using the average controls from tests and the estimated value for the chipped case it is possible to readily determine the efficiencies of the four repairs. This is shown in Fig. 8.1 in the form of a bar diagram. The darker portions of each bar represents the contribution of the respective control. The lighter shaded portion reflects the contribution of the repair.

The nonstructural repair on the formed surface provided no apparent strength gain. With all four formed surface repairs under axial loading the repair debonded from the core pile at an average load of 126 kips (Table 7.7). The structural repairs on this surface failed at 192.9 kips or a 30.5% increase compared to the controls which failed at 147.8 kips.

The chipped surfaces provided higher strength gains under axial loadings. Perhaps these repairs were pending their apparent debonding event as peak strains were recorded prior to and at failure for one test in each series. The nonstructural repair posted a 54.8% gain and the structural repair 101% gain. It is interesting to note that the structural repairs consistently offered 30% more axial capacity than the non-structural repair on a similar interface.

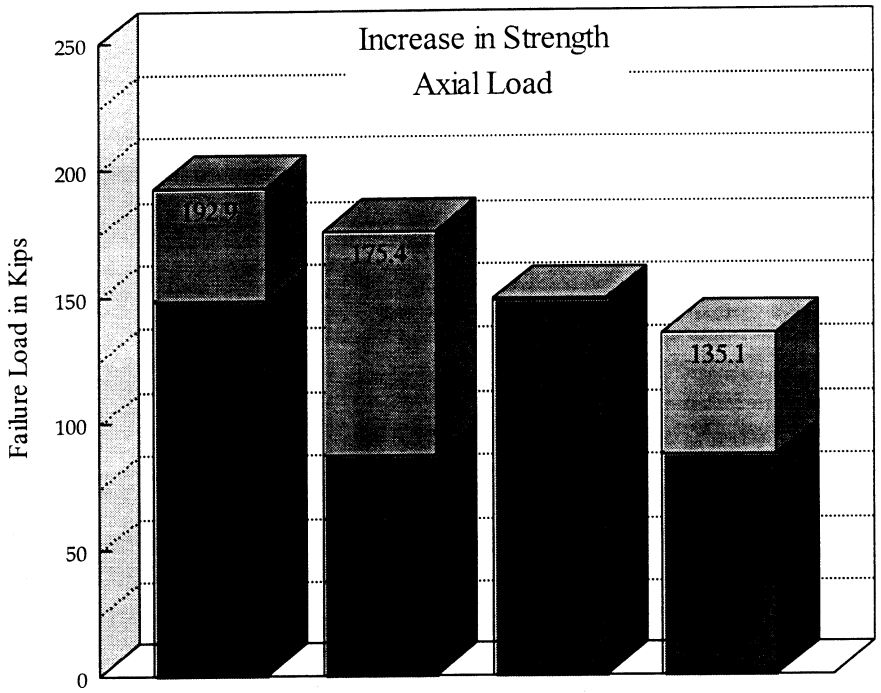

Repair Type	SF	SC	NF	NC
Core Capacity	147.8	87.3	147.8	87.3
Increase	45.1	88.1	0.89	47.8

Figure 8.1 Axial Strength Increase of Repaired Pile Specimens.

The ultimate bending capacity of a specimen with formed damage prior to a repair system was 62.3 kips (see Table 8.2). The corresponding capacity to the chipped section was calculated to be 21 kips. Fig. 8.2 plots the capacities of each type of repair with the capacity of the respective control shaded darker.

The capacity of the repaired piles was improved by each of the repair systems. These gains range from 47.4% to 355%. As for the axial results, the surface texture was the most significant contributor to enhance the strength of the repaired concrete piles. For the formed surface repairs, the nonstructural and structural specimens posted 47.4% and 78.0% increases respectively. The chipped surfaces registered gains of 265% and 355% for nonstructural and structural repairs with bending loads. Table 8.3 presents a summary of the strength gains as a percentage of the damaged controls.

In all but one of the cases some additional strength was provided by each repair system. With both loading schemes the rank order was followed. The most efficient repairs were the structural repairs on the irregular chipped surface. The second in strength gain are the non structural repairs on that same surface. This pattern is repeated with the least strength increase reported on the nonstructural repair on the formed surface.

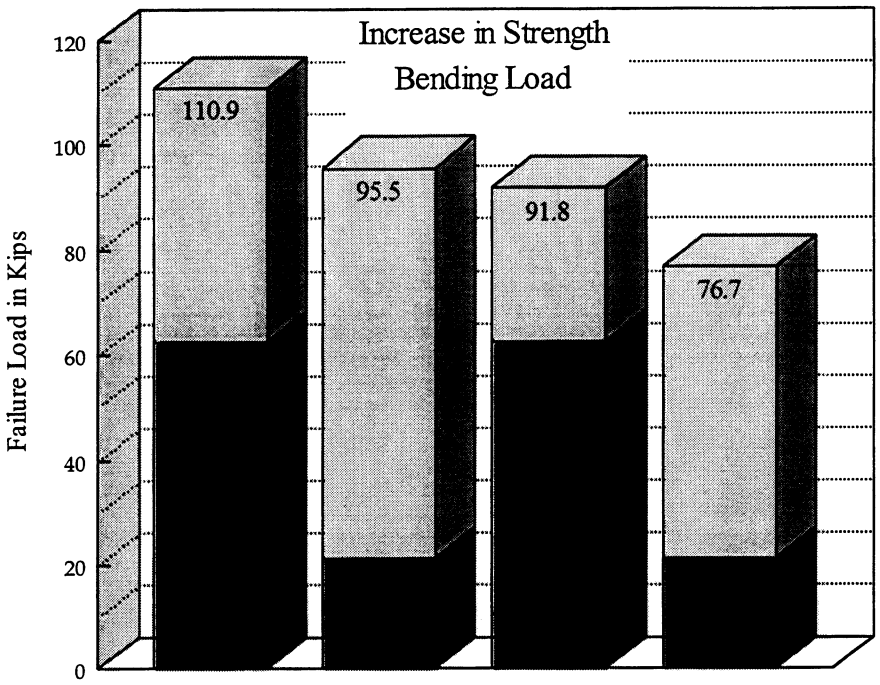

Repair Type	SF	SC	NF	NC
Core Capacity	62.3	21.0	62.3	21.0
Increase	48.6	74.5	29.5	55.7

Figure 8.2 Bending Strength Increase of Repaired Pile Specimens.

Table 8.3 Strength Gains of Repair Types.

Specimen Type	**Axial Load**	**Eccentric**
Structural Formed	30.5%	78.0%
Structural Chipped	101%	355%
Nonstructural Formed	0.6%	47.4%
Nonstructural Chipped	54.8%	265%

8.5 Discussion

This test program provided valuable data in assessing the ultimate capacity of repaired concrete piles. Furthermore, it provides the basis for identifying and measuring improved efficiency of schemes to be investigated in subsequent repair studies. Despite significant gains in most of the series tested, none of the repairs restored the damaged pile to the strength of its undamaged counterpart.

The one series that offered no strength improvement was the nonstructural repair on the formed surface in the axial case. The plots of this pair of tests clearly indicate a loss of composite action at the load level of 125 kips. Without composite action this repair system offered no additional increase in capacity. The structural repairs on this same surface also exhibited debonding at nearly the same load levels. However, the inclusion of reinforcement provided additional capacity that was about 30% higher than the damaged control.

The axial capacity of the structural repair on the chipped surface was also 1.3 times higher than the nonstructural repair on the same surface type. This surface supported higher loads prior to debonding despite having approximately 1/3 less bond surface area. This was due to the load carried by the reinforcing steel.

Significant improvements in bending capacity were reported for each of the repair systems. Reinforcement provided 1.2 times additional capacity for the formed surfaces and 1.25 for the chipped specimens compared to the respective nonstructural repairs tested in bending.

It is important to recognize the limitations of this testing program. Issues relating to durability are beyond the scope of this investigation. Furthermore, it is unlikely that a badly corroded pile would have the same surface strength as the pristinely damaged piles tested in this program. Therefore, the testing program is relative to initial bonding strengths under nearly ideal conditions.

It is recognized that the formed surface will unlikely be encountered in the field and it was assumed that the most likely condition would resemble the chipped surface. However, debonding most probably propagates from the edges of the repair where smooth surfaces are common. To this end, Phase II testing will examine the instrumentation of the interface bond and shear transfer mode.

8.6 Conclusions

Repair systems are effective in strengthening distressed piles as long as the bond strength can be maintained. The mechanical bond provided by the irregular surface of the chipped specimens generally supported higher loads prior to debonding than did the formed

surfaces. Providing a suitable bond mechanism in a pile repair is the primary critical factor for improvements in the ultimate strength in repaired piles.

Providing reinforcement is beneficial in this pursuit, but to a lessor degree. In this study reinforcement provided 1.2 - 1.3 times more strength than the nonstructural counterpart.

9. PHASE II REPAIRS

9.1 Introduction

The goal of Phase II was to identify procedures and practices that would lead to improved performance of the repaired piles. As the overall performance of the Phase I repairs was very good, Phase II testing was naturally more limited. The tests involved a total of eleven specimens and five different schemes. Only axial tests were conducted as the performance of Phase I repairs were poorer for such loading. Generally, the repair procedures were similar for both phases.

The principal difference was the use of shear connectors (described in Section 9.2) and that of a promising new material (described in Section 9.3). In addition, instrumentation was modified so that the variation in strain in the repaired region could be captured (Section 9.4). The test matrix for Phase II is summarized in Section 9.5. An outline of the repair procedure and difficulties encountered is described in Section 9.6.

9.2 Mechanical Shear Connectors

Mechanical shear connectors have been effectively used for enhancing the bond between disparate surfaces to improve shear transfer. District IV [9.1] have proposed a repair scheme that permits the use of powder activated nails as shear connectors in conjunction with Class IV concrete. In this scheme powder activated nails are placed in a rectangular grid pattern spaced 3 in. on centers extending from just below the intended pile jacket top to three pile dimensions downward but not below the high water level. Four separate investigations were carried out in this phase to assess the efficacy of such connectors. Three used powder activated nails (see 9.2.1) and the fourth used steel dowels.

Powder activated nails come in limited sizes and therefore their use in the one-third scale model presented particular problems especially since spacings could not be smaller than three inch with additional minimum edge distance requirements. A total of six specimens were prepared using powder activated nails. Two simulated District IV repairs, i.e. the nails were attached to the top region only. This scheme had a total of twenty nails (Fig. 9.a). These specimens are referred to as 'PAL'. This stands for Powder Activated Leever method (in honor of Mr. Ralph Leever of District 4). Four others extended the pins to the *entire* repair zone. Two of these were structural, i.e. additional reinforcement was provided, referred to SMP (standing for Structural Modified Powder activated nails shown in Fig.

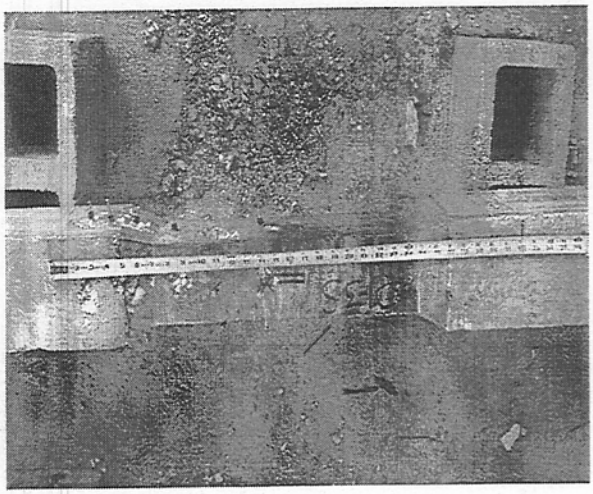

a. Powder activated nails at top only (PAL)

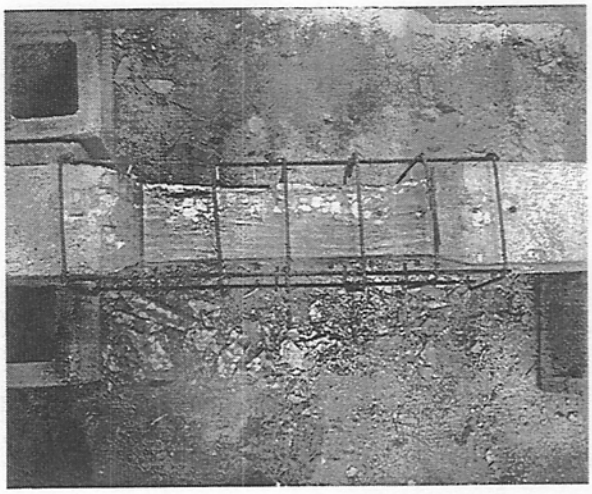

b. Structural repair with nails top/bot (SMP)

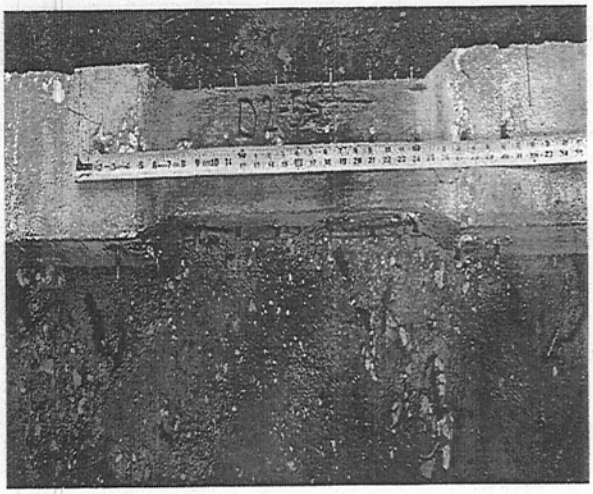

c. Non-structural - nails top/bot (MPA)

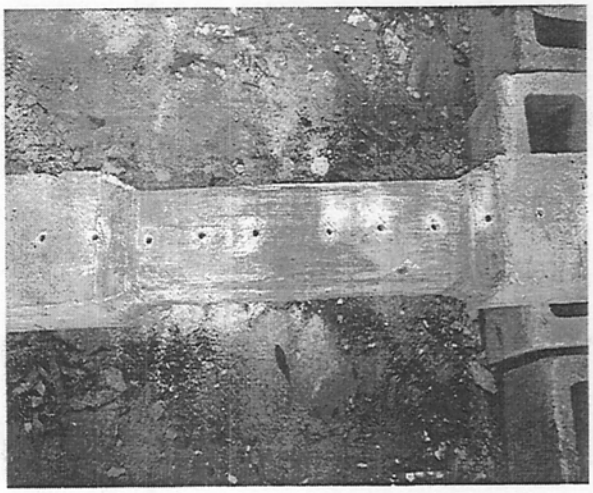

d. Holes for epoxy-doweled rebars (USF)

Figure 9.1 Repair Schemes Investigated in Phase II.

9.1b). The remaining two were non-structural referred to as MPA (standing for Modified Powder Activated shown in Fig. 9.1c).

Inspection of Fig. 9.1 shows that only a single line of powder activated nails could be installed to comply with the manufacturer's recommendation. The first nail was driven along the centerline of the pile two inches above mid height. The remaining fasteners were spaced at 3 in. intervals. These nails were placed on each of the four faces. For SMP and MPA the twice the number of nails, i.e. forty, were required.

9.2.1 Powder Activated Nails

The steel pins used in three sets of repairs, PAL, MPA, and SMP were 0.3 in. head diameter driven pins. These were 2 in. long, with a shank diameter of 0.143 in and were installed with a low velocity, semi-automatic .27 caliber tool. More details on the installation of these pins are reported in Section 9.6.

The load capacity of a powder actuated fastener installed in concrete is dependent on factors such as strength of the base material, hardness and concentration of the aggregate, dimensions and embedment depth. The manufacturer's design manual directly provides tables that lists ultimate load values for different conditions. Primarily they are listed for four different concrete strengths and three different embedment depths for the fastener [9.2]. Table 9.1 summarizes ultimate loads corresponding to 1 in. embedment in 5000 psi concrete that was closest to the repairs that were carried out.

Table 9.1 Powder Activated Nail Capacity [9.2]

Embedment Depth	5000 psi Concrete	
	Tension	Shear
1 in.	870 lbs.	1500 lbs.

In addition to the powder activated shear connectors, an identical set of non-structural repairs were carried out using 2 in. dowel rods fabricated out of the #2 bars (see Fig. 9.1d). The dowels were spaced at the same interval (3 in.) as the powder activated nails and extended over the entire repair region. This series is named USF and utilized epoxy to anchor the bars into the core of the pile in *pre-drilled* holes. The particular epoxy was selected from an approved FDOT material list and is suitable for underwater application of dowel pins and anchors (see Section 9.2.2).

9.2.2 Epoxy For Dowel Rebar

The epoxy used in the USF series was Allied Gold A-1000. This material was purchased from Allied Fastener and Tool, Lake Worth, Florida. The two in. long #2 bars were embedded 1 in. into the core pile. Technical data and design criteria is quite detailed for different lengths of embedment of reinforcing bars starting with #3 bars on up to #11's. The embedment depths indicated on these charts begin with depths of 2 1/4 in. and therefore do not pertain to this application.

Table 9.2 provides data on *ultimate* capacities of epoxied pins. These values are reported for 1/4 in. diameter anchor embedded with 1 in. embedment depth in 6000 psi concrete. The allowable loads are obtained by reducing the values in Table 9.2 by a factor of four. Note that the tension capacity of the stud is undoubtedly limited by the pullout bond strength of the bar protruding into the repair. In other words it is doubtful that this small 1/4 in. diameter bar will be developed with four diameters of embedment length.

Table 9.2 Ultimate Anchor Rod Capacity [9.3].

Anchor Size	Embedment Depth	6000 psi Concrete	
		Tension	Shear
1/4 in.	1 in.	2210 lbs.	2465 lbs.

9.3 PROTECRETE Repair

A new product, PROTECRETE-CDS, was also tested in Phase II. PROTECRETE is a concrete densifier seal that may be used in conjunction with a mix-water conditioner [9.4] . It needs to be sprayed on to the repair surface prior to addition of the filler material (Class IV concrete). The mix-water conditioner is added to the filler concrete in accordance with the manufacturer's specifications. PROTECRETE was tested because of the promising results obtained from tests conducted at the University of Illinois at Chicago [9.5]. It was thought that the sealer would improve the characteristics of the interface that would lead to improved performance of the bond between the old and new concrete.

The two specimens repaired using PROTECRETE were identified by the label PRO. Only one specimen remained and this was used as a control for all five sets of repairs that were carried out. This control was labeled CNL-1 and was similar to the PRO repair set in that no shear connectors were present. However, the series named PRO utilized a different repair mix design.

9.3.1 Protecrete Concrete Mix

The concrete used in the PRO series was batched near the concrete lab in two separate batches. A proprietary product supplied by PROTECRETE, Mix Water Conditioner, was used in this series. Each batch produced enough material for a single repair and four 6 in. cylinders. This mix design is presented in Table 9.3.

Table 9.3 Concrete Batch Design for Protecrete Mix.

Item	Quantity per batch
Cement (Type I)	57.8 lbs
Coarse Aggregate (#89 Crushed Limestone)	90 lbs
Fine Aggregate (Silica Sand)	109.2 lbs
Water	32.6 lbs
Protecrete Mix Water Conditioner (MWC)	5.8 oz
Water/Cementitious Ratio	0.56
Slump Range (in.)	7-9 in.

9.4 Strain Instrumentation

Each of the piles was instrumented with strain gages in locations similar to that in Phase I. These locations include the four faces one foot from each end and the exterior surfaces of the repair at mid height. All of these gages were mounted with epoxy instead of the fiberglass resin which was used in phase 1. This accommodated the installation of gages on vertical surfaces.

Some questions remained from the previous phase regarding the behavior of the repair system. These questions centered around the mechanics of the bond or load transfer. It appeared prudent to monitor strain data from various locations. Therefore, four additional gages were mounted in three different configurations for Phase II testing.

On four of these piles the gages were mounted on the core at the mid height. These four specimens had surfaces suitable for the installation of gages following the installation of the shear connectors. The four specimens with interior gages were CNL-1, MPA-1, PRO-1, and USF-1. These internal gages corresponded in location to the external gages on the repair surface and were separated by the thickness of the repair.

The installation of powder activated nails prevented mounting gages in this same region on two of the specimens. On these two piles the additional gages were located on the exterior Northern face of the repair. These additional gages were located at nine and 15 inches above and below the central gage. The two specimens that were configured as such are PAL-1 and SMP-1. This configuration is referred to as "5 level".

Each of the five series tested with suffix-2 had pairs of gages mounted one foot above and below the center gage on both the North and South faces. The nomenclature used for this strain gage configuration is "3 level".

9.5 Test Matrix

Phase II tests were carried out in concentric loading only with formed damaged surfaces. Recall that the axial test results of nonstructural repairs posted negligible strength gains. Also recall that the structural repair had approximately 1.3 times more capacity than its nonstructural counterpart. There was only one series of structural repair in Phase II, SMP, which was carried out on a surface prepared similar to the MPA series. The test matrix is presented in the following table that includes the instrumentation schemes unique to this phase. This is explained in the next chapter.

Table 9.4 Phase II Test Matrix.

Type of Test Specimen	**Test ID**	**Instrumentation**	
	Prefix	**-1**	**-2**
Structural Repair with P.A. Nails	SMP	5 level	3 level
Nonstructural Repair with Epoxied Pins	USF	internal	3 level
PROTECRETE Densifier and MWC	PRO	internal	3 level
P.A. Nails in Upper Half of Repair	PAL	5 level	3 level
P.A. Nails in Both Halves of Repair	MPA	internal	3 level
Non-Structural Repair Formed Surface	CNL	internal	
Totals		11	

9.6 Repair Procedures

The five repair systems utilized three different repair procedures - the first installed the powder activated nails, the second involved epoxying the dowel rebars and the third used PROTECRETE. Fig. 9.2-9.3 contain several photographs of the repair.

9.6.1 Powder Activated Nails

A total of six piles in the PAL, SMP and MPA series used powder activated nails as shear connectors. While these could be installed with the piles in the vertical position, in this study they were laid out on the ground and the positions of the nails was marked. A semi-automatic tool with .27 caliber powder load was used to install the nails. Prior to firing, the fastener with an attached spacer is inserted in the end of the barrel. Pressure is applied to the barrel through the handle. Squeezing the trigger advances the firing pen which activates the powder. A piston is propelled by the expanding gases into the fastener driving it into the base material.

Selecting the proper power load is critical in the success of installation. Naturally a load powerful enough to provide the desired embedment depth is necessary. However, too much of a load can damage the core pile and the surrounding surface. The power levels range from 1 to 6 with six as the highest level. The load levels used were 4's and 5's bearing the colors of yellow or red respectively. The appropriate load level was selected at the discretion of the operator.

Great care was taken into placement of these pins. However, there were situations which prevented the precision of placement. For example an attempt to set a pin using a yellow load was unsuccessful. Using a more powerful red load on this specific location would often produce more surface damage and a spoiled pin. In this case the pin was installed as close to the intended location as practical. Occasionally, the setting of a pin would damage the core pile. This damage was manifested in either a spall or a crack. Subsequent pins would then be set using a lower load level.

The two specimens with structural repair were fitted with the reinforcing cage after the powder activated pins were installed. These structural repairs were conducted on two of the four specimens with 40 powder activated pins. The plastic spacers were removed from all of the pins prior to the installation of the repair material.

9.6.2 Doweled Rebars

Two specimens in the USF series were provided with doweled rebars. A series of 3/8 in. holes were drilled at 3 in. intervals at marked locations on the two specimens. These holes were approximately 1 in. deep. Following drilling operations the holes were cleaned

with an air blast to remove the dust. A two component epoxy was dispensed with a manual cartridge tool through a mixing nozzle into the prepared hole. This tool was withdrawn as the drilled hole was being filled. Two inch dowel bars were then inserted into the blended epoxy with a twisting motion. The epoxy was then allowed to cure.

9.6.3 Protecrete

Protecrete Concrete Densifier Sealer was used on two of the specimens. This material was applied to the core pile using a pressureized sprayer. A total of two applications were applied approximately 10 minutes apart. This material was donated in by its manufacturer, Applied Concrete Technology of Arlington Heights, Illinois. It was applied by a manufacturers representative. The single control specimen had no additional preparation.

The repair material was cast on nine of the specimens on June 4th 1999. Eight of these specimens had mechanical shear connectors and a single control. Each of the nine repairs used Class IV concrete. The concrete was provided by Ewell Ready Mix.

The two repaired specimens were cast on June the 18th, 1999. A modified mix design resembling the Class IV mix was used. Additional water was incorporated consistent to the manufacture's recommendation. Each repair was cast from a separate mix batched with a bag mixer. Nearly six ounces of Protecrete Mix Water Conditioner was used in each of these batches. This material was donated in by its manufacturer, Applied Concrete Technology of Arlington Heights, Illinois.

9.6.4 Specifications

The specifications used to repair specimens in Phase II were very similar to those for Phase I excepting for the manner in which the surfaces were prepared. The following is a complete summary of the steps used:

1. Surfaces prepared as indicated.
2. Application of appropriate load using the pre-load simulators fitted for each repaired pile.
3. Maintenance of full water level inside the forms for a minimum of two days.
4. The orientation of the piles during repair was nearly vertical.
5. Curing occurred with the forms intact for a minimum of 27 days.
6. The repaired specimens with load simulators were instrumented and loaded.
7. Load simulator removal followed an equivalent load impressed at testing.

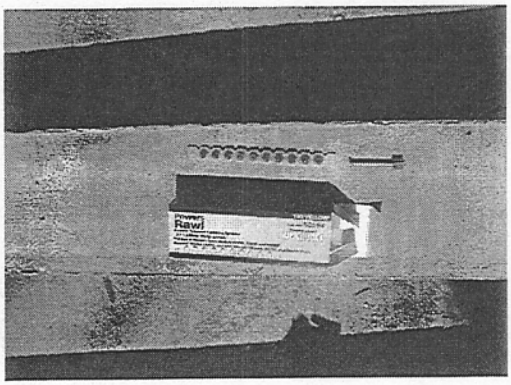

Powder Activated Charges

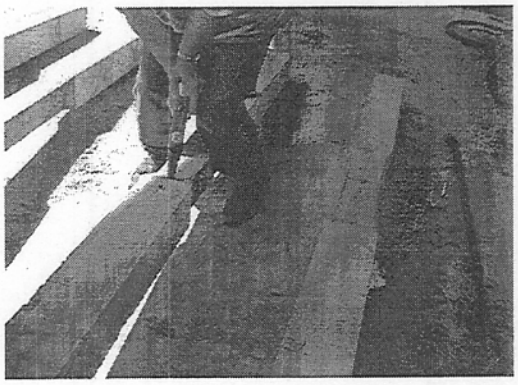

Installing Powder Activated Nails

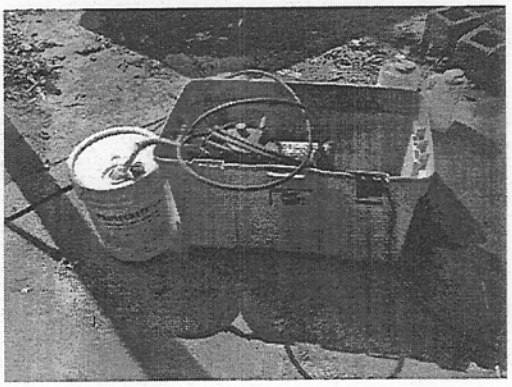

Spray Device for PROTECRETE

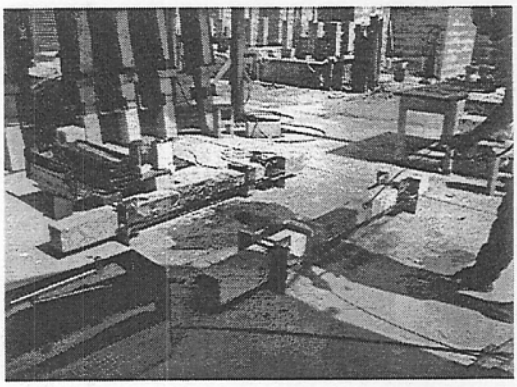

Spraying PROTECRETE-CDS

Adding PROTECRETE-MWC

Batching for PROTECRETE

Figure 9.2 Repairs of PROTECRETE.

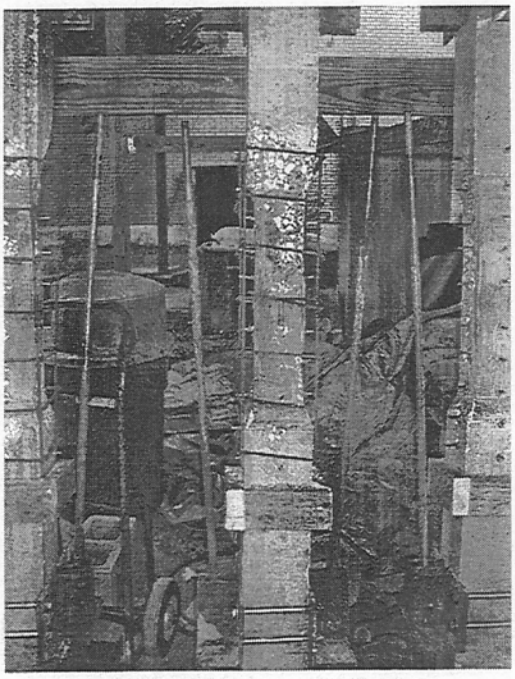

Structural Repair - SMP Series

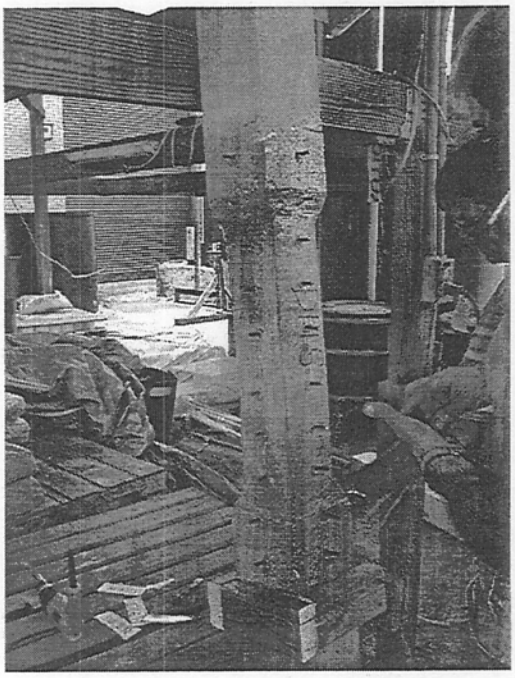

Epoxied Rebars - USF Series

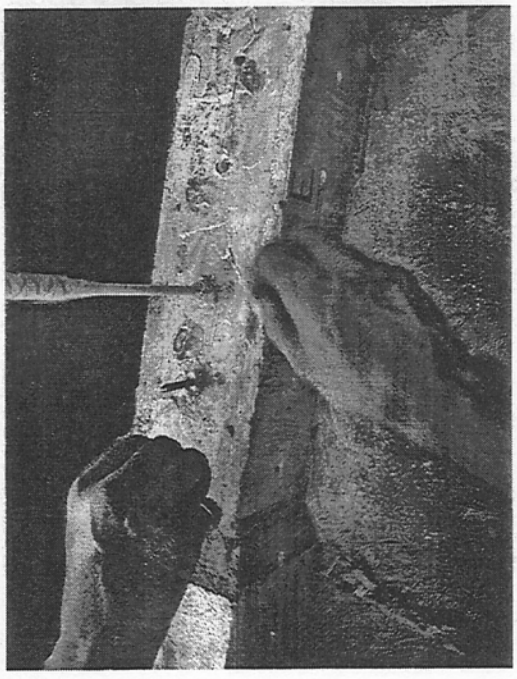

Epoxying Dowels

Epoxy Gun with Mixing Nozzle

Figure 9.3 Repairs of SMP and USF Series.

References

9.1 Leever, R. (1999). Copy of Integral Pile Jacket Drawing, Florida Department of Transportation, District IV.

9.2 Power Fastening, Inc. (No date). Fastening Systems Design Manual, Second Edition, New Rochelle, NY, p. 38.

9.3 Allied Fastener & Tool (No date). Allied Gold A-1000 Design Manual, Lake Worth, FL, pp. 12-15.

9.4 Applied Concrete Technologies, Inc. (No date). Arlington Heights, IL, Technical Data Sheet for PROTECRETE-MWS, PROCRETE-CDS..

9.5 Issa, M. A., Johnson, D. T., Issa, M.A., Faraj, M. and Bickers, R. (1998). "Mechanical Properties and Durability of High Performance Protecrete Concrete," Symposium, Proceedings on Performance of Concrete Structures in the Arabian Gulf Environment, Dhahran, Saudi Arabia, November, pp. 37-49.

10. ASSESSMENT OF PHASE II RESULTS

10.1 Introduction

This chapter presents the results from the concentric load tests conducted in Phase II. All eleven specimens tested were sections where the repair had been carried out on the formed surfaces. Five different repair schemes were examined, each involving two specimens. These included structural repairs (Type V), non-structural repairs (Type II) and a single (Type II) repair which served as a control. The results are evaluated with respect to the capacity of the undamaged controls that were tested in the first phase.

The test setup in Phase II was identical to that in Phase I described in Section 7.2. Details of the specimens tested and information on the additional strain gages provided appear in Section 10.2. The ultimate capacity results are presented in Section 10.3. The interpretation of the information from the additional gage instrumentation is discussed in Section 10.4. The principal conclusions and observations from Phase II testing are summarized in Section 10.5.

10.2 Test Program

The focus of Phase I testing was to determine if current repair methods enhanced the ultimate strength of repaired piles. Generally, strength gains were reported in all cases. However, the non-structural repair carried out on a formed surface tested axially posted minimal gains.

The focus of Phase II testing was to identify measures which could improve the efficiency of pile jacket repairs. As described in the previous chapter, shear connectors were utilized on four pairs of the five repair schemes that were investigated. The remaining pair of specimens were treated with a material believed to strengthen the existing pile core and improve certain bond characteristics of the repair material.

Details of the 11 specimens tested are summarized in Table 10.1. In each of the 11 repairs the surface utilized for the bonding interface was characterized as formed damage. A full explanation of the nomenclature used to identify the specimens is presented in the previous chapter (see Section 10. 2). Table 10.1 also provides information on the strain gages used on the specimens.

Table 10.1 Specimen Details.

Type of Test Specimen	Specimen	Interface Gage	No of Exterior Gages/face
Control - no shear connectors	CNL-1	Yes	3
Structural Repair with powder activated shear connectors over the entire repair zone but no strands cut	SMP-1 SMP-2	- -	5 3
Non-Structural Repair with epoxied rebar shear connectors over the entire repair zone	USF-1 USF-2	Yes -	- 3
Non-Structural Protecrete Repair with no shear connectors	PRO-1 PRO-2	Yes -	- 3
Non-Structural Repair with powder activated shear connectors from top of jacket to above high water line (District IV option)	PAL-1 PAL-2	- -	5 3
Same as above excepting that powder activated shear connectors extended over the entire region (Modified District IV option)	MPA-1 MPA-2	Yes -	- 3
Total	11		

Inspection of Table 10.1 shows that no shear connectors were provided for the control (CNL-1) or for the PRO specimens. Thus, a direct comparison of the capacities of these piles would provide an index of the improvement that was achieved by using the new material. The remaining specimens were all provided with shear connectors that were either powder activated (SMP, PAL, MPA series) or used epoxied rebars (USF).

One important difference may be noted for the structural repairs: unlike Phase I where strands where cut prior to the installation of the reinforcement cage, in this phase no strands were cut. As a result, comparison of the results from the MPA and SMP series directly provide an index of the confinement provided by the reinforcement and ties to improve the interface bond between the pile core and the repair material.

10.2.1 Instrumentation

The set-up, testing and instrumentation to measure displacement was identical to that used in Phase I as described in Sections 6.2-6.3. However, additional gages were attached

to gain a better understanding of bond transfer and the mechanism of failure. The original intent was to place gages at the repair interface in *all* the specimen types. Unfortunately, the powder activated nails ripped the concrete surface sufficiently to make this task impossible (see Fig. 10.1). Consequently, such gages could only be provided in some of the test specimens. For those specimens where interior gages could not be provided, additional gages were attached symmetrically on the exterior face(s). Table 10.1 provides a summary of this information.

Inspection of Table 10.1 shows that strain gages were mounted using three specific schemes. In the first scheme, a single gage was provided at the mid-point of each of the interfaces prior to the repair. The specimens instrumented in this manner were CNL-1, USF-1, PRO-1 and MPA-1. As a gage was also placed at the corresponding exterior location, the load at which debonding occurred at the mid-height location could be directly assessed. For such specimens, no additional strain gages were affixed on the exterior repair surfaces.

The second scheme was used in cases where no interface gage had been provided. In this case, three gages were attached symmetrically on two opposite exterior faces of the repair - one at mid-height and two others one foot from the ends of the repaired zone. The specimens instrumented in this manner were the ones with a suffix 2, i.e. SMP-2, USF-2, PRO-2, PAL-2 and MPA-2. Where three gages were provided, specimens are referred to as '3 level'.

The final scheme was similar to the previous scheme excepting that five gages were placed instead of three with the specimens being referred to as '5 level'. In this case, the gages were bonded to a *single face*. The gages were equally spaced and located symmetrically with respect to the center line with the first and last ones being 6 in. from the ends of the repair zone. Only two specimens were prepared in this manner. These were SMP-1 and PAL-1.

10.2.2 Specimen Preparation

Prior to the installation of the repair system the cross-sectional dimensions in the repair zone were measured. Additional measurements of the outside dimensions of the repair and its position in the pile were recorded prior to testing. The calculated cross sectional areas summarized in Table 10.2. correspond to the mid-height location.

As before, each of the 11 specimens was repaired under simulated loads. The procedure for the removal of the load simulators was identical to that used in Phase I. A target load of 20 kips was applied and maintained throughout the removal of the preload hardware. Under this sustained load the strain gages were referenced to zero. The load cell readings had a sensitivity constant error (0.8524) as in the previous phase. The actual load applied was closer to 17 kips.

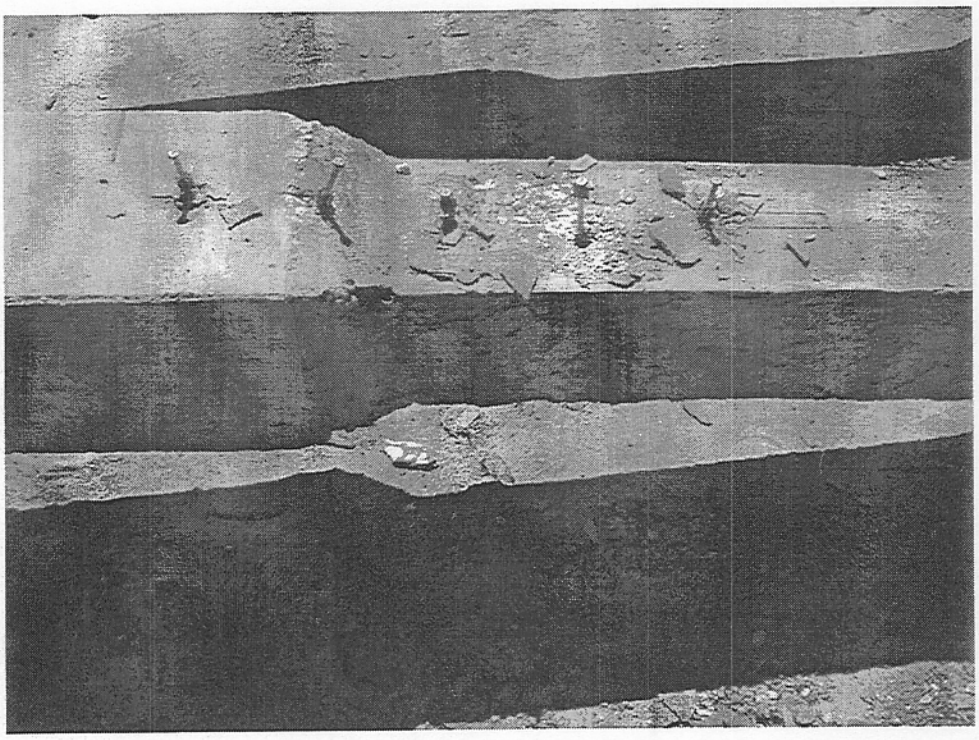

Figure 10.1 Damage to Surface by Powder Activated Nails.

Table 10.2. Cross-Sectional Area of Specimens in Phase II.

Item #	Test Type	Specimen	Gross Area in^2	Core in^2	Area of in^2
1	CNL-1	D2-9	75.5	21.1	54.4
2	SMP-1	D1-6	77.1	20.3	56.8
3	SMP-2	D2-6	77.1	20.8	56.3
4	USF-1	D1-1	74.9	20.3	54.6
5	USF-2	D1-2	76.6	21.1	55.5
6	PRO-1	D2-1	74.9	20.3	54.6
7	PRO-2	D2-2	76.0	20.8	55.2
8	PAL-1	D2-3	76.1	21.4	54.7
9	PAL-2	D1-3	75.5	20.3	55.2
10	MPA-1	D1-5	76.1	21.4	54.7
11	MPA-2	D2-5	77.1	22.6	54.5

10.3 Results

This section presents results from the six series of tests conducted in Phase II and compares the results with the axial capacity of undamaged piles obtained previously. Table 10.3 provides a summary of the ultimate load values. The results in this table are also presented in a bar graph in Fig. 10.2.

Table 10.3 provides information on the individual failure load, the average failure load and the *average* failure load from each of the six series as a percentage of the *average* of the three undamaged controls from Phase I.

Table 10.3. Summary of Phase II Test Results.

Test#	Type	Specimen	Failure Load kips	Average kips	% U.Control	% Phase I
1-4	Controls	Phase I		239.0	100.0	
34	NS Control	CNL-1	132.8	132.8	55.6	
36	Type V	SMP-1	177.6			na
40	Type V	SMP-2	175.7	176.7	73.9	
32	NS - Rebar	USF-1	166.2			
39	NS - Rebar	USF-2	167.4	166.7	69.8	+12.1
35	NS-No nails	PRO-1	160.5			
41	NS-No nails	PRO-2	159.8	160.2	67.0	+7.7
37	NS-PA nails	PAL-1	153.6			
42	NS-PA nails	PAL-2	149.4	151.5	63.4	+3.3
33	NS-PA nails	MPA-1	135.3			
38	NS-PA nails	MPA-2	143.5	139.4	58.3	-6.3

NS - Non Structural (Type II) ; PA - Powder Activated

Inspection of Table 10.3 shows that the greatest capacity increase was for the structural repairs (SMP) that had 73.9% of the capacity of the undamaged control. This was however, lower than that realized in Phase I (see Table 6.3) presumably because of the effective prestress that remained. The doweled epoxy bars (USF) and PROCRETE (PRO) provided the next highest increases (12.1% and 7.7% increases respectively over Phase I). The worst performance was the modified powder activated scheme (MPA) where powder activated nails were driven over the entire repaired region - this showed a 6.3% *decrease.* District IV's original scheme (PAL) fared better and showed a modest increase of 3.3% over Phase I results (see Table 6.3).

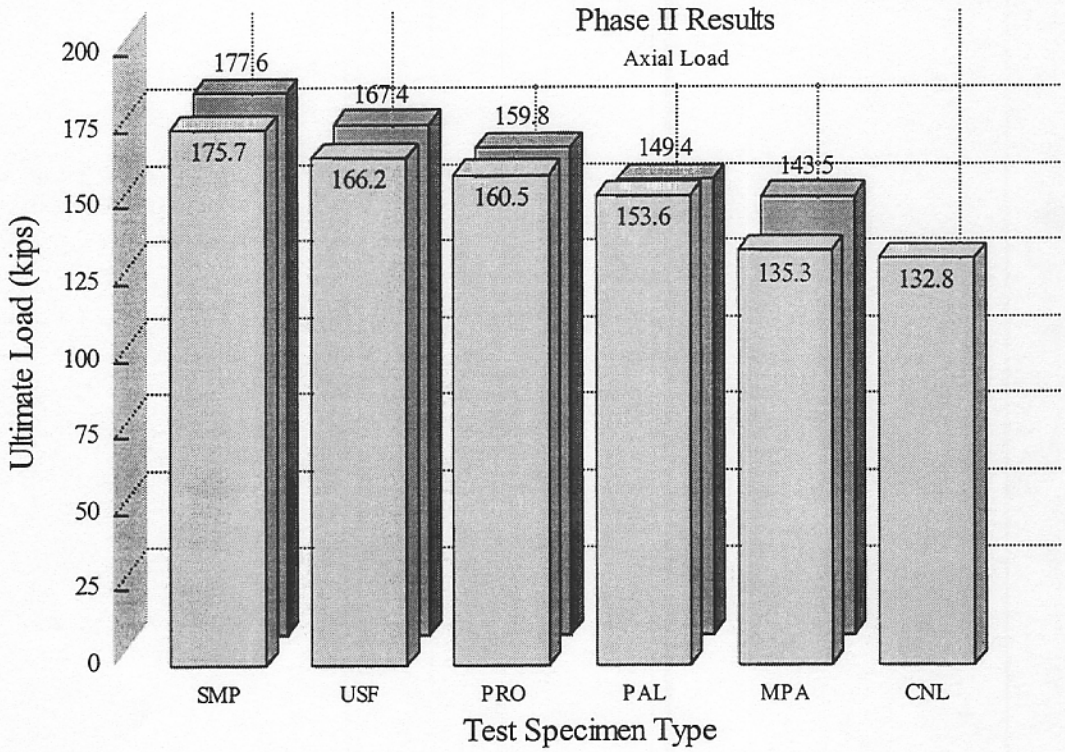

Figure 10.2. Summary of Phase II Capacities Under Axial Loading.

Failure modes for the repaired specimens are shown in Fig. 10.3-10.7. They are in the same order as the specimen listing in Table 10.3. As for Phase I, the structural repair jacket did not disintegrate though it was cracked (Fig. 10.3). The jackets in the other repairs fell in chunks (Fig. 10.4) or nearly completely in other cases (Fig. 10.5-10.6). To assess debonding, a detailed analysis of the strain gage data is presented later in Section 10.4. Plots of load vs strain are omitted to be prevent clutter and may be found in Appendix C.

10.3.1 Repaired Control

Due to the limited number of suitable specimens available for repair, a single control was prepared using the same material as the four other sets. The ultimate load at failure for this specimen was 132.8 kips. This load level is compared to the average values of the undamaged controls from Phase I. The repaired specimen had 55.6 % of the average ultimate capacity of 239.0 kips recorded from the undamaged specimens. These values are reported in tabular form (see Table 10.4).

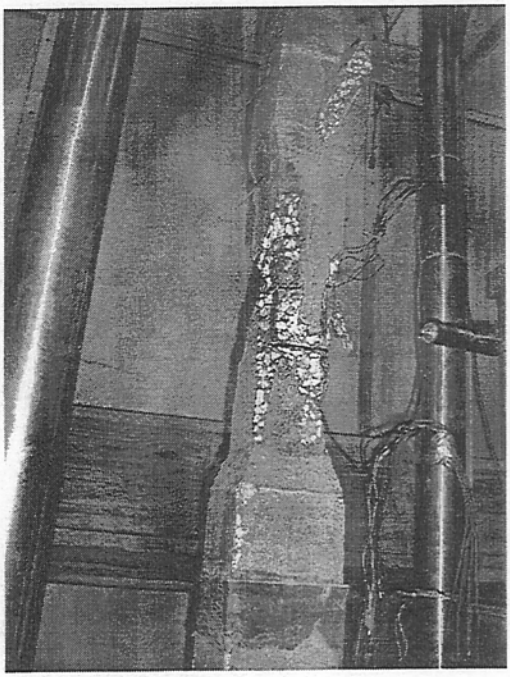

View of Failed Repaired Control

View of Jacket Bottom

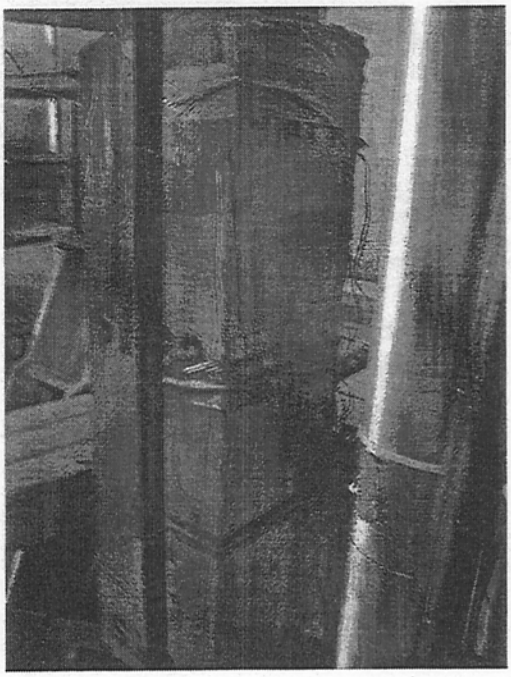

Note Splitting at Edges

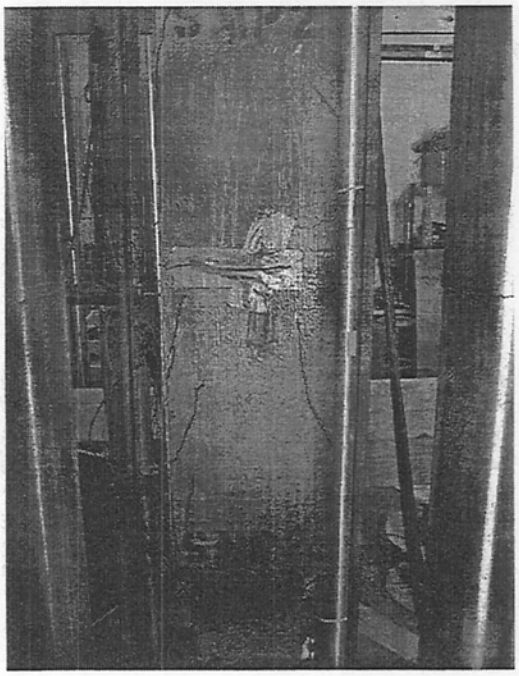

Failure Mode for SMP 2

Figure 10.3 Failure Mode of Control and SMP Specimen Under Axial Loads.

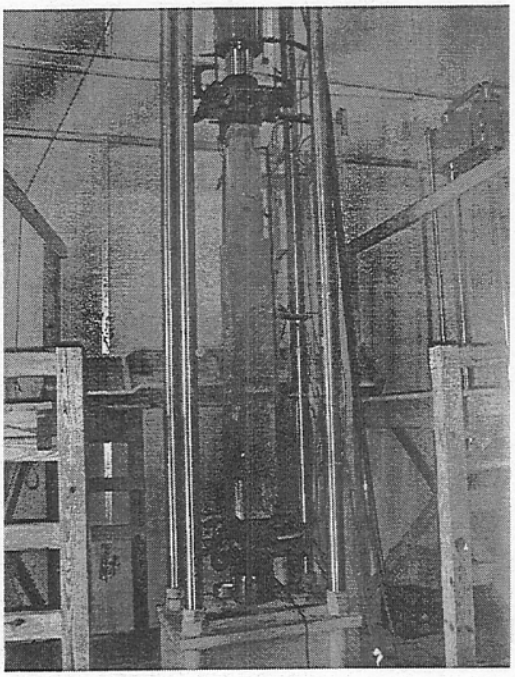

Test Set-Up

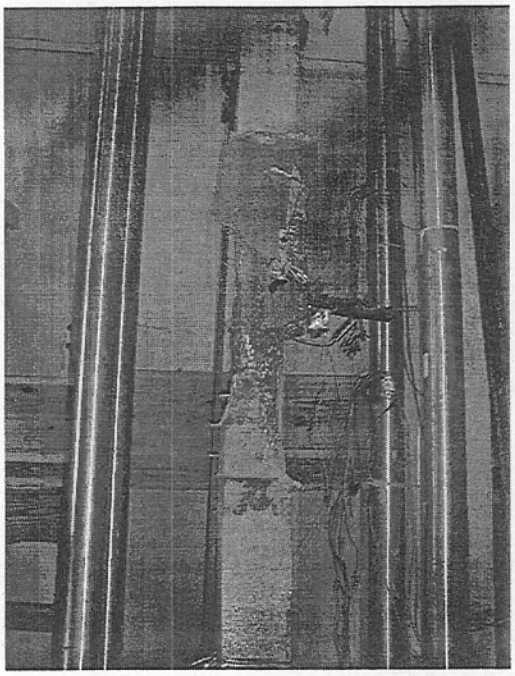

Failure Mode for USF-1

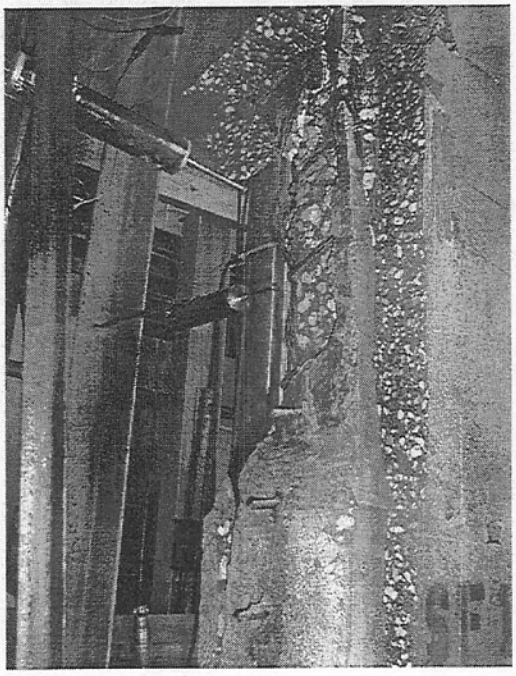

View of Jacket Bottom

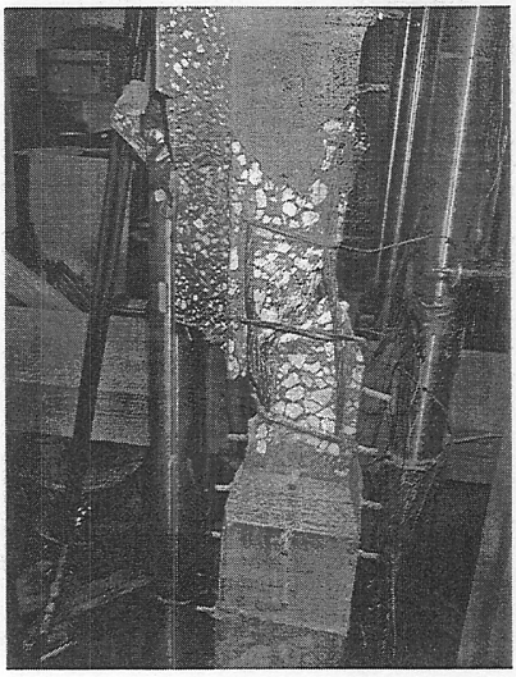

View of Failed Specimen

Figure 10.4 Failure Mode of USF Repairs Under Axial Loads.

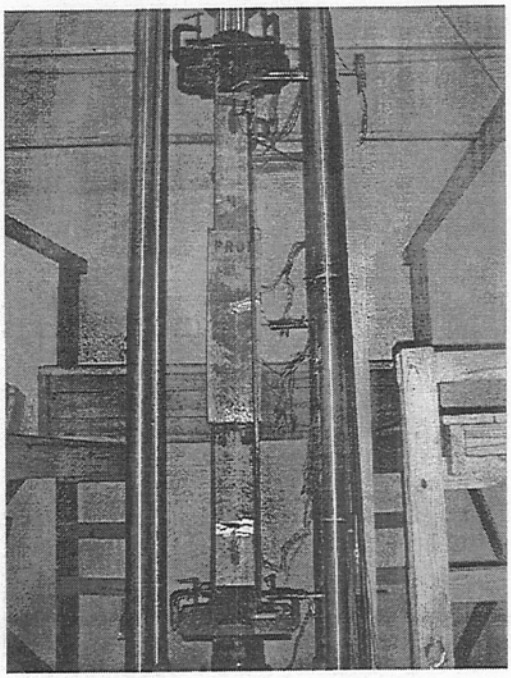

Test Set-Up - PRO 1

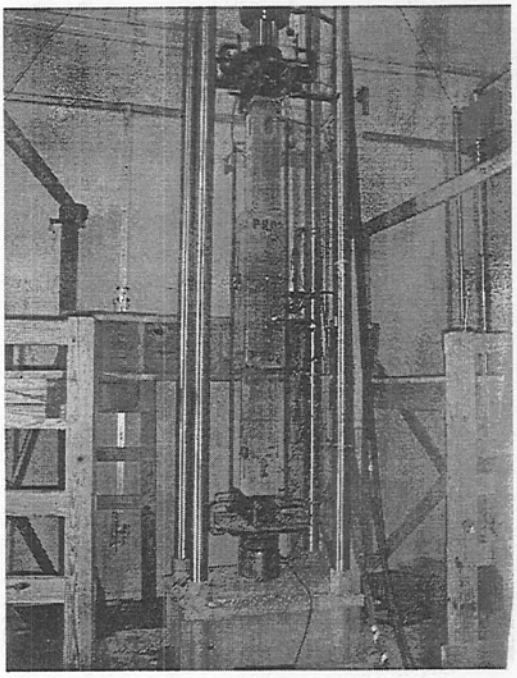

Test Set-Up - PRO 2

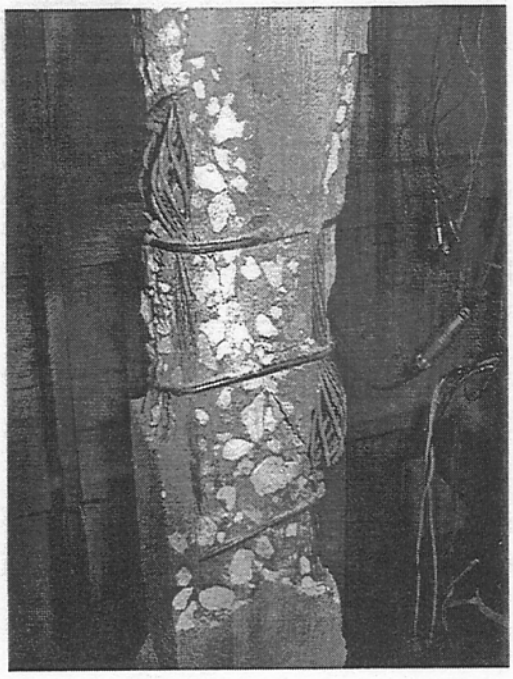

Note Core Failure

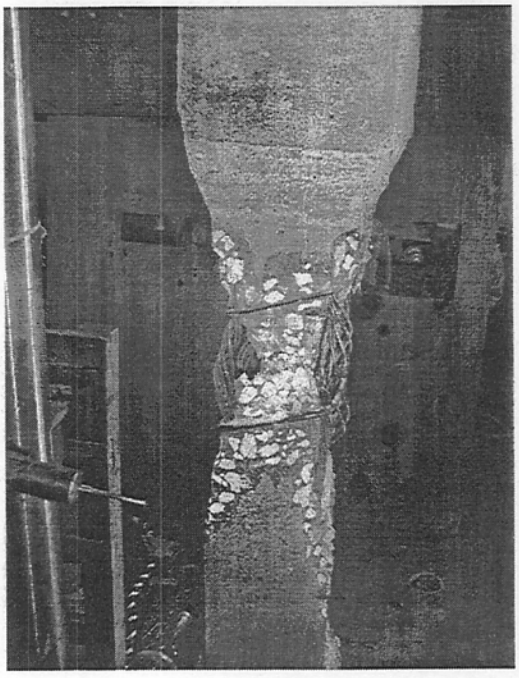

Buckling of Strands

Figure 10.5 Failure Mode of PROTECRETE Specimen Under Axial Loads.

View of PAL 1

View of PAL 2

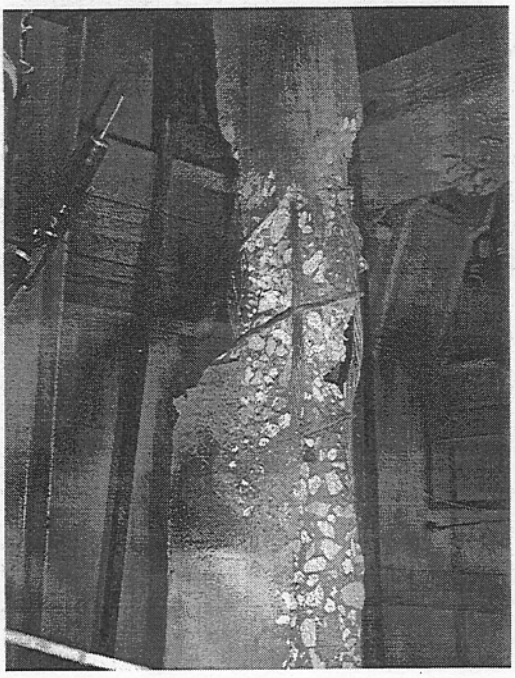

Jacket Partially Bonded at Bottom

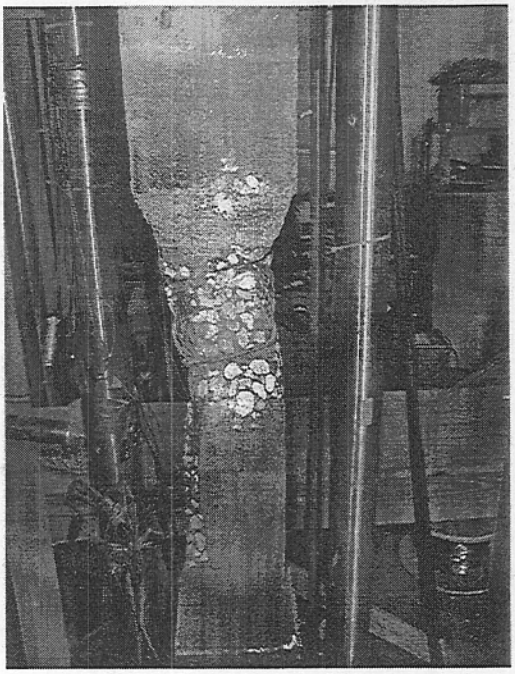

Note Failure Location at Top

Figure 10.6 Failure Mode of PROTECRET Specimen Under Axial Loads.

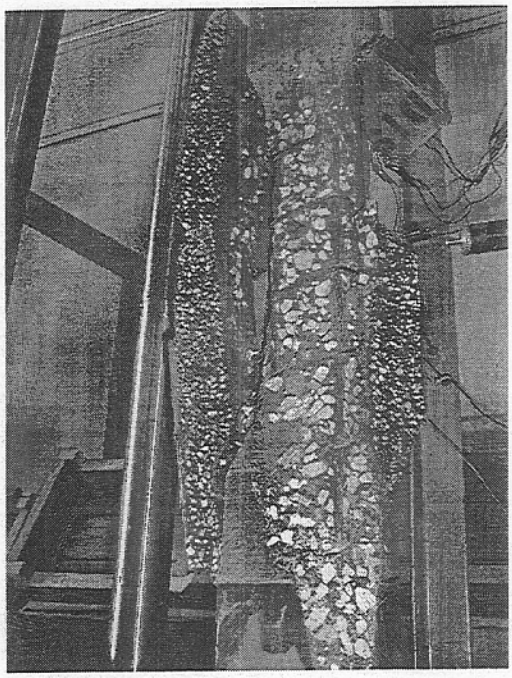

View of Failed MPA 1

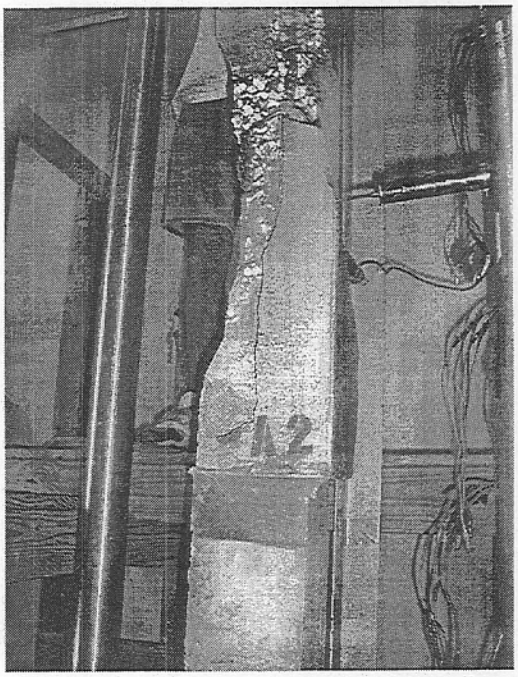

View of Failed MPA 2

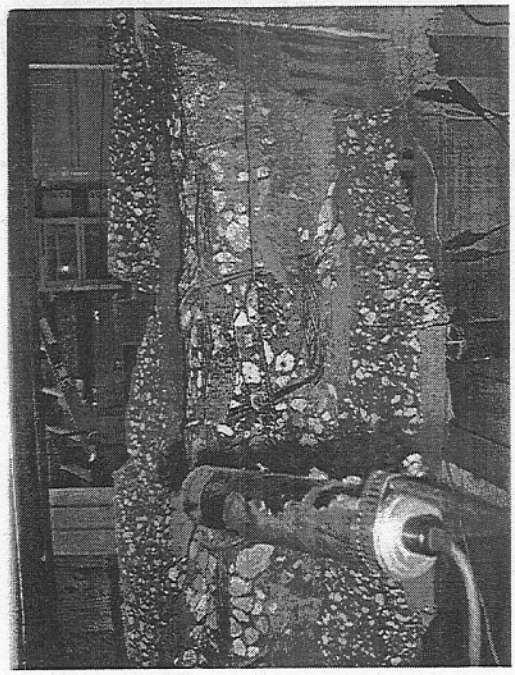

Note Damage Along Core

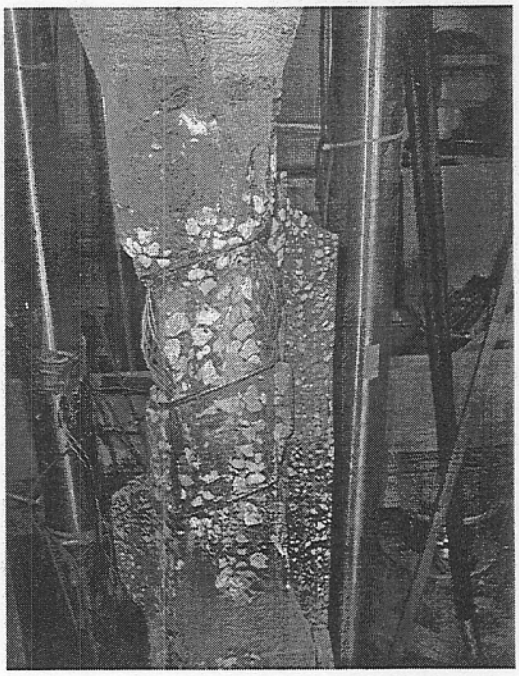

View of Damage

Figure 10.7 Failure Mode of MPA Specimen Under Axial Loads.

Table 10.4. Control Test Results.

Specimen	Test #	Debond Load	Ultimate Load	Debond % Ultimate	% Repaired Control	%Undamaged Control
Undamaged	Ph I	na.	239.0	na.	na.	100.0
CNL-1	34	111	132.8	83.6	100.0	55.6

At 111 kips the repair debonded from the core pile. This event occurred at 83.6% of the ultimate capacity of the single control. Evidence of debonding was provided by the disparity between the strain measurements at the interface and at the exterior both mounted at mid height. Additional evidence of debonding may be detected by the dramatic change in strain measured at the core and by changes in deflection or axial shortening. Plots showing variation of axial strain with load are shown in Fig. C.1.

10.3.2 Structural Repairs with Powder Activated Nails

A pair of structural repairs were carried out on piles whose surfaces were identical to the series MPA. Forty powder activated nails were installed on piles with formed damage. In addition, model reinforcement was placed representing the structural repairs that were tested in Phase I.

The SMP specimens failed at 177.6 and 175.5 kips. In terms of averages this was nearly 74 percent of the undamaged control and 133 percent of the repaired control. Compared to the sister series, MPA, this structural sibling posted 27 percent gains. Details on the MPA series are reported in Section 10.3.6.

Plots showing the axial strain variation with load may be found in Figs. C.2-C.3.

Table 10.5. Axial Test Results for Structural Repairs.

Specimen	Test #	Debond Load	Ultimate Load	Debond % Ultimate	% Repaired Control	%Undamaged Control
SMP-1	36	171	177.6	96.5	133.7	74.3
SMP-2	40	176	175.7	100.0	132.3	73.5
	Average	174	176.7	98.3	133.0	73.9

10.3.3 Non-Structural Repairs with Epoxied Rebars

A pair of non-structural repairs were performed on specimens that contained epoxied rebar studs. Forty dowels were fabricated from #2 bars studded the formed surface. The USF specimens failed at 166.2 and 167.4 kips. The averages of this series indicate the ultimate capacities to be nearly 70 percent of the undamaged control specimens.

The mechanical connectors did not appear to have much impact on increasing the debond loads. In Phase I this loading level fell consistently around 125 kips for the formed surfaces. For this pair of test the debond loads were 121 and 128 kips. The average ultimate capacity exceeded those in Phase I by 7.7%.

Plots showing the strain variation with load may be found in Figs. C.4-C.5.

Table 10.6. Axial Test Results for Dowel Rebar Repairs.

Specimen	Test #	Debond Load	Ultimate Load	Debond % Ultimate	% Repaired Control	%Undamaged Control
USF-1	32	121	166.2	72.6	125.2	69.5
USF-2	39	128	167.4	76.3	126.1	70.0
	Average	124	166.8	74.5	125.6	69.8

10.3.4 PROTECRETE Repairs

A pair or of non-structural repairs were conducted using unique procedures and materials in this phase. Prior to the repair the core surface was treated with a Protecrete - CDS. This densifier sealer was also applied to the external surface of the repair following the 28 day cure. Also a mix water conditioner was used in the repair mix. This series had no steel or connecters in the repair.

The PRO specimens failed at 160.5 and 159.8 kips. The debonding load for this pair averaged 115 kips. Nevertheless, this repair system provided 20 percent additional capacity compared to the single control. Similar tests in Phase I (NF) provided nearly zero additional capacity. The PRO repairs were 67 percent as strong as the undamaged controls. The ultimate capacity showed a 7.7% improvement over Phase I.

Plots showing the strain variation with load may be found in Figs. C.6-C.7.

Table 10.7. Axial Test Results for Protecrete Repair System.

Specimen	Test #	Debond Load	Ultimate Load	Debond % Ultimate	% Repaired Control	%Undamaged Control
PRO-1	35	120	160.5	74.5	120.9	67.2
PRO-2	41	111	159.8	69.1	120.3	66.9
	Average	115	160.2	71.8	120.6	67.0

10.3.5 Non-Structural Repairs with Powder Activated Nails At Top

A pair of non-structural repairs was installed on specimens with 20 powder activated nails. These pins were located in the upper portion only of the form damaged piles to agree with District IV's scheme.

The PAL specimens failed at 153.6 and 149.4 kips. This represents a 14 percent improvement compared to the control. This capacity is 63 percent of the undamaged piles used as controls. The debond loads were the highest of all non-structural repairs in this phase. The ultimate capacity showed a 3.3% increase over Phase I.

Table 10.8. Axial Test Results for Powder Activated Pins in Upper Half of Repair.

Specimen	Test #	Debond Load	Ultimate Load	Debond % Ultimate	% Repaired Control	%Undamaged Control
PAL-1	37	144	153.6	93.6	115.7	64.3
PAL-2	42	141	149.4	94.2	112.5	62.5
	Average	142	151.5	93.9	114.1	63.4

10.3.6 Structural Repairs with Powder Activated Nails At Top and Bottom

A pair of non-structural repairs were performed on specimens that had twice as many nails as the PAL series. The same pattern and spacing were used. However, both the top and bottom portion of the repair contained nails in this MPA series. This same spacing was used in the SMP repairs.

The test MPA-1 was conducted like all the other tests except for a single detail. The test data was only manually recorded. Hence, the failure load was estimated by those

individuals positioned at the monitoring station during the test. The data points plotted were obtained from the printout obtained at ten kip intervals up to 130 kips.

Table 10.9. Axial Test Results for Powder Activated Pins in Both Halves of Repair.

Specimen	Test #	Debond Load	Ultimate Load	Debond % Ultimate	% Repaired Control	%Undamaged Control
MPA-1	33	128	135.3	94.5	101.9	56.6
MPA-2	38	130	143.5	90.9	108.1	60.0
	Average	129	139.4	92.7	105.0	58.3

Table 10.10. Axial Test Result Summary of Phase II.

Test Series	Debond Load	Ultimate Load	Debond Percent of Ultimate	Percent of Undamaged Control
	kips	kips	%	%
Undamaged Controls	na.	239.0		100.0
Repaired Control	111	132.8	83.9	55.6
Structural Repair w/ PA Nails	174	176.7	98.3	73.9
NS Repair w/ Epoxied Dowels	124	166.8	74.5	69.8
Protecrete NS Repair w/o Nails	115	160.2	71.8	67.0
NS Repair w/ PA Nails in Top	142	151.5	93.9	63.4
NS w/ PA Nails Top & Bottom	129	139.4	92.7	58.3

10.4 Analysis of Strain Data

As mentioned earlier, additional concrete gages were attached to several of the specimens (see Table 10.1) that were tested. These included internal gages attached at the interface, and additional external gages on the repaired surface. This section presents an

10.4.2 Strain Variation - Three Readings

One specimen from each of the five repair schemes had additional strain gages fixed on two opposite faces to monitor strain variation in the repaired zone at three levels. These were at mid-height and symmetrical locations nine inches above and below respectively. These positions coincided with the top and bottom of the simulated damage (see Fig. 3.2).

A summary of the strain variation at the three levels at the respective debonding loads is contained in Table 10.12. In this table, strains at levels 1 and 3 are the average of two strain readings while those for level 3 (at mid-height) are averaged from four readings. Corresponding strain plots for the five specimens may be found in Figs. C.16-C.20.

Table 10.12 Strain Variation in Repair Zone.

Location	MPA-2 ($\mu\epsilon$)	USF-2 ($\mu\epsilon$)	SMP-2 ($\mu\epsilon$)	PRO-2 ($\mu\epsilon$)	PAL-2 ($\mu\epsilon$)
Top	175	227	218	128	177
Mid-Height	353	334	495	289	382
Bottom	294	294	190	254	141
Debonding Load (kips)	130	128	176	111	149

Inspection of Table 10.12 shows that the strains are lowest at the top and highest at the middle. In other words, the load is transferred *non-linearly* to the repair material. The strain variation is most pronounced in two of the three specimens using powder activated nails - SMP and PAL but not MPA. This could be because the powder activated nails could not always be installed uniformly with the same embedment at all the locations. This is supported by the more uniform distribution of strains in the USF repairs where there was far more uniformity in the placement of the doweled bars.

Confinement effects of the ties used in the structural repair appear to be small prior to debonding. Comparisons for the *same load* between the non-structural (MPA) and structural (SMP) repairs - identical but for the provision of a reinforcing cage (see Fig. 10.1) - confirm this. Assuming the strain variation as linear, for a load corresponding to 130 kips the strain in the SMP specimen at mid-height is (130)(495)/176 = 366 $\mu\epsilon$ vs 353 $\mu\epsilon$ in the non-structural repair MPA. This is not surprising because of the relatively large tie spacings used in the repair.

The debond loads detected at the various levels are tabulated in Table 10.13. All loads reported are in kips. For completeness, the failure load is also included in the same table.

10.4.3 Strain Variation - Three Readings

One specimen from each of the five repair schemes had additional strain gages fixed on two opposite faces to monitor strain variation in the repaired zone at three levels. These were at mid-height and symmetrical locations nine inches above and below respectively. These positions coincided with the top and bottom of the simulated damage (see Fig. 3.2).

A summary of the strain variation at the three levels at the respective debonding loads is contained in Table 10.12. In this table, strains at levels 1 and 3 are the average of two strain readings while those for level 3 (at mid-height) are averaged from four readings. Corresponding strain plots for the five specimens may be found in Figs. C.16-C.20.

Table 10.12 Strain Variation in Repair Zone.

Location	MPA-2 ($\mu\epsilon$)	USF-2 ($\mu\epsilon$)	SMP-2 ($\mu\epsilon$)	PRO-2 ($\mu\epsilon$)	PAL-2 ($\mu\epsilon$)
Top	175	227	218	128	177
Mid-Height	353	334	495	289	382
Bottom	294	294	190	254	141
Debonding Load (kips)	130	128	176	111	149

Inspection of Table 10.12 shows that the strains are lowest at the top and highest at the middle. In other words, the load is transferred *non-linearly* to the repair material. The strain variation is most pronounced in two of the three specimens using powder activated nails - SMP and PAL but not MPA. This could be because the powder activated nails could not always be installed uniformly with the same embedment at all the locations. This is supported by the more uniform distribution of strains in the USF repairs where there was far more uniformity in the placement of the doweled bars.

Confinement effects of the ties used in the structural repair appear to be small prior to debonding. Comparisons for the *same load* between the non-structural (MPA) and structural (SMP) repairs - identical but for the provision of a reinforcing cage (see Fig. 10.1) - confirm this. Assuming the strain variation as linear, for a load corresponding to 130 kips the strain in the SMP specimen at mid-height is (130)(495)/176 = 366 $\mu\epsilon$ vs 353 $\mu\epsilon$ in the non-structural repair MPA. This is not surprising because of the relatively large tie spacings used in the repair.

The debond loads detected at the various levels are tabulated in Table 10.13. All loads reported are in kips. For completeness, the failure load is also included in the same table.

Inspection of Table 10.13 indicates that the quality of the bond in the upper portion of the repair to be generally less superior to the lower portion.

Table 10.13 Debonding Load Variation in Repair Zone.

Location	MPA-2	USF-2	SMP-2	PRO-2	PAL-2	Average
Top	78 (60%)	93 (73%)	100 (57%)	100 (90%)	107 (71%)	71%
Mid-Height	130 (100%)	128 (100%)	176 (100%)	111 (100%)	141 (100%)	100%
Bottom	127 (98%)	150 (117%)	145 (82%)	120 (108%)	145 (103%)	102%
Failure Load	144	167	176	160	149	

All loads are in kips

The lower debonding load at the top indicates that debonding starts at the top and proceeds towards the bottom. The stress state at this location are more complex than at the middle where conditions are more uniform. Nonetheless, a likely cause for the lower load is weaker concrete arising out of bleed water rising towards the top.

The average debonding load was 71% of that at mid-height. ACI 318-99 uses a 30% penalty for situations such as those in this study where there is 12 in. or more of concrete below a rebar for the very same reason. Interestingly, debonding took place at higher loads at the bottom compared to the top.

10.4.3 Strain Variation - Five Readings

Two specimens were configured to accommodate strain readings at five levels along a *single* face of a repair. The gages were positioned symmetrically with respect to the mid-height of the repair zone at 6 in. on centers. As the distance between the first and fifth gage was 2 ft., these gages were located partly in the 3:1 transition zone (see Fig. 3.2).

As before, the strain variation and the determination of the manner in which the jacket debonded was of particular interest. These results are tabulated in Table 10.14. In this table, the level 3 strain values are the average of four readings unlike the remaining entries that correspond to a single gage. Corresponding plots may be found in Figs. C.21-C.22.

Table 10.14 Strain and Debonding Load Variation in Repair Zone.

Location	Strain Readings at Debond Load		Debond Load for Gage Level (kips)	
	SMP-1	**PAL-1**	**SMP-1**	**PAL-1**
12 in. above Mid-Height	53	236	100 (58.5%)	82 (54.7%)
6 in. above Mid-Height	437	479	167 (97.7%)	144 (96%)
Mid-Height	502	390	171 (100%)	144 (96%)
6 in. below Mid-height	252	434	125 (73.1%)	150 (100%)
12 in. below Mid-Height	101	172	90 (52.6%)	70 (46.6%)

Inspection of Table 10.14 shows that the trends observed previously for the three level (Table 10.12) readings are also repeated here. Thus, the strains are lower at the top and debonding starts at the top. However, there are some differences. The strain variation pattern for PAL-1 and SMP-1 are different - the distribution is more uniform. This could be because the powder activated nails were placed more evenly in this case.

The first and last gages are located outside of the damaged area. Inspection of Table 10.14 indicates that the strains are lower in this region. This is in part because they are located in the transition region where proportionately smaller loads are transferred by shear since some load can be directly transferred by bearing.

10.5 Conclusions

The capacity of the repair is enhanced if the core can transfer load to the repair material. This chapter showed that mechanical connectors can provide some increase provided the core is not damaged. Powder activated nails used in this study were found to damage the core and led to relatively poor performance. In contrast, doweled epoxy bars performed better. The PROTECRETE material also performed moderately well. From the practical standpoint, this would be the easiest to use.

Analysis of strain data showed that shear lag effects were minimal. Readings from gages attached at the interface and external gages showed very similar readings until debonding. The bond appeared to be the weakest at the top of the jacket presumably because of bleed water weakening the concrete. As failure was initiated at this location in many instances, measures that could reduce the water cement ratio could lead to improved performance.

11. FINITE ELEMENT MODELING

11.1 Introduction

This chapter presents results of numerical analyses conducted using the finite element program ANSYS. A three-dimensional finite element model was developed to predict the experimental results reported in Chapters 6, 7 and 10.

General aspects of the finite element model are described in Section 11.2. Material properties used in the analysis are discussed in Section 11.3. Models specific to Phase I study are presented in Section 11.4. This is followed by a discussion of the axial and bending test simulation results in Sections 11.5 and 11.6 respectively. Phase II models and results are presented in Sections 11.7 and 11.8 respectively. Finally, a brief discussion and conclusions based on the finite element results appears in Section 11.9.

11.2 Finite Element Model

The finite element analysis program, ANSYS (version 5.5) was used to analyze the columns. The models utilize SOLID65, an eight node, three-dimensional element with three degrees of freedom per node. This element is capable of cracking under tensile loads, and crushing under compressive loads. The status of the element, i.e., if it is cracked, uncracked, or crushed, is determined at each element integration point. The element can crack in three orthogonal directions at each integration point. Once cracking occurs, the finite element program modifies the stiffness by creating a plane of weakness normal to the *open* crack, thereby preventing load transfer in that direction. However, the crack can be *closed* due to compressive loads, and still transfer load in compression. Unlike cracking, once the element is crushed, the element can no longer transfer any loads. This is implemented in ANSYS by reducing the element stiffness to very small number once the element is crushed. The element can also model reinforcement. The reinforcement is assumed to be smeared uniformly along the specified direction in the concrete elements.

Due to modeling of cracking and crushing, the analysis is non-linear. This requires that the loads be applied slowly. Also, a fairly dense mesh is required to accurately model concrete under bending loads. The mesh density used for the analysis was selected based on preliminary studies and a typical mesh is shown in Fig. 11.1. The model shown has about 2400 nodes and 1800 elements. The number of nodes and elements for repaired columns is about 3600 and 2800 respectively.

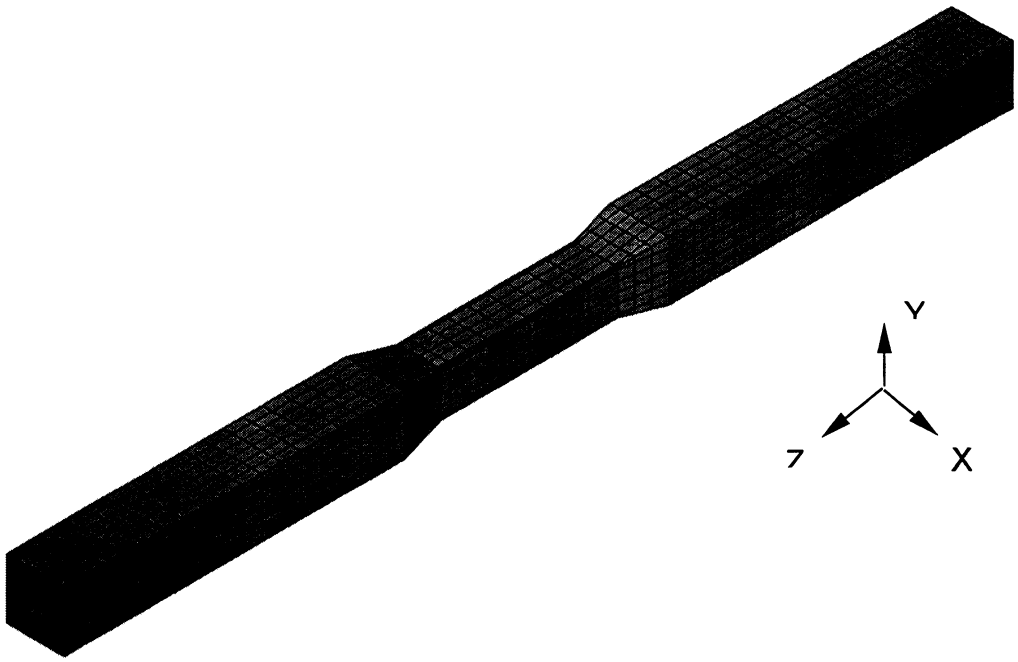

Figure 11.1 Typical Mesh.

11.3 Material Properties

The finite element analysis program requires that the geometry, loading, and material properties be specified. Geometry and loading are presented in Sections 11.4 and 11.7 for Phase I and Phase II results respectively. The material properties used for analysis are the same as presented earlier in Chapter 3 and 10.

Since the compressive strength of the concrete is above 6000 psi, it is considered to be high strength concrete. The modulus of elasticity of the concrete was calculated using the following equation from [11.1] for high strength concrete.

$$E = 40{,}000\sqrt{f'_c} + 10^6 \quad \text{(psi)} \tag{11-1}$$

where f'c is the compressive strength of the concrete in psi. The tensile strength of concrete was obtained using equation 11.2 [11.1] for high strength.

$$f'_t = 12\sqrt{f'_c} \quad \text{(psi)} \tag{11-2}$$

The modulus of elasticity and tensile strengths for ordinary concrete was found using the following equation [11.1].

$$E = 57{,}000\sqrt{f_c'} \quad \text{(psi)} \tag{11-3}$$

$$f_t' = 7.5\sqrt{f_c'} \quad \text{(psi)} \tag{11-4}$$

11.4 Phase I Models

Seven different types of columns were tested under axial load and bending during Phase I of this study. This section describes the finite element models that were used.

11.4.1 Geometry

The nominal dimensions of the undamaged, damaged and repaired column sections are shown in Fig. 2.1, Fig. 2.2 and Fig. 5.1 respectively. Although the actual dimensions vary slightly, for the purpose of the finite element analysis, all columns were modeled using the nominal dimensions. Only the dimensions of the damaged cross-sections with the chipped surface and columns with strands cut were based on actual measurements.

As stated previously, concrete was modeled using the element SOLID65 from the ANSYS element library. Prestressing steel and the spiral ties were modeled as smeared reinforcements in the concrete element. The effective prestress was taken as 1000 psi. The typical mesh used for the formed damage section is shown in Fig. 11.1.

11.4.2 Axial Test Boundary Conditions

The ends of the columns were pinned in the axial tests. This allowed the ends to rotate, but prevented any translation. This was simulated in the finite element model by restraining the translation of the center nodes at the top and bottom ends of the columns. The load was applied at the top end of the column as a uniform pressure, while the axial motion of the other end was restrained. In order to ensure that the load was distributed uniformly, a steel plate with 1 in. thickness was used in the test. This was modeled using a four node shell element (SHELL63) that was overlaid on the top and bottom surface of the column. This stiffens the ends and makes the axial displacement uniform. The top and bottom 6 in. of the column were modeled with higher strength material to simulate the confinement of the ends during the actual tests (see Fig. 6.1).

11.4.3 Bending Test Boundary Conditions

Rollers were used at the ends during bending tests to apply an eccentric load about

a single axis. Eccentric load was applied to the columns by placing the bottom roller at the centerline of the column, while offsetting the top roller end by 1.2 in. about the centerline. This was simulated in the finite element model as follows: the translation of the center nodes were restrained at both ends of the column. A uniform force was applied at the top end on to all nodes placed at 1.2 in. from the centerline of the section. The stiffness of the plates fixed to the rollers was modeled with spring elements (COMBIN14) placed along the corners of the top and bottom end sections. As with the axial test model, shell elements were used to ensure uniform load transfer at the ends. Also, the top and bottom 6 in. of the columns were again modeled with higher strength material to simulate confinement.

11.4.4 Modeling Repaired Columns

The damaged sections of the columns were repaired by casting additional concrete repair material at the section. The repair was modeled by generating the geometry of the repaired column (see Fig. 11.2). The key factor determining the strength of the repaired column is the bond strength between the old and new concrete. Since the bond strength is dependent on several factors, such as the material properties, the surface conditions, etc., it is difficult to determine it analytically. Therefore, the bond strengths used for the finite element analysis was based on the experimental results. Initially, a perfect bond was assumed to exist between the old and new concrete. The bond was assumed to fail when the strains at the interface exceeded a certain value. This critical value of strain was based on the experimental results.

Bond failure is simulated in the analysis by using the element "death" option provided in ANSYS. This feature allows elements to be disabled during parts of the analysis, thereby removing it from the model. The elements of the repair geometry were disabled when bond between it and the old concrete failed. In order to decide when to disable the elements of the repaired geometry, the load was applied gradually over a number of steps, and the strains developed at the interface between the old and new concrete were compared with the critical value after every step. An element from the repair geometry is disabled (or killed) if the strains determined above exceed the critical value.

11. 5 Phase I Axial Test Results

Two types of comparisons were made between the experimental and finite element analysis results. First, the failure load, the mode of failure (i.e., crushing or cracking), and the region of failure were compared. Second, the experimental strains were compared.

As with the experimental results, the central portion of the column was found to fail due to crushing in the finite element model (Figs. 6.3-6.9). Table 11.2 presents the failure load obtained from the finite element analysis, and the average failure load obtained from the tests. The finite element results were adjusted to account for the initial prestressing load.

It may be seen that the predictions are fairly close to the test results. The failure load predictions for the repaired columns are higher than the experimental data. This is because a perfect bond was assumed throughout prior to debonding. This assumption makes the column stiffer and therefore the critical strain is attained at a higher load.

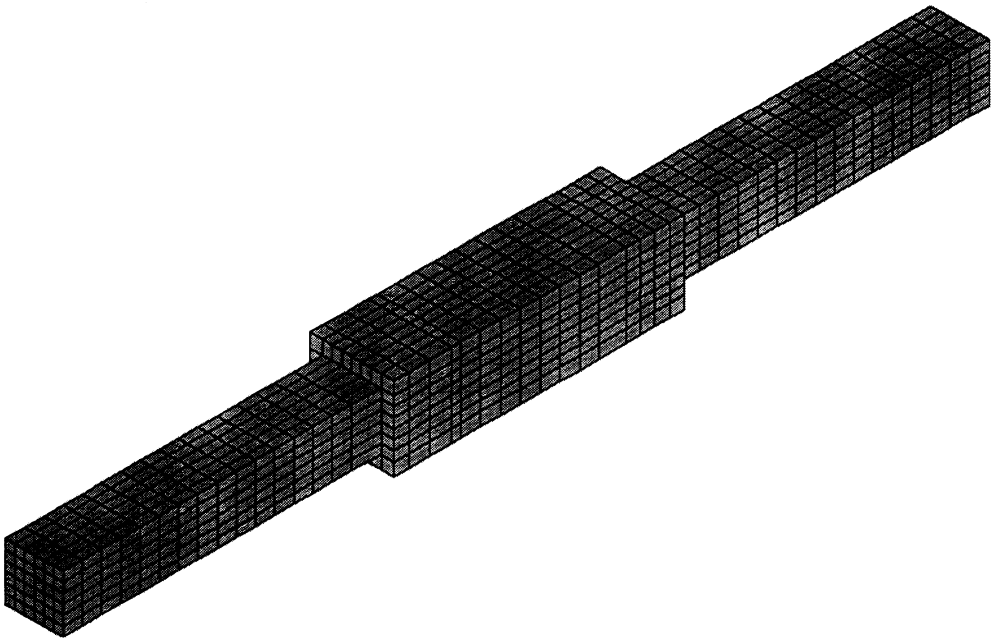

Figure 11.2 Typical Mesh of a Repaired Column.

Strain measurements were obtained at different locations in the tests as explained in Chapters 6-7. For the purposes of comparison, the average mid level strains were compared to the finite element results. The results are presented in Appendix D, Figs D.1-D.15. It may be seen that although the finite element model predictions are necessarily linear, there is a reasonable match with the experimental results. For the most part, the finite element model of the repaired columns is seen to be stiffer than the actual test columns. As already stated, this was because of the assumption of perfect bond between the damaged column and the repair section.

Table 11.1 Finite Element Result Comparison for Phase I Axial Tests.

Test Type	Specimens	Avg. Test Results (kips)	FEM Results (kips)	FEM/Test Ratio
Undamaged Control	C1-5, C1-6, C2-6, C1-7	239	250	1.1
Structural Repair Formed Surface	SF-1, SF-2	192.9	210	1.1
Structural Repair Chipped Surface	SC-1, SC-2	175.4	200	1.1
Non-Structural Repair Formed Surface	NF-1, NF-2	148.7	180	1.2
Non-Structural Repair Chipped Surface	NC-1, NC-2	135.1	165	1.2
Damaged Controls	D1-10, D2-10	147.8	120	0.8
Damaged Controls with Strands Cut	D2-4, D2-9	100	80	0.8

11.6 Phase I Bending Test Results

As with the axial test case, the experimental strains, and failure loads are compared with the finite element analysis results..

Table 11.2 presents the failure load under obtained from the finite element analysis and the corresponding average experimental failure load. The finite element predictions are reasonably close to the test results. All columns were found to fail at the central portion due to crushing as was observed experimentally (see Figs. 7.3-7.9).

11.7 Phase II Models

The geometry of the columns used for Phase II of the study was the same as that of the Phase I, except for the use of nails in certain repair sections as described in Chapter 9. The finite element model was essentially the same as used for Phase I, except that the nails used in the repairs were modeled using beam elements (BEAM4). The beam elements are two node elements capable of carrying axial and bending loads. A perfect bond was assumed to exist between the nail and the concrete.

Table 11.2 Finite Element Result Comparison for Phase I Bending Tests.

Test Type	Specimens	Avg. Test Results (kips)	FEM Results (kips)	FEM/Test Ratio
Undamaged Control	C1-5, C2-7	119.5	110	0.9
Structural Repair Formed Surface	SF-3, SF-4	110.9	120	1.1
Structural Repair Chipped Surface	SC-3, SC-4	95.5	110	1.2
Non-Structural Repair Formed Surface	NF-3, NF-4	91.8	110	1.2
Non-Structural Repair Chipped Surface	NC-3, NC-4	76.7	90	1.2
Damaged Controls	D1-7, D2-7, D2-8	62.3	50	0.8
Damaged Controls with Strands Cut	D1-8, D1-9	28.9	30	1.0

The following modification were also made to model the Phase II repairs. In columns using powder activated nails, the concrete region around the nails was found to crack (see Fig. 10.1) during installation. This was accounted for in the model by reducing the effective cross-section of the concrete. As Protecrete led to increased strength of the core, a higher concrete strength was used in the model. The magnitude of increase was based on experimental results.

The boundary conditions for the finite element model used for Phase II were the same as those used for the Phase I axial test models. Also, the methodology used for modeling the repair was exactly the same.

11.8 Phase II Results

As with the Phase I axial results, the failure loads and the strains are compared. Table 11.3 presents the failure load data, while the strains are presented in Figs. D.16-D.26. As with the Phase I axial tests, the two results are reasonably close.

In the Phase II tests, in addition to the strains on the external surface, the strains were also measured on the internal surface and at different levels of the repair. The large variation between these strains occurred due to the variation of the bond strength in these regions.

Since a perfect bond was assumed in the finite element model, the two results cannot be compared. The results from the two phases are comparable.

Table 11.3 Finite Element Result Comparison for Phase II Axial Tests.

Test Type	Specimens	Avg. Test Results (kips)	FEM Results (kips)	FEM/Test Ratio
Structural Repair with P.A. Nails	SMP-1, SMP-2	151.7	160	1.1
Non-Structural Repair with Epoxied Pins	USF-1, USF-2	166.7	190	1.1
PROTECRETE Densifier and MWC	PRO-1, PRO-2	160.2	200	1.2
P.A. Nails in Upper Half of Repair	PAL-1	151.6	165	1.1
P.A. Nails in Both Halves of Repair	MPA-1, MPA-2	139.5	160	1.1
Non-Structural Repair Formed Surface	CNL-1	132.8	180	1.4

11.9 Conclusions

The finite element analysis results are reasonably close to the experimental results for axial tests. It is important to realize that this was obtained only because the analysis used experimental values. The bending test results were found to be more sensitive to the assumption of perfect bond. The major hurdle in obtaining good correlation is in modeling bond. The simplified bond model used can provide qualitative information about the repair process.

The primary mode of failure in all repaired columns was found core crushing which often occurred following bond failure. It is likely that capacity of the columns may be restored if the bond strength between the old concrete and the repair material is increased. Structural reinforcements in the repaired section were found to reduce the radial stresses (not reported here), which may explain the higher ultimate values. Simulation of Phase II results also point to the effectiveness of nails in increasing the capacity of the columns, but the advantage may be easily offset by damage to the core section (see Fig. 10.1).

References

11.1 MacGregor, J. G. (1997). *Reinforced Concrete Mechanics and Design,* Third Edition, Prentice- Hall, NJ

11.2 ANSYS, Inc (1998), *ANSYS Reference Manuals, Revision 5.5,* ANSYS, Inc, Canonsburg, PA

12. CONCLUSIONS AND RECOMMENDATIONS

12.1 Introduction

This chapter summarizes the results from this two phase experimental study to assess the efficacy of repairs carried out on damaged piles. In the first phase, existing practice was assessed. These conclusions are described under Phase I Axial (Section 12.2) and Phase I Bending (Section 12.3). Attempts at increasing the ultimate capacity of the repaired pile were carried out in the second phase. These findings are described under Phase II Axial (Section 12.4). The principal recommendations are presented in Section 12.5.

12.2 Phase I Axial

The focus of Phase I one testing was to determine the extent to which currently used pile jacketing methods restored pile capacity. Seven series of axial load tests were conducted, three of which were used as controls; the remaining investigated the effects of structural (Type V) and non-structural (Type II) repairs for two distinct damage surfaces - formed and chipped.

The following conclusions may be drawn from the test results:

1. Structural repairs provide higher increase in axial capacity. Non-structural repairs on *formed* surfaces led to practically no increase in capacity (see Table 6.11).

2. The roughness of the interface contributes significantly to composite action. Chipped surfaces resulted in composite action practically to failure. The repair material debonded more readily in case of formed specimens and was the same for structural and non-structural repairs.

3. None of the repairs led to full restoration of the original strength. The highest increase was 80.7% (Type V - formed); the lowest was 56.6% (Type II - chipped).

12.3 Phase I Bending

Seven series of eccentrically loaded compression tests were conducted, three of which

were used as controls, the remaining investigated the effects of structural (Type V) and non-structural (Type II) repairs. As with the axial testing series, two distinct damage surfaces were evaluated, formed and chipped. All "bending" tests used a 1.2 inch off-center load line producing an eccentricity (e/h = 0.2).

The following conclusions may be drawn from the test results:

1. Structural repairs are very efficient and lead to significant increases in ultimate capacity. Non-structural repairs on *formed* surfaces are much more efficient under eccentric loading rather than axial loading where there was practically no increase in capacity (see Table 7.11).

2. The bond between the old concrete and the repair material is less important under eccentric load than with concentric loading.

3. None of the repairs led to a full restoration of the original strength. The highest increase was 93.1% (Type V - formed); the lowest was 64.3% (Type II - chipped). These are however, higher than those for axial loads.

12.4 Phase II Axial

The focus of Phase II was to identify measures which could lead to improved ultimate capacity. As axial tests on formed piles provided the least improvement, only axial loads were considered in this phase. Five systems - four powder activated nail systems and a chemically-based proprietary repair system were tested in this phase.

The following conclusions may be drawn from the test results:

1. Improvement in capacity as a result of the use of powder activated nails was disappointing. When installed only above the water line (District IV's original scheme) increases in capacity over Phase I were only 3.3%. However, when these nails were used both above and below the waterline there was a 6.3% *decrease* (see Table 10.3). This was because of the damage induced in the core during the installation of the nails (see Fig. 10.1).

2. The best results were obtained when enhanced bond did not result in damage to the core. Capacity increases of 12.1% were recorded for the cases where dowels were epoxied into pre-drilled holes (see Fig. 9.3 and Table 10.3).

3. The chemically based proprietary system provided a greater increase (7.7%) than powder activated nails. This system is simple to use and may provide the most cost effective solution.

12.5 Recommendations

Based on the findings from this study, the following recommendations may be made:

1. Extreme care should be exercised in installing mechanical fasteners to improve interface bond using impact and impact-momentum tools so as to minimize damage. If powder-activated nails are used, consideration should be given to using longer nails into pre-drilled holes to minimize surface degradation.

2. An alternative to powder-activated nails is the use of epoxy reinforcing bars into pre-drilled holes that can be used for both dry and underwater installations. This system gave the best results in the study.

3. The chemically based proprietary system tested showed promise and consideration should be given to its use in field applications.

Corrosion protection is of utmost importance in any pile repair but this was outside the scope of this investigation. A self-regulated, self-powered, cathodic protection system based on research conducted at FDOT's State Materials Office known as Lifejacket is currently available and is marketed by Altrista Corporation's Zinc Products Company, TN. The proposed enhancements incorporated with this system may provide an enduring solution to Florida's substructure pile corrosion problem.

APPENDIX A Axial Results - Phase I

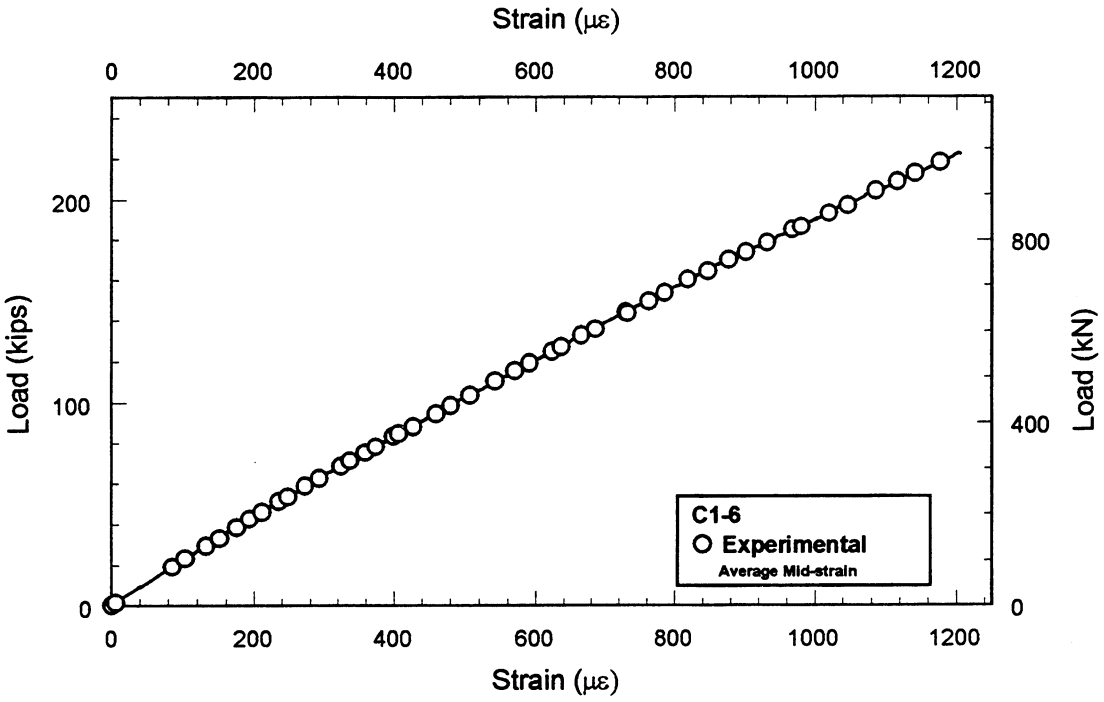

Figure A.1 Axial Strain Variation for Undamaged Control.

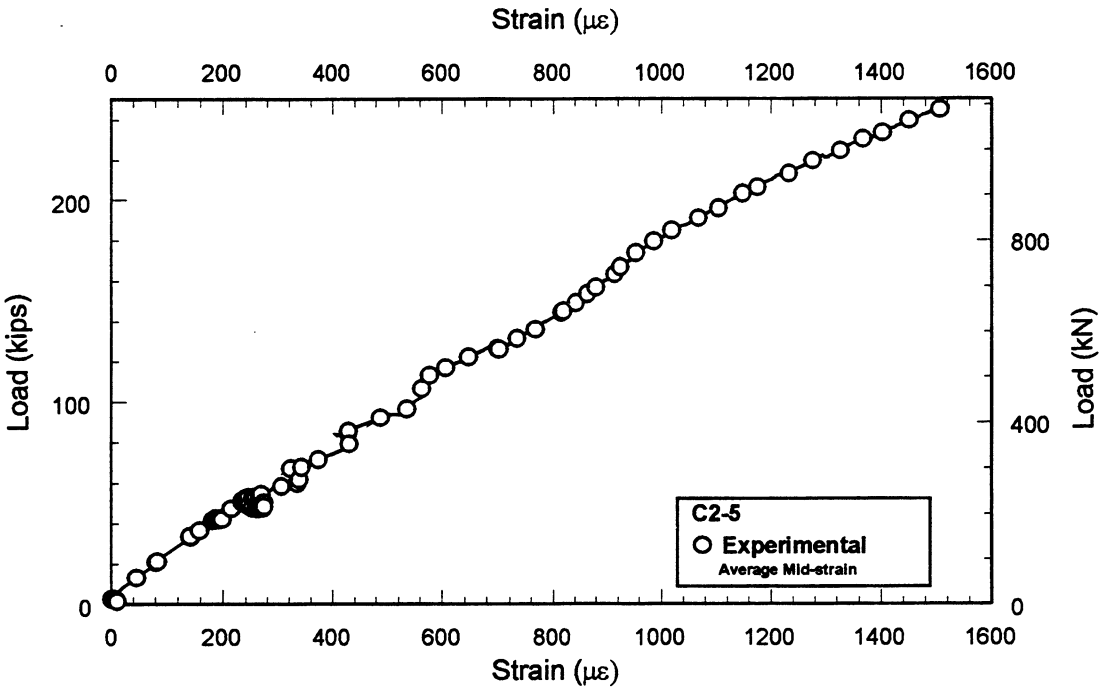

Figure A.2 Axial Strain Variation for Undamaged Control.

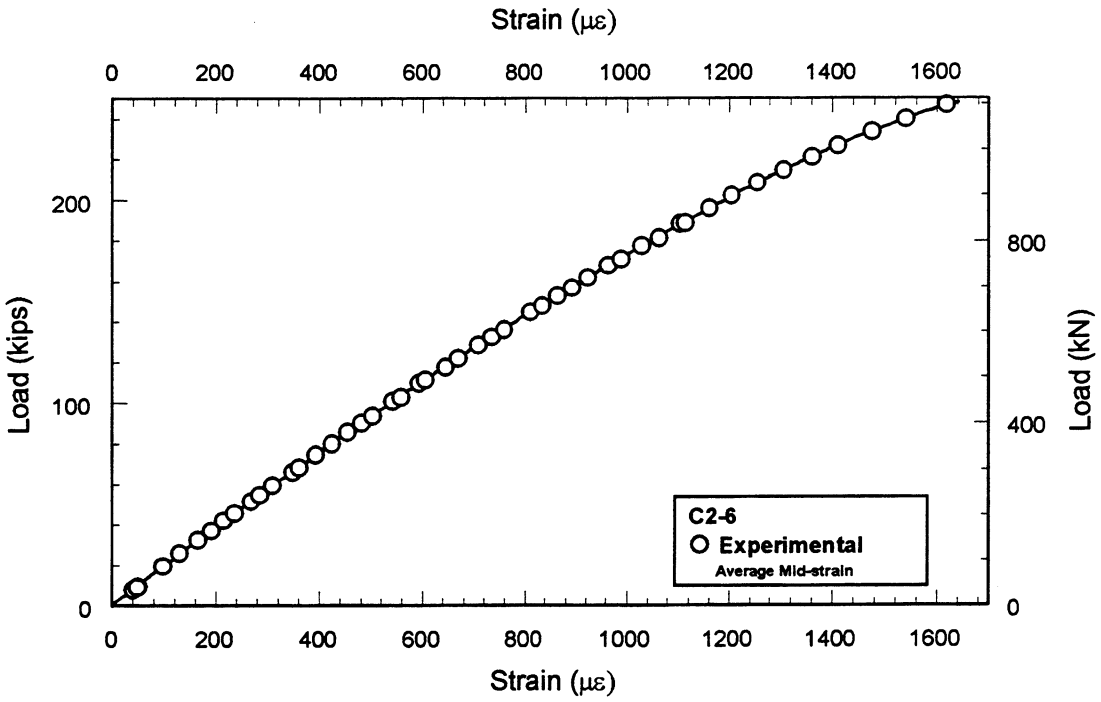

Figure A.3 Axial Strain Variation for Undamaged Control.

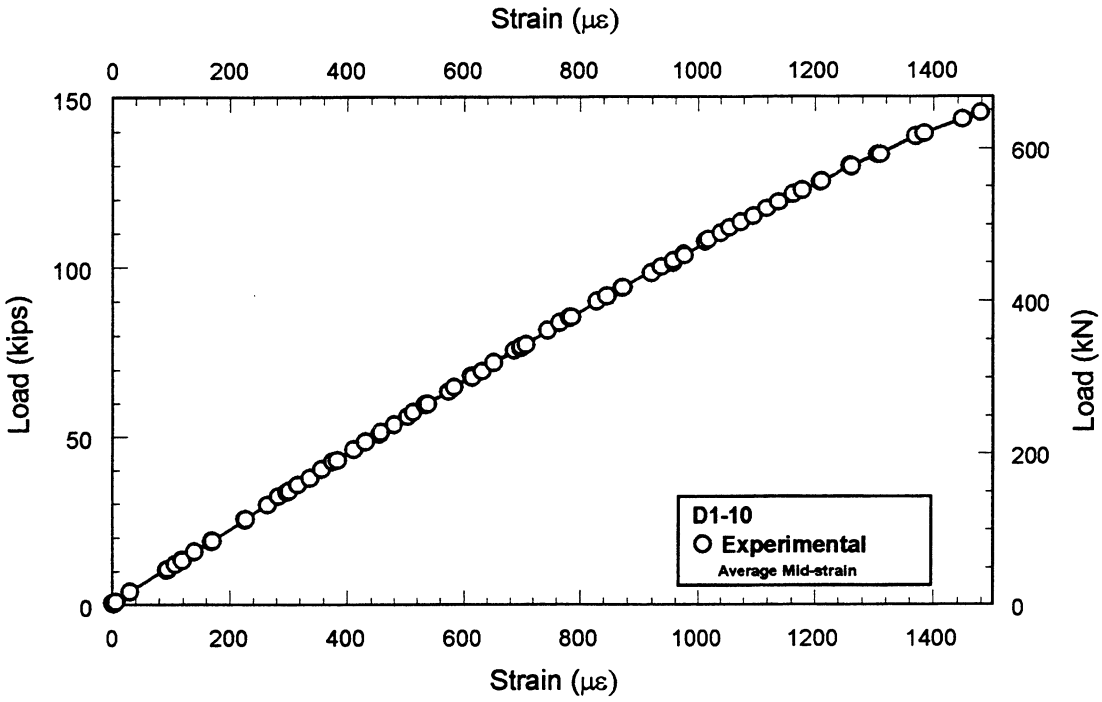

Figure A.4 Axial Strain Variation for Formed Damage Control.

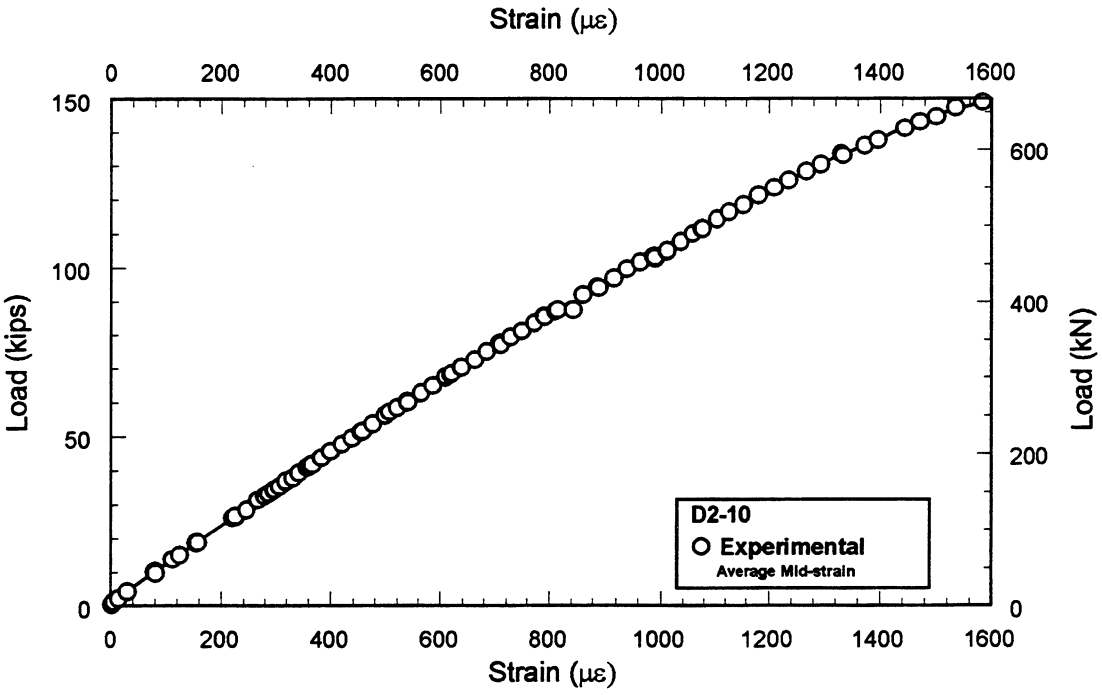

Figure A.5 Axial Strain Variation for Formed Damage Control.

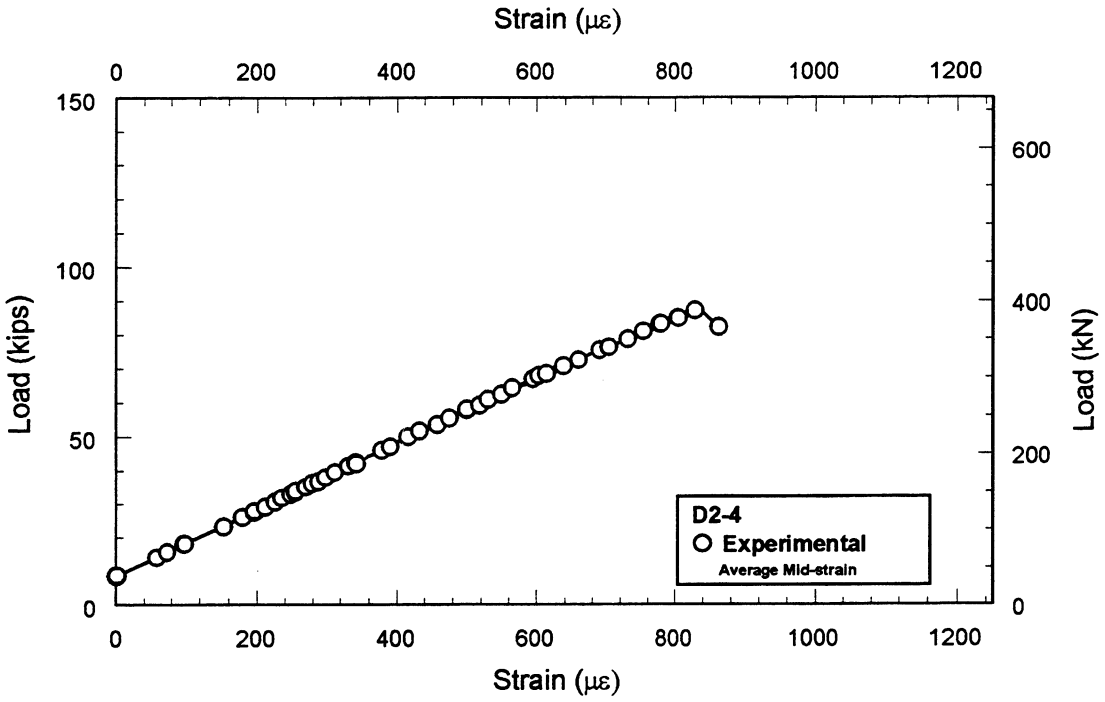

Figure A6 Axial Strain Variation for Formed Damage with Cut Strands.

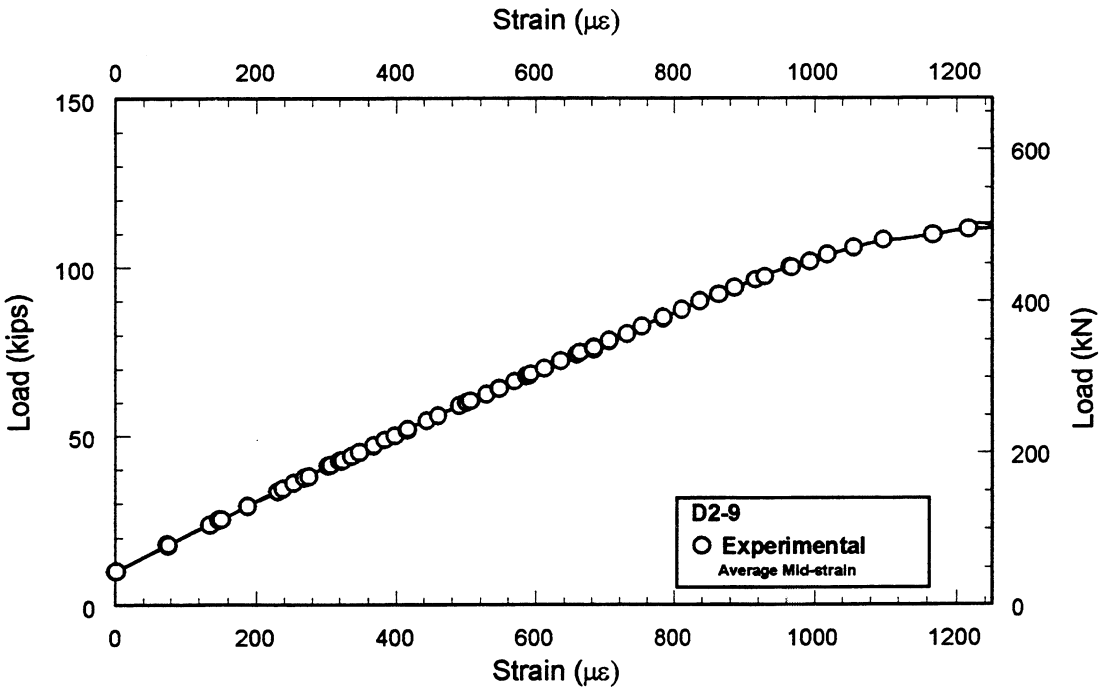

Figure A7 Axial Strain Variation for Formed Damage with Cut Strands.

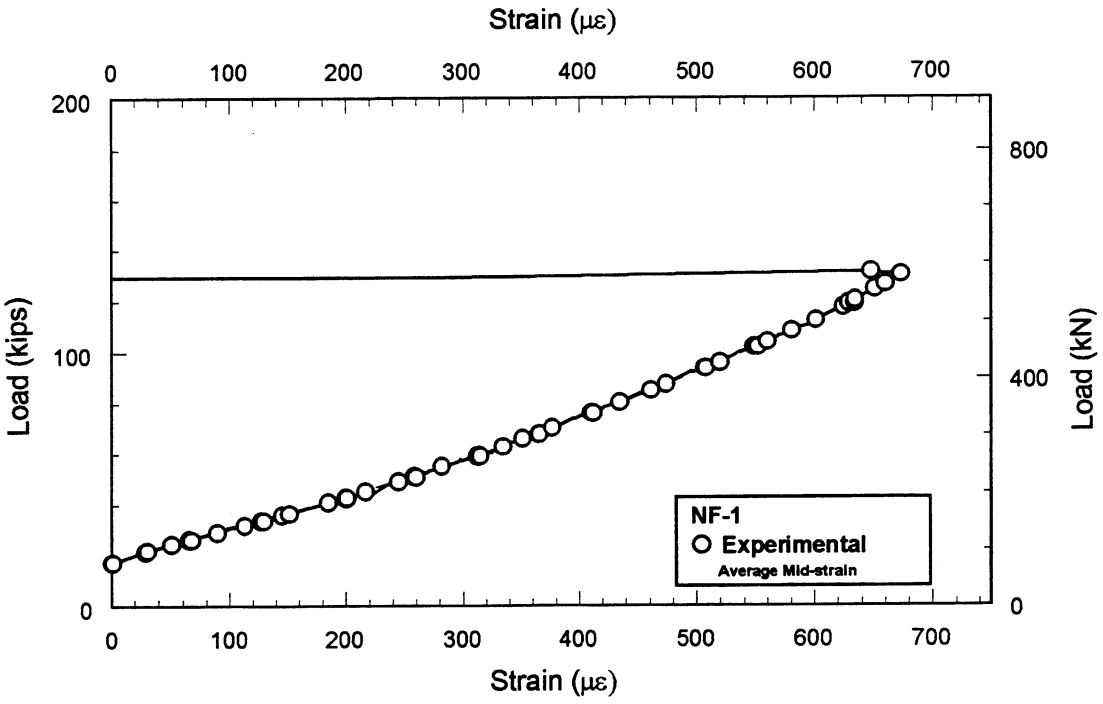

Figure A.8 Axial Strain Variation for Formed Non-Structural Repair.

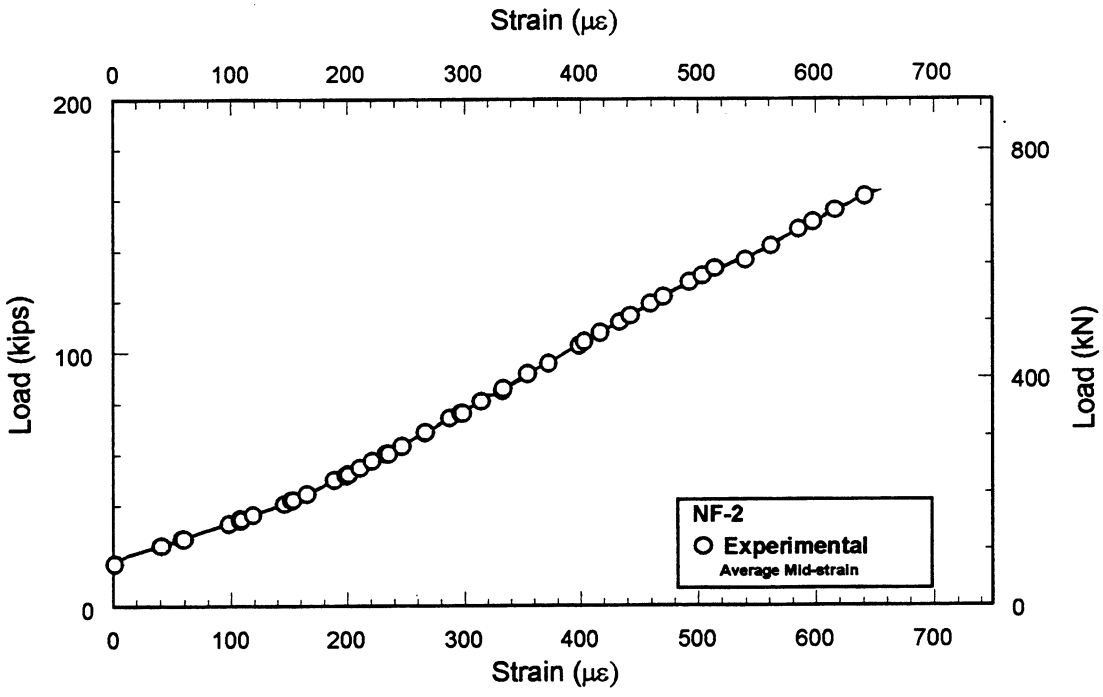

Figure A.9 Axial Strain Variation for Formed Non-Structural Repair.

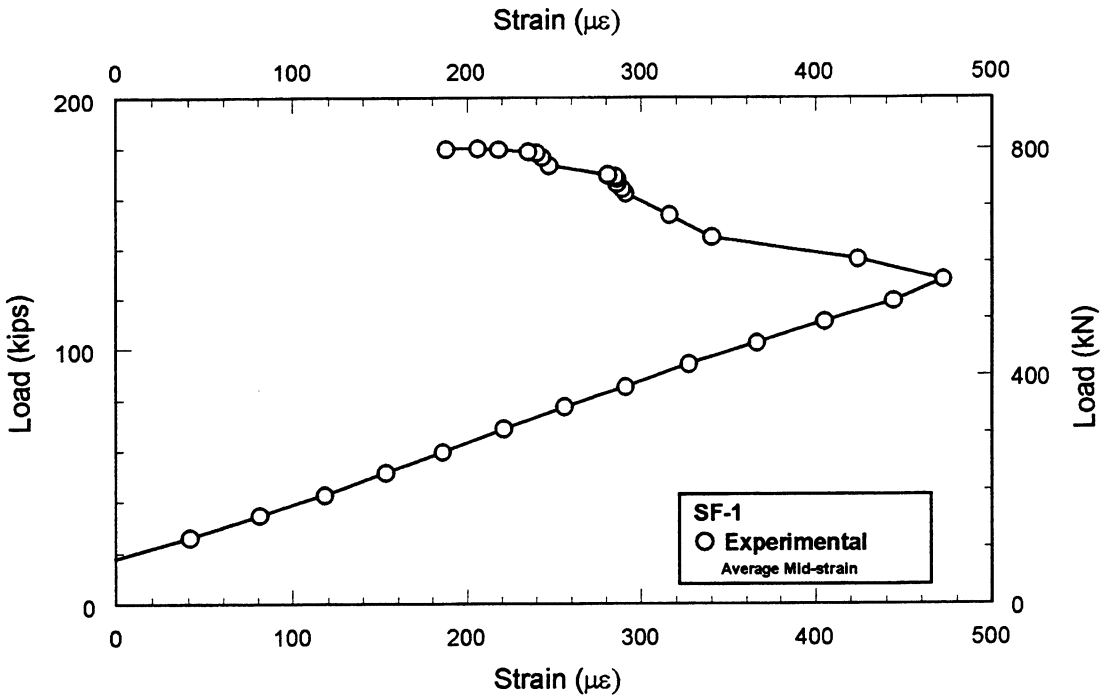

Figure A.10 Axial Strain Variation for Formed Structural Repair.

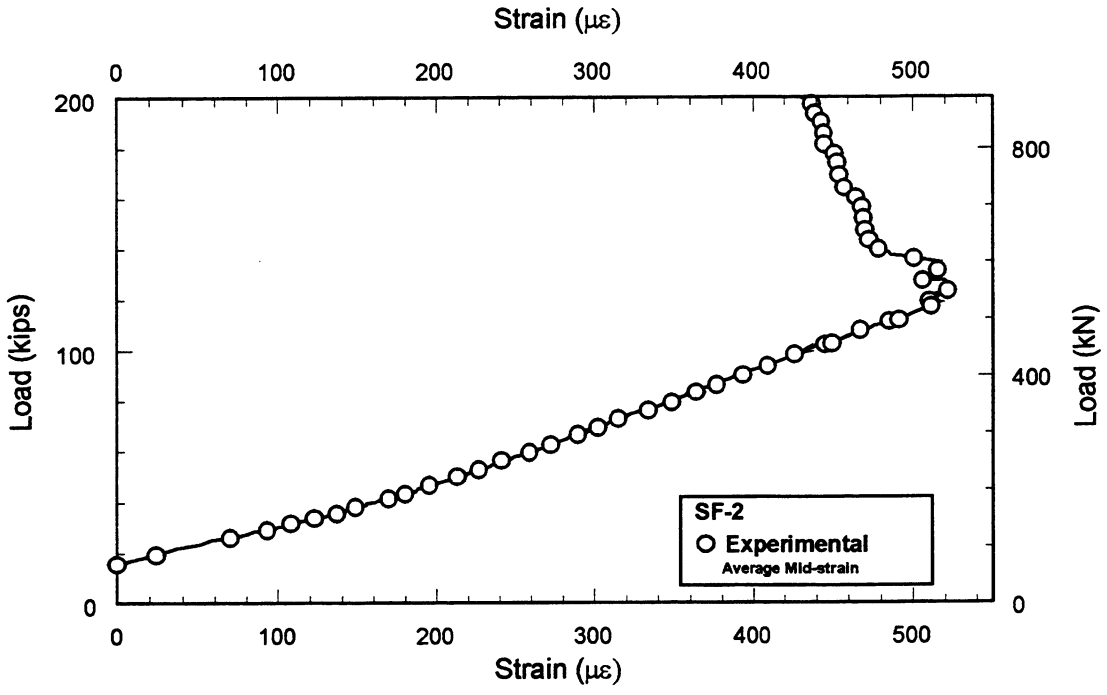

Figure A.11 Axial Strain Variation for Formed Structural Repair.

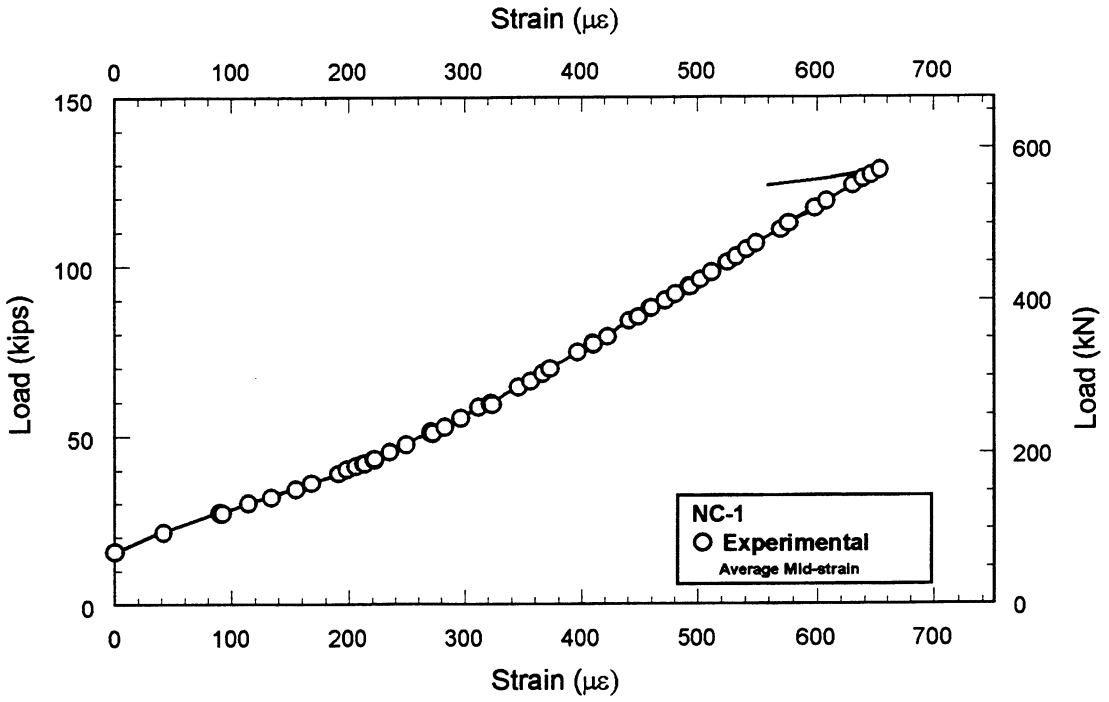

Figure A.12 Axial Strain Variation for Chipped Non-Structural Repair.

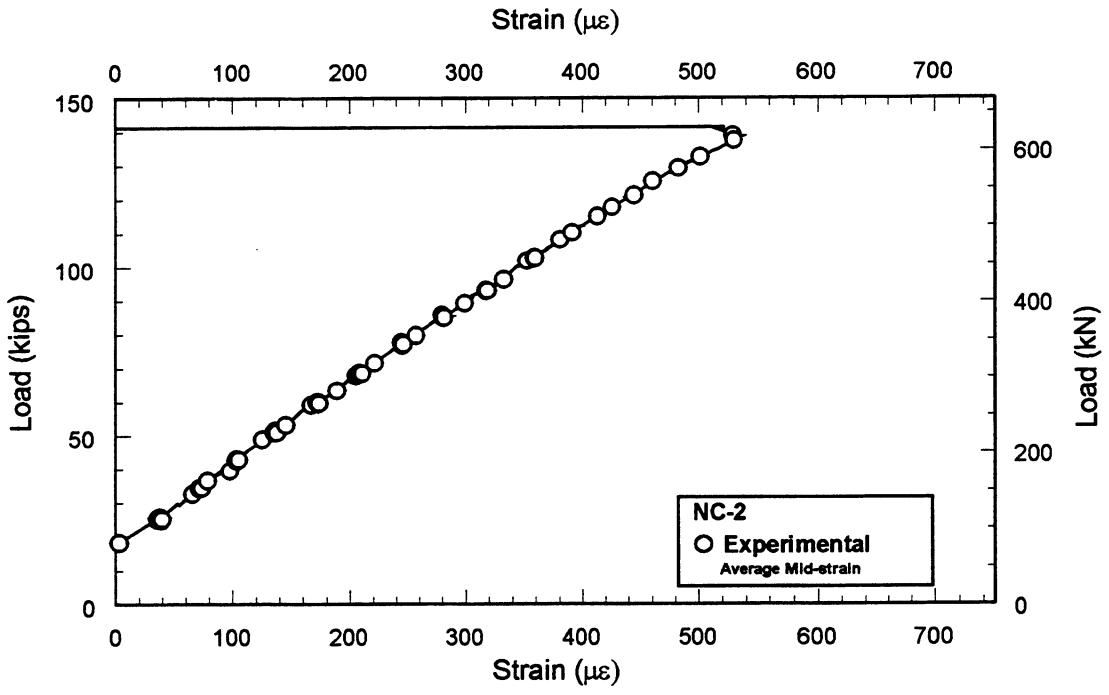

Figure A.13 Axial Strain Variation for Chipped Non-Structural Repair.

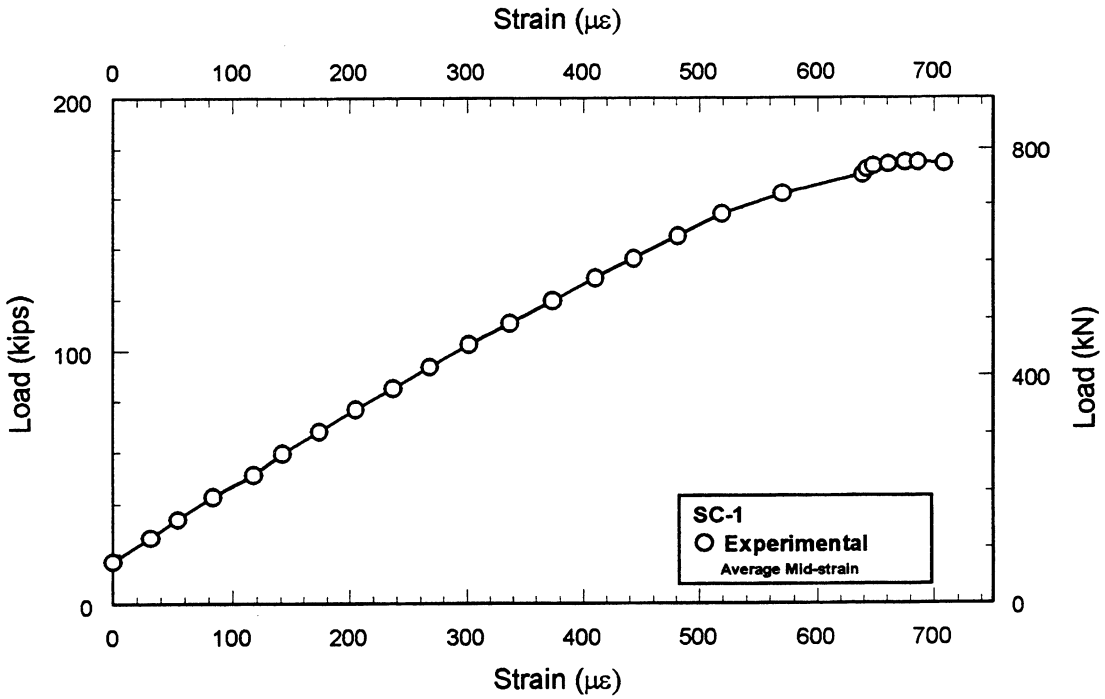

Figure A.14 Axial Strain Variation for Chipped Structural Repair.

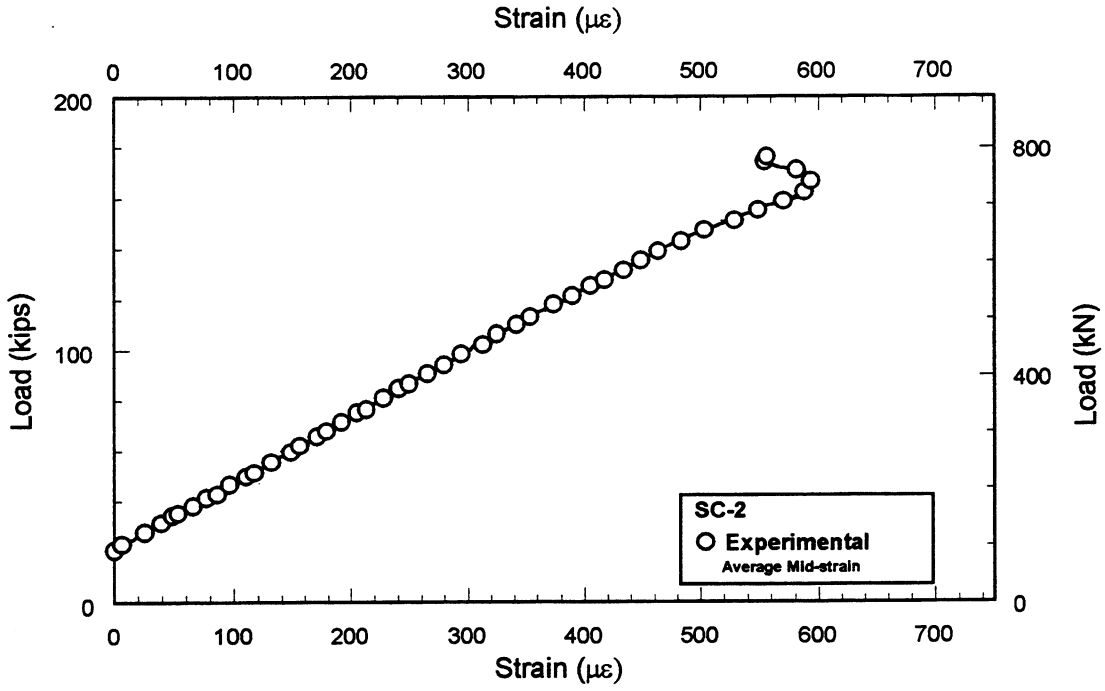

Figure A.15 Axial Strain Variation for Chipped Structural Repair.

APPENDIX B Bending Results - Phase I

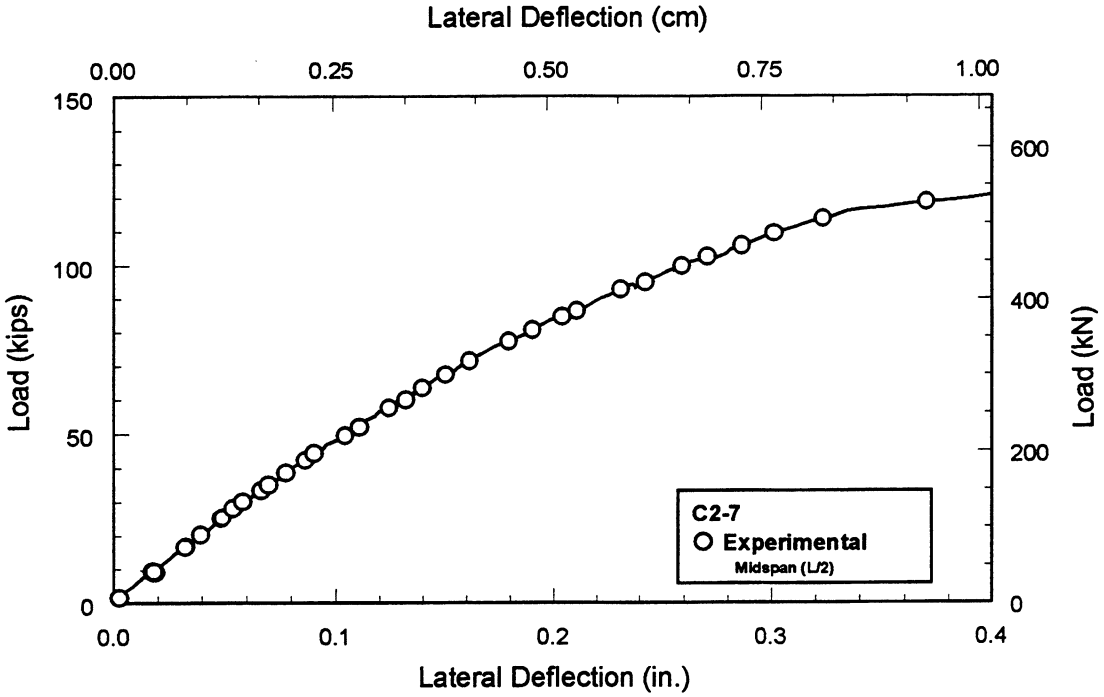

Figure B.1 Load vs Deflection Plot for Undamaged Control.

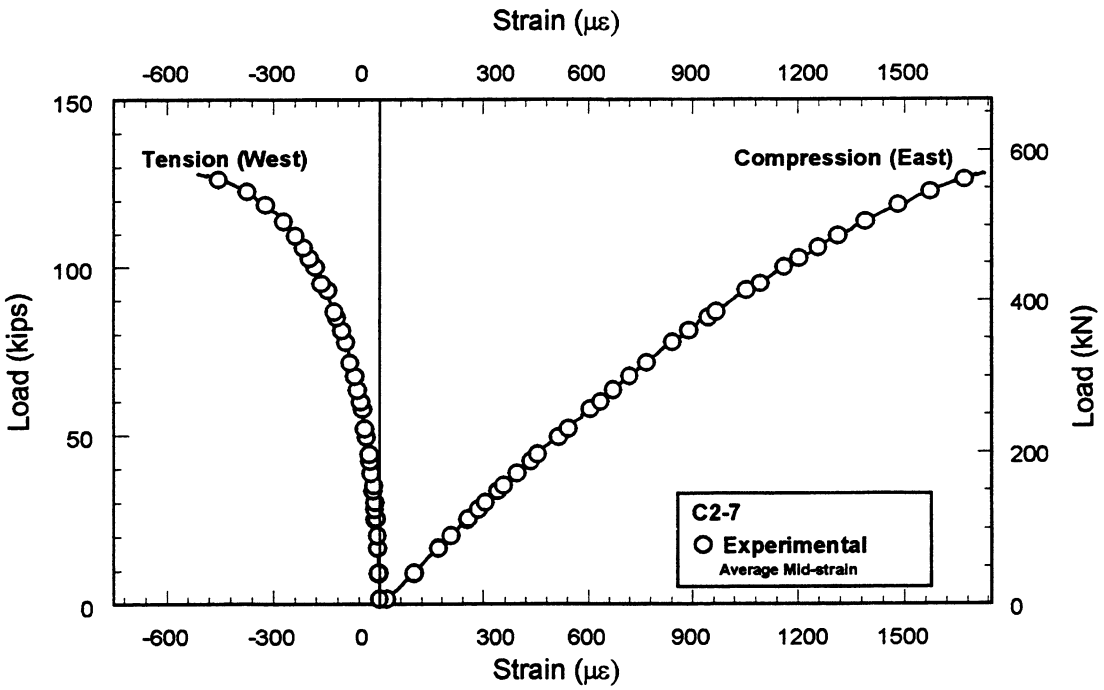

Figure B.2 Strain Variation for Undamaged Control.

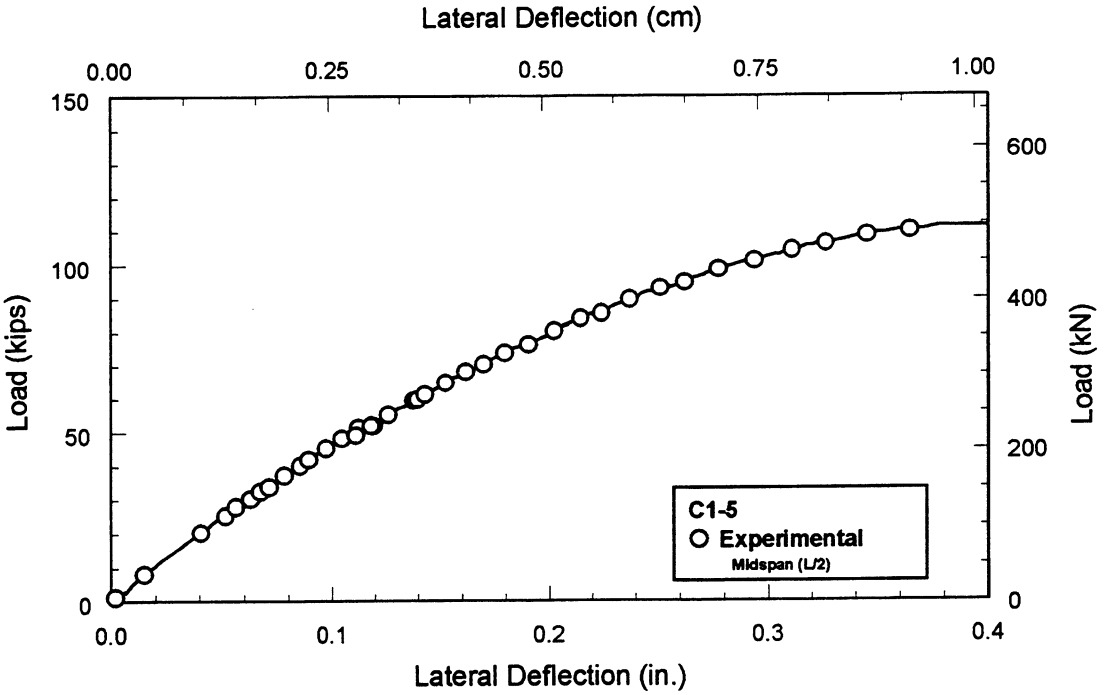

Figure B.3 Load vs Deflection Plot for Undamaged Control.

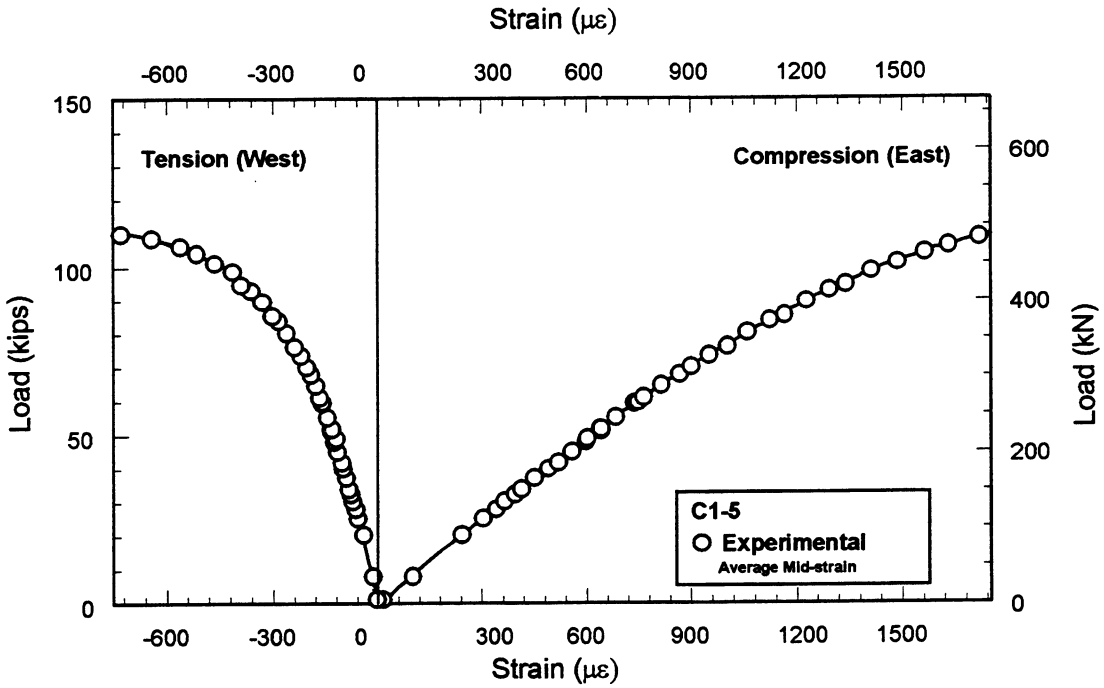

Figure B.4 Strain Variation for Undamaged Control.

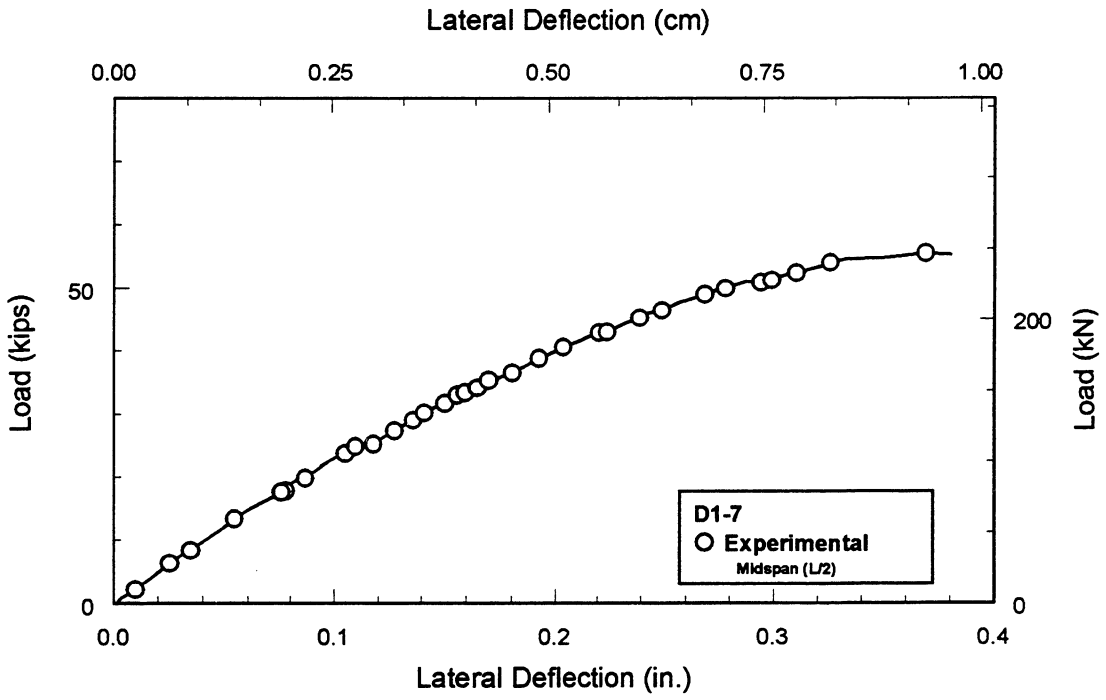

Figure B.5 Load vs Deflection Plot for Formed Damage Control.

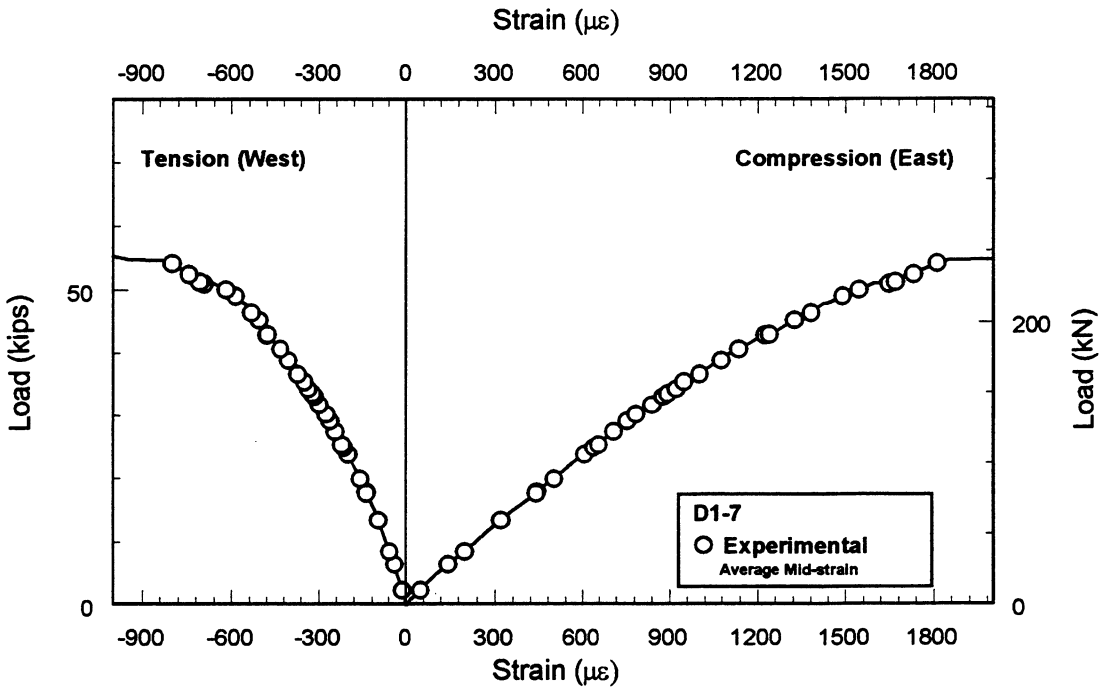

Figure B.6 Strain Variation for Formed Damage Control.

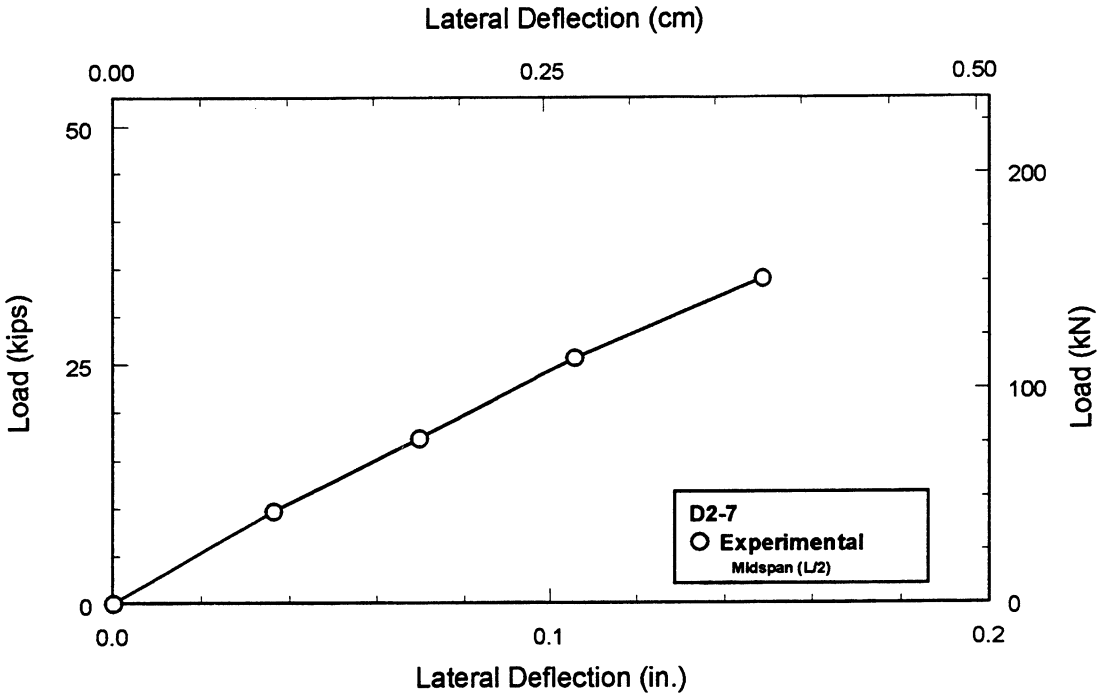

Figure B.7 Load vs Deflection Plot for Formed Damage Control.

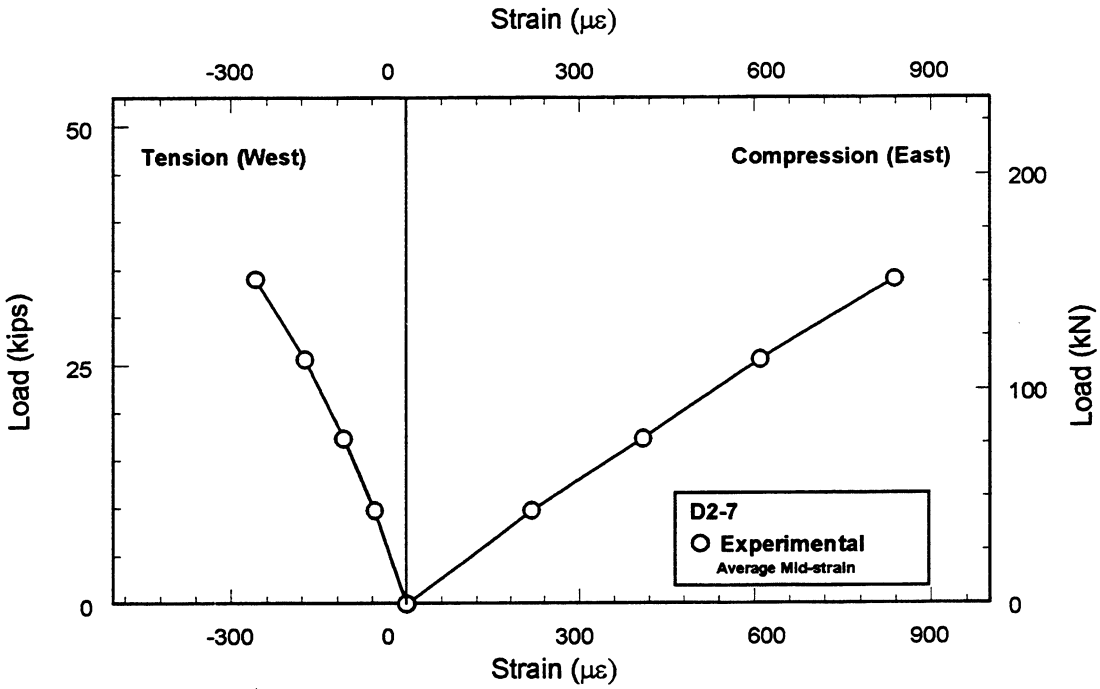

Figure B.8 Strain Variation for Formed Damaged Control.

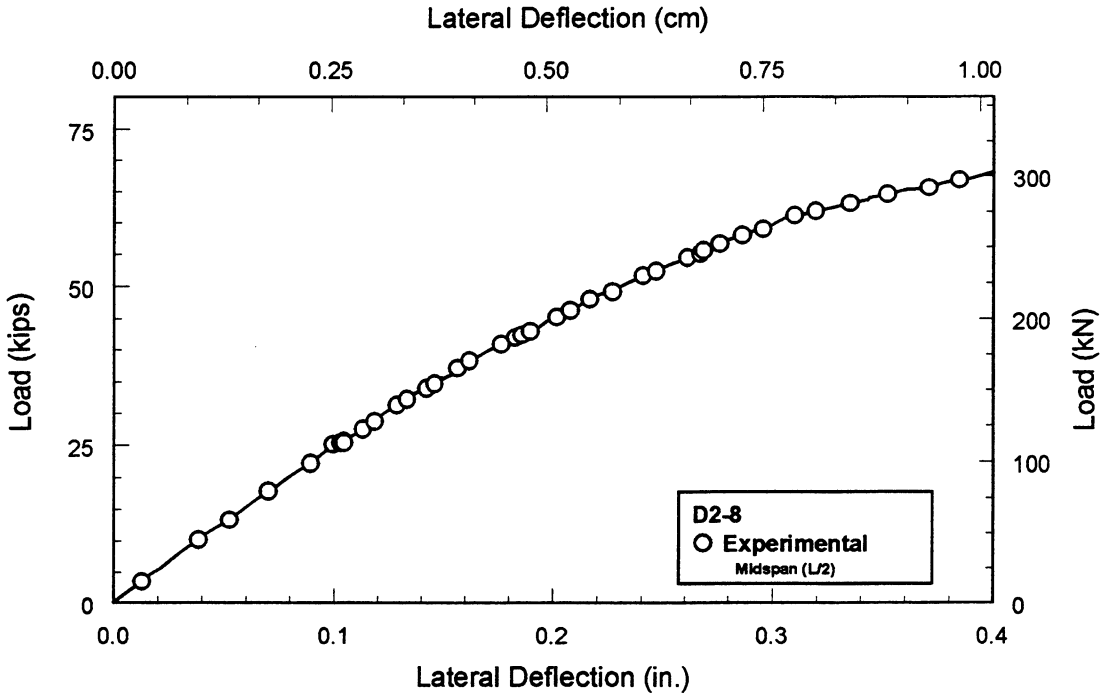

Figure B.9 Load vs Deflection Plot for Form Damaged Control.

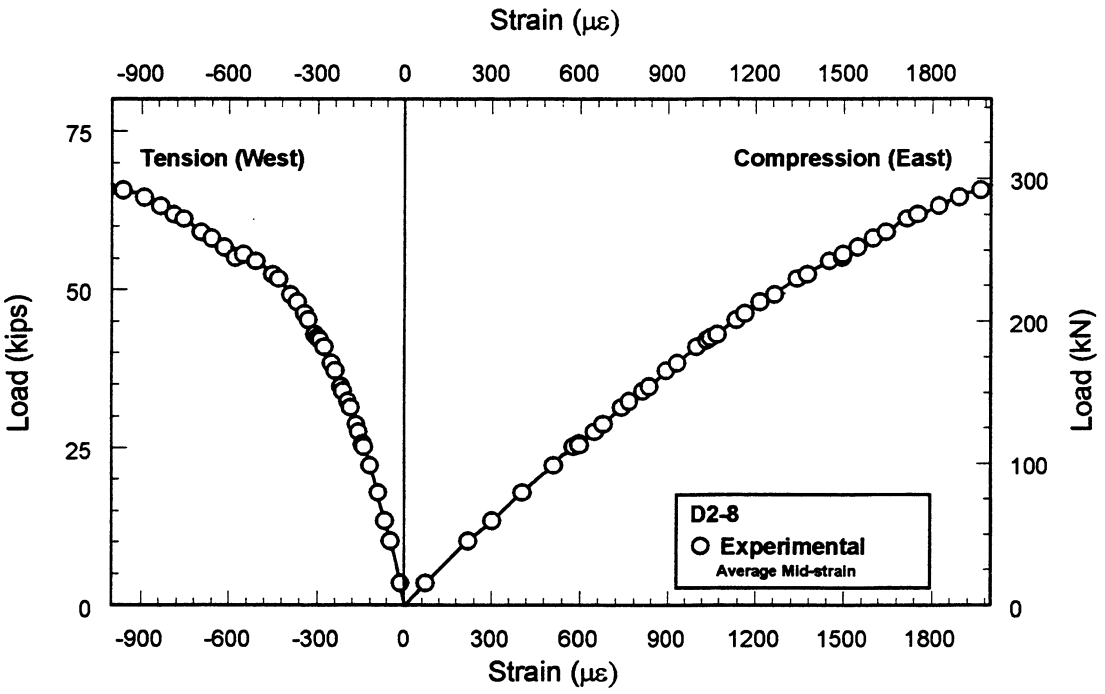

Figure B.10 Strain Variation for Formed Damaged Control.

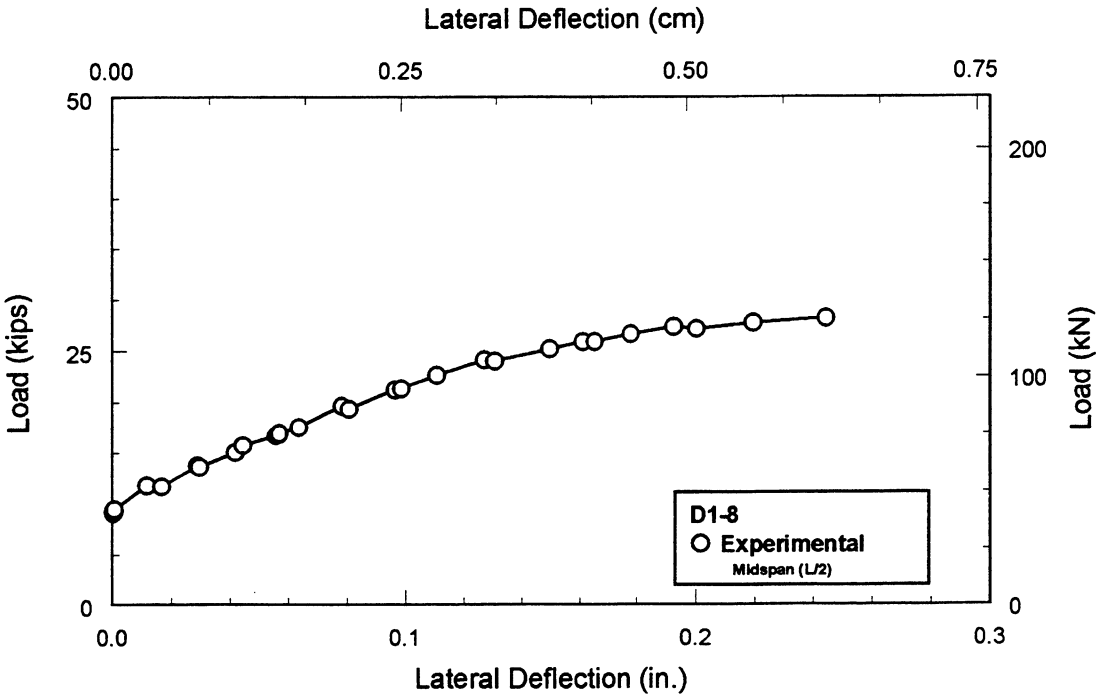

Figure B.11 Load vs Deflection Plot for Control with Cut Strands.

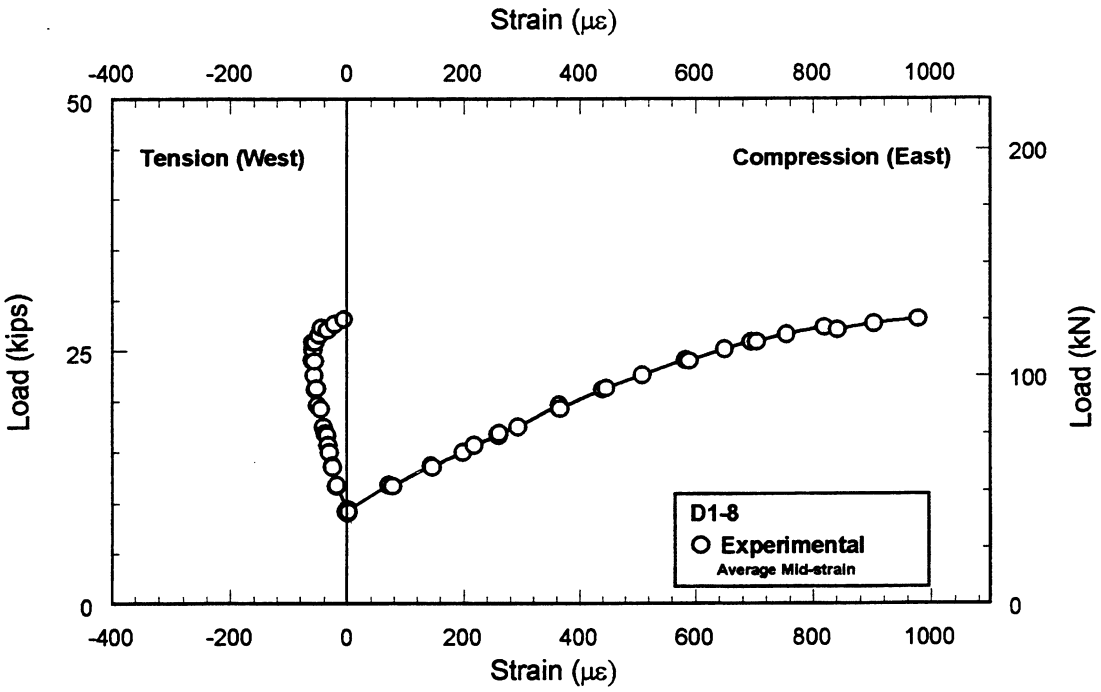

Figure B.12 Strain Variation for Control with Cut Strands.

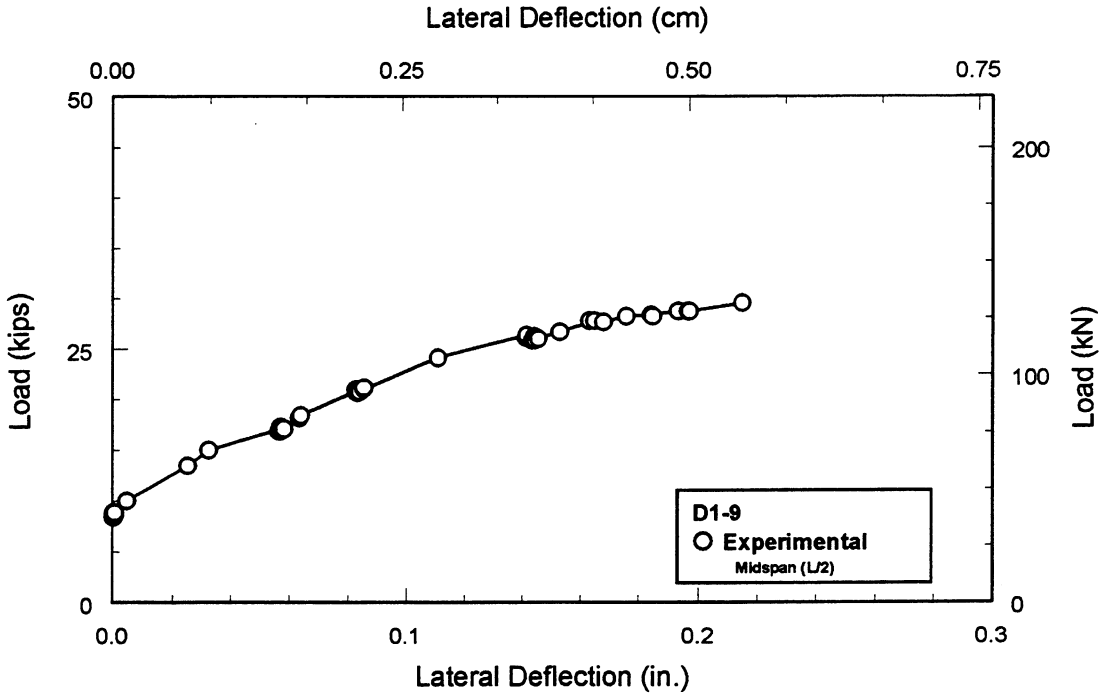

Figure B.13 Load vs Deflection Plot for Control with Cut Strands.

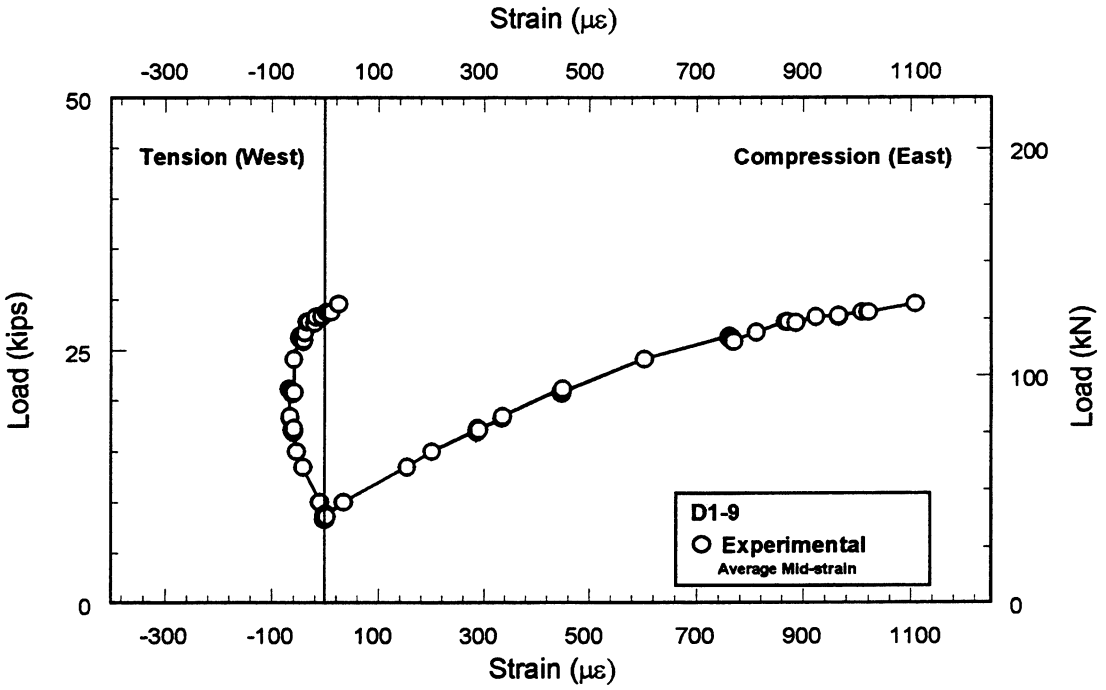

Figure B.14 Load vs Strain Variation for Control with Cut Strands.

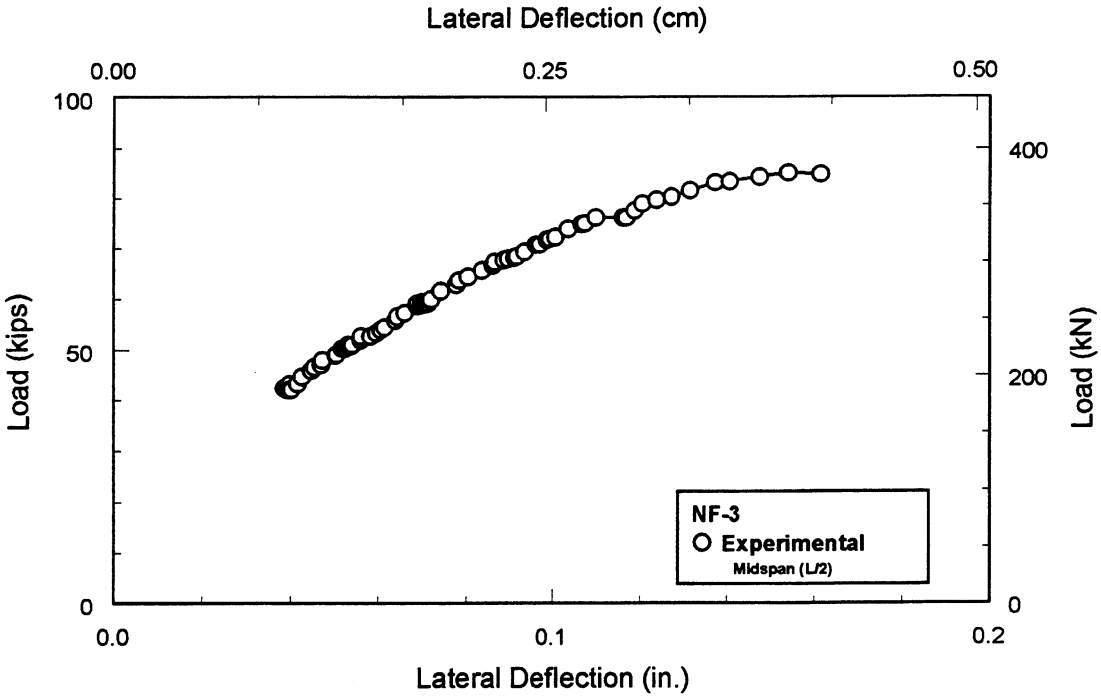

Figure B.15 Load vs Deflection Plot for Non Structural Formed Repair.

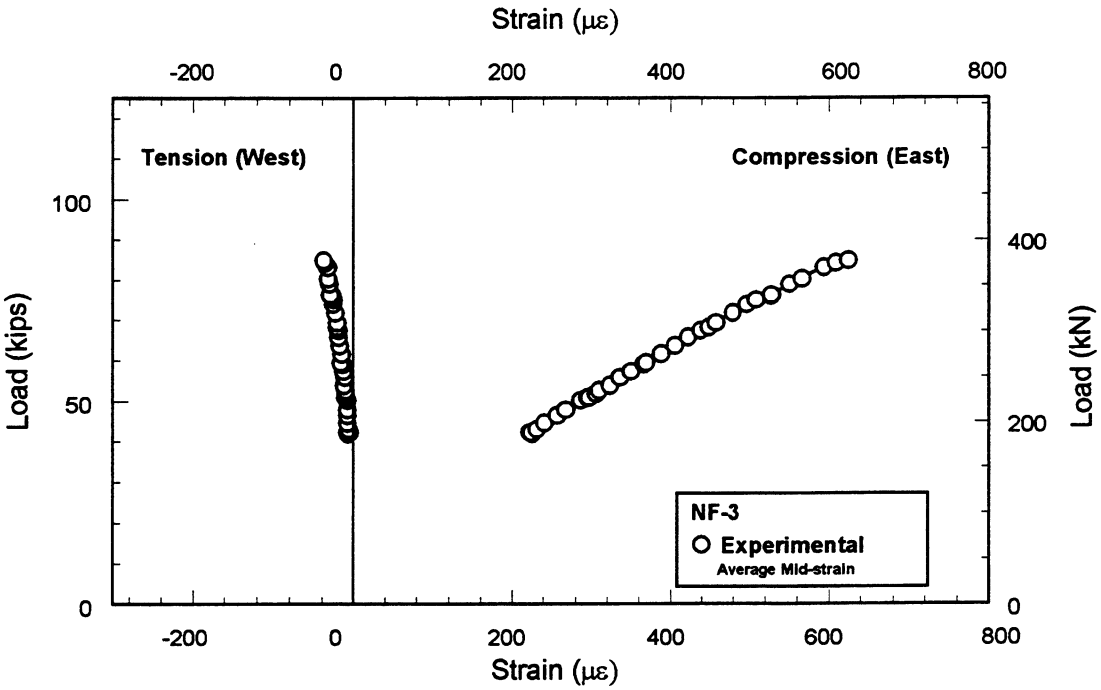

Figure B.16 Load vs Strain Variation for Non Structural Formed Repair.

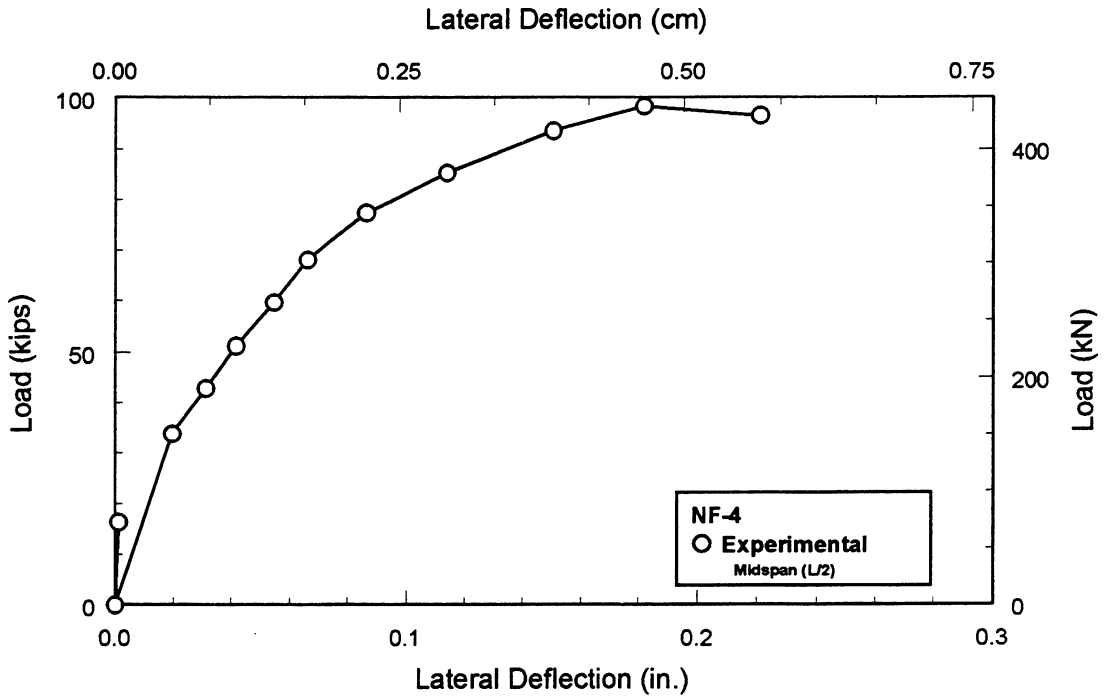

Figure B.17 Load vs Deflectition for Non Structural Formed Repair.

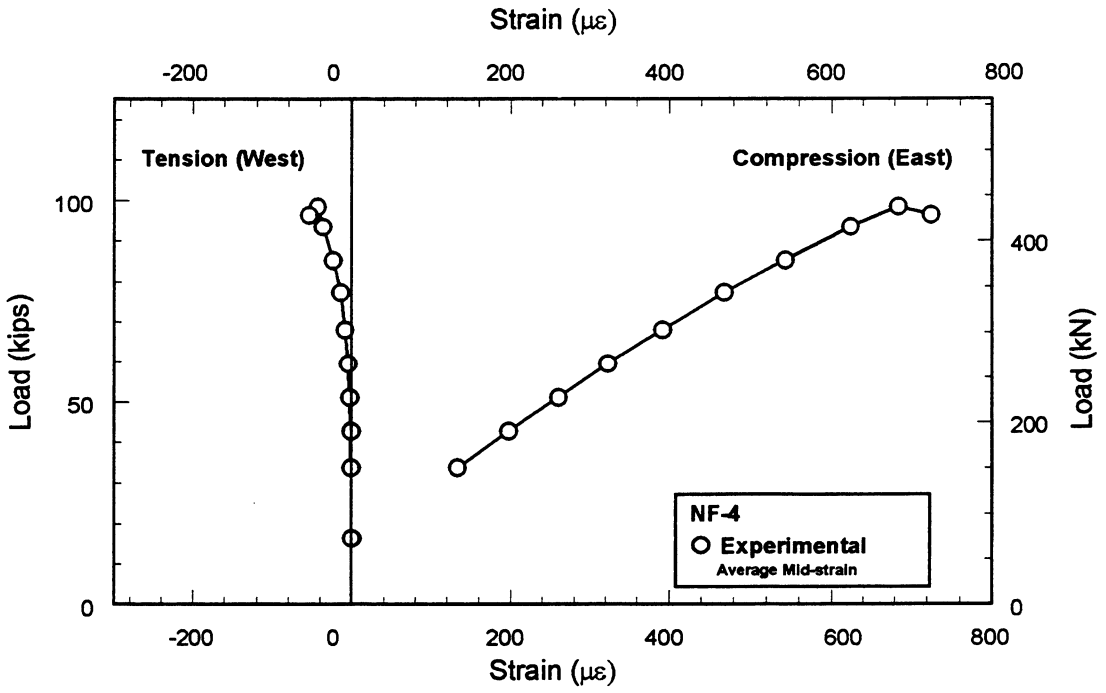

Figure B.18 Load vs. Strain Variation on Non Structural Formed Repair.

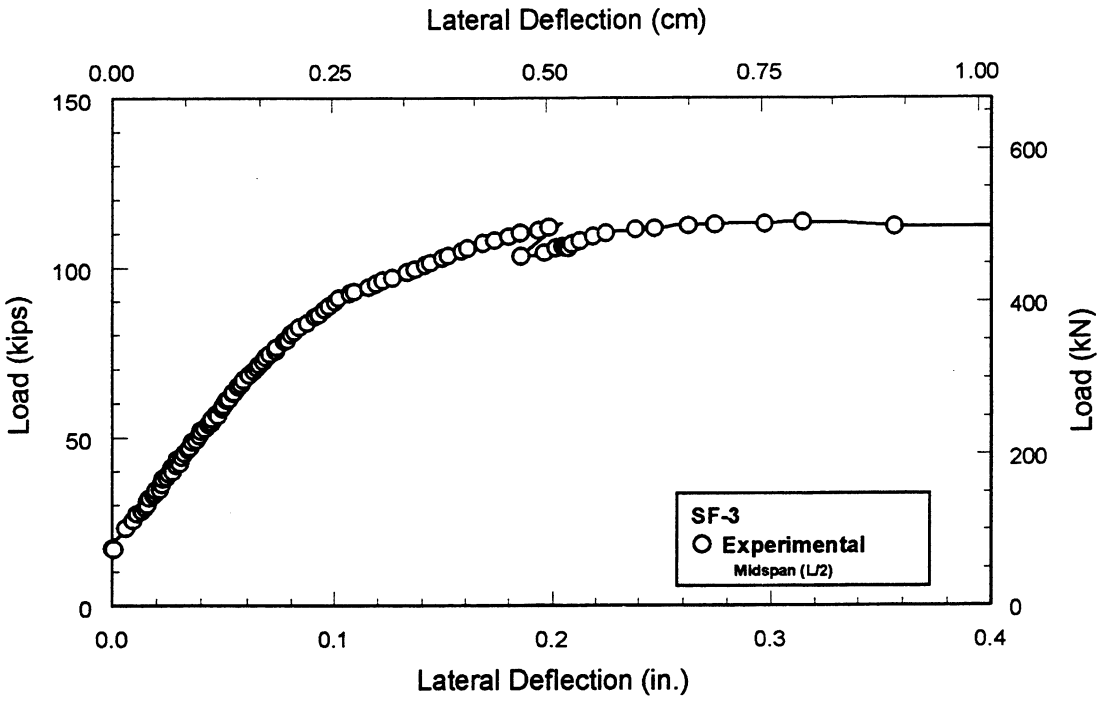

Figure B.19 Load vs Deflection Plot for Structural Formed Repair.

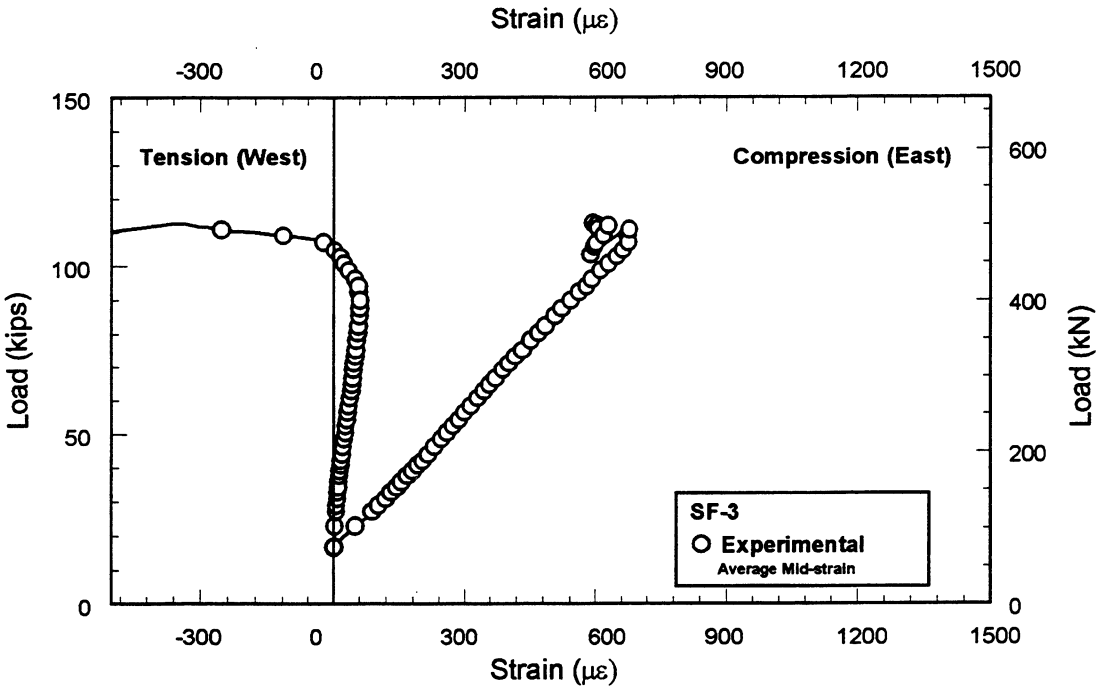

Figure B.20 Load vs Strain Variation for Structural Formed Repair.

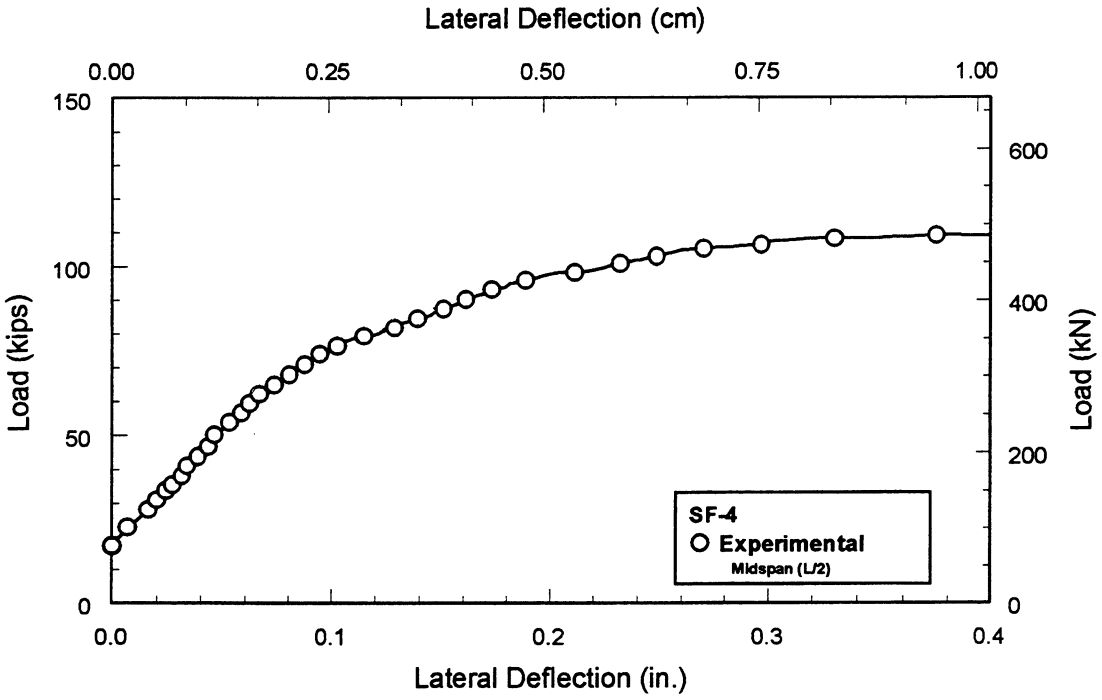

Figure B.21 Load vs Deflection Plot Structural Formed Repair.

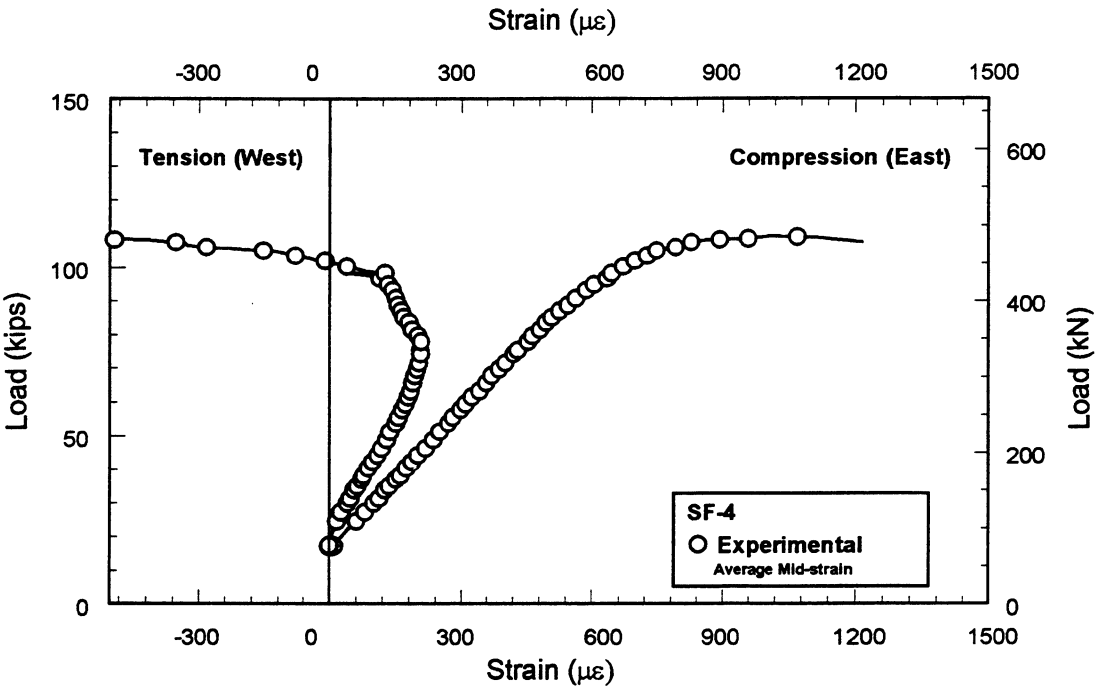

Figure B.22 Load vs Strain Variation for Structural Formed Repair.

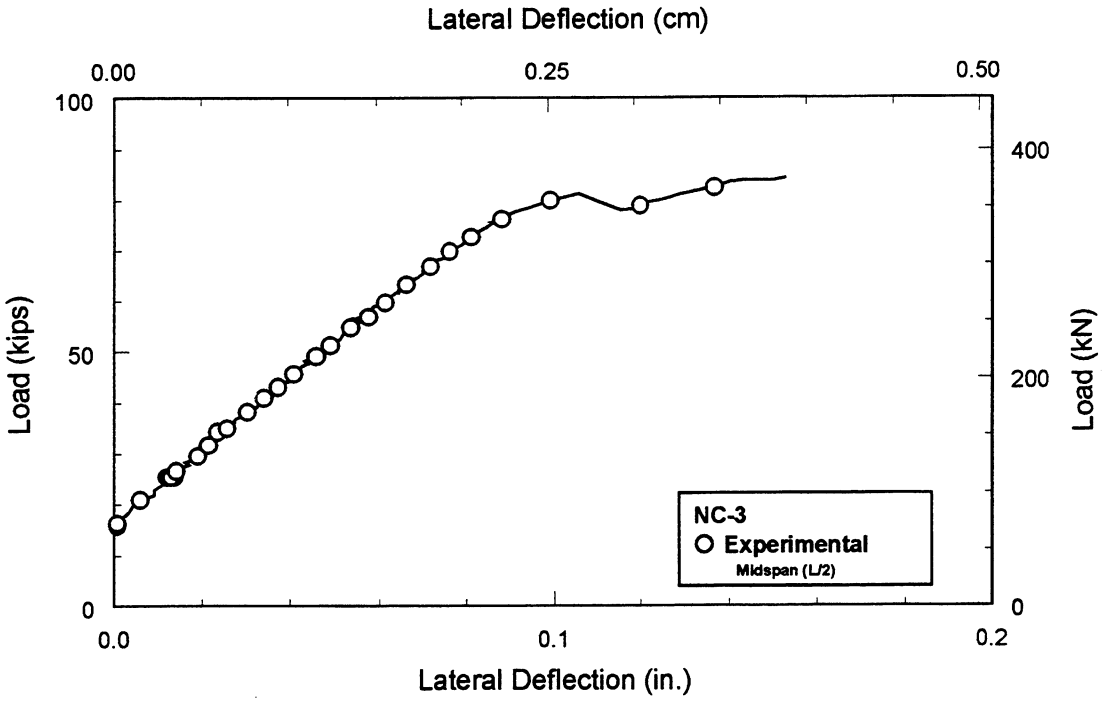

Figure B.23 Load vs Deflection Plot for Non Structural Chipped Repair.

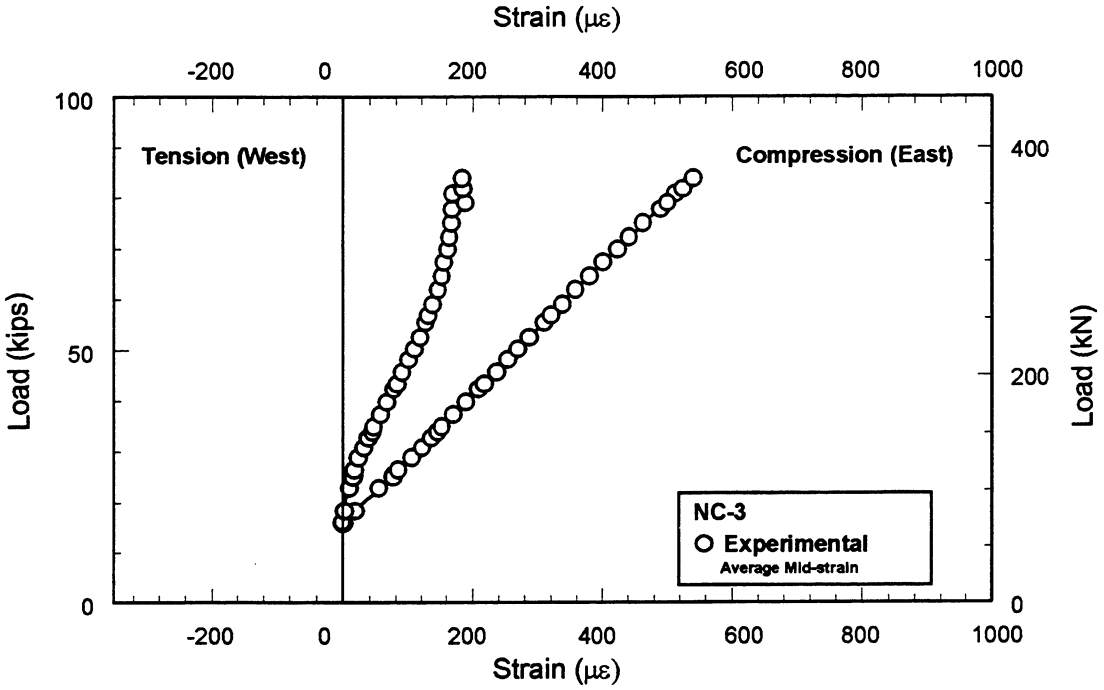

Figure B.24 Load vs Strain Variation for Non Structural Chipped Repair.

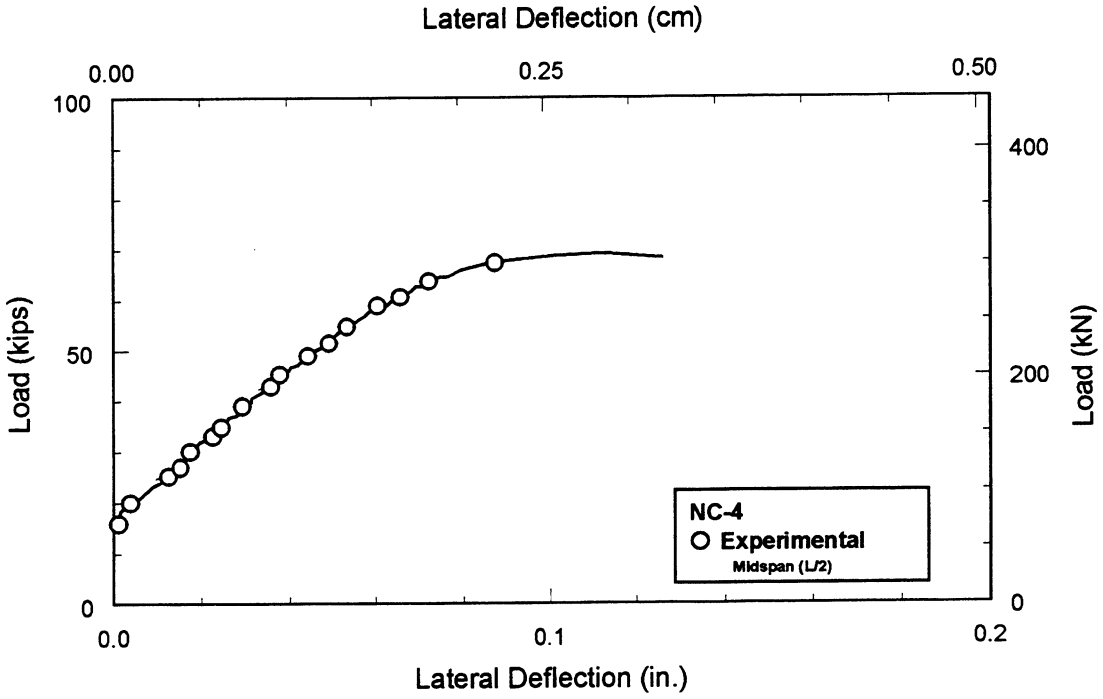

Figure B.25 Load vs Deflection Plot for Non Structural Chipped Repair.

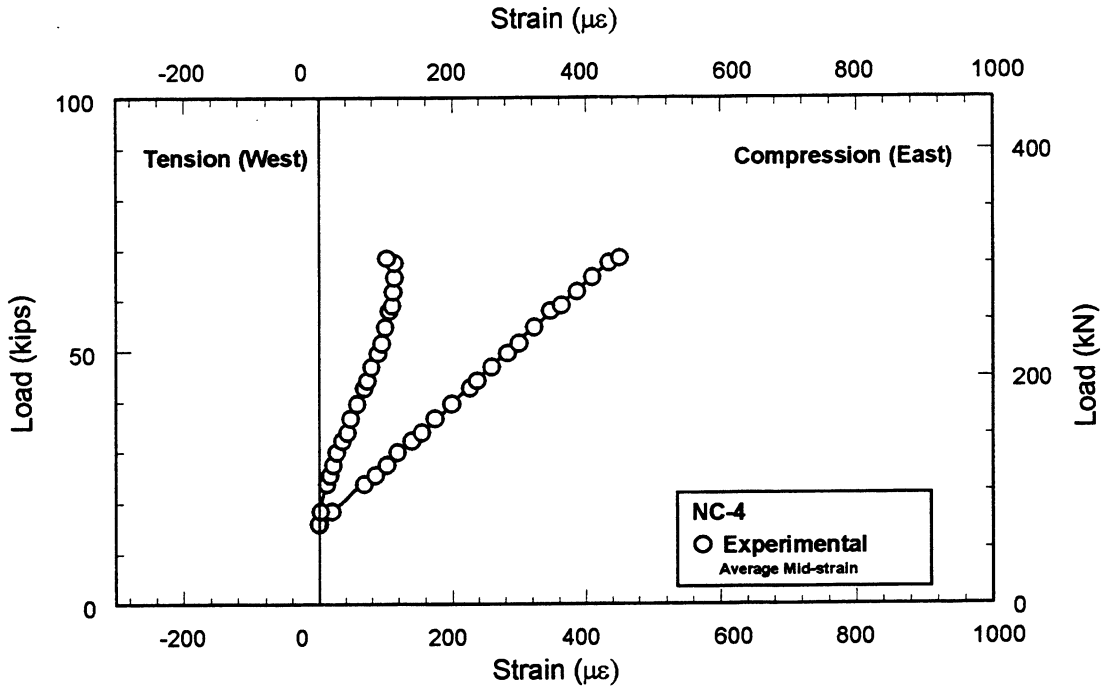

Figure B.26 Load vs Strain Variation for Non Structural Chipped Repair.

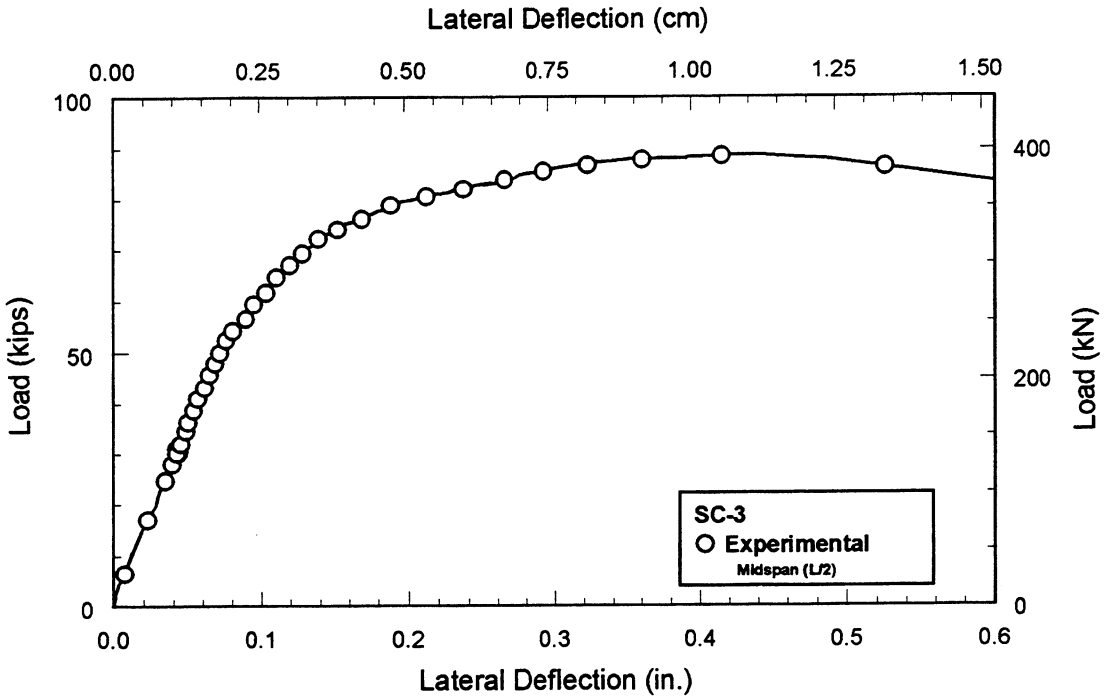

Figure B.27 Load vs Deflection Plot for Structural Chipped Repair.

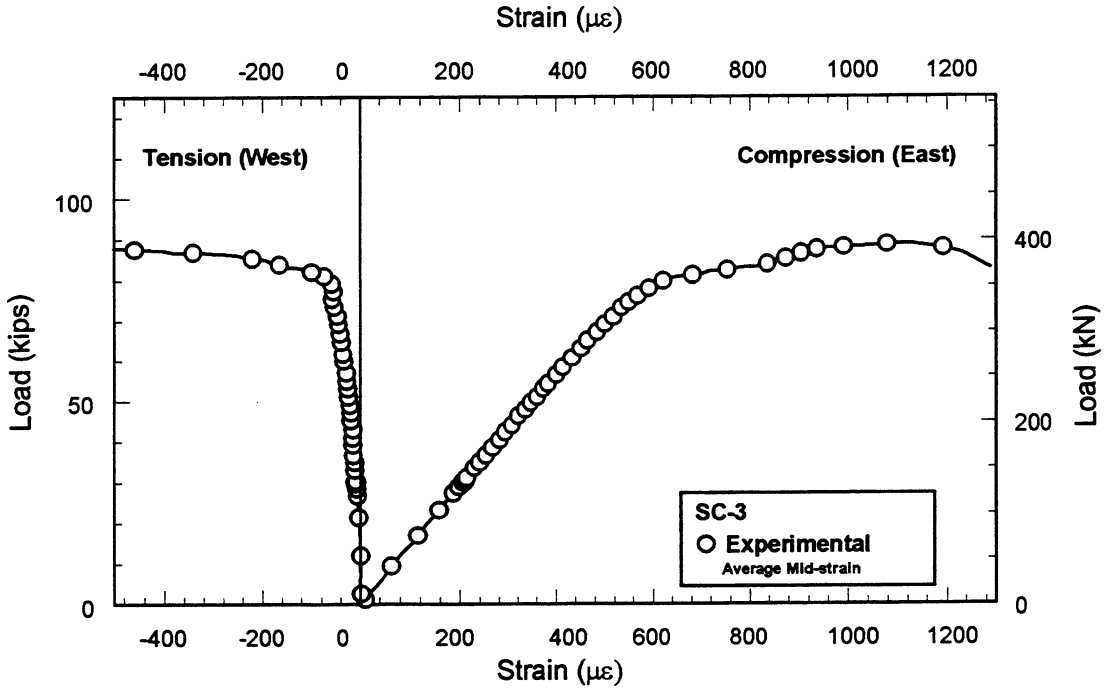

Figure B.28 Load vs Strain Variation for Structural Chipped Repair.

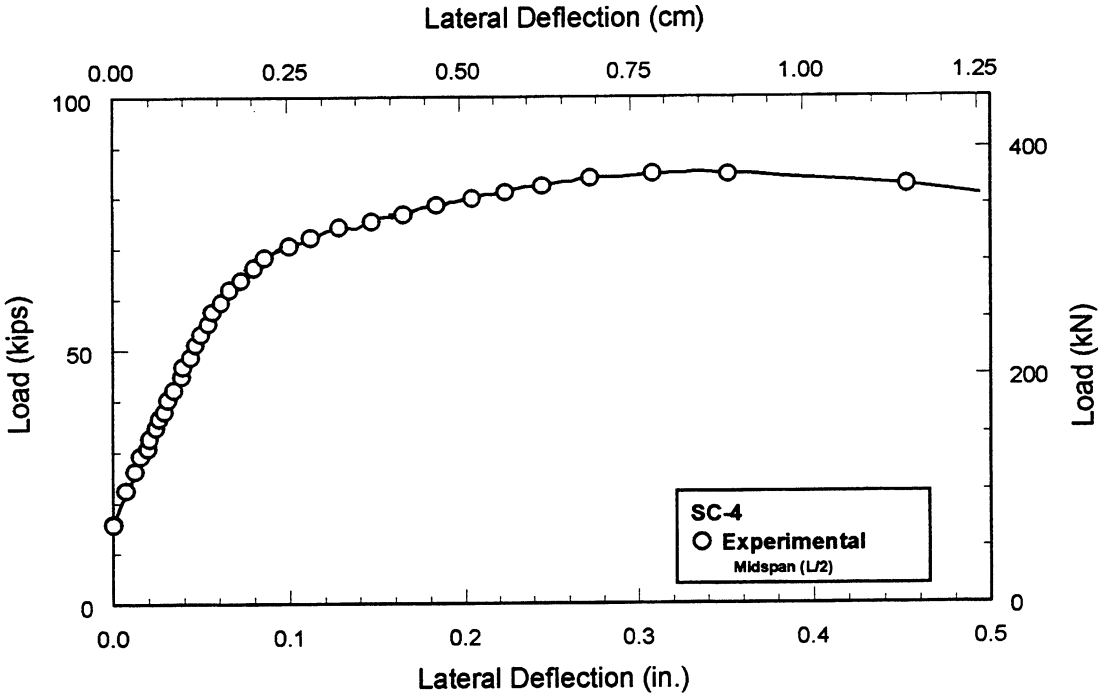

Figure B.29 Load vs Deflection Plot for Structural Chipped Repair.

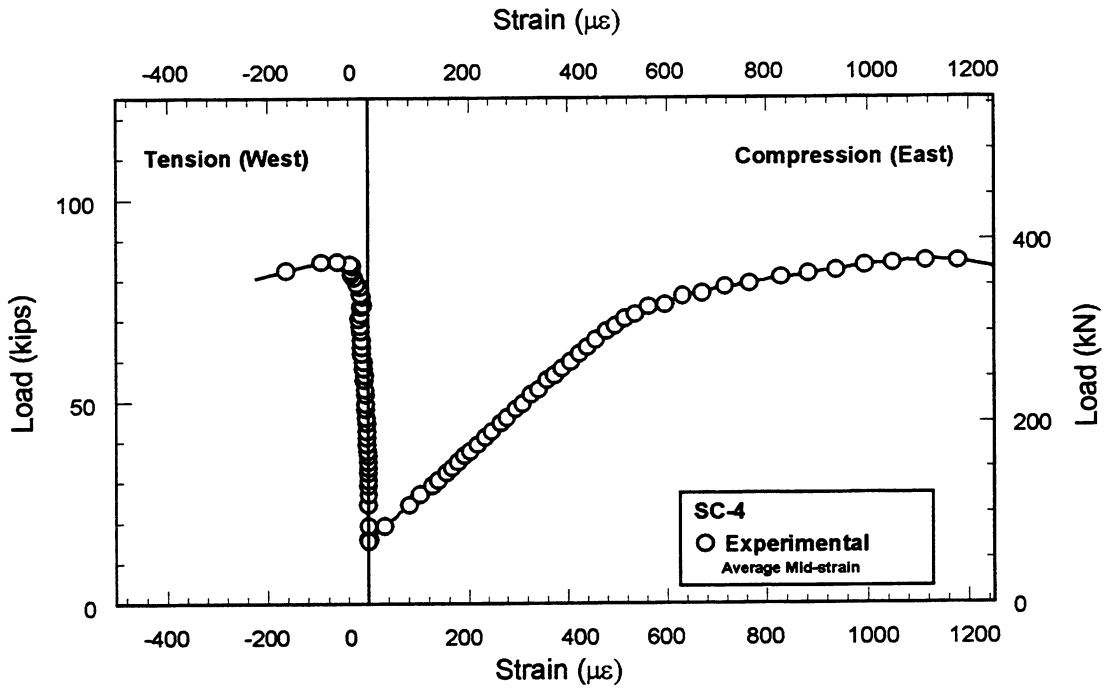

Figure B.30 Load vs Strain Variation for Structural Chipped Repair.

APPENDIX C Axial Results - Phase II

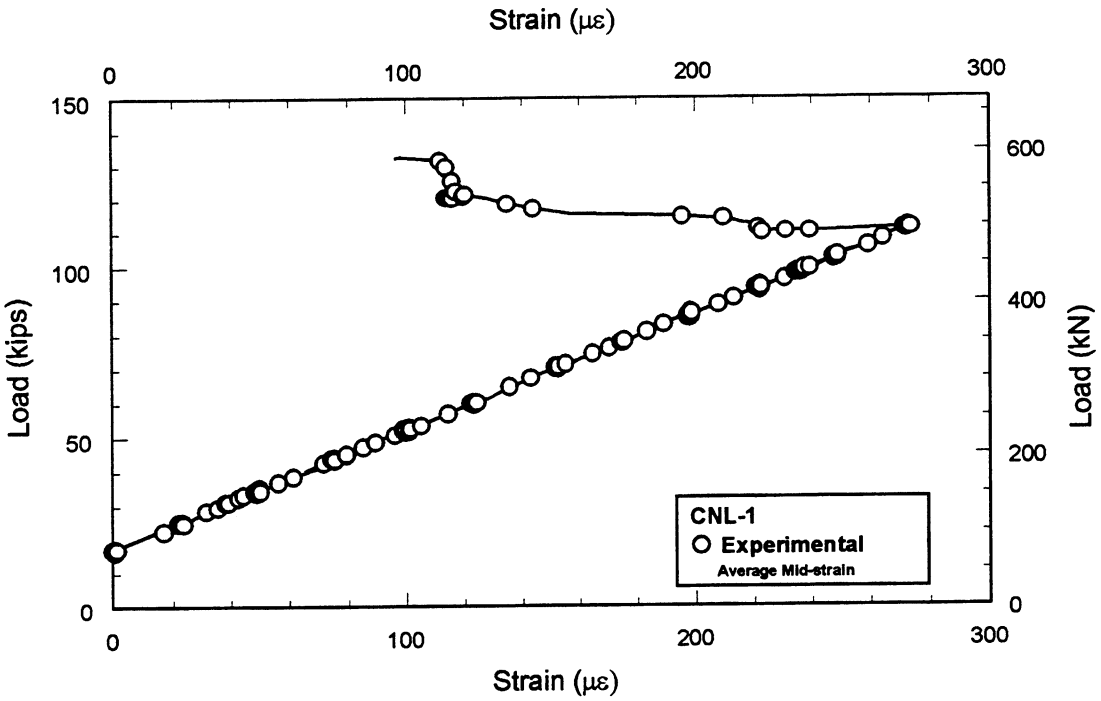

Figure C.1 Axial Strain in Control Non-Structural Repair without Nails.

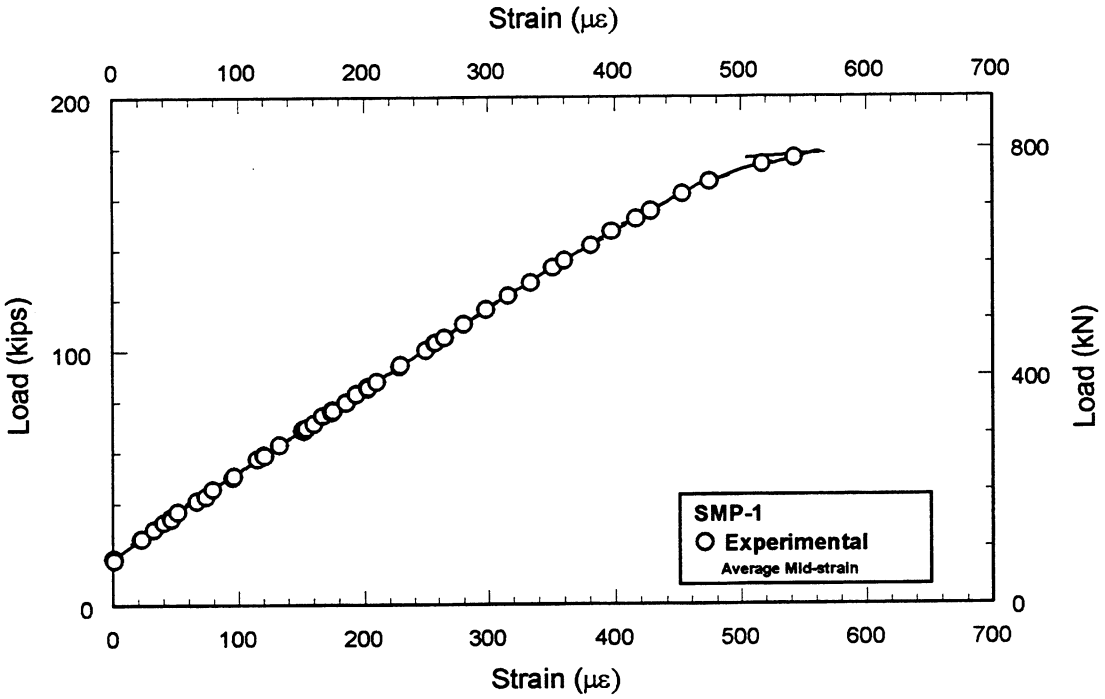

Figure C.2 Axial Strain in Structural Repair with Nails.

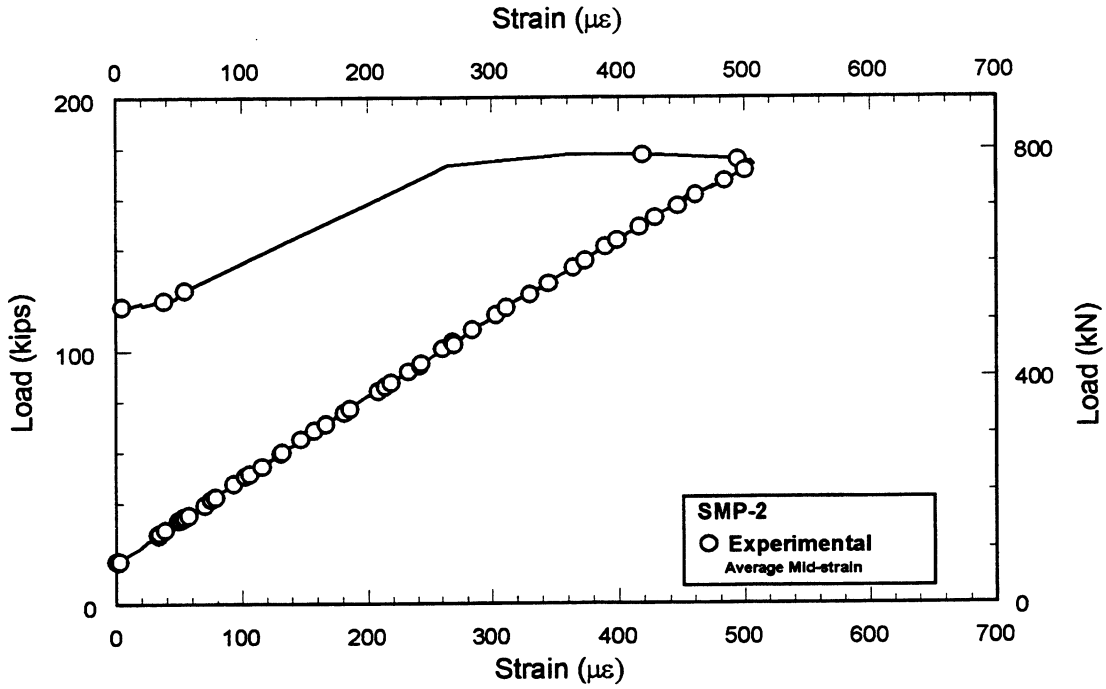

Figure C.3 Axial Strain in Structural Repair with Nails.

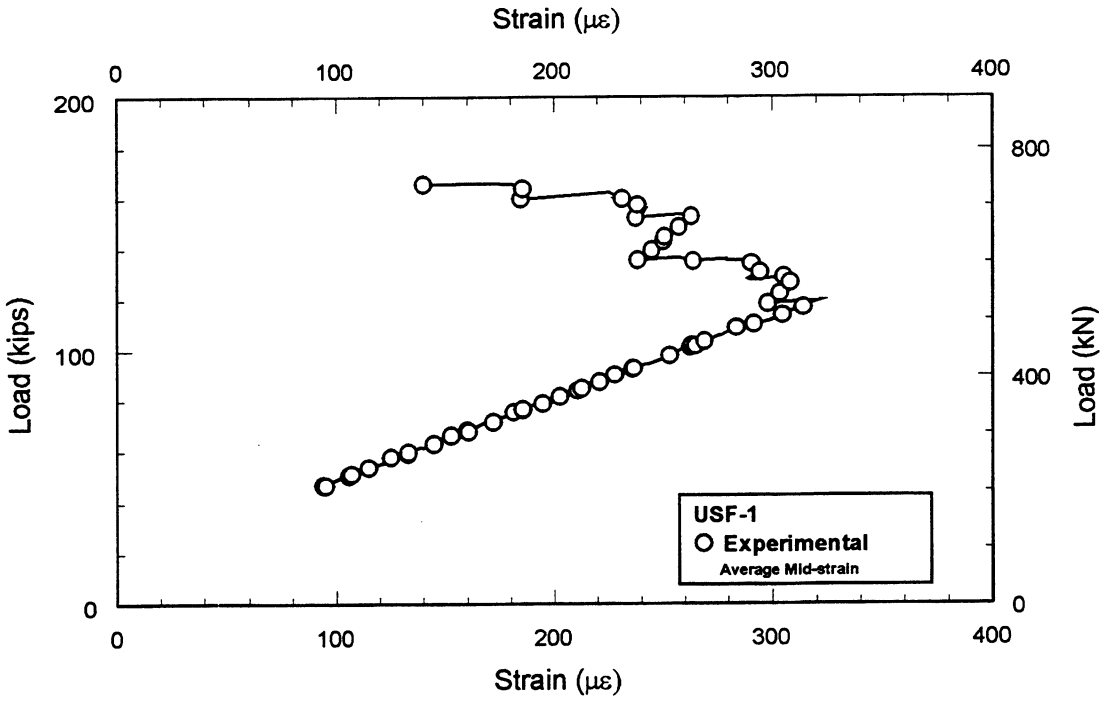

Figure C.4 Axial Strain in Non-Structural Repair with Epoxied Rebars.

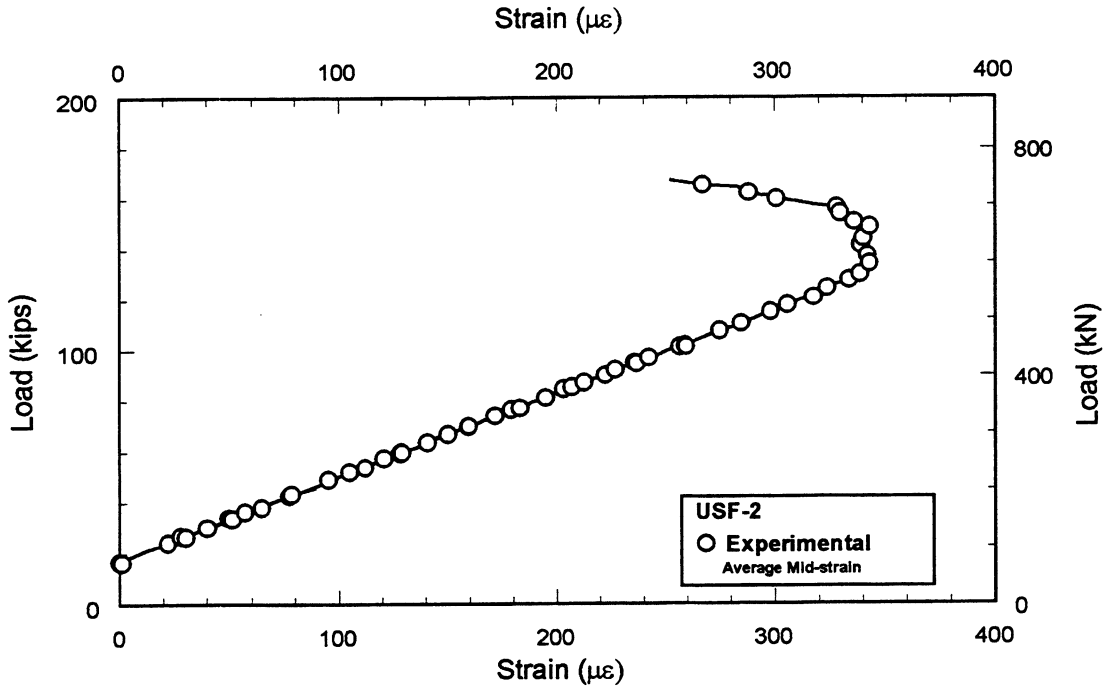

Figure C.5 Axial Strain in Non-Structural Repair with Epoxied Rebars.

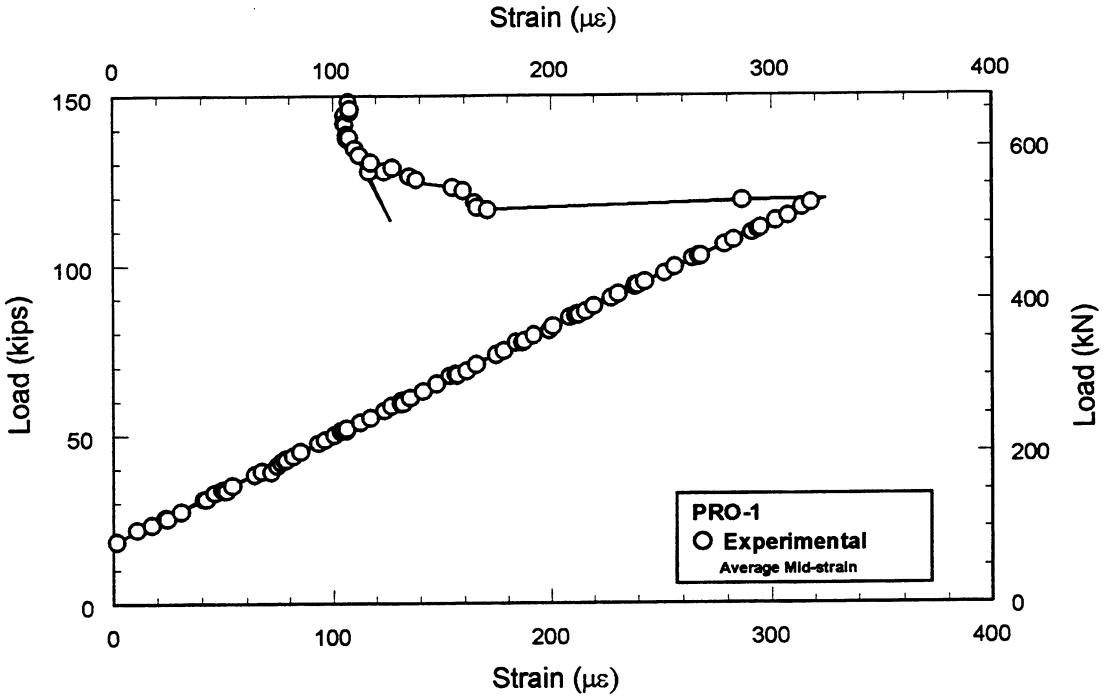

Figure C.6 Axial Strain in Non-Structural Protecrete Repair.

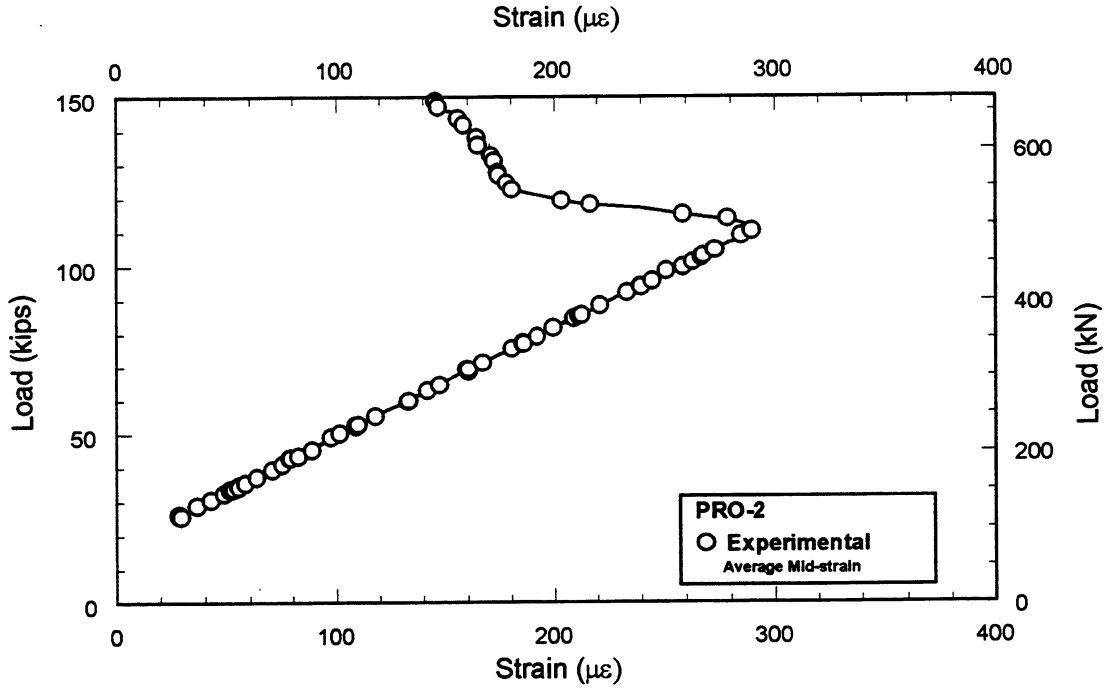

Figure C.7 Axial Strain in Non-Structural Protecrete Repair.

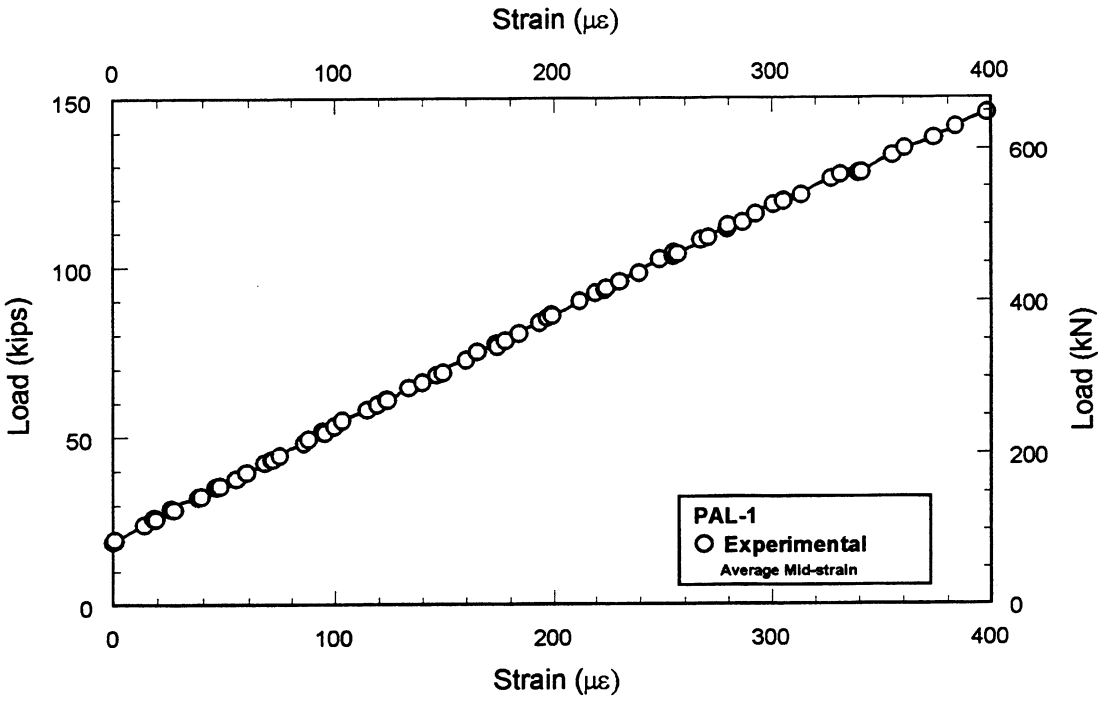

Figure C.8 Axial Strain in Non-Structural Repair with Nails at Top.

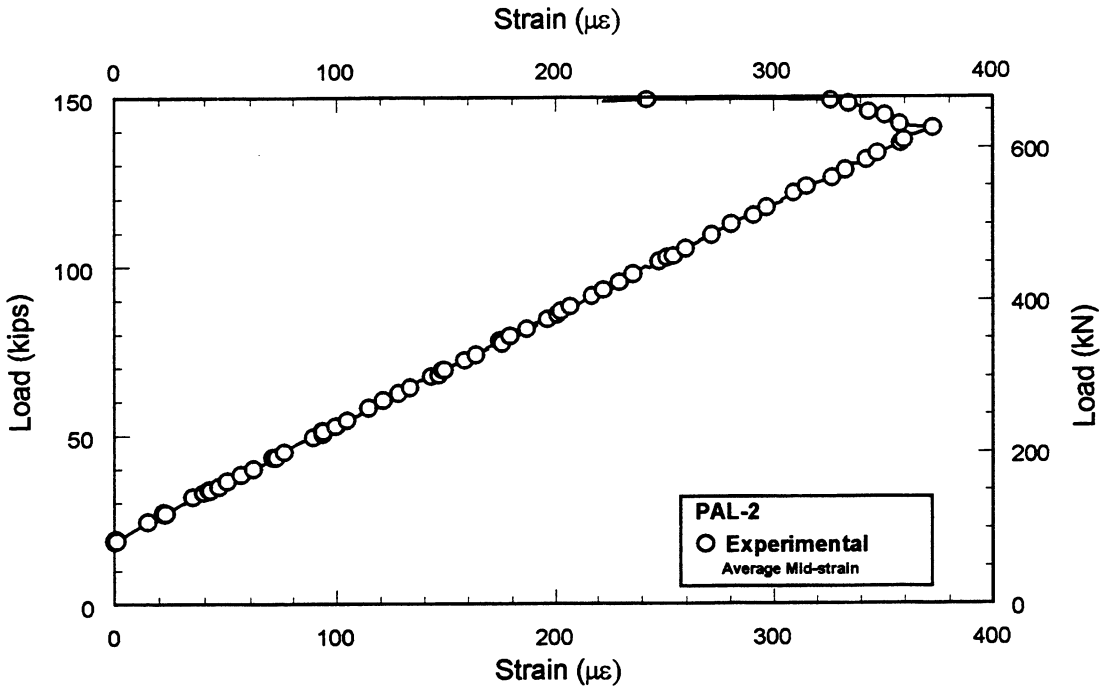

Figure C.9 Axial Strain in Non-Structural Repair with Nails at Top.

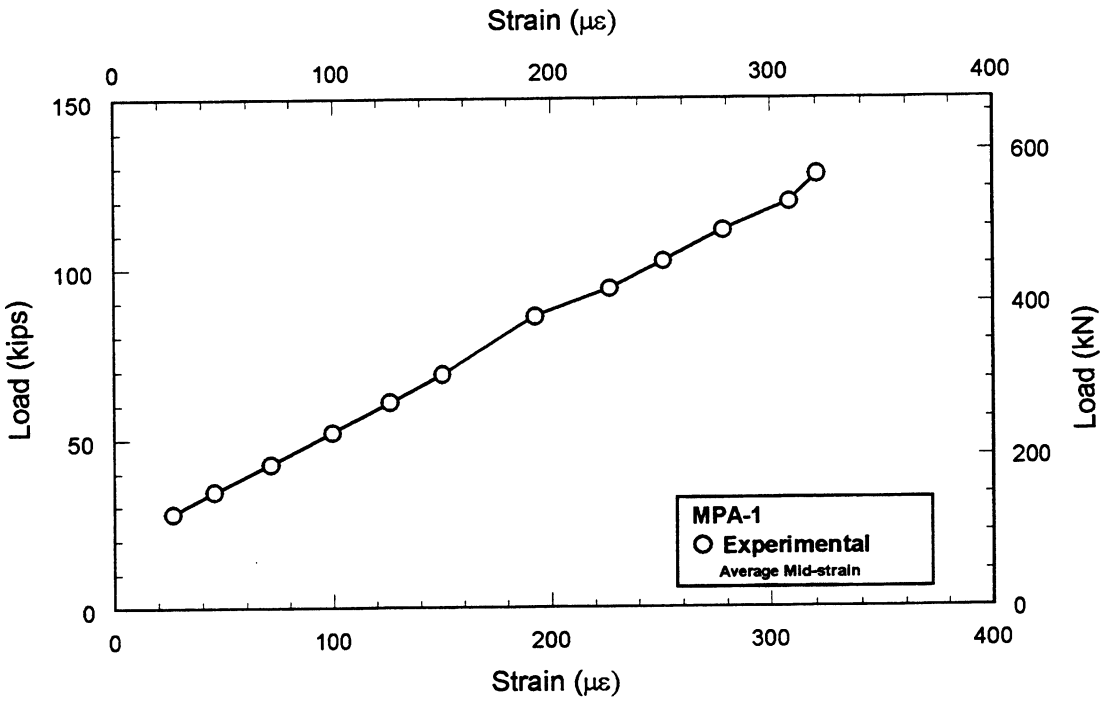

Figure C.10 Axial Strain in Non-Structural Repair with Nails at Top and Bottom.

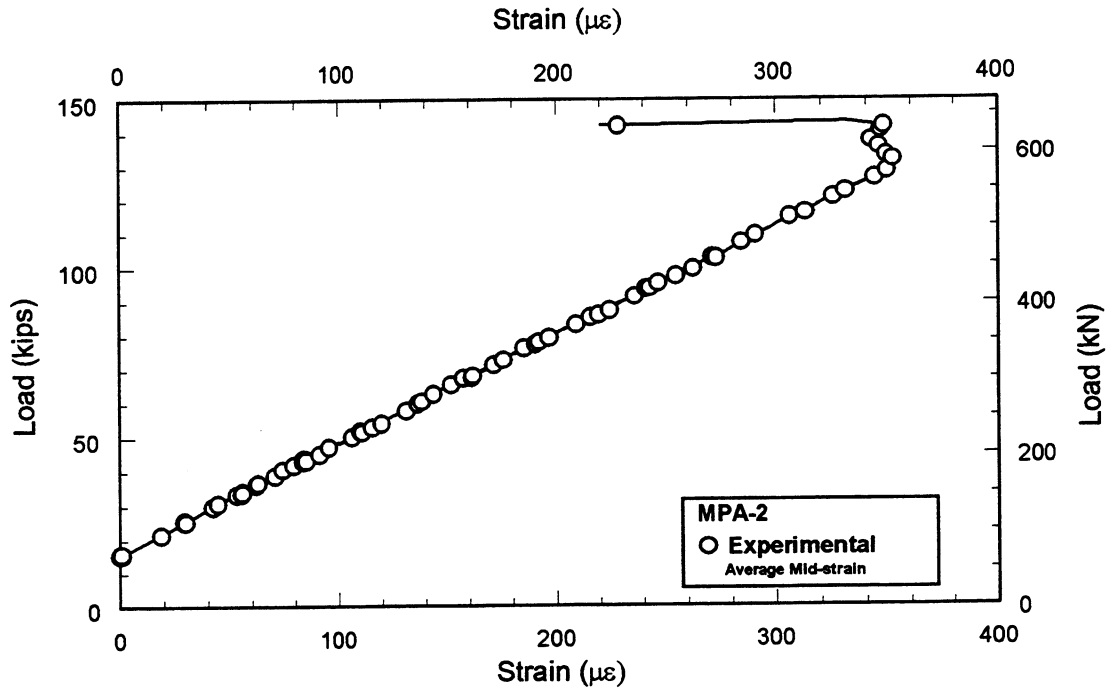

Figure C.11 Axial Strain in Non-Structural Repair with Nails at Top and Bottom.

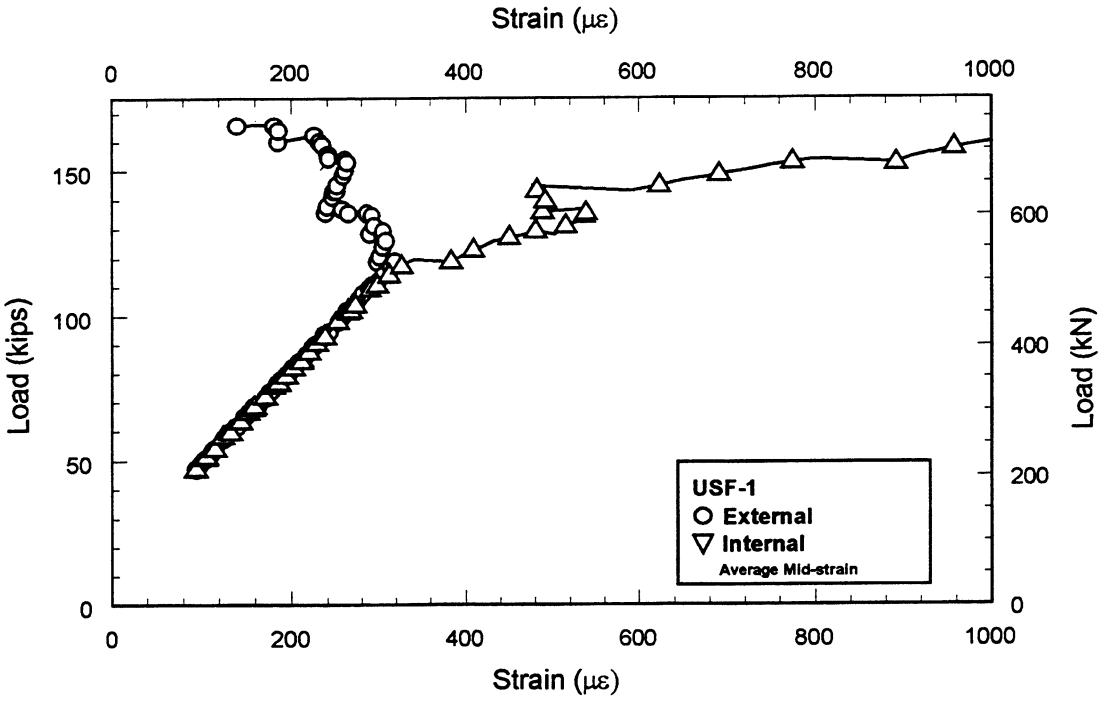

Figure C.12 Load vs Internal and External Strain in Specimen USF.

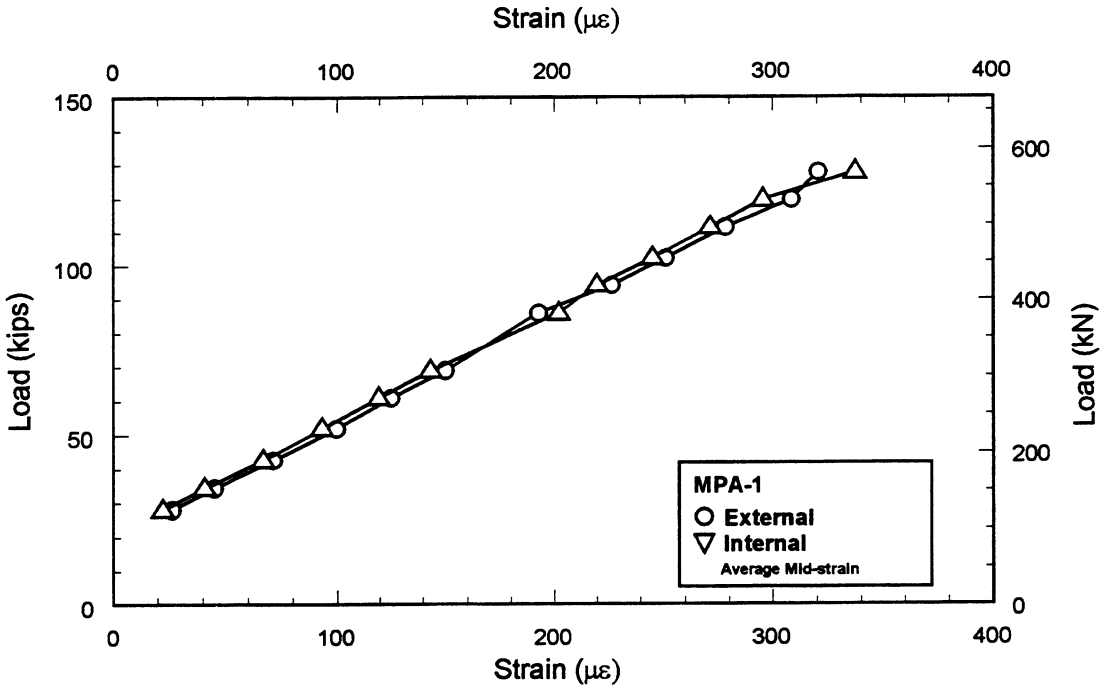

Figure C.13 Load vs Internal and External Strain in Specimen MPA.

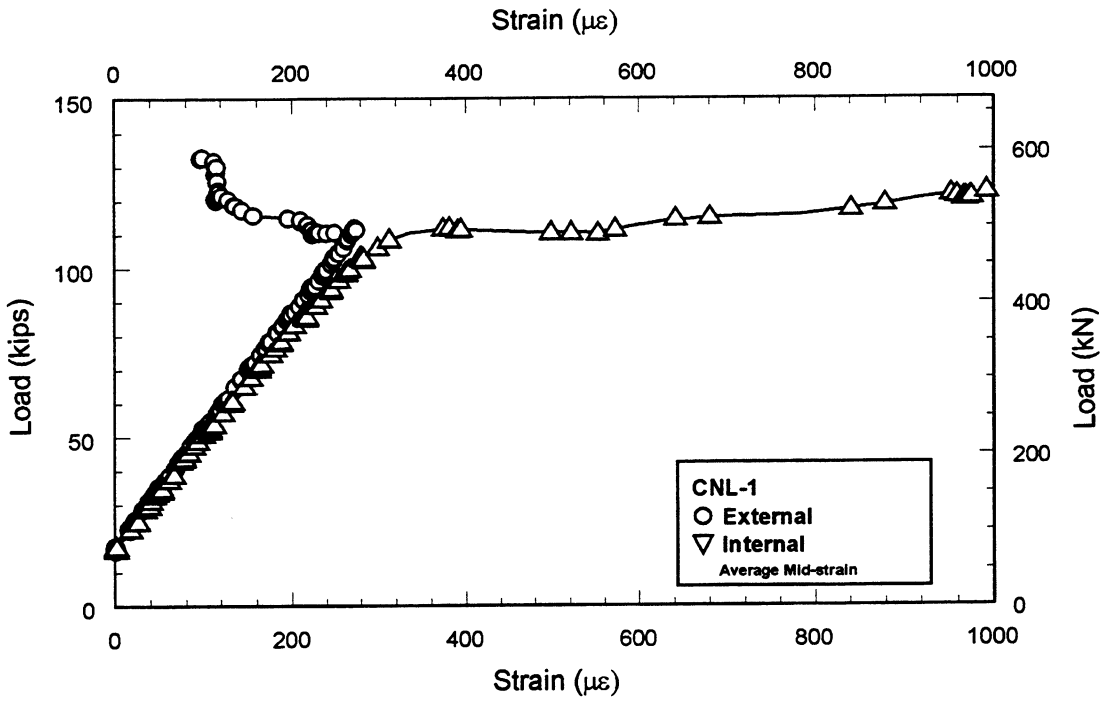

Figure C.14 Load vs Internal and External Strain in Specimen CNL.

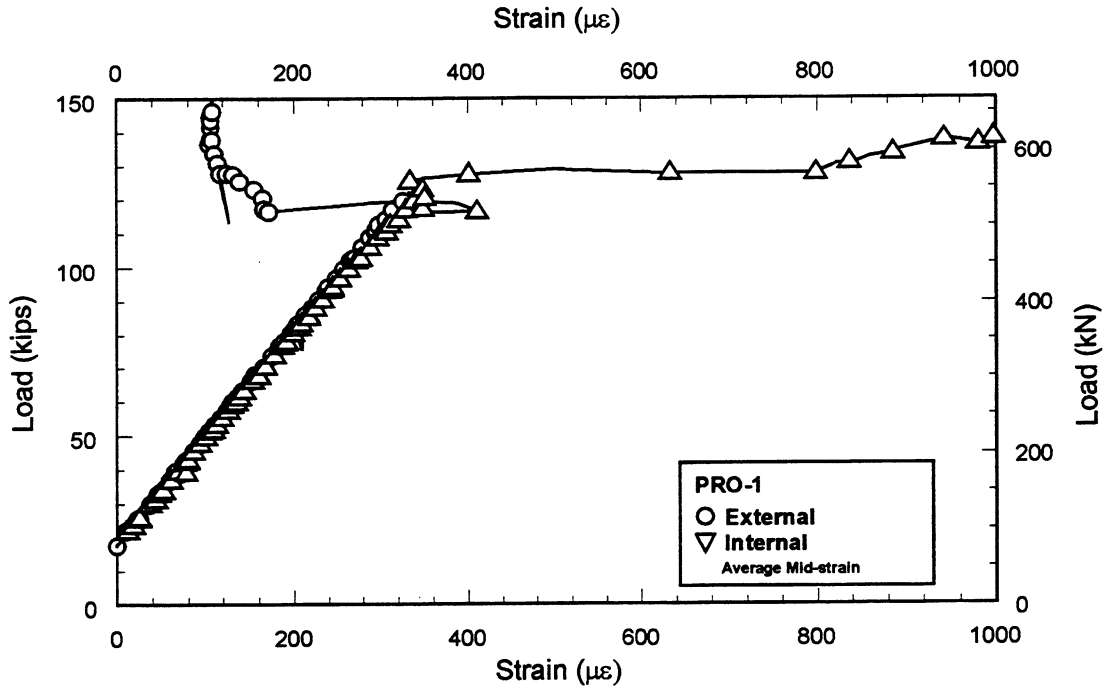

Figure C.15 Load vs Internal and External Strain in Specimen PRO.

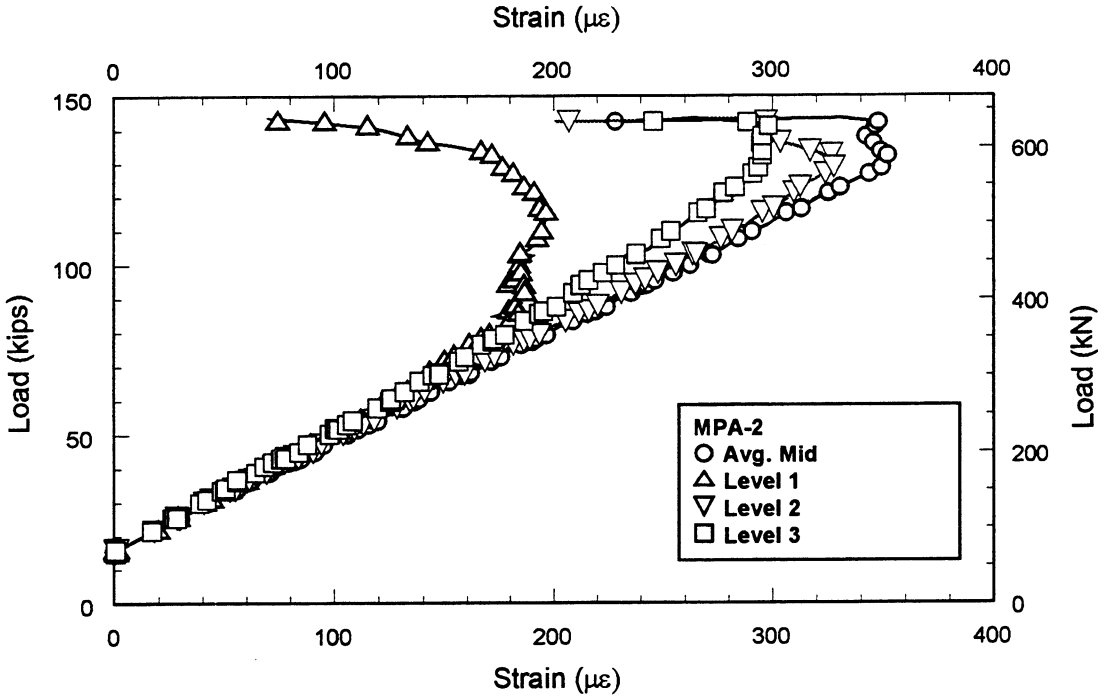

Figure C.16 Load vs Strain in Specimen MPA-2 at Three Levels.

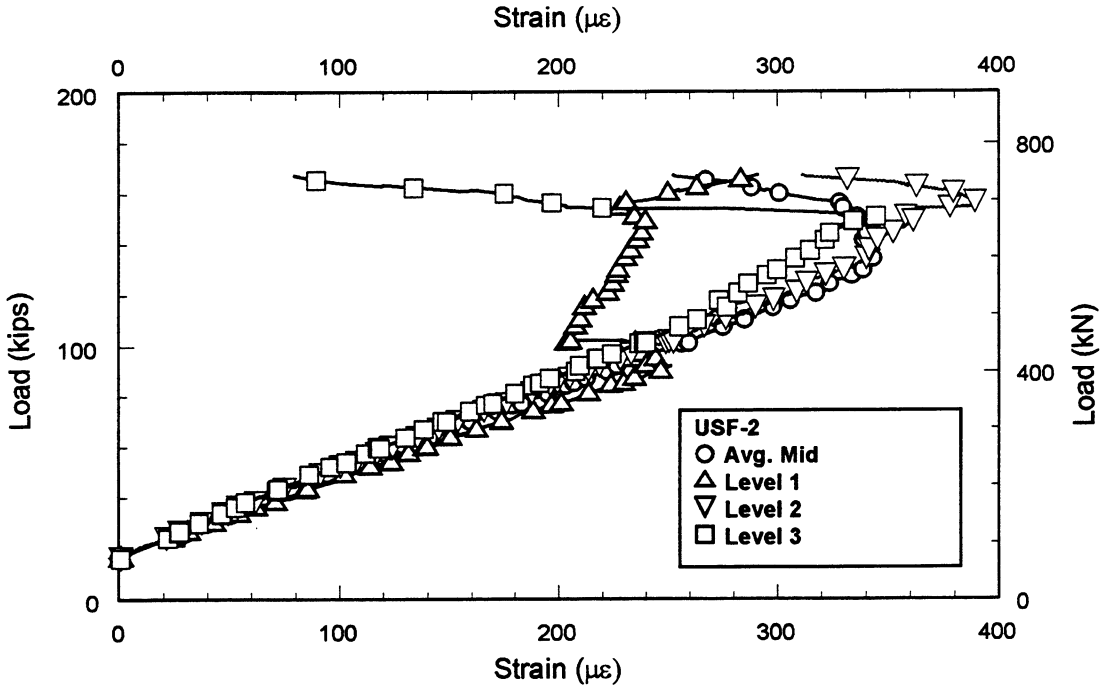

Figure C.17 Load vs Strain in Specimen USF-2 at Three Levels.

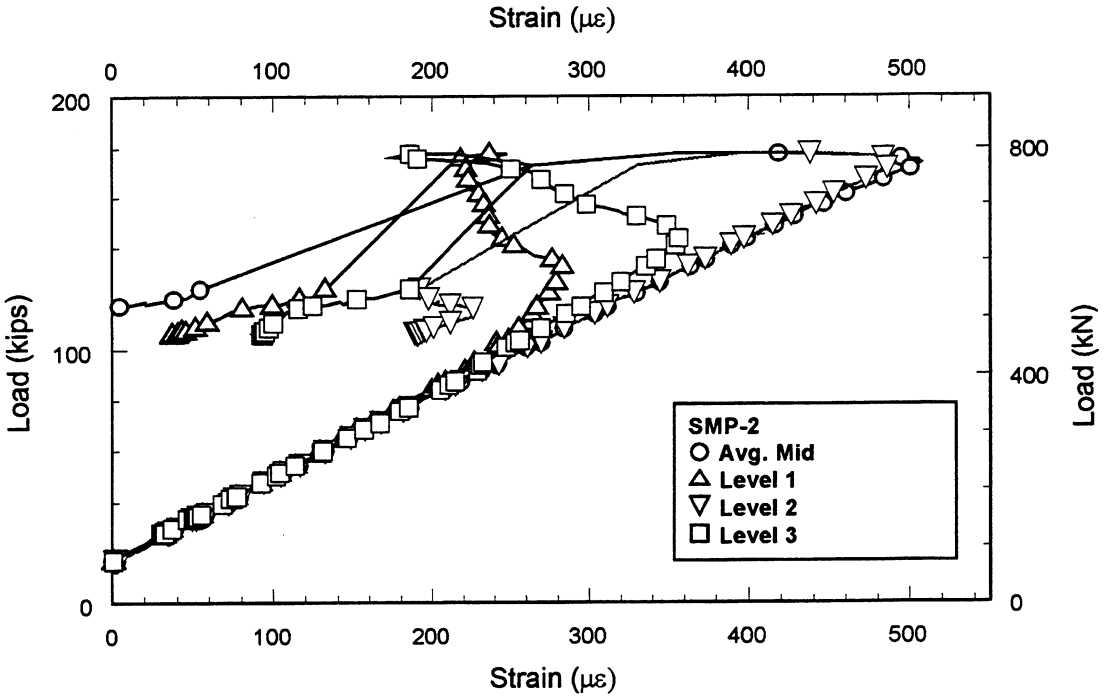

Figure C.18 Load vs Strain in Strain in Specimen SMP-2 at three Levels.

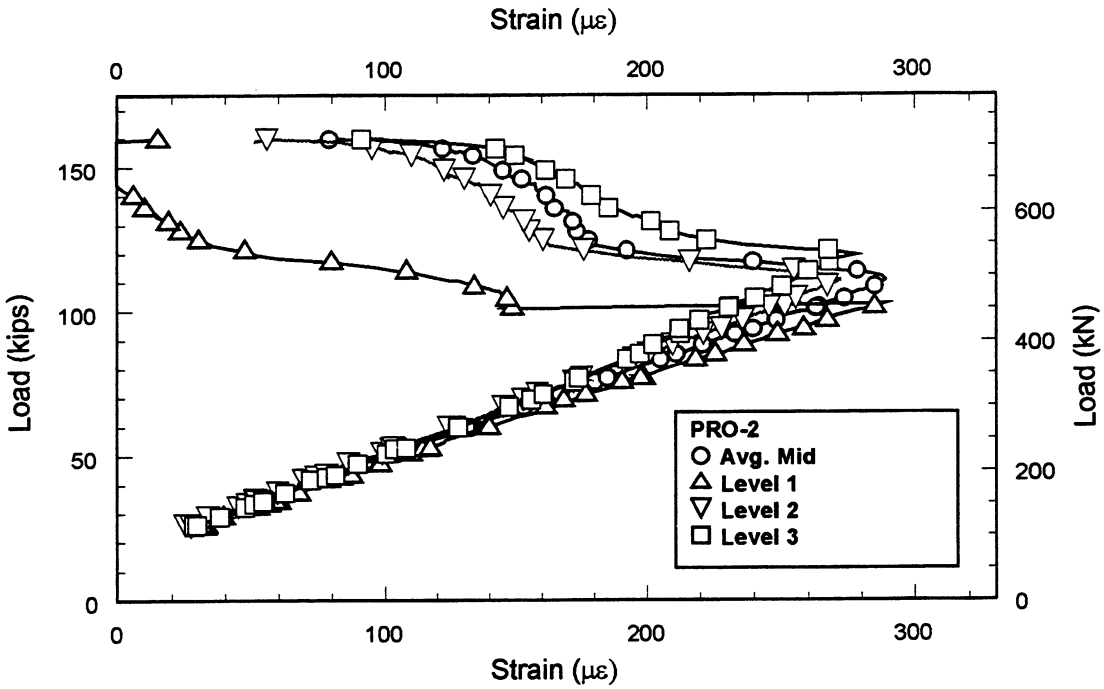

Figure C.19 Load vs Strain in Specimen PRO-2 Repair at Three Levels.

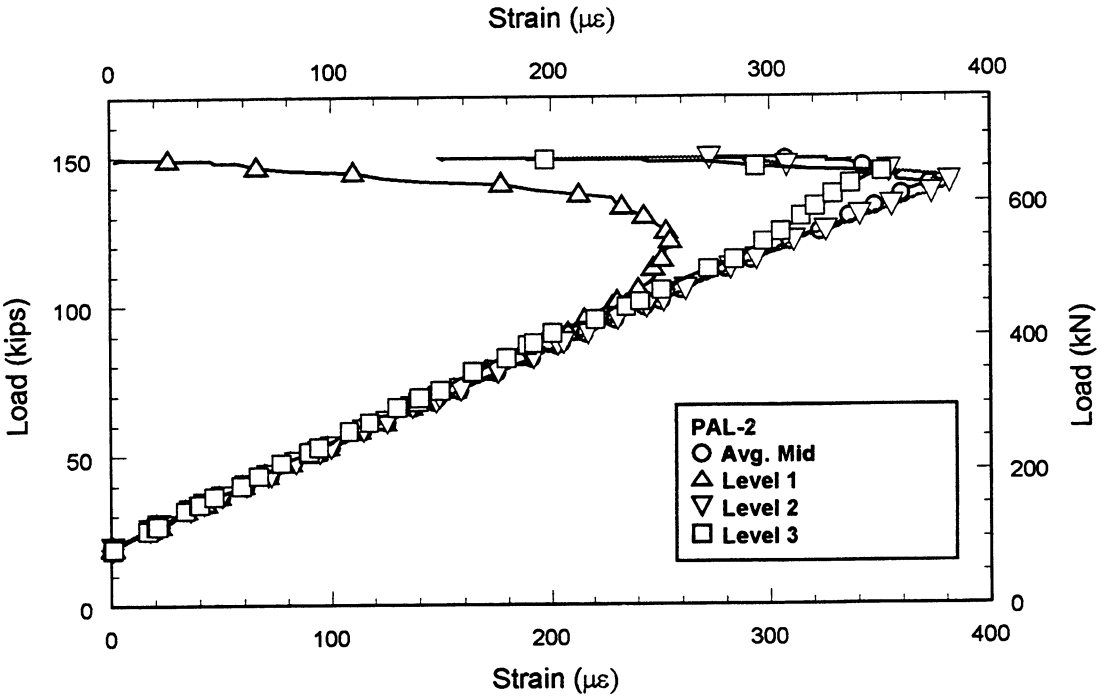

Figure C.20 Load vs Strain in Specimen PAL-2 Repair at Three Levels.

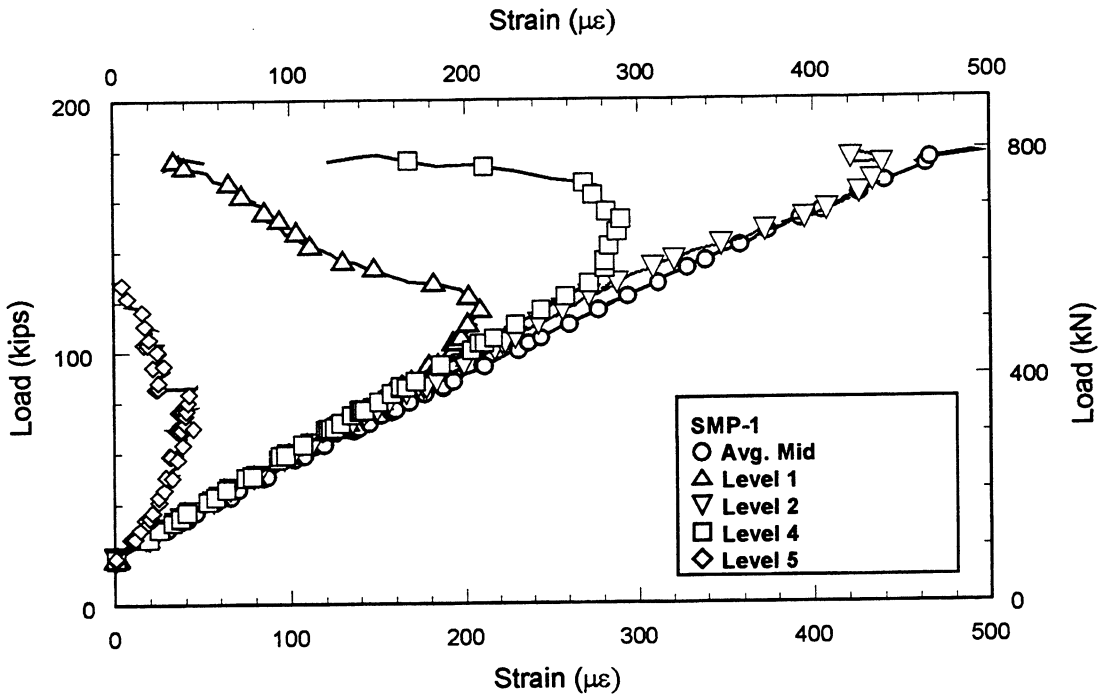

Figure C.21 Load vs Strain in Specimen SMP-1 Repair at Five Levels.

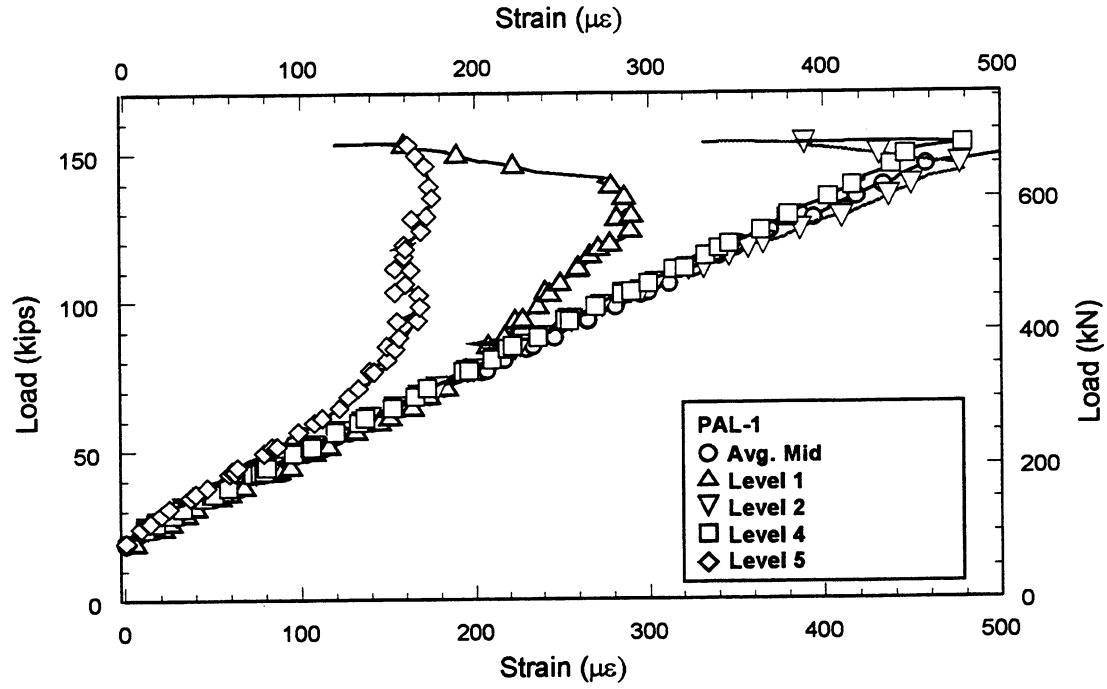

Figure C.22 Load vs Strain in Specimen PAL-1 Repair at Five Levels.

APPENDIX D Finite Element Comparison

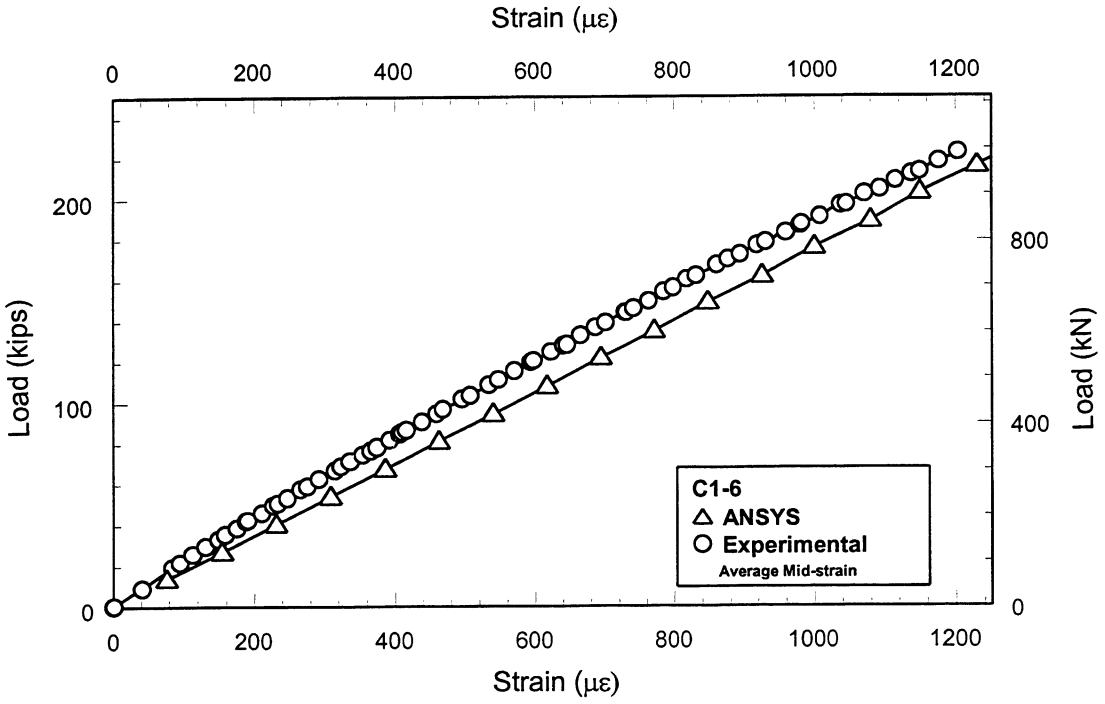

Figure D.1 Finite Element Comparison - Phase I Axial Test C1-6.

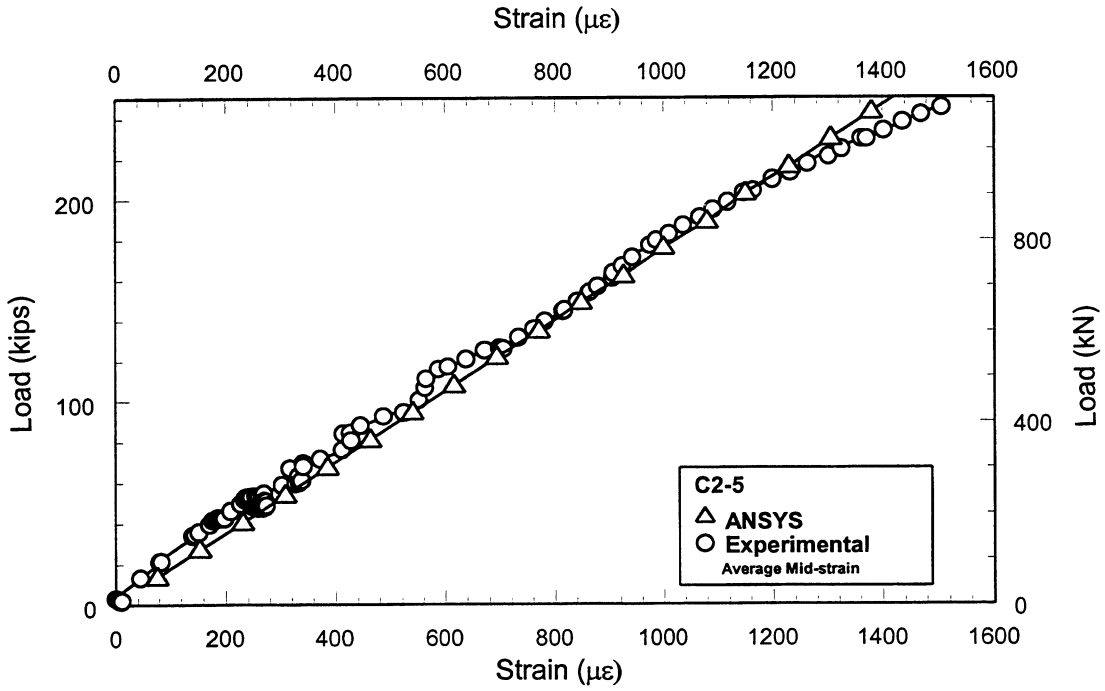

Figure D.2 Finite Element Comparison - Phase I Axial Test C2-5.

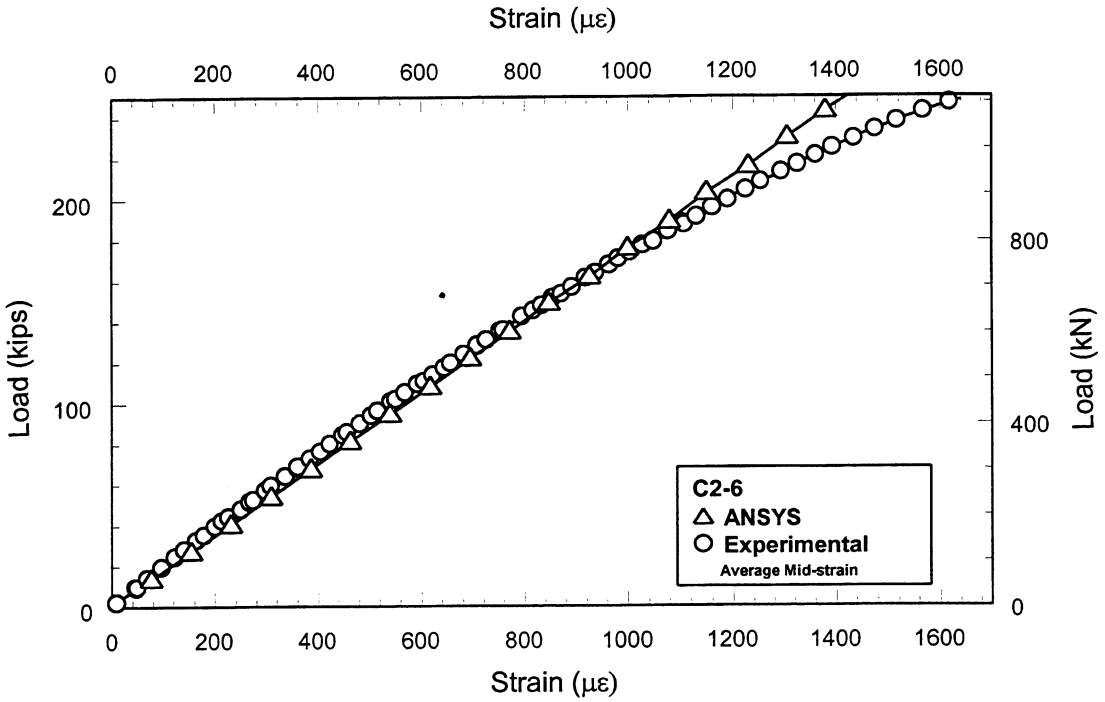

Figure D.3 Finite Element Comparison - Phase I Axial Test C2-6.

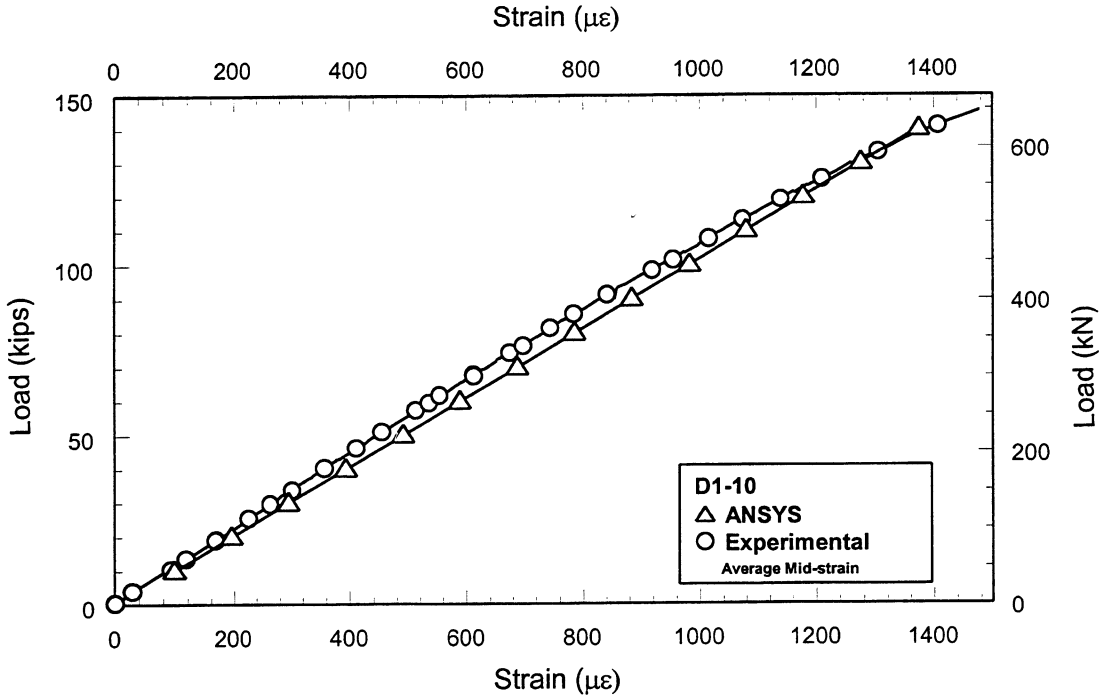

Figure D.4 Finite Element Comparison - Phase I Axial Test D1-10.

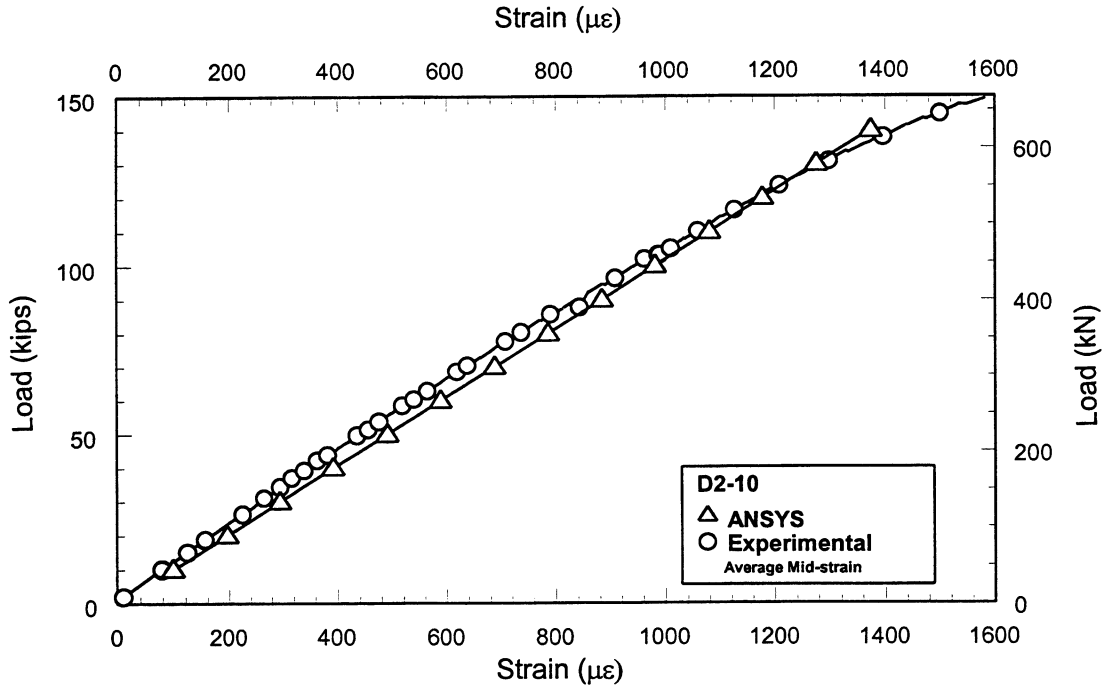

Figure D.5 Finite Element Comparison - Phase I Axial Test D2-10.

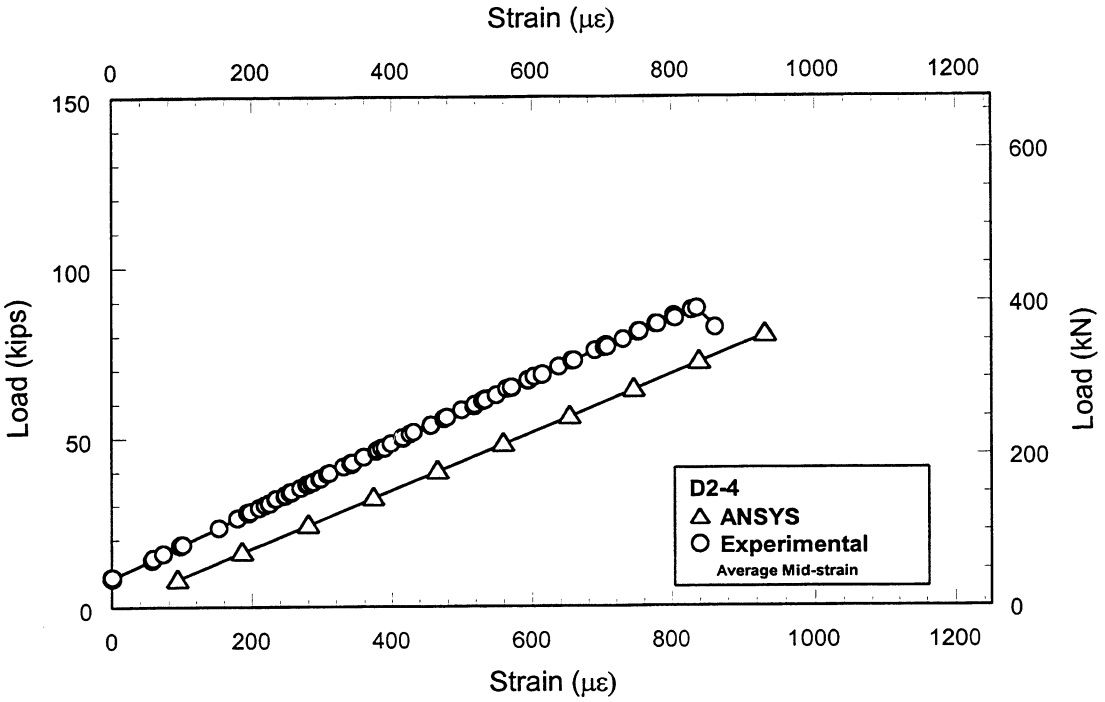

Figure D.6 Finite Element Comparison - Phase II Axial Test D2-4.

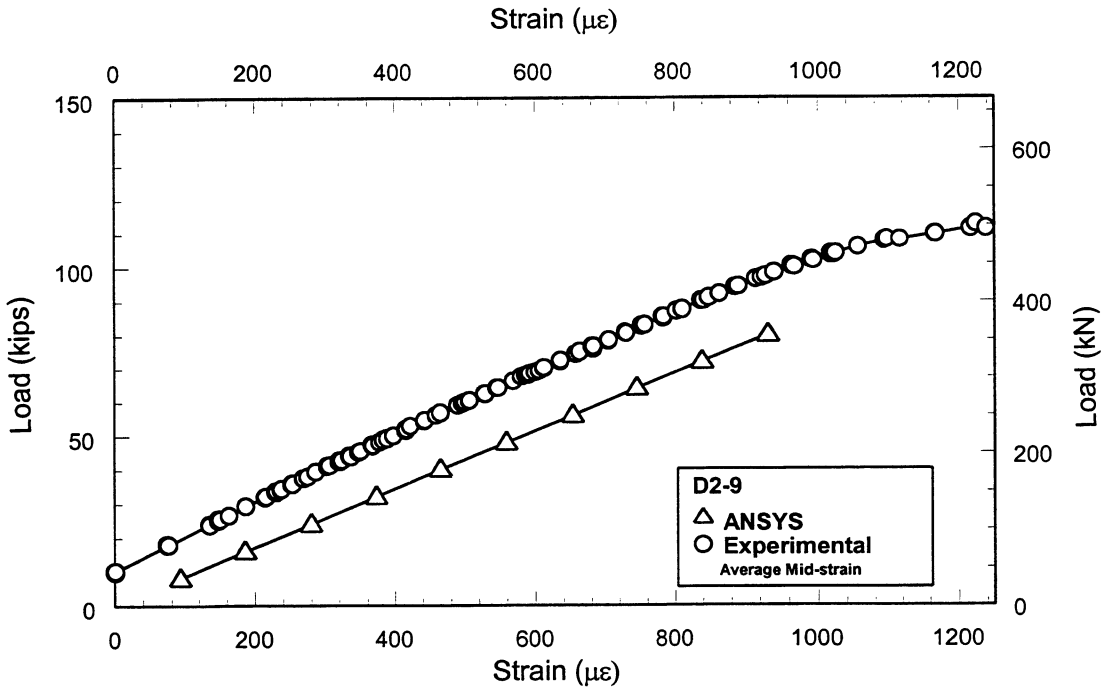

Figure D.7 Finite Element Comparison - Phase II Axial Test D2-9.

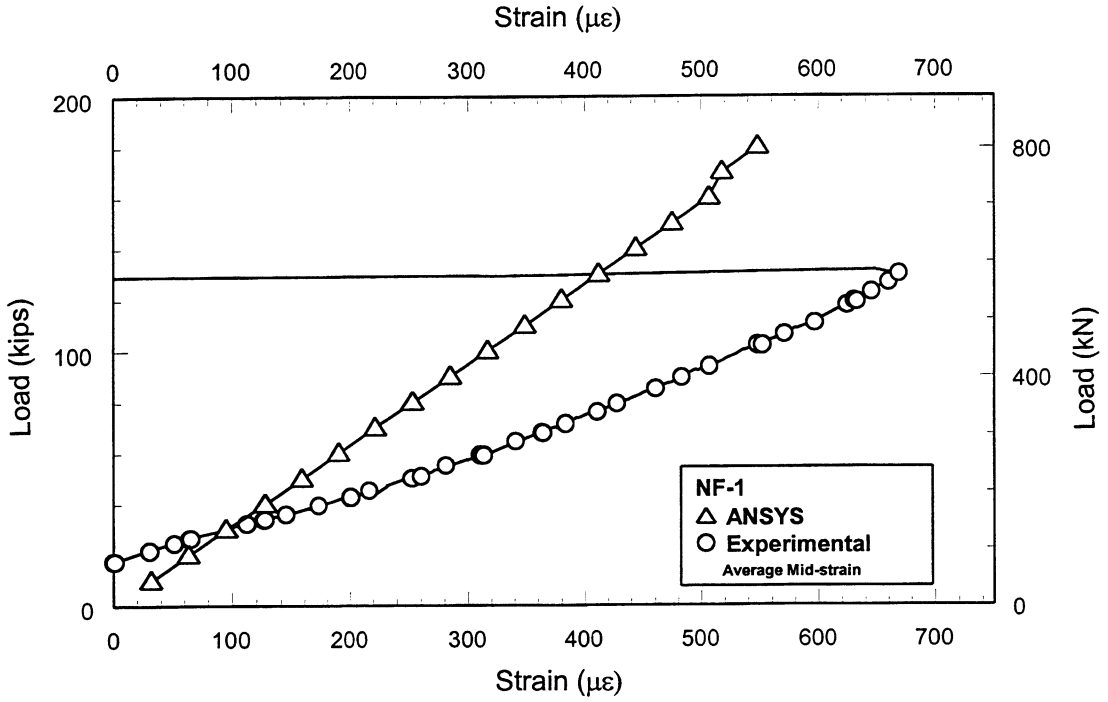

Figure D.8 Finite Element Comparison - Phase I Axial Test NF-1.

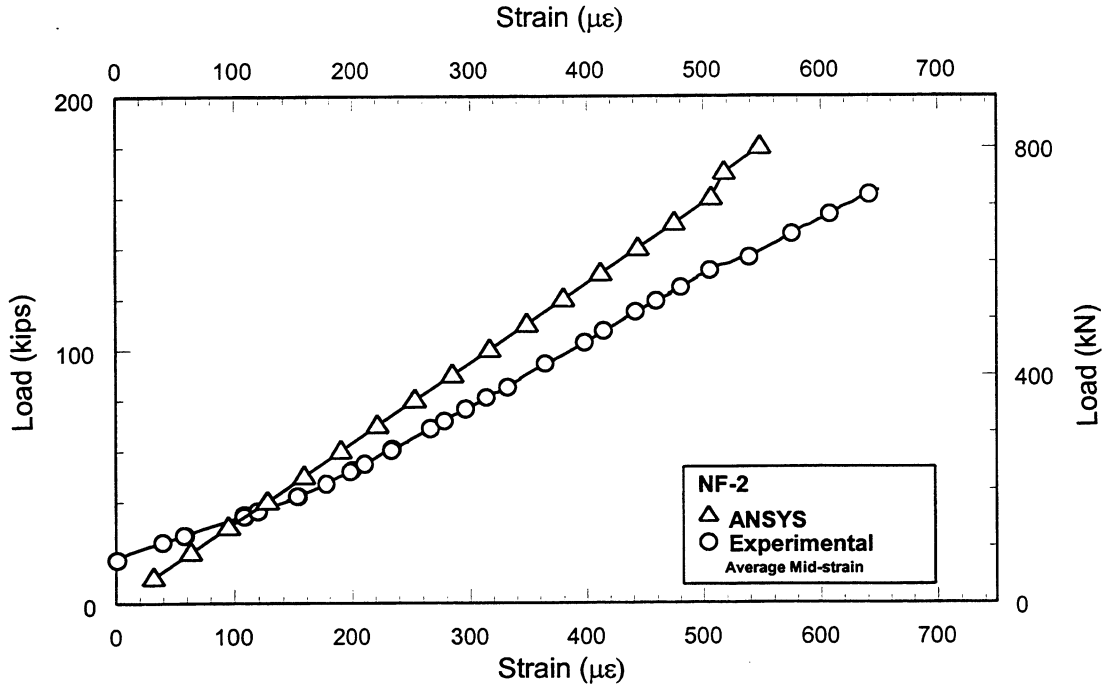

Figure D.9 Finite Element Comparison - Phase I Axial Test NF-2.

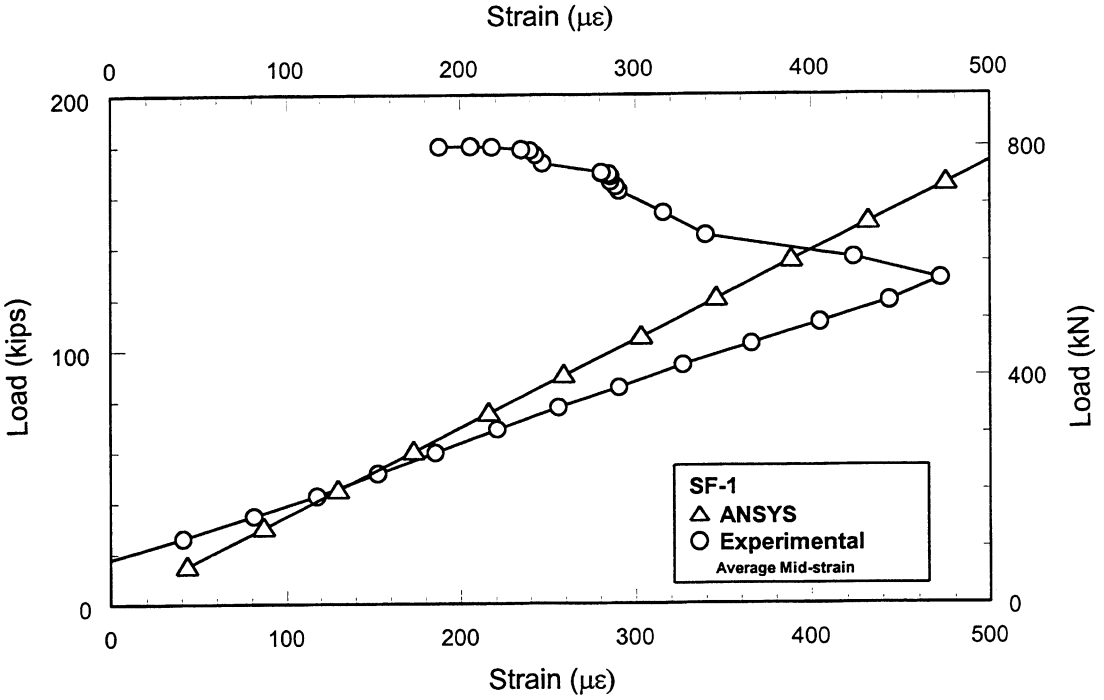

Figure D.10 Finite Element Comparison - Phase I Axial Test SF-1.

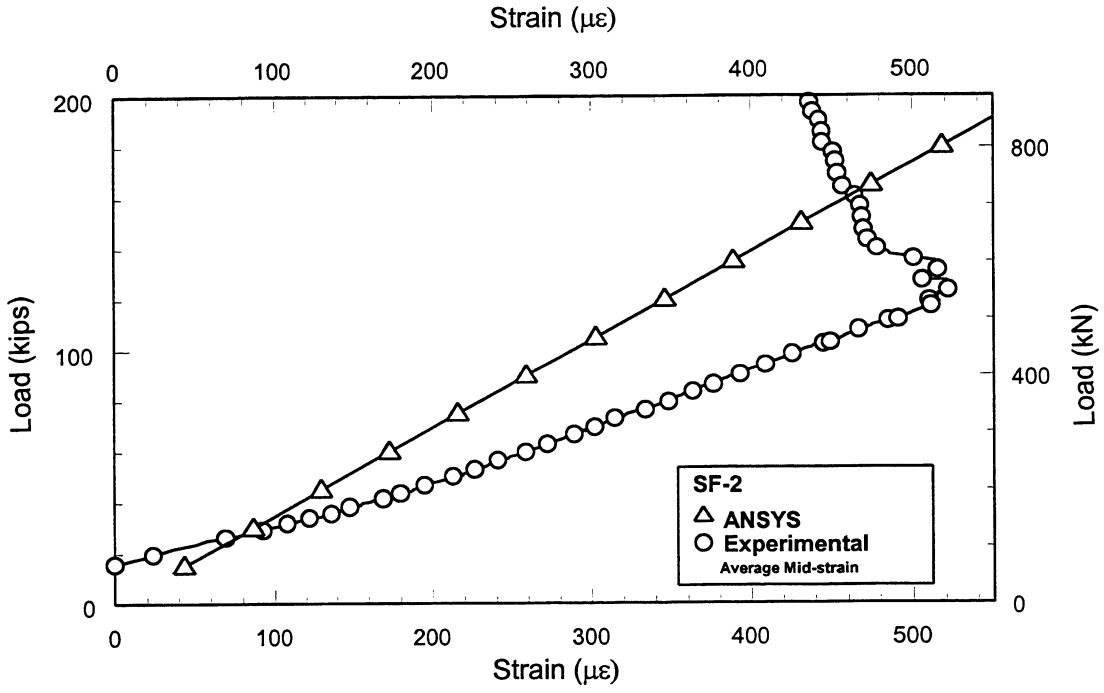

Figure D.11 Finite Element Comparison - Phase I Axial Test SF-2.

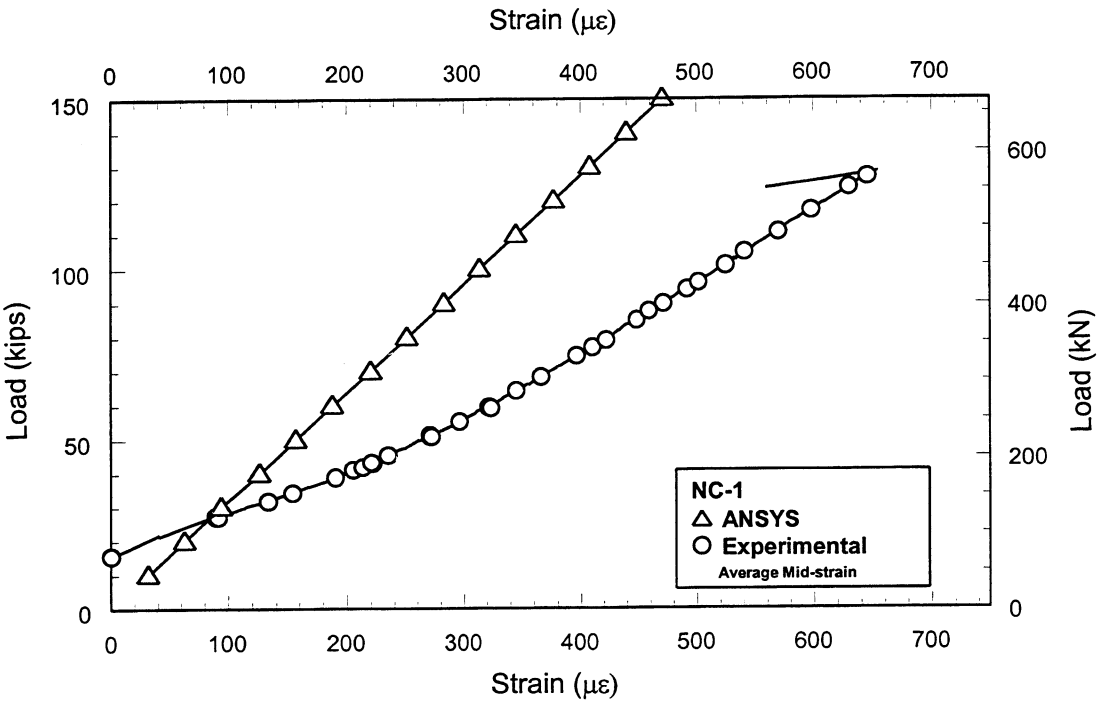

Figure D.12 Finite Element Comparison - Phase I Axial Test NC-1.

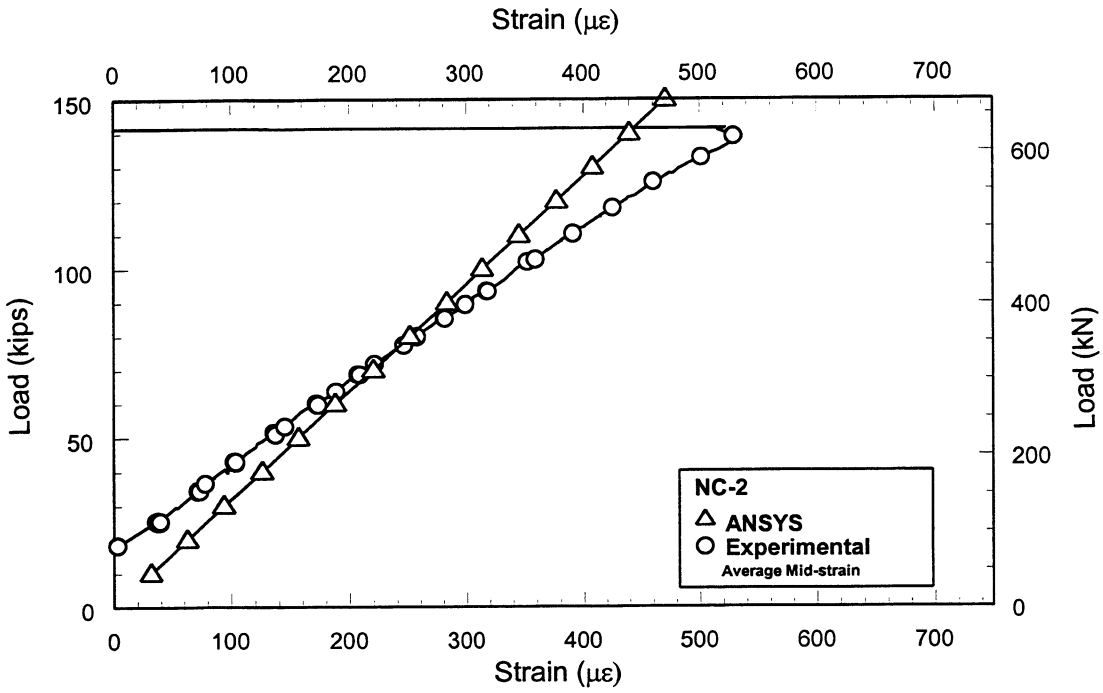

Figure D.13 Finite Element Comparison - Phase I Axial Test NC-2.

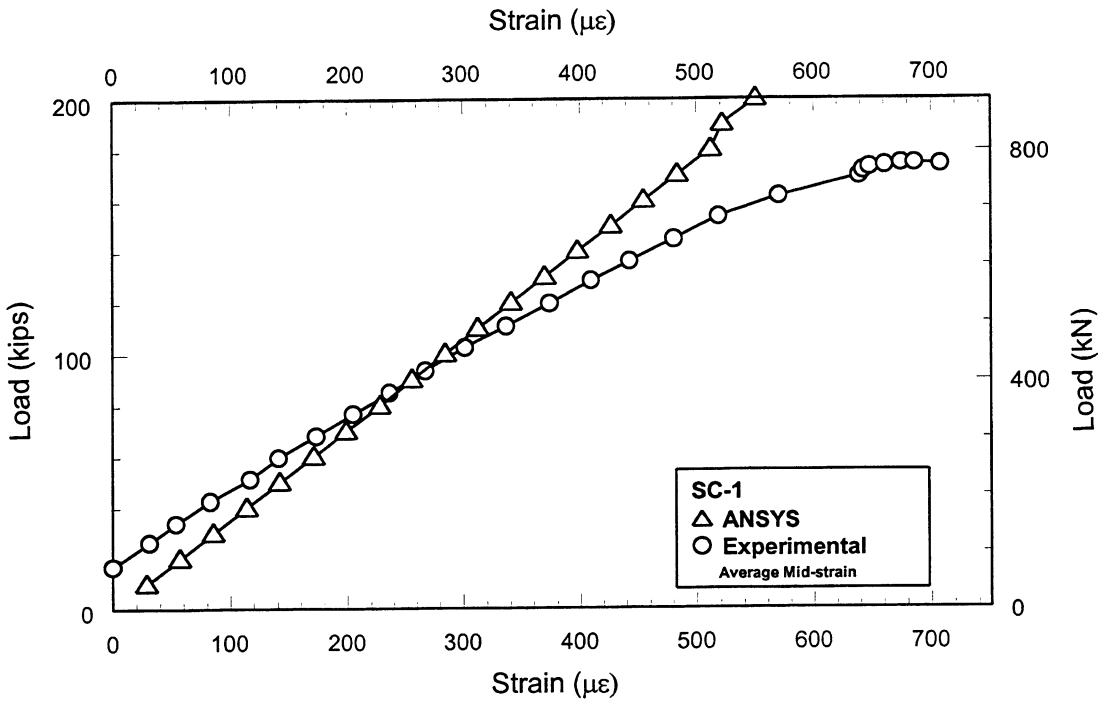

Figure D.14 Finite Element Comparison - Phase I Axial Test SC-1.

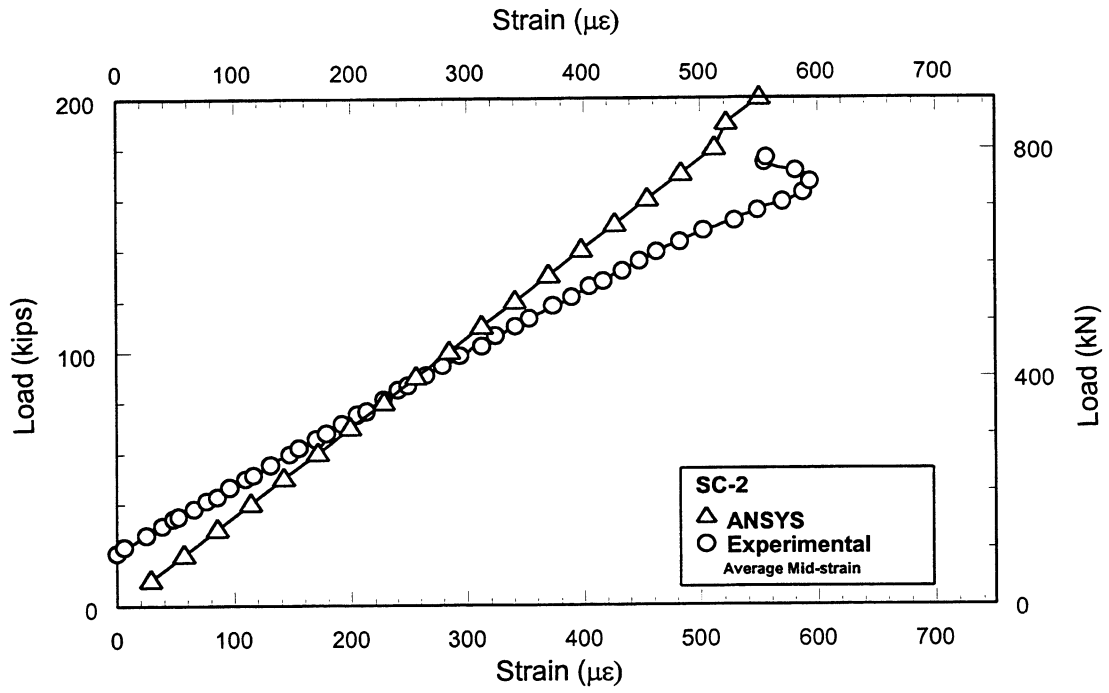

Figure D.15 Finite Element Comparison - Phase I Axial Test SC-2.

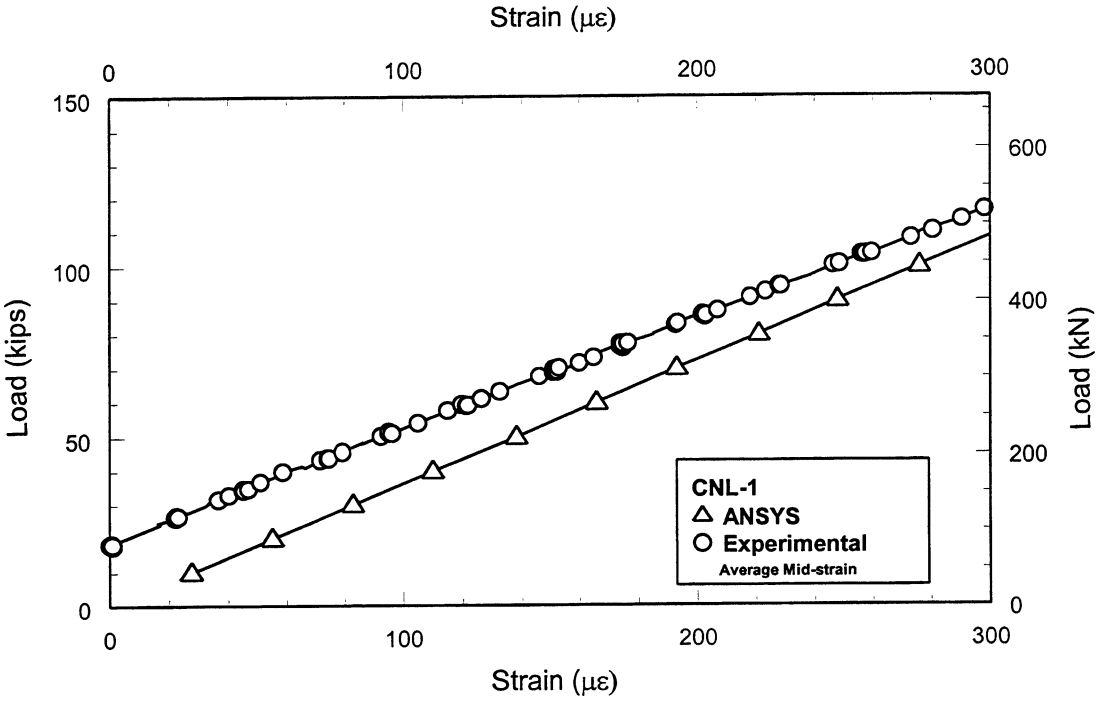

Figure D.16 Finite Element Comparison - Phase II Axial Test CNL-1.

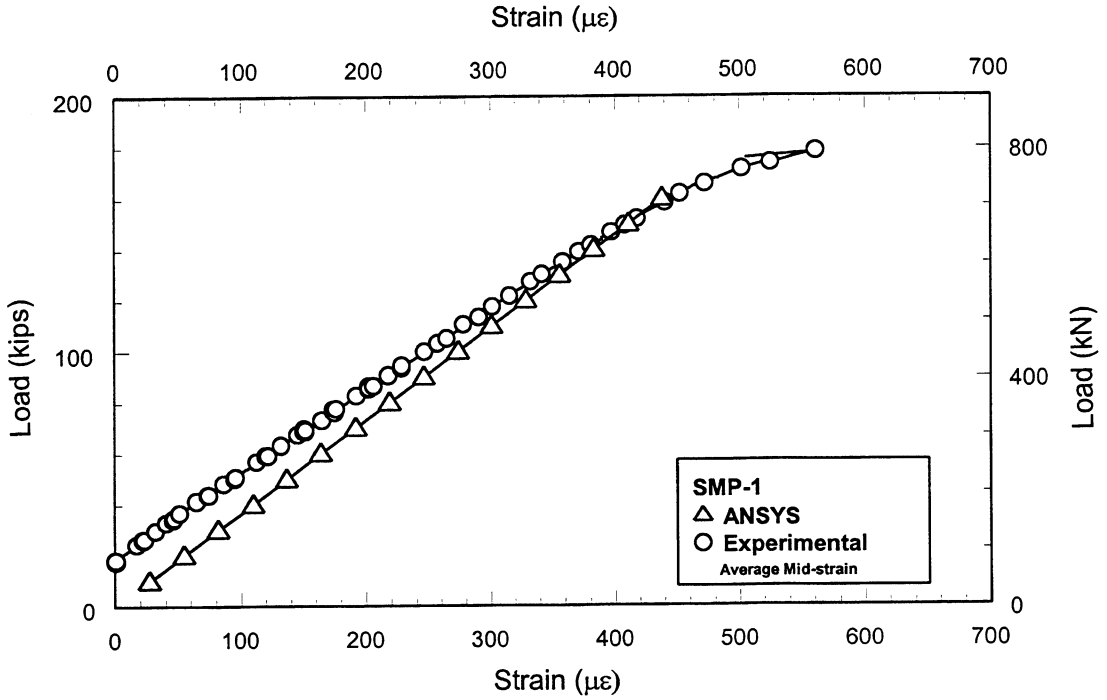

Figure D.17 Finite Element Comparison - Phase II Axial Test SMP-1.

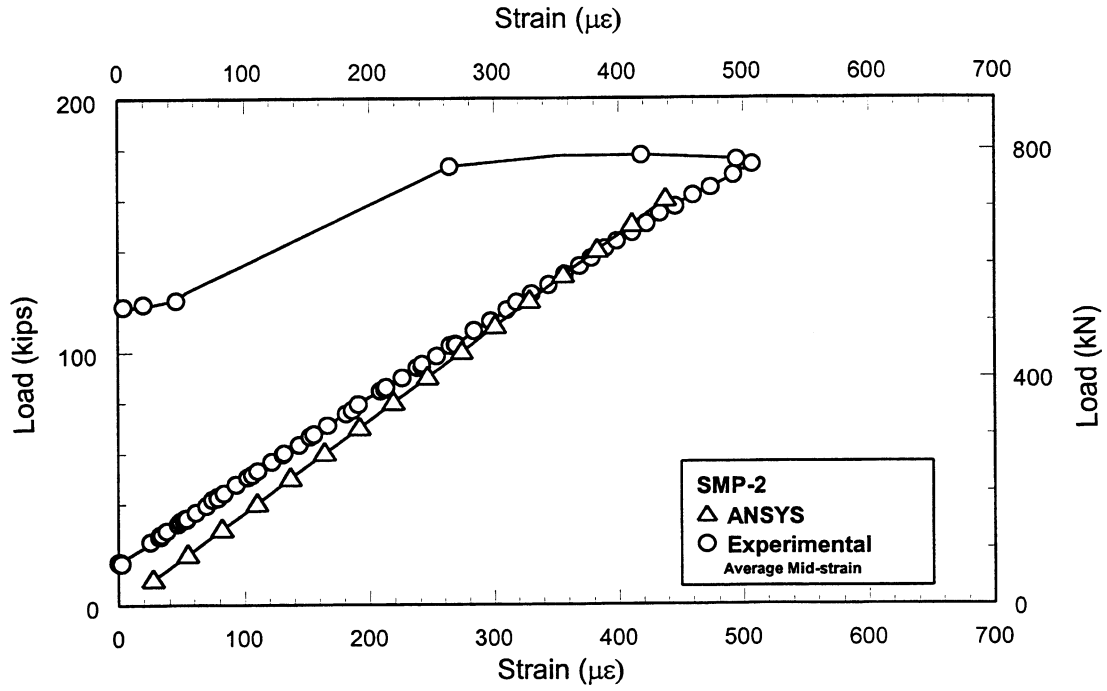

Figure D.18 Finite Element Comparison - Phase II Axial Test SMP-2.

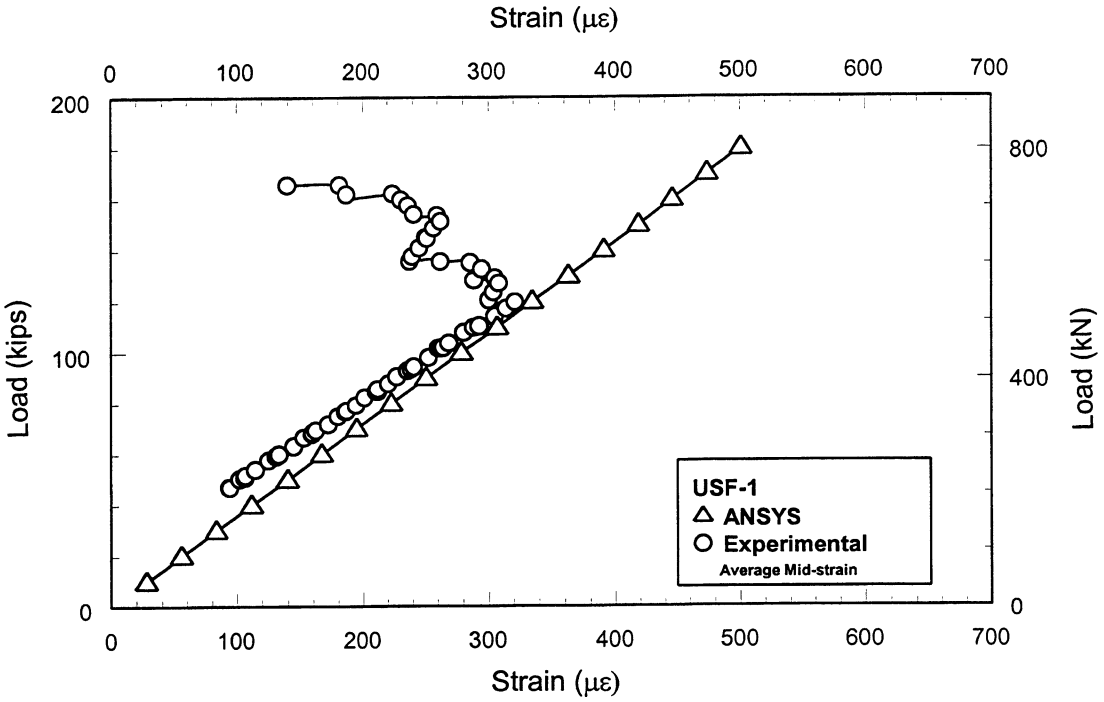

Figure D.19 Finite Element Comparison - Phase II Axial Test USF-1.

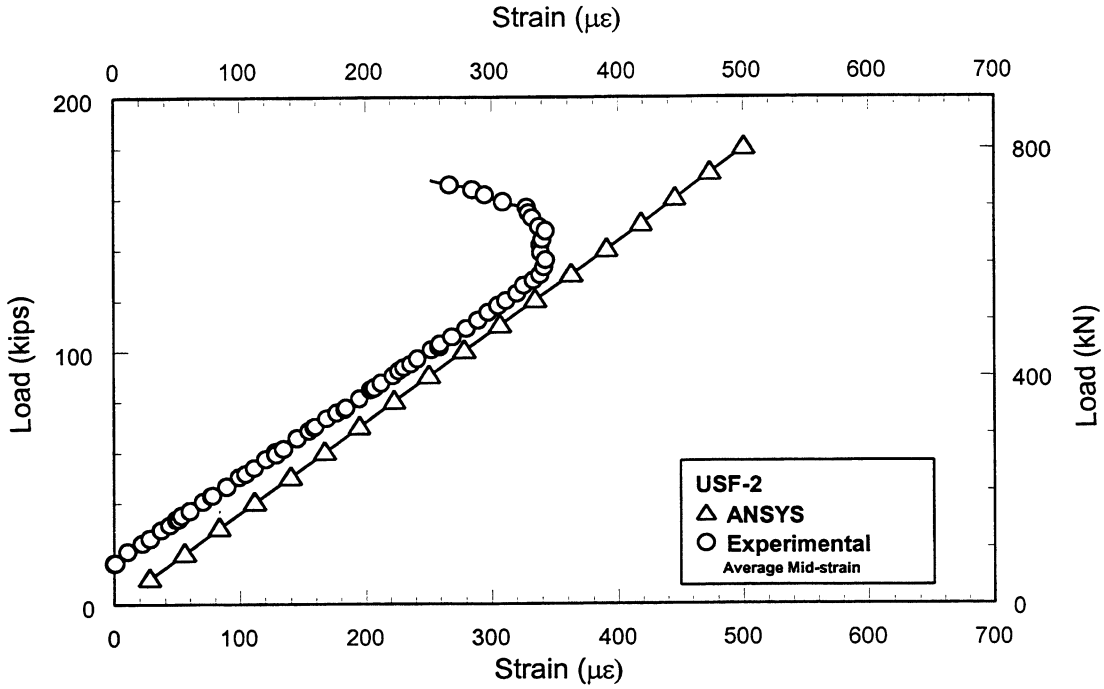

Figure D.20 Finite Element Comparison - Phase II Axial Test USF-2.

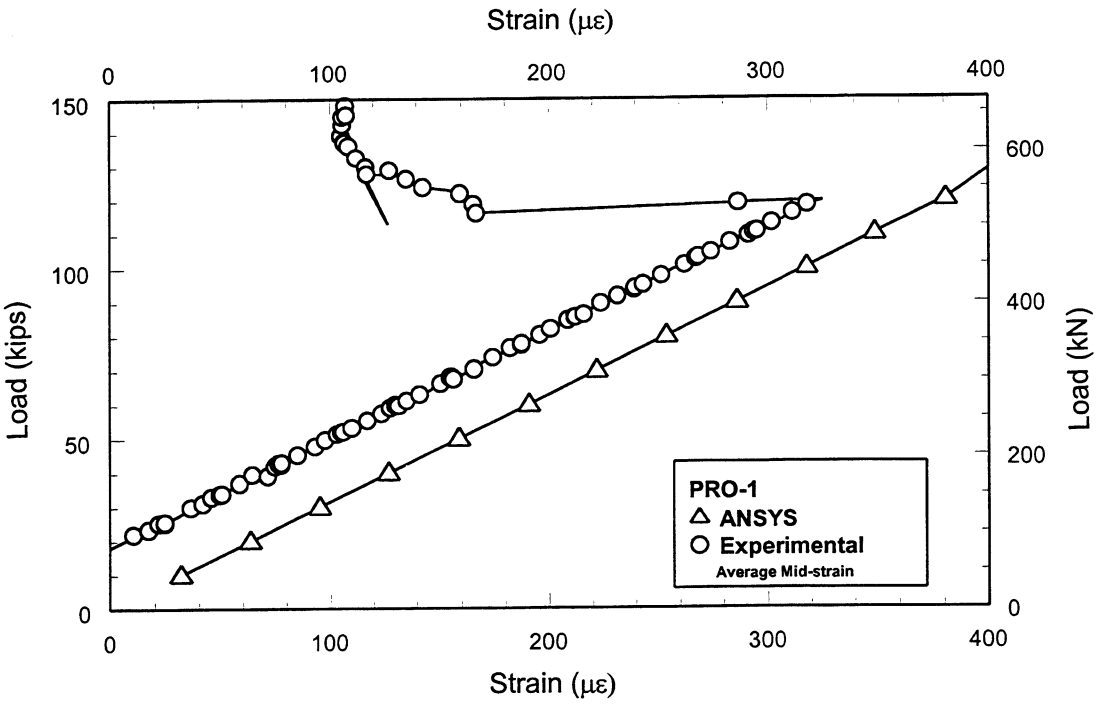

Figure D.21 Finite Element Comparison - Phase II Axial Test PRO-1.

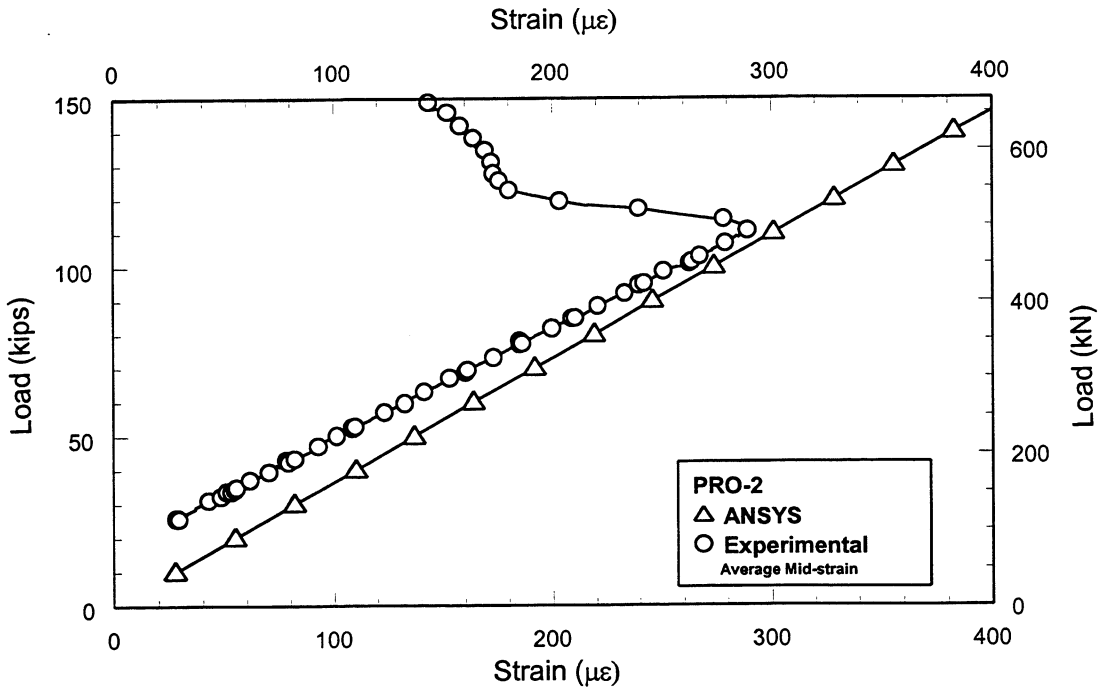

Figure D.22 Finite Element Comparison - Phase II Axial Test PRO-2.

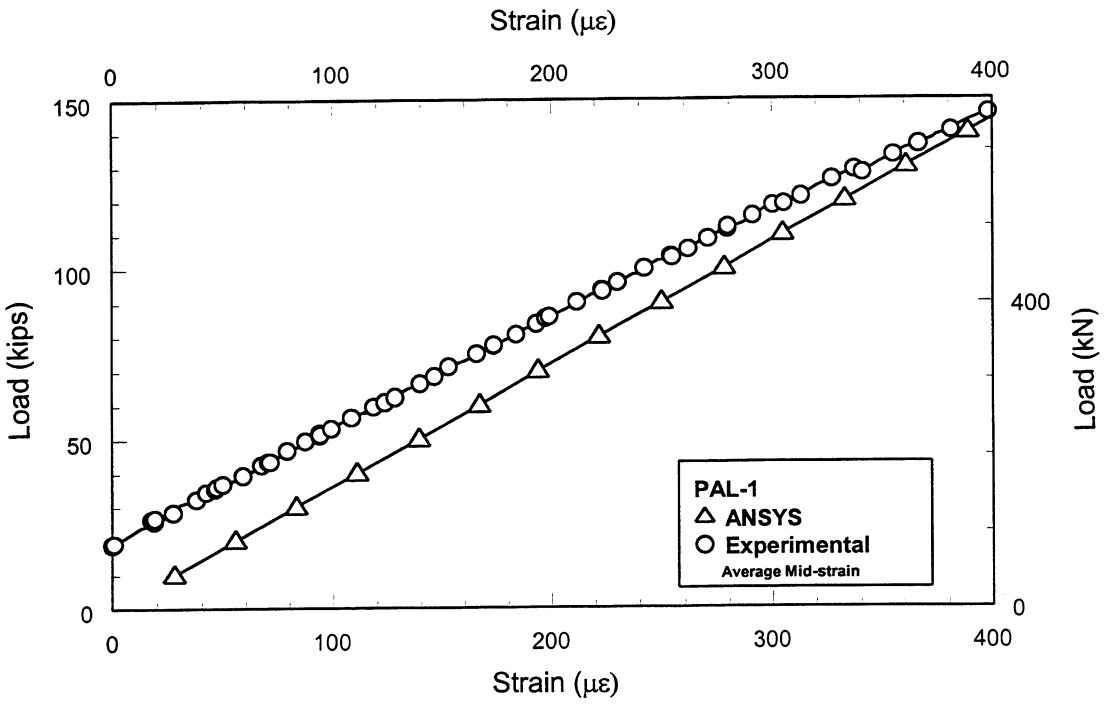

Figure D.23 Finite Element Comparison - Phase II Axial Test PAL-1.

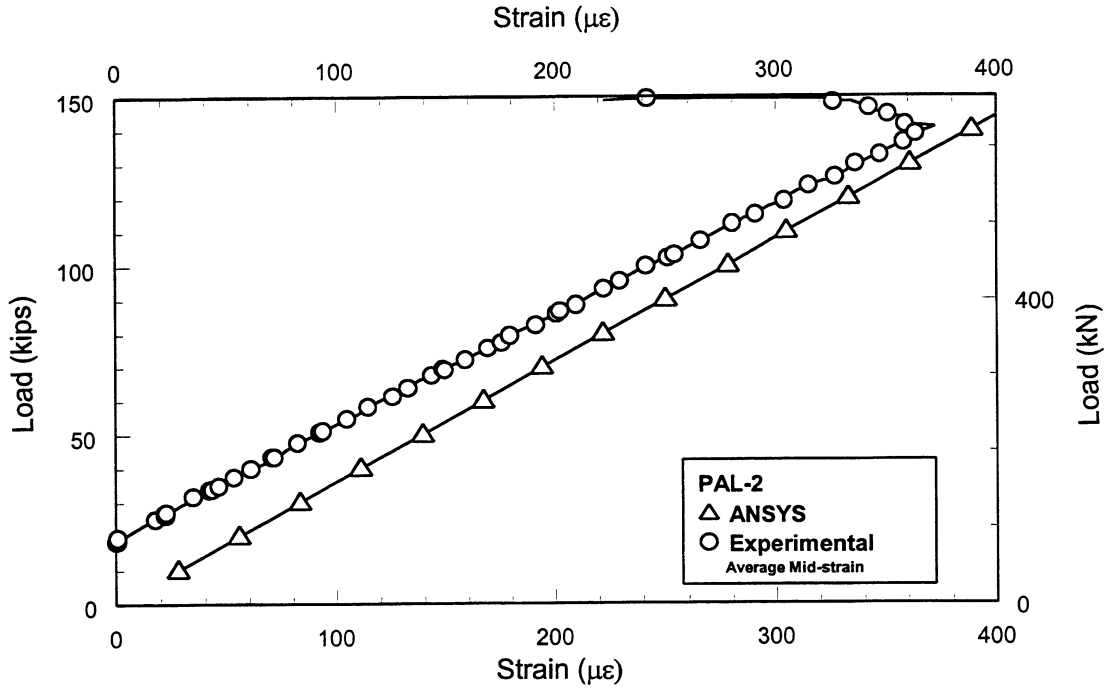

Figure D.24 Finite Element Comparison - Phase II Axial Test PAL-2.

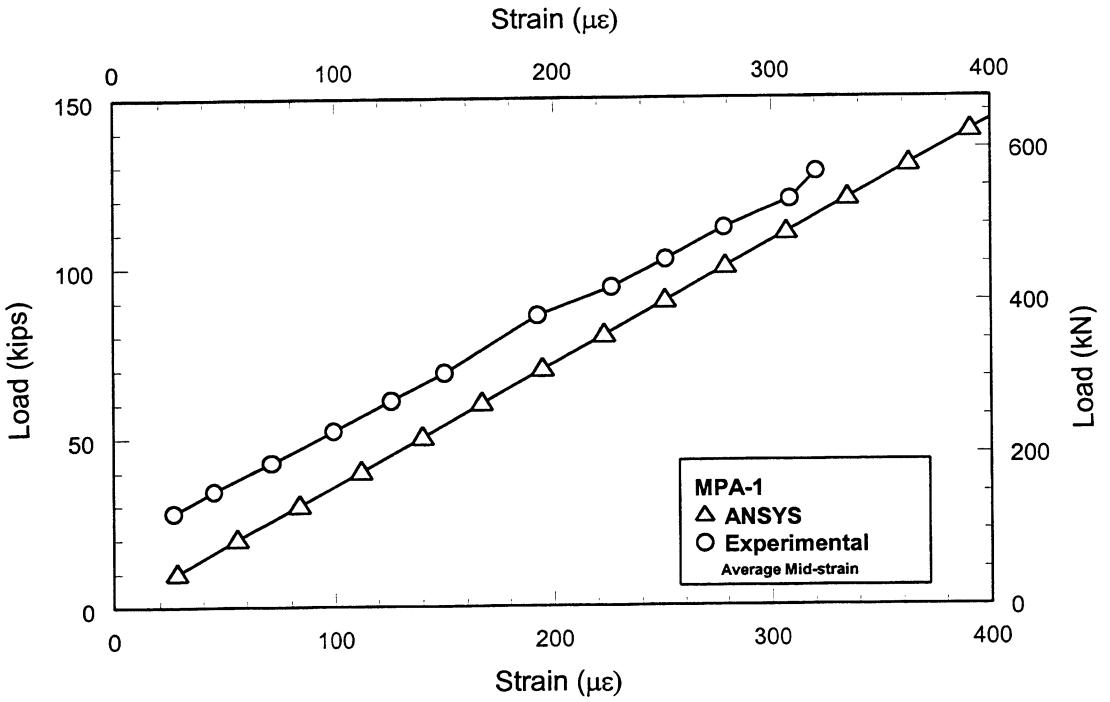

Figure D.25 Finite Element Comparison - Phase II Axial Test MPA-1.

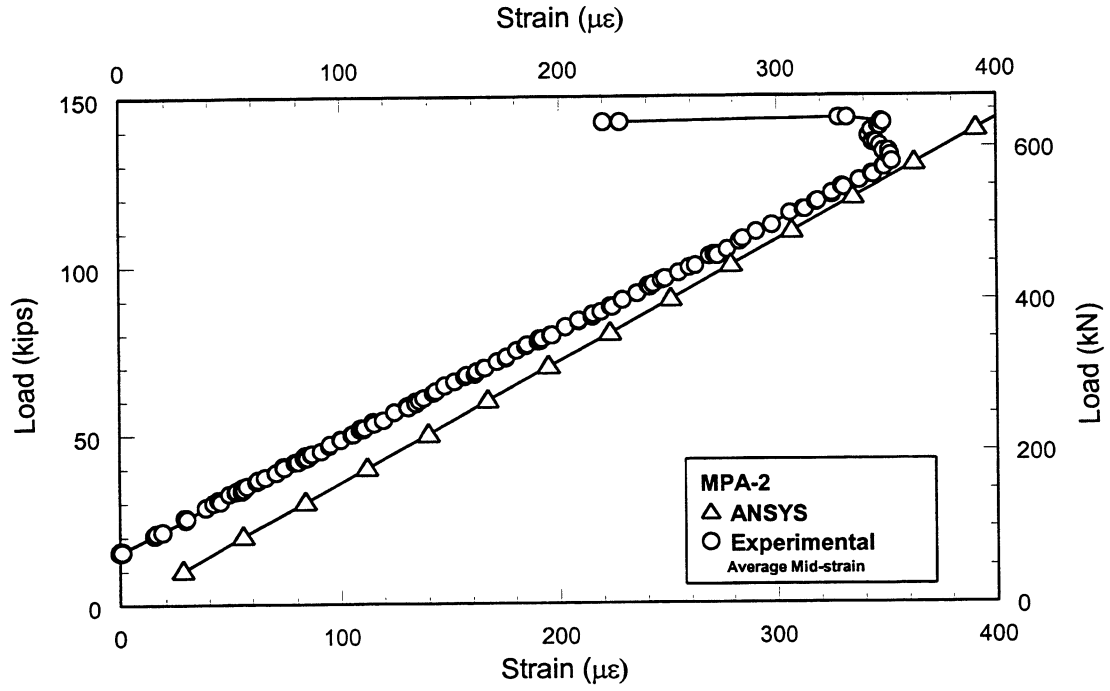

Figure D.26 Finite Element Comparison - Phase II Axial Test MPA-2.